Cellular and Intraviral Interaction Partners of Papillomavirus E6 Protein

Dissertation

der Mathematisch-Naturwissenschaftlichen Fakultät

der Eberhard Karls Universität Tübingen

zur Erlangung des Grades eines

Doktors der Naturwissenschaften

(Dr. rer. nat.)

vorgelegt von

Jia Wen Lim

aus Johor Bahru/Malaysia

Tübingen

2023

Gedruckt mit Genehmigung der Mathematisch-Naturwissenschaftlichen Fakultät der Eberhard Karls Universität Tübingen.

Tag der mündlichen Qualifikation:	31.01.2023
Dekan:	Prof. Dr. Thilo Stehle
1. Berichterstatter/-in:	Prof. Dr. Thilo Stehle
2. Berichterstatter/-in:	Prof. Dr. Thomas Iftner

Table of Contents

List of Abbreviations

°C	Degree Celsius
A	Alanine
AUC	Analytical ultracentrifugation
BPV	Bovine papillomavirus
C	Cysteine
$CaCl_2$	Calcium chloride
Co-IP	Co-immunoprecipitation
CPV	Canine papillomavirus
CR	Conserved region
CRPV	Cottontail rabbit papillomavirus
CSL	DNA-binding proteins CBF-1/RBPjk/Su(H)/Lag1
D	Aspartic acid
DLG-1	Disk Large homolog 1
DNA	Deoxyribonucleic acid
DoL	Degree of labeling
E. coli	*Escherichia coli*
E6AP	E3 ubiquitin ligase E6 associated protein
E6C	E6 C-terminal domain
E6N	E6 N-terminal domain
EV	*Epidermodysplasia verruciformis*
F	Phenylalanine
FACS-FRET	Flow cytometry-based FRET
fl	Fluorescein
FL	Full-length
FP	Fluorescence polarization
FRET	Förster resonance energy transfer

G	Glycine
GPCA	Gaussia Princeps complementary assay
H	Histidine
HA	Hemagglutinin
HECT	Homologous to the E6-AP carboxyl terminus
His_6	Hexa-histidine
hMAML1	Human MAML1
HPV	Human papillomavirus
IPTG	Isopropyl β- d-1-thiogalactopyranoside
K	Lysine
K_D	Dissociation constant
kDa	Kilodalton
M	Methionine
MAGI-1	Membrane-associated guanylate kinase
MAML1	Mastermind-like 1 protein
MBP	Maltose binding protein
mg	Milligram
$MgCl_2$	Magnesium chloride
mL	Millilitre
mM	Millimolar
MmuPV	*Mus musculus* papillomavirus
MnPV	*Mastomys natalensis* papillomavirus
N	Asparagine
NICD	Notch intracellular domain
nm	Nanometer
ORF	Open reading frame
PBM	PDZ-binding motif

PDZ	Postsynaptic density protein (PSD95), Drosophila disc large tumor suppressor (DlgA), and zonula occludens-1 protein (ZO-1)
pRb	Retinoblastoma protein
PTPN14	Protein tyrosine phosphatase non-receptor type 14
R	Arginine
rMAML1	Rabbit MAML1
rpm	Rotation per minute
S	Serine
s_{app}	Sedimentation coefficient
SCC	Squamous cell carcinoma
SDS-PAGE	Sodium dodecyl sulfate-polyacrylamide gel electrophoresis
SE	Sedimentation equilibrium
SEC	Size exclusion chromatography
SfPV	*Sylvillagus floridan*us papillomavirus
Srt A	*Sortase A*
SV	Sedimentation velocity
TB	Terrific Broth
UBR4	Ubiquitin protein ligase E3 component N-recognin 4
UV	Ultra-violet
W	Tryptophan
$ZnCl_2$	Zinc chloride
µg	Microgram
µM	Micromolar

Zusammenfassung

Papillomviren sind kleine DNA-Tumorviren, die Menschen und Tiere infizieren. Eine anhaltende Infektion mit Hochrisiko-Alpha- -HPV kann sich zu Gebärmutterhals- und Anogenitalkrebs entwickeln. HPV16, der krebserregendste Alpha-Hochrisikotyp, verursacht >50 % der HPV-assoziierten Gebärmutterhalskrebsfälle. Das kutane Beta-HPV steht in hohem Maße mit Hautkrebs bei Patienten mit *Epidermodysplasia verruciformis* und bei Personen mit Immunsuppression in Verbindung. Die karzinogenen E6- und E7-Proteine sind die Hauptverantwortlichen für die Entstehung von HPV-assoziierten Krebserkrankungen. Es ist bekannt, dass sie zahlreiche zelluläre Proteine und Signalwege stören, die für die Tumorsuppression wichtig sind.

Das Baumwollschwanz-Kaninchen-Papillomavirus (CRPV) löst in der Haut von Kaninchen Papillome aus. Es ist ein etabliertes Tiermodell für die HPV-vermittelte Karzinogenese, bei der das virale E6-Protein eine entscheidende Rolle spielt. Studien haben gezeigt, dass E6-Proteine von kutanem Beta-HPV, Rinder-PV und Maus-PV E6 mit dem Mastermind-ähnlichen 1-Protein (MAML1) assoziieren und anschließend den Notch-Signalweg hemmen, wodurch die Zelldifferenzierung und -proliferation beeinträchtigt wird. Das CRPV E6 unterscheidet sich jedoch von anderen E6-Proteinen, da es für ein verlängertes E6-Protein (langes E6, LE6) und ein N-terminal verkürztes Produkt (kurzes E6, SE6) kodiert. In dieser Arbeit wird die Interaktion zwischen CRPV-E6-Proteinen und MAML1 und ihre Fähigkeit beschrieben, den Notch-Signalweg herunterzuregulieren, was ein Weg sein könnte, wie eine CRPV-Infektion die Karzinogenese ähnlich wie bei beta-HPV induziert.

Das E6-Protein interagiert nicht nur mit zellulären Proteinen, um den zellulären Signalweg zu stören, sondern kann auch mit E7-Proteinen zusammenarbeiten, um Keratinozyten zu immortalisieren. Die Rolle von E6 und E7 im HPV-Lebenszyklus und bei der Entwicklung der Karzinogenese wurde bisher unabhängig voneinander untersucht. Eine dirkte Interaktion zwischen E6 und E7 ist jedoch noch nicht gezeigt. In dieser Arbeit wird eine direkte Interaktion zwischen E6- und E7-Proteinen von HPV16 und HPV31 in einem zellbasierten Assay nachgewiesen. Darüber hinaus wurde durch analytische Ultrazentrifugation die Beteiligung eines E7-Dimers und zweier E6-Monomere an der Komplexbildung nachgewiesen. Der Fluoreszenzpolarisationstest zeigte eine Bindungsaffinität der Komplexe im

mikromolaren Bereich. Diese Interaktion wirft Fragen über die Funktion des Komplexes in der Karzinogenese und im viralen Lebenszyklus auf, die weiter untersucht werden müssen.

Abstract

Papillomaviruses are small DNA tumor viruses that infect humans and animals. Persistent infection with high-risk alpha- -HPV can develop into cervical and anogenital cancer. HPV16, the most carcinogenic high-risk alpha type, causes >50% of HPV-associated cervical cancers. In addition, cutaneous beta HPV is highly associated with skin cancer in patients with epidermodysplasia verruciformis and individuals with immunosuppression. The carcinogenic E6 and E7 proteins are the major contributors to HPV-associated cancers. They are known to disrupt numerous cellular proteins and signaling pathways essential for tumor suppression.

Cottontail rabbit papillomavirus (CRPV) induces papillomas in rabbit skin. It is an established animal model for HPV-mediated carcinogenesis, in which the viral E6 protein plays a critical role. Studies have shown that cutaneous beta-HPV, bovine PV, and mouse PV E6 proteins associate with mastermind-like 1 protein (MAML1) and subsequently inhibit Notch signaling, thereby impairing cell differentiation and proliferation. However, CRPV E6 differs from other E6 proteins in that it encodes an extended E6 protein (long E6, LE6) and an N-terminally truncated product (short E6, SE6). In this work, we describe the interaction between CRPV E6 proteins and MAML1 and their ability to down-regulate Notch signaling, which may be a way CRPV infection induces carcinogenesis similar to beta-HPV.

The E6 protein interacts with cellular proteins to disrupt the cellular signaling pathway and can cooperate with E7 proteins to immortalize keratinocytes. The roles of E6 and E7 in the HPV life cycle and the development of carcinogenesis have previously been studied independently. However, a direct interaction between E6 and E7 has yet to be shown. In this thesis, a direct interaction between the E6 and E7 proteins of HPV16 and HPV31 is demonstrated in cell-based assays and verified using biophysical methods. In addition, the involvement of two E7 molecules and two E6 molecules in complex formation was demonstrated by analytical ultracentrifugation. Furthermore, the fluorescence polarization assay showed the binding affinity of the complexes is in a micromolar range. This interaction raises questions about the function of the complex in carcinogenesis and in the viral life cycle that requires further investigation.

Publication

Parts of this thesis have already been published.

Lim, J., Frecot, D. I., Stubenrauch, F., Iftner, T., & Simon, C. (2022). Cottontail rabbit papillomavirus E6 proteins: Interaction with MAML1 and modulation of the Notch signaling pathway. Virology, 576, 52–60.

Lim, J., Straub, E., Stubenrauch, F., Iftner, T., Schindler, M., & Simon, C. (2022). An enhanced triple fluorescence flow-cytometry-based assay shows differential activation of the Notch signaling pathway by human papillomavirus E6 proteins. Scientific Reports, 12(1), 1–13.

Lim, J., Iftner, T., & Simon, C. (2021). Native Isolation of 3×HA-Tagged Protein Complexes to Characterize Protein-Protein Interactions. *Current Protocols*, *1*(2), 1–20.

Lim, J., Lilie, H., Kalbacher, H., Roos., N, Frecot, D. I., Feige. M., Conrady, M., Votteler, T., Cousido-Siah, A., Corradini Bartoli, G., Iftner, T., Trave, G., & Simon, C. Evidence for direct interaction between the oncogenic proteins E6 and E7 of high-risk human papillomavirus (HPV). J Biol Chem, 2023. **299**(8): p. 104954.

1 Introduction

1.1 Papillomaviruses

Papillomaviruses (PVs) are small, circular, non-enveloped, double-stranded DNA viruses with a virion size of ~ 55 nm, infecting humans and animals. To date, there are more than 400 types of PVs from more than 20 different mammalian host species as well as birds and reptiles sequenced (according to Papillomavirus Episteme (PaVE); https://pave.niaid.nih.gov/#home), of which more than 200 types belongs to human papillomaviruses (HPVs) [1].

1.2 Genome Organization and Classification of Papillomaviruses

Most PVs genomes are approximately 8,000 base pairs containing eight or nine open reading frames. The genomes of the papillomaviruses mentioned in this dissertation are shown in ***Figure 1***. The organization of PVs' genomes shows three regions, which include i) the early coding region consisting of the early genes E1, E2, E4, E5, E6, and E7; ii) a region containing late genes which encode major (L1) and minor (L2) capsid proteins, and iii) a non-coding region named upstream regulatory region (URR) that contains most of the regulatory elements that play essential roles in viral DNA replication and transcription. The genomes of all PV are highly conserved with some exceptions, such as (i) the absence of E5 open reading frame (ORF) in beta HPV types; (ii) an elongated E6 ORF in cottontail rabbit PV (CRPV) in which it encodes an elongated E6 protein named long E6 (LE6) and a second ORF within LE6, which encodes short E6 (SE6) protein.

Papillomaviruses are classified into different genera based on the differences in their L1 nucleotide sequences [8]. PVs of the same genera share approximately 60 % or more nucleotide sequence identity [8]. Of the same genera, PVs are further grouped into different species based on their phylogenetic relationship whereby they share the common biological and pathological properties [8]. HPVs are divided into five genera (alpha, beta, gamma, mu, and nu), of which the majority belong to the alpha genus which infects anogenital and mucosal epithelial while HPVs from the beta genus infect cutaneous epithelial. Alpha HPVs are further divided into high-risk and low-risk types based on their carcinogenic potential [9, 10]. Several other genera that should be mentioned

include delta papillomaviruses such as bovine papillomavirus 1 (BPV1) that infect cows, kappa papillomaviruses such as CRPV that infect rabbits and pi papillomaviruses such as Mus musculus papillomavirus type 1 (MmuPV1) that infect mice as these papillomaviruses have been studied and employed as animal models in the last decades.

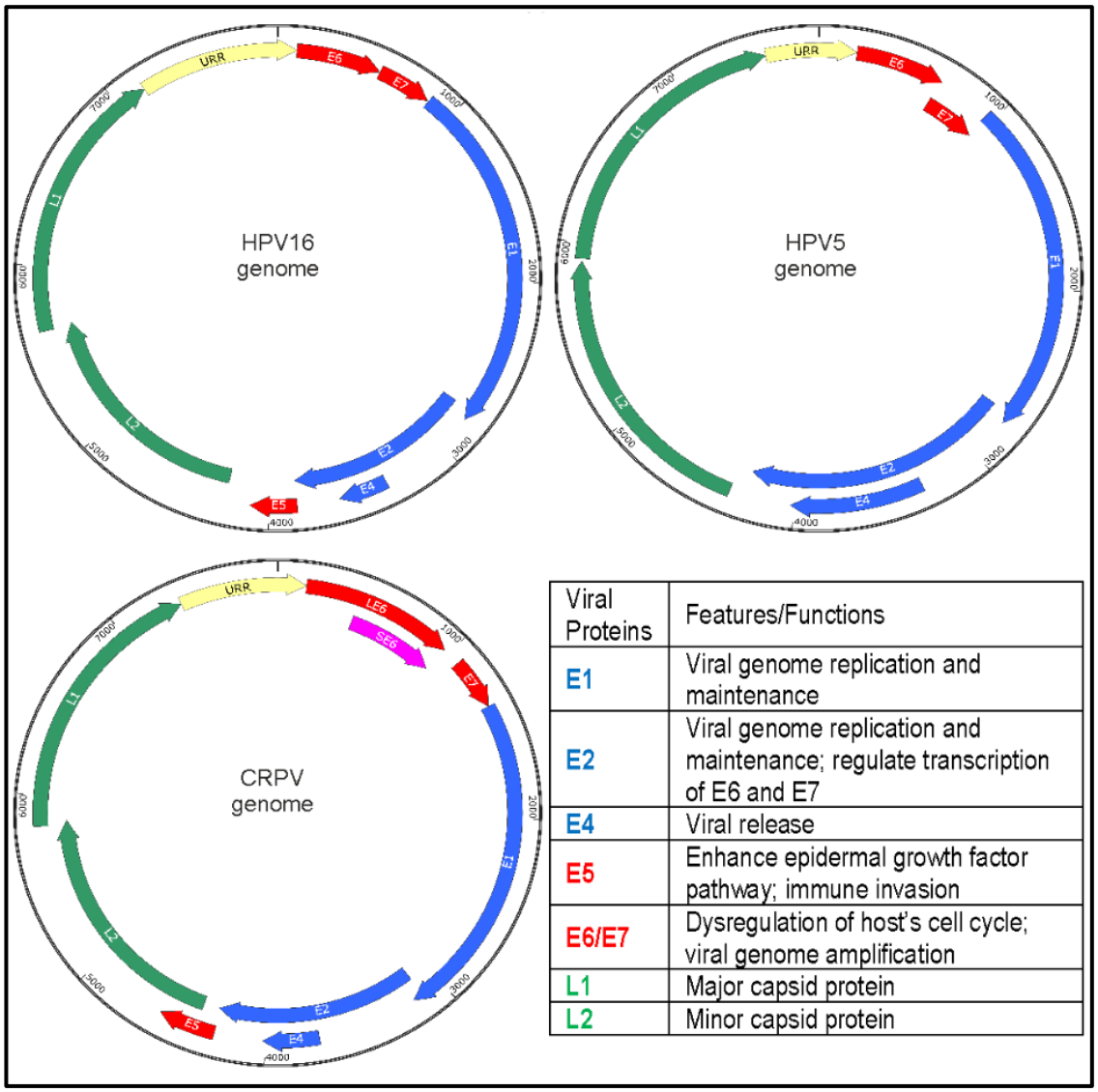

Viral Proteins	Features/Functions
E1	Viral genome replication and maintenance
E2	Viral genome replication and maintenance; regulate transcription of E6 and E7
E4	Viral release
E5	Enhance epidermal growth factor pathway; immune invasion
E6/E7	Dysregulation of host's cell cycle; viral genome amplification
L1	Major capsid protein
L2	Minor capsid protein

Figure 1 Genome organization of papillomaviruses and the functions of each viral protein. Genome map generated with SnapGene® version 4.1.9 and edited with CorelDrawX7 version 17.5.0.907. Late genes are in green; early genes are in turquoise; oncogenes are in red; yellow is the upstream regulatory region magenta is the SE6 which is unique in kappa PV. The functions of each protein are indicated below the genomes.

1.3 Human Papillomaviruses - Infection and Clinical Manifestations

Infection with HPV is common among sexually active women at some stage of their life. However, it is uncommon for an infection to develop into cervical cancer, as a cell-mediated immune response may clear these infections. Only persistent

infection with high-risk alpha HPVs (HPV16, HPV18, HPV31, HPV33, HPV35, HPV39, HPV45, HPV51, HPV52, HPV56, HPV58, HPV59, HPV68, HPV73, and HPV82) may progress into cervical cancer. There were approximately 604,000 new cases of cervical cancer reported in 2020, of which 342,000 reported death; with most new cases and deaths (~90 %) occurring in low-income and middle-income countries [11]. Persistent infection with high-risk HPV could lead not only to cervical cancer but also several other cancers, including cancers of the vulva, vagina, penis, anus, and head and neck cancer [12, 13]. Of these cancers, it should be noted that head and neck cancer accounts for more than 800,000 new cases and more than 400,000 deaths globally in 2020 [11], and it is highly associated with HPV16 infection [14-16]. The low-risk alpha HPVs (HPV6, HPV11, HPV40, HPV42, HPV43, HPV44, HPV54, HPV61, HPV70, HPV72, and HPV81) are rarely associated with cancers but may induce the formation of genital warts [13].

Exposure to cutaneous beta HPV is common for an individual. Healthy individuals' hair follicle stem cells have been proposed to be the reservoir for the persistent infection of beta HPVs, in which beta HPV types are detected in up to 90 % of healthy individuals [17-20]. Studies have shown that the infection may occur in childhood via skin-to-skin contact [21, 22]. There were over one million new non-melanoma skin carcinoma (NMSC) cases and 64,000 deaths cases reported worldwide in 2020 [11]. It remains unclear if the infections of beta HPV types in healthy individuals may contribute to NMSC. However, they are highly prevalent in *epidermodysplasia verruciformis* (EV) patients and immunosuppressed individuals [23, 24]. The infections may progress into cutaneous squamous cell carcinoma (cSCC), especially at sun-exposed anatomical sites [23]. Beta HPV5 and HPV8 are detected in 90% of these cancers in EV patients [24-26]. Serological assays have also detected not only the presence of beta HPV in cSCC but also gamma, mu and nu HPV, with beta HPV being detected in most cases and nu HPV the least detected [27, 28]. A ‘hit-and-run’ mechanism has recently been proposed for beta HPV E6 that it may be required to initiate carcinogenesis, but it is not required to maintain the phenotypes [29]. Hence, the association of beta HPV with carcinogenesis remains under debate.

1.4 HPV Life Cycle

The life cycle of HPVs relies on the differentiation of the infected epithelium (***Figure 2***). This is initiated through their invasion of the basal cells in the stratified epithelium via a micro-abrasions wound [30]. The HPV genomic DNA enters the nucleus following viral entry and uncoating. The DNA copy number is maintained at 50-100 copies per cell in the basal layer, which is crucial to establish the early phase of the viral life cycle [31, 32]. Then, the infected cells migrate into suprabasal layer, initiate differentiation and induce viral gene expression. The E6 and E7 proteins are expressed to ensure continuous cell division in infected, differentiating cells by co-operatively inactivating p53 and retinoblastoma protein (pRb), respectively [31, 33]. In the suprabasal layer, the expression of the viral early genes (E1, E2, E4, E6, E7) involved in viral genome replication elevates and promotes viral genome amplification to thousands of copies per cell [34, 35]. The terminal differentiation of infected cells activates the expression of L1, and L2 proteins promoting the assembly [36, 37] and the release [38, 39] of the progeny virions.

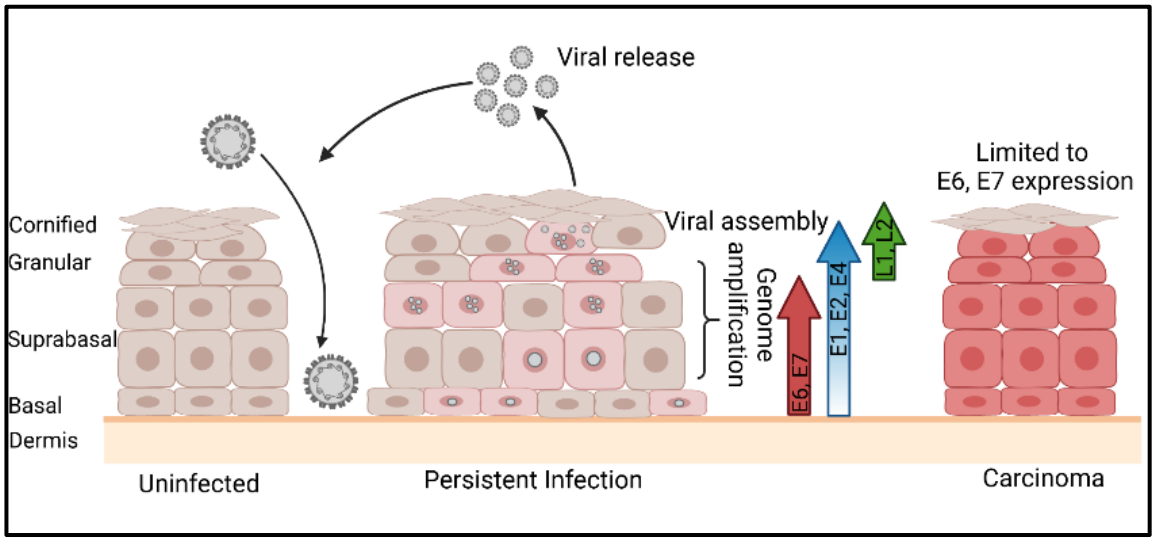

Figure 2 HPV viral life cycle. Diagram illustrates the progression of HPV infection to malignancy. Figure created with Biorender.com.

Persistent infection may result in the accumulation of secondary genetic changes in infected host cells and the progression of cancer. Cervical intraepithelial neoplasia (CIN) are distinguished from grade 1 to grade 3 based on the extent of abnormal dividing cells within the epithelium. CIN1 lesions retain the ability to complete the HPV life cycle, producing viral particles and resembling flat warts

but the level of cell proliferation in basal and parabasal layers is lower [40]. Integration of viral genome into the host cells together with DNA aneuploidy is observed in CIN2 and CIN3 lesions as well as in cervical carcinoma [41, 42]. The integration is suggested to be the end of the viral life cycle and the loss of differentiation accompanied by high E6 and E7 expression due to the mutation or deletion of other viral genes may lead to the progression of carcinoma [43, 44].

1.5 E6 Protein

HPV E6 is a multifunctional protein (***Figure 3A***) with approximately 150 amino acids and is partly conserved among PVs in sequences and structure (***Figure 3B*** & ***Figure 3C***). E6 consists of four zinc-binding motifs that give rise to the two E6 domains, E6N and E6C [45, 46]. E6 proteins target the LXXLL motifs of cellular proteins that are commonly found in transcriptional coregulators such as E3 ubiquitin ligase E6 associated protein (E6AP/UBE3A) and Mastermind-like 1 protein (MAML1) (***Figure 3D***).

Among all interacting targets, the best-studied model is the association of alpha high-risk E6 proteins to E6AP, followed by the recruitment of p53, forming an E6/E6AP/p53 ternary complex and resulting in ubiquitination and degradation of p53 via proteasomal pathway [5, 45, 47]. This allows infected cells to escape from p53-dependent apoptosis [31]. Moreover, a unique and conserved PDZ (**P**ostsynaptic density protein (PSD95), **D**rosophila disc large tumor suppressor (DlgA), and **Z**onula occludens-1 protein (ZO-1))-binding motif (PBM) at the C-terminal of all high-risk HPV E6 proteins (***Figure 3B***), allows these E6 to associate with PDZ-domains containing proteins, such as membrane-associated guanylate kinase 1 (MAGI-1) and Disk Large homolog 1 (DLG-1) that play crucial roles in apoptosis, and cell polarity [48-51].

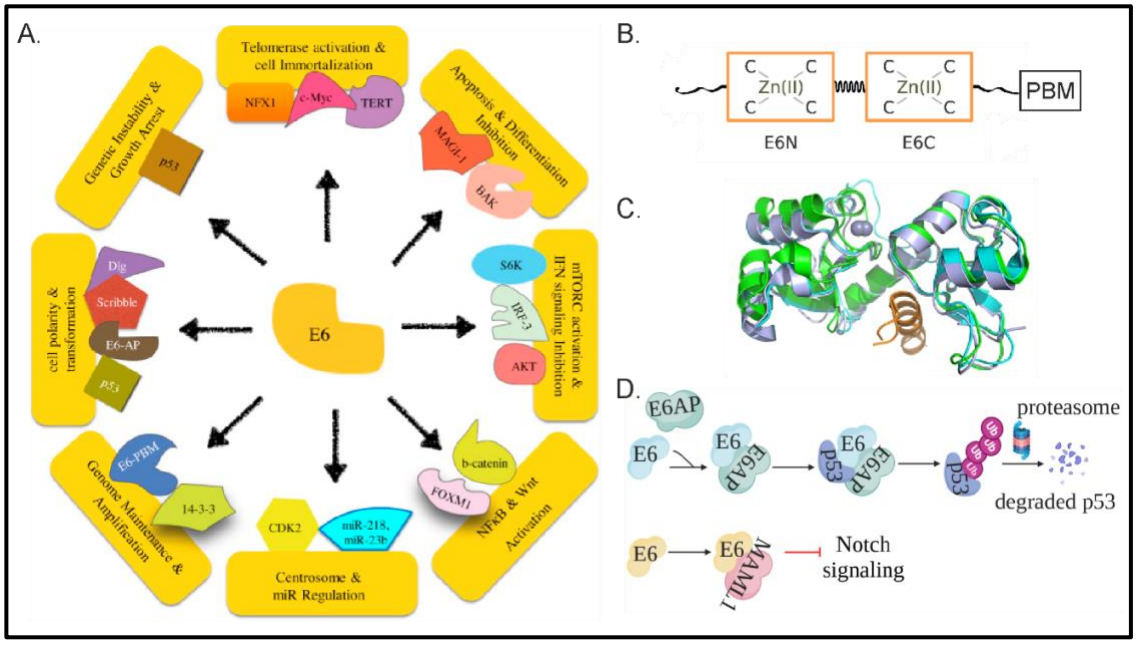

Figure 3 The structure of E6 and functional role of E6. A. E6 interacts with many cellular proteins. *Adapted from* [1]. **B.** The schematic domain organization of E6. *Adapted from* [3]. **C.** The superimposition of E6 structure from HPV16E6/LxxLL(E6AP) in green; HPV16E6/LxxLL(E6AP)/p53 in grey; HPV31E6/LxxLL(E6AP) in cyan and LxxLL (E6AP) in orange *Adapted from* [5] . **D.** Alpha HPV E6 recruits E6AP and binds p53 for p53 proteasomal degradation; beta HPV E6 bind MAML1 and inhibits Notch signaling. *Figure created with Biorender.com*.

Beta HPV is much less studied. However, it is known that most of the beta HPV E6 proteins neither interact nor degrade p53 [52, 53]. However, they associate with MAML1 via the LxxLL motif and lead to the inhibition of the Notch signaling pathway [54-56] that is responsible for keratinocyte differentiation [57], though the mechanism remained unclear.

1.6 E7 Protein

The HPV E7 protein is a highly phosphorylated, acidic polypeptide that consists of approximately 100 amino acid residues and interacts with many cellular proteins (***Figure 4A***). E7 contains three conserved regions (CR), namely CR1 (amino acids 1 to 15), CR2 (amino acids 16 to 37), and CR3 (amino acids 38 to 98) (***Figure 4B***). CR1 and CR2 are highly unstructured, with CR2 of E7 containing a conserved LXCXE motif, a high-affinity binding site for tumor suppressor pRb [58, 59] (***Figure 4B***). CR3 is highly structured and composed of two CXXC motifs building a zinc-binding domain (***Figure 4B*** & ***Figure 4C***). It allows the E7 to form a stable dimer with its unique β1β2α1β3α2 topology that is not present in any other known zinc-binding protein [60, 61]. CR3 was also reported as the binding site of many cellular targets, such as tumor suppressor

non-receptor protein tyrosine phosphatase type 14 (PTPN14), and is a secondary low-affinity binding site for pRb [4, 62].

Among all interactive targets (***Figure 4A***), the most understood cellular target for E7 is the pRb tumor suppressor. The association of E7 with pRb drives the proteasome-mediated degradation of pRb via the recruitment of cullin 2 ubiquitin ligase, which disrupts the interaction between pRb and E2F transcription factor (***Figure 4D***). Thus, it leads to the activation of the E2F-regulated S-phase gene, promoting G1/S phase cell cycle transition, resulting in continuous cell cycle progression and cellular transformation [1, 63, 64]. In addition, the interaction of E7 with PTPN14 has recently drawn attention in the field. E7 targets PTPN14 for ubiquitination and proteasomal degradation by recruiting E7-associated ubiquitin protein ligase E3 component N-recognin 4 (UBR4) to its N-terminus (**Figure 4*D***) hence impairing keratinocyte differentiation [65].

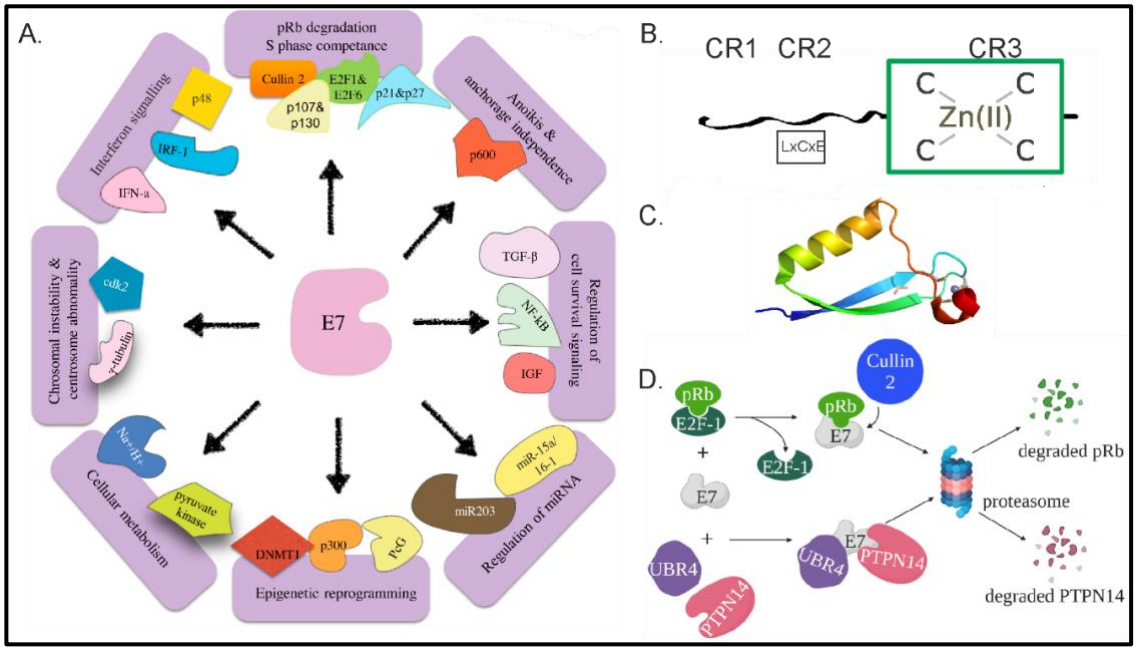

Figure 4 The structure and functional roles of E7. A. E7 interacts with many cellular proteins. Adapted from [1]. **B.** The schematic domain organization of E7. *Adapted from* [3]. **C**. The 3D-structure of HPV18 E7CR3 45-98. *Adapted from* [4]. **D.** E7 recruits cullin 2 and UBR4 ubiquitin ligase to initiate proteasomal degradation of pRb and PTPN14, respectively. *Figure created with Biorender.com*.

1.7 The Synergy Effect between E6 and E7 in Carcinogenesis

Both E6 and E7 are required to maintain the malignant phenotype and cell survival [66, 67] though the mechanism employed by E6 and E7 is not clear so far. It has been mentioned earlier that the inactivation of pRb by E7 proteins induces uncontrolled cell cycle progression in infected cells. The elevation of p53

levels has been shown in cells expressing E7, thus inducing p53-dependent growth arrest and apoptosis [68-70]. However, this effect from p53 is circumvented by HPV-infected cells through E6 expression, whereby E6 employs E6AP to degrade p53 [47], possibly targeting only p53 cellular pools that are involved in the activation of the transcription pro-apoptotic factors [71], thus inhibiting the p53-dependent apoptotic pathway [31]. Furthermore, both E6 and E7 target interferon (INF) responses and manipulate the corresponding cellular pathways to overcome immune invasion. HPV16 E6 was shown to downregulate the expression of INF-α and IFN- β mRNA in cervical keratinocytes [72]. It also decreases the nuclear STAT-1 proteins and the effect is more efficient when E6 is co-expressed with E7 and subsequently inhibit the transactivation of IFN-responsive genes [72]. Besides, HPV18 E6 inhibits Tyk-2 kinase to downregulate INF-α induced JAK-STAT signaling [73]. Moreover, E6 and E7 also trigger cellular proliferation in concert with the Hippo signaling pathway by inducing the Yes-associated protein (YAP1) activation [74]. E7 does this by inhibiting PTPN14 [78, 85], while E6 targets DLG-1, MAGI-1, and Scrib through its PBM [48, 49, 75-77]. Furthermore, HPV E6 and E7 activate angiogenesis which plays a critical role in the development and progression of cancers by downregulating anti-angiogenic factor prolyl 4-hydroxylase PHD2 [78] and upregulating the pro-angiogenic factors oxygen-sensitive transcriptional activator HIF-1α (hypoxia-inducible factor-1) and VEGF (vascular endothelial growth factor) [79, 80]. It has been reported that inhibition of PI3K/Akt and ERK1/2 signaling pathway represses the HPV16 E6 and E7-induced HIF-1α protein and VEGF expression [79] even though the precise molecular mechanism of whether E6 or E7 is dysregulating the balance between pro- and anti-angiogenic factors are not well understood. Studies have shown that for VEGF, E6 stimulates the VEGF promoter by binding to the VEGF proximal promoter region [81], whereas E7 induces VEGF expression via hTERT and telomerase activity [82]. However, it is not clear whether the upregulation of VEGF by E6 and E7 is a direct or indirect effect. It is known that E6 and E7 cooperate in immortalizing human keratinocytes, E7 alone has lower immortalizing effect but E6 alone cannot do so [83]. Inhibition of E6 or E7 by siRNAs efficiently suppresses or kills the growth of HPV-positive cells [66, 67, 84, 85]. These studies show that E6 and E7 work synergistically in developing and maintaining the HPV-associated carcinogenesis.

1.8 E6/E7 Complex

The transcriptomic and proteomic analyses of HPV E6 and E7 proteins have been explored in single expression for their critical roles in HPV-associated carcinogenesis, revealing many cellular proteins and pathways they interfere with [53, 86-92]. In addition, the intraviral interactions between E6/E2 and E7/E2 have also been described, in which they interact to regulate the functional roles of each other [93, 94]. However, the direct interaction between E6 and E7 has not been described in the literature.

Nevertheless, the interaction between E6 and E7 of HPV31 has first observed in the Ph.D. dissertation of Giada Corradini Bartoli through a systematic intraviral interaction screening using a cell-based flow cytometry-FRET (FACS-FRET) assay. This interaction in HPV31 was verified, and the same interaction from HPV16 was investigated in my master thesis via FACS-FRET analysis and co-immunoprecipitation. In the master thesis of Marcel Conrady, the interaction between E6 and E7 of HPV16, HPV18, and HPV31 was also seen in *Gaussia* Princeps complementary assay (GPCA), and he further verified the interaction of HPV16 E6 and E7 *in vitro* with co-elution and co-purification experiments. Desiree Frecot and Tobias Votteler started to characterize the HPV31 E6/E7 complex in their master thesis and bachelor thesis, respectively, in which they established and optimized the condition of the fluorescence polarization assay and obtained a binding affinity for the mentioned complex. The function of the complex is so far non-disclosed and it is also unclear if this complex formation affects the interactomes of E6 and E7.

1.9 Cottontail Rabbit Papillomavirus (CRPV)

The cottontail rabbit is the first animal host of PV discovered in 1922 [95] and is the first DNA virus reported to be associated with tumorigenesis [96, 97]. CRPV belongs to the kappa genus and is named CRPV or *Sylvilagus floridan*us papillomavirus 1 (SfPV1). Like HPV infection, persistent infection with CRPV induces papilloma in domestic rabbits that may progress into cancer depending on the host [98, 99]. In the last decades, the CRPV-rabbit tumor model remains an important animal model for studying the latent infection [100-102], the

mechanism behind the carcinogenesis associated with the cutaneous PVs [103-106], the development of anti-viral therapy [107-110] and immunotherapy [108-110], and the development of prophylactic and therapeutic vaccines [111-115].

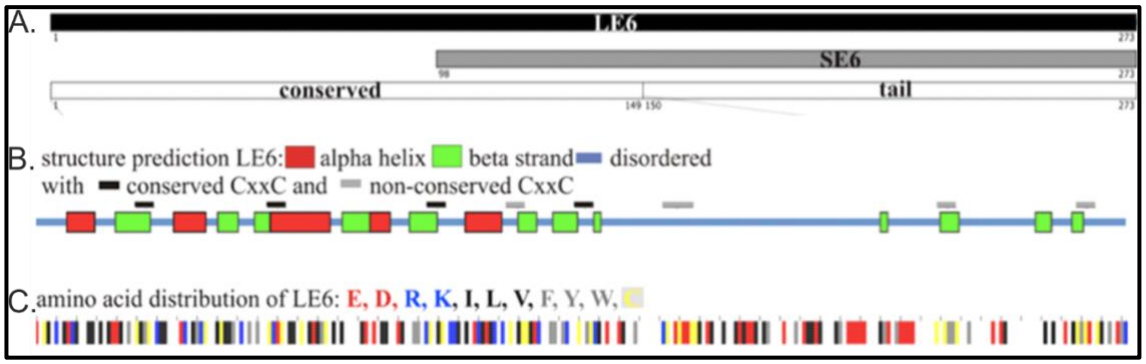

Figure 5. The unique schematic structure of CRPV E6. A. Schematic structure of CRPV E6 shows the N-terminus (1-149) of CRPV E6 is conserved with other E6 proteins of papillomaviruses. **B.** Structure prediction and CxxC motif of CRPVE6. The conserved CxxC motifs are black, whereas the additional non-conserved CxxC motifs are grey. **C.** The amino acid composition shows a highly acidic tail region. *Adapted from* [7].

CRPV E6 encodes a unique E6 protein consisting of an elongated tail structure while retaining the N-terminal region that is conserved with other E6 proteins (***Figure 5A***). The structure prediction of CRPV E6 showed that the four CxxC motifs in the N-terminus of CRPV E6 are conserved to the common four CxxC motifs in the E6N-E6C domain organization of other E6 proteins (***Figure 5B***). In contrast, the tail region is predicted to be highly unstructured, highly acidic with low complexity and is neither conserved with any E6 proteins nor any protein on the swiss protein database (***Figure 5C***). Notably, CRPV E6 full-length proteins consist of five additional CxxC motifs, one located in the conserved region of E6C and four other CxxC motifs located in the tail region (***Figure 5B***). However, the function of these additional motifs still needs to be discovered.

1.10 Notch Signaling

Notch signaling plays key role in the cell differentiation and proliferation [116]. It occurs through cell-to-cell contact in which the membrane-anchored Jagged receptors bind to the Notch receptors, subsequently leading to a series of proteolytic cleavage. The Notch intracellular domain is released upon gamma-secretase cleavage allowing its translocation to the nucleus and its binding to the DNA-binding proteins CBF-1/RBPjk/Su(H)/Lag1 (CSL). Upon binding, CSL is dislocated from the co-repressor that keeps Notch signaling inactive and recruits other cellular proteins such as MAML1, p300, and other co-activators, forming a

Notch initiation complex thus activating Notch responsive genes such as *HES1* [6, 117, 118] (***Figure 6***).

The dysregulation of Notch signaling has been observed in cancers [119-122], viral infections [123-125], and some other diseases [126-128]. Notch activity has been suggested to be a tumor suppressor in SCC due to the observable loss of functions mutation in the Notch pathway [129, 130]. This suppressive effect in the context of keratinocytes is suggested to be due to the induced differentiation that inhibits cell proliferation and activation of keratinocyte growth arrest [131].

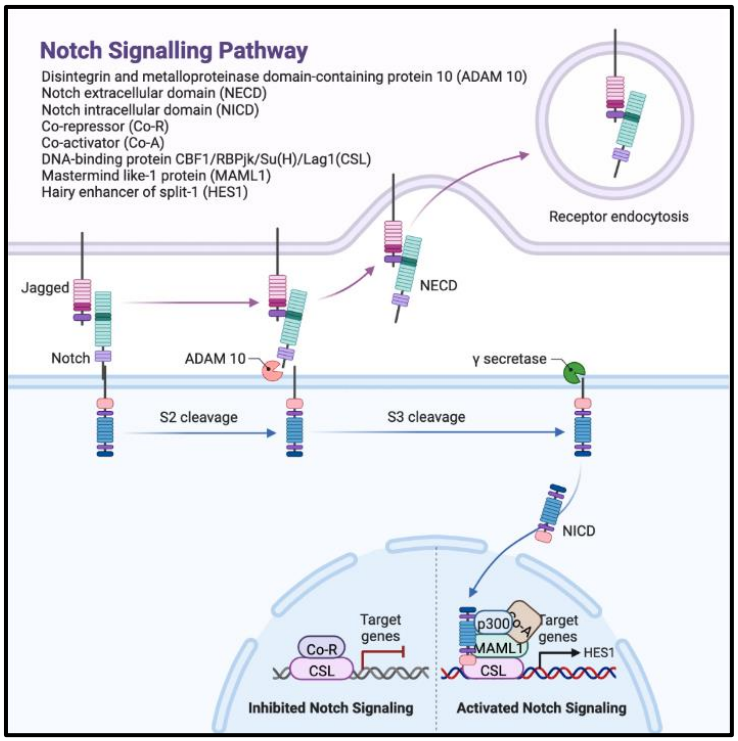

Figure 6 Scheme of the Notch signaling pathway. The binding of Jagged from neighboring cells to the Notch receptor initiates the cleavage at the S2 cleavage site by ADAM 10 protease, releasing Notch extracellular domain (NECD) for receptor endocytosis. Gamma-secretase cleaves Notch intracellular domain (NICD) at the S3 cleavage site, followed by the translocation of NICD into the nucleus. NICD binds CSL and recruits MAML1, p300, and other co-activators to activate the expression of the Notch target gene, *HES1*. *Adapted from* [6].

2 Objectives

This thesis investigates the cellular and intraviral interaction partners of the carcinogenic E6 protein from papillomaviruses.

The first part of this thesis focuses on the cellular targets of the CRPV E6 protein. The molecular mechanism of cutaneous beta HPV-induced tumorigenesis remains understudied due to the lack of suitable animal models. Notch signaling is crucial in determining cell fate and differentiation [116]. MAML1 is one of the essential components of the Notch initiation complex [117]. It consists of an LxxLL motif at its C-terminus. This motif is known to be targeted by the E6 proteins of beta HPV8 and HPV38, animal BPV1, and MmuPV1, subsequently downregulating the Notch signaling [54-56] thus impairing cell differentiation. However, the interaction between CRPV E6 and MAML1 remains unclear. Hence, this thesis aims to investigate the interaction between MAML1 and CRPV E6 using co-immunoprecipitation and flow cytometry-FRET assay (FACS-FRET). Besides, we aim to study the effect of CRPV E6 on Notch signaling using a novel triple fluorescence reporter assay in order to address the possibility of CRPV as a suitable animal model to study beta HPV-associated cancers.

In the second part, we investigate the intraviral target of HPV E6 protein, mainly on its interaction with E7 carcinogenic protein. This interaction has not been described in the literature so far. The interaction between E6 and E7 of HPV16 in previous cell-based experiments was unclear due to the non-specific signal observed in the control samples. Furthermore, the binding affinity obtained for HPV31 using the final optimized assay condition was incomplete. Hence, in this thesis, we aim to further optimize the co-immunoprecipitation protocol to verify the interaction between HPV16 E6 and E7 proteins. Besides that, we sought to screen the E6 and E7 interaction in various HPV types using FACS-FRET to verify the results obtained from GPCA. Next, we intend to characterize the HPV16 and HPV31 E6/E7 complex with purified recombinant proteins by applying analytical ultracentrifugation and fluorescence polarization to determine the stoichiometric and binding affinity of the complex, respectively.

3 Results and Discussion

3.1 Part I: Cottontail rabbit papillomavirus E6 proteins interact with MAML1 and downregulate the Notch signaling pathway in rabbit keratinocytes

3.1.1 Interaction between CRPV E6 and MAML1

Lim, J., Frecot, D. I., Stubenrauch, F., Iftner, T., & Simon, C. (2022). Cottontail rabbit papillomavirus E6 proteins: Interaction with MAML1 and modulation of the Notch signaling pathway. Virology, 576, 52–60.

3.1.1.1 In silico analysis of CRPV E6 Protein and the Putative Interaction with MAML1

The mechanism of the carcinogenesis specific with cutaneous beta HPV is not well understood due to the shortage of suitable animal models. CRPV has been an excellent animal model for studying the biology of HPV as mentioned in Section 1.9. CRPV E6 protein is unique from E6 of other PVs as it encodes an elongated E6 protein, with its N-terminus conserved to other E6 proteins, while the C-terminus tail is not conserved to any other protein. In addition, it encodes an N-terminus truncated E6, SE6. Hence, we sought to determine if CRPV E6 can interact with MAML1 and interfere with the Notch signaling pathway.

First, we aligned the conserved region of CRPV LE6 (N-terminus) to other E6 protein sequences to identify the sequence identity, followed by a comparison to the E6 sequences of i) animal PV BPV1 and MmuPV1 due to their known association to MAML1, ii) alpha HPV16 and 31, focusing on the amino acid residues that bind E6AP iii) beta HPV5 and HPV8, focusing on the amino acid residues that bind MAML1. Furthermore, we compared the amino acid residues at position ±3 of the E6AP LxxLL motif and hMAML1 LxxLL motif to the rMAML1 LxxLL motif as they are crucial for their interaction with E6.

The pairwise sequence alignment of BPV1 E6, MmuPV1 E6, and the N-terminus of CRPV E6 to the different human PV E6 proteins revealed a similar sequence identity percentage [7]. They share the crucial CxxC motifs mentioned in Section 1.9 and Section 1.5. The critical amino acid residue R102 in HPV16 E6, which bridges the E6N and E6C, is conserved among all HPV E6 [5] and with CRPV E6 [7]. As for the amino

acid residues that bind to the E6AP LxxLL motif, HPV16 E6 L50 is not only conserved among HPV E6 but also in CRPV LE6 [7]. Regarding MAML1 binding, residue K64 in beta HPV8 E6 is crucial [56] and is shown as WHK in CRPV E6 (51/52/53) and as R55 in alpha HPV16 E6 and HPV31E6 [7]. It is known that R55 binds to the negatively charged E3 of the LxxLL motif of the E6AP. The positively charged K64 and protonated H52 may allow their association with the negatively charged D3 to the MAML1 LxxLL motif. The K142 in HPV8 E6 is another critical residue that binds MAML1 [56] and is conserved in all beta HPV as WHK. It is conserved in CRPV E6 as WRG (W+G) [7].

The alignment of the amino acid residues at position ±3 of the MAML1 LxxLL motifs showed that these amino acids are highly conserved in hMAML1 (MSD**L**DD**LL**GSQ) and rMAML1 (MND**L**DD**LL**GSQ). The negatively charged E3 of the LxxLL motif from E6AP (ELT**L**QE**LL**GEE) that binds alpha HPV E6 [5, 132] corresponds to the negatively charged D3 in the LxxLL motif of hMAML1 and rMAML1. The asparagine (N) in rMAML1 is shown as serine (S) in hMAML1, but it is conserved in canine (MND**L**DD**LL**GPQ) and murine (INE**L**DD**LL**GSQ) MAML1, which is known to bind to CPV2 and MnPV1 E6 proteins [133].
Hence, with these results, we postulate an association between CRPV LE6 and MAML1 as it shares the primary structure required for the common two-domain E6N and E6C of E6 proteins in the N-terminus and further retains the essential amino acids for the interaction with MAML1 LxxLL motif.

3.1.1.2 CRPV E6 Association with hMAML1 in Cell-based Assays

To study the interaction between CRPV LE6 and CRPV SE6 with MAML1, we performed HA co-immunoprecipitation with FLAG-HA-E6 proteins to co-immunoprecipitate hMAML1 in the HPV-negative cervix cell line, C33A which is the most commonly used cell line in HPV research. A mutation of M98S was introduced into the CRPV LE6 to avoid the expression of CRPV SE6 from M98. Hence, we co-transfected C33A cells with FLAG-HA-E6 and pHAGE-V5-hMAML1 full-length (FL) (1-1016). We showed the interaction between HPV5 E6 and full-length hMAML1 (1-1016). HPV5 E6 belongs to the same species as HPV8 E6 whose association with MAML1 has been shown several times [54-56, 133]. This interaction was also shown clearly for CRPV LE6M98S, whereas CRPV SE6 showed only a faint signal of MAML1 in the pull-down (***Figure 7A***). It is known that cutaneous beta HPV8 E6 bind to MAML1

predominantly via the LxxLL motif [55, 56]. Thus, we repeated the experiment by substituting pHAGE-V5-MAML1 FL (1-1016) with pHAGE-V5-MAML1 dLxxLL (1-990), in which the C-terminus acidic domain of MAML1 (DLIDSLLKNRTSEEWMSD**L**DD**LL**GSQ) was deleted. Notably, hMAML1-dLxxLL was co-immunoprecipitated with HPV5 E6 and CRPV LE6M98S but not CRPV SE6 (***Figure 7B***). These results indicate that CRPV LE6M98S can interact with hMAML1 while CRPV SE6 can only interact weakly. The interactions between HPV5 E6 and CRPV E6 are not limited to the LxxLL motif. It is plausible that another domain in hMAML1 may participate in this interaction.

Next, to further verify the interaction, we co-transfected C33A cells with different variants of EYFP-hMAML1 and various types of mTagBFP2-E6 to screen the interaction with FACS-FRET. For FRET to occur, the excited donor fluorophore needs to transfer the energy to an acceptor fluorophore that comes into close proximity, thus resulting in an enhanced fluorescence emission of acceptor [134]. There are three criteria that need to be met for this phenomenon, which include i) the emission spectra of the donor fluorophore have to overlap with the excitation spectra of the acceptor fluorophore; ii) the distance between the donor and acceptor must be within the Förster radius of less than 10 nm; and iii) the donor and acceptor fluorophores are in the same orientation, as reviewed in [135]. Hence, with proper gating, as described in [136] , a positive FRET signal indicates an interaction has occurred. Briefly, we first gated the living cells with the forward and sideward scatter. Next, the compensation of EYFP-hMAML1 or mTagBFP2-E6 expressing cells and the double positive cells exhibiting FRET signals were examined explicitly by adjusting the photomultiplier tube (PMT) voltages. As a control, the combination of mTagBFP2 + EYFP-hMAML1s and EYFP + mTagBFP2-E6s were included to gate out false positive FRET cell population as EYFP exhibits some emission in the FRET channel when it is excited at 405 nm. A genetic fusion of mTagBFP2-EYFP is employed as a positive control to gate for the positive FRET signals. The beta HPV5 and HPV8 E6 are the biological positive controls. The different MAML1 variants included in the analysis are: i) full-length MAML1 (hMAML1 FL 1-1016), ii) a variant resembles the LxxLL motif of rMAML1 (hMAML1 FL S1007N), iii) C-terminal truncated hMAML1 (hMAML1 1-990), iv) N-terminal truncated hMAML1 (hMAML1 759-1016), and v) N-terminal and C-terminal truncated hMAML1 (hMAML1 759-990).

As a result, FACS-FRET analysis showed no interaction in the control samples. CRPV LE6M98S interacts with hMAML1 1-1016 as reported for beta HPV8, animal BPV1, and MmuPV1 [54-56]. Besides, CRPV LE6M98S interacts with hMAML1 1-990 as opposed to HPV5 and HPV8 E6, which showed lower % FRET with hMAML1 1-990. This result indicates that the MAML1 N-terminus may interact with CRPV E6, and the interaction is not limited to the LxxLL motifs. HPV5 E6 and HPV8 E6 interact with hMAML1 759-1016 but do not interact with hMAML1 759-990, indicating the involvement of LxxLL motifs in the interaction (***Figure 7C***). In contrast, the interaction seems to be lost in both hMAML1 759-1016 and hMAML1 759-990 for CRPV E6. These results again suggest that the binding of CRPV LE6M98S to MAML1 may depend on the N-terminus of MAML1. All tested E6s show interaction with hMAML1 S1007N that resembles the LxxLL motif of rMAML1 (***Figure 7C***). This result implies a potential binding of all tested E6s to rMAML1. None of the E6 interacts with hMAML1 759-990. CRPV SE6 binding to MAML1 is unclear due to the low FRET positive cells of <500 that is below the statistically relevant cell population threshold. Notably, the FRET signals between the different E6 and MAML1 variants are not comparable due to the different expression levels of E6 and MAML1 variants [7]. Thus, only qualitative evaluation could be applied here.

Taken together, it is clear from the co-immunoprecipitation and FACS-FRET analysis that the CRPV LE6M98S is binding to hMAML1, while the interaction of CRPV SE6 remains elusive. The binding of CRPV LE6M98S does not seem to be LxxLL dependent as compared to HPV5 and HPV8 E6 but rather depends on the hMAML1 N-terminus. The hMAML1-FL S1007N reduced the binding to HPV5 and HPV8 E6 but did not affect the binding of CRPV LE6M98S. The E6 proteins of different papillomaviruses may not always interact with the same cellular proteins in the same way. It has recently been shown that the E6 proteins of several types of HPV and animal PV employ different association mechanisms with E6AP. These interactions are divided into two groups, Type I interaction and Type II interaction [137]. E6 proteins that interact directly with the LxxLL motif of E6AP to recruit p53 tumor suppressor are grouped in the Type I interaction [137]. Type II interaction includes E6 proteins from HPV types that require either the N-terminus or C-terminus HECT (Homologous to the E6AP carboxyl terminus) domain of E6AP for the binding [137]. Hence, we postulate

that CRPV E6 may employ a different mechanism than beta HPV, animal BPV1, and MmuPV1 in binding to MAML1.

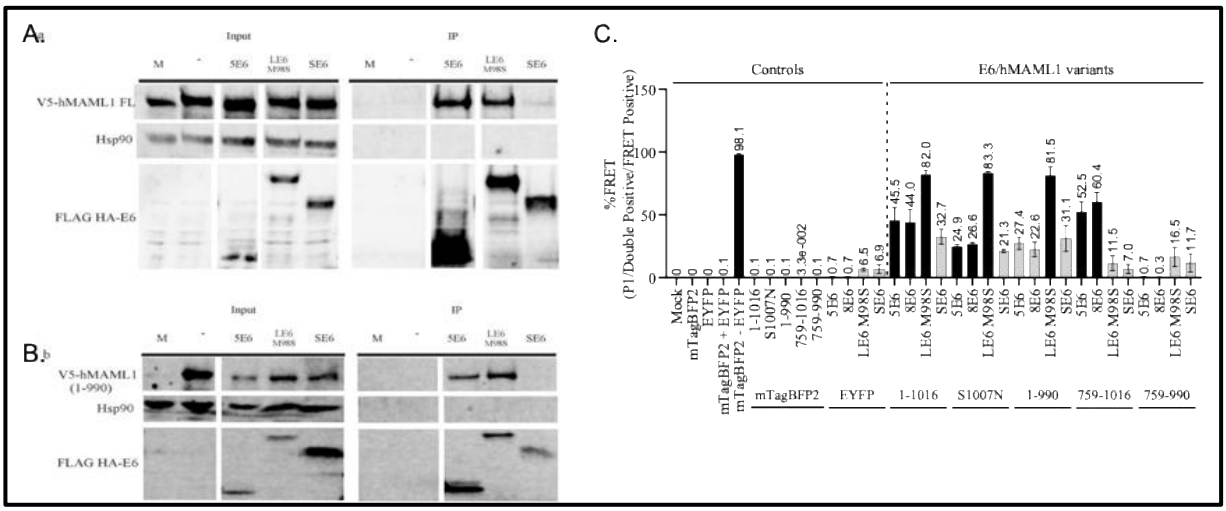

Figure 7 CRPV E6 interacts with hMAML1. The HA co-immunoprecipitation shows HPV5 E6 and CRPV LE6M98S pull down **A.** hMAML1 1-1016 and **B.** hMAML1 1-990. CRPV SE6 only co-immunoprecipitated hMAML1 1-1016 weakly but not hMAML1 1-990. **C**. HPV 5 and 8 E6 bind hMAML1 1-1016, S1007N, 1-990 and 759-1016 while CRPV LE6M98S showed only positive FRET signal with hMAML1 1-1016, S1007N and 1-990. CRPV SE6 did not fulfill the threshold that concludes a positive FRET signal. No FRET was observed for all E6s with hMAML1 759-990. Samples with cell numbers lower than 500 are in grey and are considered as negative FRET. In contrast, the black bar with more than 500 FRET positive cells and % FRET > 10 % are positive, indicating an observed interaction. *Adapted from* [7].

3.1.2 A Novel Triple Fluorescence Flow Cytometry-Based Assay Shows CRPV E6 Represses Notch Signaling in A Species-Specific Manner

3.1.2.1 The Establishment of a Triple Fluorescence Flow Cytometry-Based Assay

Lim, J., Straub, E., Stubenrauch, F., Iftner, T., Schindler, M., & Simon, C. (2022). An enhanced triple fluorescence flow-cytometry-based assay shows differential activation of the Notch signaling pathway by human papillomavirus E6 proteins. Scientific Reports, 12(1), 1–13.

The E6 proteins of beta HPV8, HPV38, MmuPV1, and BPV1 repressed the Notch responsive gene *HES1* via their association with the LxxLL motif of MAML1 [54-56]. Hence, we would like to investigate the influence of CRPV LE6 on Notch signaling, focusing downstream of the gamma-secretase cleavage, in which the Notch intracellular domain translocates to the nucleus forming a Notch initiation complex with other cellular proteins to activate the Notch signaling.

As proof of principle, we explored the effect of E6 on Notch signaling similarly to the studies mentioned above [55] in C33A cells using a dual-luciferase assay by starting with the controls, BPV1 E6 and HPV5 E6 that are known to downregulate Notch-responsive *HES1* genes [54, 55]. Unfortunately, a repression activity by BPV1 E6 and HPV5 E6 was not seen (***Appendix 1***). The advantage of the dual-luciferase assay is that it allows the examination of the promotor activity coupled with the variations in the transfection efficiency. However, there are some drawbacks of this assay: i) the necessity to lyse the cells for the measurement, but the variation in lysis efficiency could not be accounted for; and ii) the different expression levels of the co-transfected modulatory protein (in this case, the E6 protein) that is affecting the gene of interest (in this case, the *HES1* gene) from experiment to experiment could not be assessed within the assay. Furthermore, the abovementioned limitations could contribute to a high signal-to-noise ratio in the assay, thus interfering with the actual signal.

To overcome these obstacles, we established a triple-fluorescence flow cytometry-based assay to study the effect of CRPV LE6 on the Notch signaling [6]. One of the advantages of fluorescent proteins over luciferases is that it does not require any co-factor or substrate for their fluorescence activity. In addition, this assay does not require the cell lysis step. Instead, it monitors the fluorescence activity in living cells, making it possible to eliminate the variation in the lysis efficiency. Moreover, transfecting the same amount of plasmid DNA does not assure the same expression levels for different proteins or their variants. Every protein is expressed in different amounts, and its turnover rate in cells varies. The intracellular levels of E6 proteins of varying HPV types are different [138]. Therefore, the genetic fusion of fluorescence proteins to the E6 allows for assessing the E6 expression level with an appropriate laser. In contrast to analyze the protein amount of the modulator with a concomitant Western blot analysis, which is offline of promotor activity measurement, this assay allows a direct assessment to compare the effect of the modulator on the activity of the reporter. With proper gating, this assay also evaluates a single cell to eliminate the background from dead and non-transfected cells, allowing only assessment for the triple-positive cells (activator, modulator, reporter).

Hence, we changed the reporter readout from luciferases to fluorescence activity in order to assess *P-HES1* activity with three fluorescent proteins reporting i) the

activator plasmid, NICD, which co-expressed EGFP (hereafter NICD), to examine the transfection efficiency; ii) the modulator (mTagBFP2 fused to the N-terminus of E6, hereafter mTagBFP2-E6); and iii) the promotor activity of *P-HES1* by DsRed2 expression. This allows us to assess living cells that are triple positive (P1/EGFP/mTagBFP2/DsRed2) for EGFP (activator transfected, NICD), mTagBFP2 (modulator, E6), and DsRed2 (*P-HES1* promotor).

To further develop and validate this assay, we used two different cell lines: i) the HPV-negative cervix carcinoma cell line C33A, the cell line chosen for this project, and ii) p53-null lung cancer cell line H1299 (hereafter H1299) to eliminate the effect of p53 in this assay because there is a crosstalk between p53 and the Notch pathway [139, 140]. Inevitably, fluorescent protein excitation and emission spectra could overlap when using more than two fluorescent proteins in an assay. Hence, we examined the background signal of the fluorescent proteins of choice (EGFP, DsRed2, and mTagBFP2). As a result, we showed minimal and compensable crosstalk between the three fluorescence proteins in other channels by applying proper gating and obtaining a background signal of <0.5 % cell population [6]. Furthermore, we transfected both C33A and H1299 cells with *P-HES1*-DsRed2, with or without exogenous NICD, to address the background signal of the endogenous Notch signaling. We showed that the activation follows the expression of the exogenous NICD, as the endogenous NICD cannot activate the Notch signaling to a statistically relevant level [6].

Next, we included alpha HPV (16, 31, 18, 6) and beta HPV (5, 8, 38) E6 for their effect on Notch signaling by co-transfecting C33A and H1299 cells with NICD, mTagBFP2-E6 and *P-HES1*-DsRed2. Then, we applied a triple fluorescence gating strategy by gating viable cells expressing EGFP (activator transfected, NICD) followed by mTagBFP2 (modulator, E6) and finally the DsRed2 (*P-HES1* promotor) to analyze the DsRed2 signal in triple positive cells. We monitored the percent cells (% cell) which is the change in the DsRed2 cell population, and the mean fluorescence intensity (MFI), representing the intracellular level of DsRed2 expression upon *P-HES1* activation. All tested beta HPV E6 repressed DsRed2 in % cells and MFI in both cell types [6]. The repression of the Notch signaling is in line with the reported data [55, 56, 141]. The modulation effects of alpha HPV E6s are highly divergent. HPV16 shows evident activation in both cell types. This result is consistent with the higher levels of Notch

signaling observed in HVP16-positive keratinocytes and high-grade lesions [142-144]. HPV31 and HPV6 E6 activate Notch signaling in both cell types slightly in both % cell and MFI [6]. HPV18 represses the DsRed2 % cell slightly and does not impact the MFI [6].

The protein activity and the protein amount of a modulatory protein impact the gene regulations. We observed different signals for mTagBFP2-E6 for % cells and MFI indicating different intracellular expression levels of the mTagBFP2-E6 from various HPV types [6], consistent with the different intracellular expression levels of various HPV E6 proteins described previously [138]. The amount of E6 proteins may influence gene regulation differently. The higher protein activity and higher protein amount may have an enormous impact. The expression of E6 on protein levels in the native environment during infection or transformation remained unresolved. The assay shown here may not resemble the native environment regarding the amount of NICD, E6, and *P-HES1* promotor. The MFI per cell of a fluorescence protein is principally equivalent to its fluorescent protein per cell. Thus, the MFIs of mTagBFP2 and DsRed2 are equivalent to the amount of mTagBFP2-E6 and DsRed2 (the reporter for *P-HES1* promotor activity), respectively. Hence, we introduced a semi-quantitative analysis by calculating the ratio of normalized MFI of DsRed2 to the MFI of mTagBF2-E6 only in triple positive cells to assess the specific activity of E6 proteins concerning the different E6 expression levels.

We showed in both cell types that beta HPV5 and HPV8, which belong to the beta-1 species, displayed similar repression potential, while HPV38, which belongs to the beta-2 species, showed higher repression potential. These results indicate an association between function and phylogeny. For alpha HPV, HPV16 showed evident activation in C33A cells, while HPV31, HPV18, and HPV6 showed no significant impact on Notch signaling. In H1299 cells, the activation of alpha high-risk HPV31 is similar to that of alpha high-risk HPV16 and much more potent than low-risk HPV6. HPV16 and HPV31 belong to alpha-9. It remains unclear why the activity of HPV16 is similar in both cell types, while HPV31 seems to be more potent in H1299 cells. One major difference between the two cell types is the presence of p53. Hence, we speculate that the different activity observed for HPV31 in C33A and H1299 may be related to its lower potential in interacting and degrading p53. Surprisingly, HPV18, the

second most carcinogenic HPV type, does not show significant impact on Notch signaling in both cell types. Notably, this assay focused only on the *P-HES1* promotor downstream of the Notch signaling pathway. The effect of HPV18 on Notch signaling remains undiscovered, to our knowledge. Other than Notch signaling, there are many other alternatives to dysregulate cell proliferation and differentiation. Thus, we postulate that HPV18 E6 may employ a different mechanism in interfering with the cell proliferation and differentiation.

In summary, with a Notch-responsive fluorescence reporter plasmid, we showed that the established triple fluorescence flow-cytometry-based assay is an appropriate approach to studying the effect of exogenous proteins on the Notch signaling pathway. This assay also allows a semi-quantitative comparison of the activity of the modulator. We validated the assay by showing the repression of Notch signaling by E6 of beta-1 (HPV5 and HPV8) and beta-2 (HPV38), as reported previously [54-56]. HPV38 E6 is the most potent repressor among the tested beta HPV. Additionally, the activation effect of E6 proteins of alpha-9 (HPV16 and HPV31) and alpha-10 (HPV6) on Notch signaling, especially in H1299 cells on Notch signaling provides new insights into the function of E6 proteins from a phylogenetic perspective.

3.1.2.2 The Repression of Notch Signaling by CRPV E6 in Rabbit Keratinocytes

Lim, J., Frecot, D. I., Stubenrauch, F., Iftner, T., & Simon, C. (2022). Cottontail rabbit papillomavirus E6 proteins: Interaction with MAML1 and modulation of the Notch signaling pathway. Virology, 576, 52–60.

We used C33A cells and immortalized rabbit keratinocytes (hereafter RK1) to study the modulation effect of CRPV LE6M98S on Notch signaling. In addition, we employed E6 of HPV5 and HPV8 as positive controls. First, we co-transfected NICD, mTagBFP2-E6, and the *P-HES1*-DsRed2 in C33A and RK1 cells. Then, we applied the established triple fluorescence gating strategy (P1/EGFP/mTagBFP2/DsRed2) as described above to assess the activity of the *P-HES1* promotor with % DsRed2 cell population. The beta HPV5 and HPV8 E6 proteins showed a significant decrease in DsRed2 % cell populations in both cell types indicating inhibition of Notch signaling, which is in line with the reported data [55, 56]. However, CRPV LE6M98S interfered

differently with the Notch-responsive *HES1* gene in the two cell types. In C33A cells, both CRPV LE6M98S and CRPV SE6 show no changes in the % cell population. In RK1, CRPV LE6M98S significantly repressed the *P-HES1* promotor activity, leading to a lower % cell population similar to HPV5 and HPV8 E6.

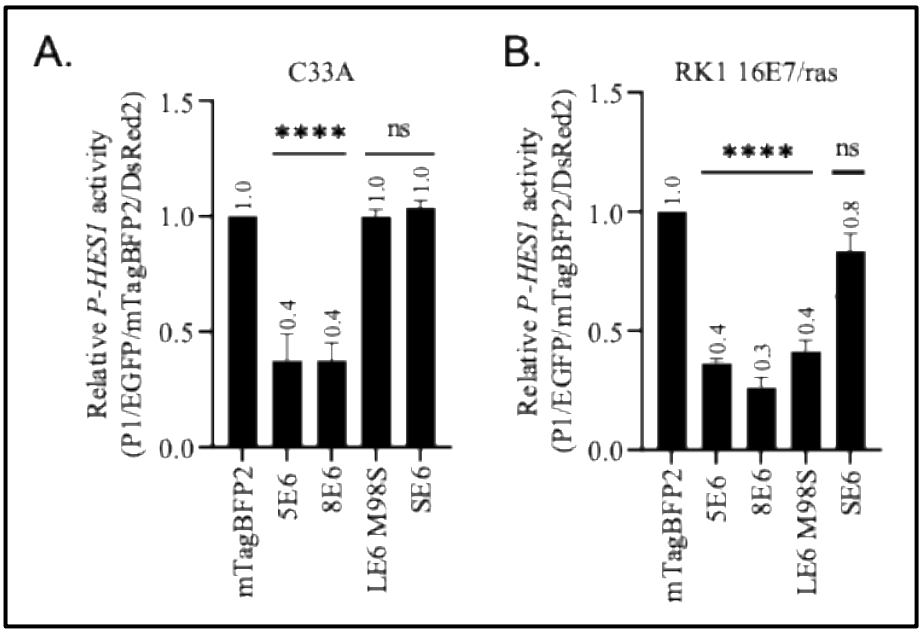

Figure 8 CRPV E6 inhibits Notch signaling in rabbit keratinocytes. Viable cells co-expressing Notch activator (NICD) with EGFP, mTagBFP2-E6, and *P-HES1*-DsRed2 are triple gated (P1/EGFP/mTagBFP2/DsRed2) as described. HPV5 and HPV8 E6 repressed Notch signaling in C33A and rabbit keratinocytes. CRPV LE6M98S inhibits Notch signaling significantly, while CRPV SE6 weakly inhibits it only in rabbit keratinocytes. Data were derived from three independent biological replicates with the mean value plotted and labeled on top of each bar. The error bars are the standard deviation of the mean value. P values were calculated using One-Way ANOVA with Fischer's LSD test by comparing the mean value of each sample to the control sample, where **** = P≤0.0001, ns = P>0.05. *Adapted from* [7].

As mentioned earlier, the expression of different E6 proteins varies, which may impact their activity on gene regulation. Notably, by applying the semi-quantitative analysis as described in *Section 3.1.2.1*, we revealed a similar Notch repression activity by CRPV LE6M98S compared to beta HPV5 and HPV8 E6 in RK1 (***Figure 9A***), despite a 2-fold lower *P-HES1* repression activity shown with the MFI of the DsRed2 (***Figure 9B***). The lower MFI repression is due to the marginal 2-fold lower MFI of mTagBFP2 for CRPV LE6M98S in the triple-positive cells (***Figure 9C***) compared to beta HPV5 and HPV8 E6, indicating a lower intracellular expression of mTagBFP2-LE6, which in turn, shows a lower repression activity.

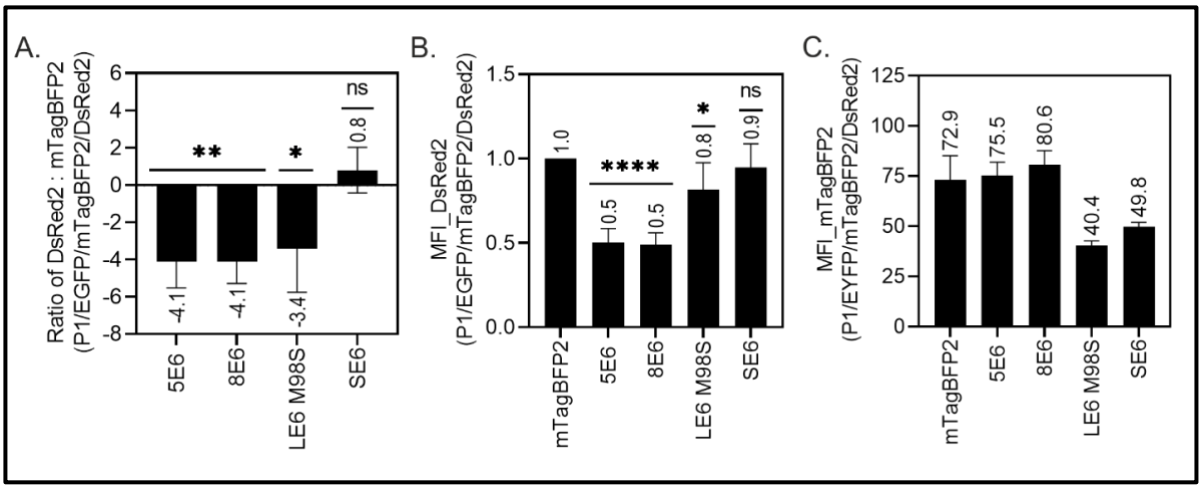

Figure 9 CRPV E6 Notch inhibition with regard to its intracellular expression level in rabbit keratinocytes. A. Ratio of MFI of DsRed2 and mTagBFP2 showed similar repression activity of CRPV LE6M98S compared to beta HPV5 and HPV8 E6 in rabbit keratinocytes. B. Viable cells co-expressing Notch activator (NICD) with EGFP, mTagBFP2-E6, and *P-HES1*-DsRed2 are triple gated (P1/EGFP/mTagBFP2/DsRed2) as described to assess the MFI of DsRed2 in response to *P-HES1* promotor activity. HPV5, HPV8 E6, and CRPV LE6M98S repressed Notch in rabbit keratinocytes. CRPV SE6 weakly inhibits Notch in rabbit keratinocytes. C. Intracellular expression level of E6 in triple-positive cells. CRPV LE6M98S and CRPV SE6 showed about 2-fold lower expression levels than beta HPV5 and HPV8 E6 proteins. This explained the higher MFI signal seen in B. Data were derived from three independent biological replicates with the mean value plotted and labeled on top of each bar. The error bars are the standard deviation of the mean value. P values were calculated using One-Way ANOVA with Fischer's LSD test by comparing the mean value of each sample to the control sample, where **** = P≤0.0001, ** = P≤0.01, * = P≤0.05, ns = P>0.05. [Unpublished data].

In short, CRPV LE6M98S repressed the Notch signaling pathways in rabbit keratinocytes but not in human C33A cells at a comparable levels as shown for beta HPV E6. However, CRPV SE6 do not show a significant effect on Notch signaling. These results indicate that the repression of CRPV LE6M98S on Notch signaling could be species-specific. Indeed, CRPV E6 is known to have another species-specific function: it can only immortalize rabbit keratinocytes but not human keratinocytes [145]. Several different cellular proteins have been found in forming the Notch initiation complex to initiate the transcription of Notch target genes. These include MAML1, CSL, p300, and other co-activators. It is known that CRPV LE6 can immortalize keratinocytes and induce tumorigenesis by inhibiting p53-mediated apoptosis through their association with p300 [146]. Therefore, the Notch inhibition that CRPV E6 mediates may not be limited to its association with MAML1 but may also be the p300 or other not-yet-defined cellular targets. Nonetheless, CRPV E6 can repress the Notch signaling, which is observed to be species-specific. Hence, CRPV E6 remains a promising model for studying further beta-HPV-associated carcinogenesis.

3.2 Part II: Human Papillomavirus E6 Proteins: Interaction with E7 Proteins and The Complex Characterization

Lim, J., Iftner, T., & Simon, C. (2021). Native Isolation of 3×HA-Tagged Protein Complexes to Characterize Protein-Protein Interactions. *Current Protocols*, *1*(2), 1–20.

Lim, J., Lilie, H., Kalbacher, H., Roos., N, Frecot, D. I., Feige. M., Conrady, M., Votteler, T., Cousido-Siah, A., Corradini Bartoli, G., Iftner, T., Trave, G., & Simon, C. Evidence for direct interaction between the oncogenic proteins E6 and E7 of high-risk human papillomavirus (HPV). J Biol Chem, 2023. **299**(8): p. 104954.

*I contributed to 80% of this work.

3.2.1 Interactions Between E6 and E7 Proteins in The Cell-Based Assay

To investigate the interaction between E6 and E7, we screened the E6 and E7 of various HPV types through FACS-FRET assay, including alpha high-risk HPV16, HPV31, HPV18, alpha low-risk HPV6, and beta HPV38 in C33A cells. To do this, we fused EYFP to the N-terminus of E7 and fused mTagBFP2 to the N-terminus of E6. The negative controls mTagBFP2-E6 + EYFP and mTagBFP2 + EYP-E7 were included in the analysis. No non-specific signals were detected with these controls. We observed interaction between E6 and E7 of alpha high-risk HPV16, HPV31, HPV18, and beta HPV38 (***Figure 10A***). As mentioned in *Section 3.1.1.2*, a comparison of the % FRET signal should be avoided because expression levels of mTagBFP2-E6 and EYFP-E7 vary. Notably, HPV6 E6 did not meet the threshold of at least 10 % of the FRET signal and at least 500 FRET-positive cells despite a significant % FRET signal to conclude an observed interaction. The low FRET is due to the extremely low expression of mTagBFP2-6E6.

To further verify the results, we carried out co-immunoprecipitation. Previously in my Master thesis, I investigated the interaction between E6 and E7 of HPV16 and HPV31 using N-terminally 3xHA tagged E7 (bait) and N-terminally mTagBFP2 tagged E6 (prey). However, the non-specific binding of mTagBFP2 and mTagBFP2-E6 to the HA antibodies as well as the high non-specific background from the antibodies have made the analysis difficult. It was impossible to conduct the co-immunoprecipitation with untagged E6 due to the absence of suitable anti-16E6 antibodies at that time. Later,

Arbor Vita Corporation generously provided anti-16E6 and anti-31E6 antibodies for this project, allowing us to conduct co-immunoprecipitation for untagged E6 with 3xHA-E7.

We co-transfected 3xHA-16E7 and 16E6 in C33A cells, followed by HA co-immunoprecipitation. As expected, we detected a non-specific signal in the control sample when 16E6 was transfected alone in C33A cells in the IP. To circumvent this, we developed a protocol utilizing a 3xHA peptide to perform competitive elution of 3xHA-tagged proteins and their interactors [147]. The 3xHA peptide allows 3xHA-tagged proteins to elute in their native form with their complexes while leaving any proteins that bound non-specifically to the matrix as well as the Co-IP antibodies to retain. We systematically tested the elution temperature, kinetic, and concentration of the 3xHA peptides to determine the optimal elution conditions, as described in [147]. Finally, considering protein stability, protein degradation, and aggregation issues with the optimal condition tested, we decided to elute the 3xHA-16E7 protein complex after overnight incubation with 250 µM 3xHA peptide at 4 °C followed by Western blotting to check for 3xHA-16E7 and untagged 16E6 signals in the pull-down. The non-specific signal of 16E6 was eliminated, and 16E6 was detected in the native pull-down when it was co-transfected with 3xHA-16E7, indicating an interaction (***Figure 10B***). Next, we conducted CoIP also with 3xHA-31E7 and untagged 31E6. Since no non-specific signal of 31E6 to the antibodies was detected, the proteins were eluted in denaturing condition with pre-heated 1xSDS sample buffer. The 31E6 was seen clearly precipitated by the 3xHA-31E7 (***Figure 10C***). This result indicates that 31E7 interacts with 31E6.

In short, based on the FACS-FRET and co-immunoprecipitation, the interactions between E6 and E7 proteins of HPV16 and HPV31 were confirmed. We have seen the same interaction in HPV18 and HPV38 with FACS-FRET, but it remains elusive for HPV6. These results agree with the GPCA performed by Marcel Conrady in his master thesis, where he showed interactions between E6 and E7 for HPV16, HPV31, and HPV18. The interaction in alpha low-risk HPV6 needs to be examined and validated further.

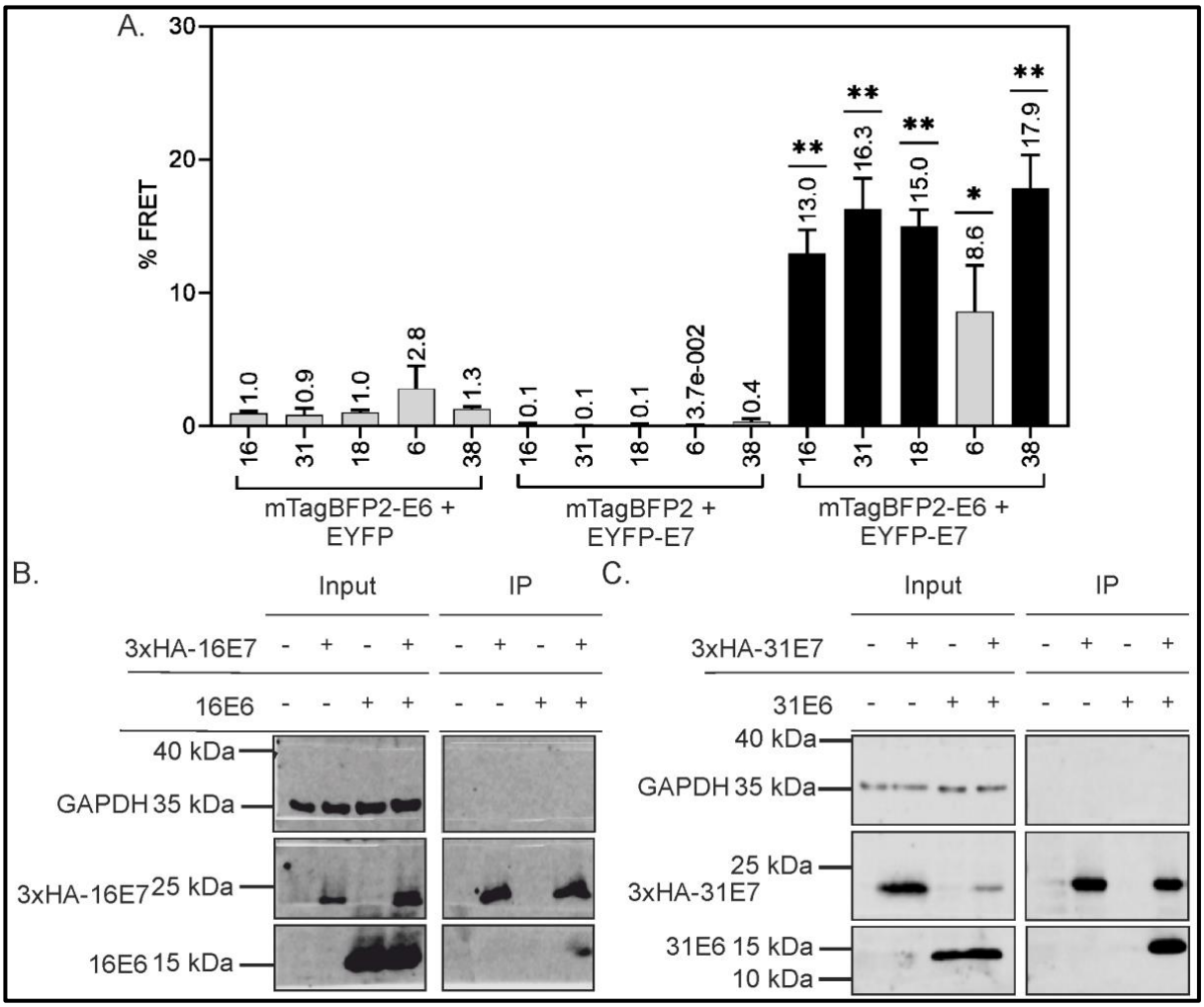

Figure 10 Interaction between E6 and E7 in cell-based assay. A. FACS-FRET assays showed interaction between E6 and E7 of HPV16, HPV31, HPV18 and HPV38. HPV6 E6 and E7 show % FRET that is below the threshold, hence an interaction was not concluded. **B. & C.** Co-IP showed untagged E6 of HPV16 (**B**) and HPV31 (**C**) were pulled down by 3xHA-16E7 and 3xHA-31E7, respectively. Adapted from [2].

3.2.2 Characterization of HPV16 And HPV31 E6/E7 Complexes

To further characterize the E6/E7 complex, we moved on to determine the stoichiometry of the complex through analytical ultracentrifugation and quantify the binding through fluorescence polarization. We conducted these experiments using recombinant proteins expressed in *Escherichia coli* (*E. coli*) and purified them as described briefly below.

3.2.2.1 Production and Purification of MBP-E6-LxxLL / MBP-16E6_4C4S

HPV E6 protein exerts solubility and stability issues [3]. Hence, all E6 were cloned into the pETxM1 vector with maltose binding protein (MBP) fused to the N-terminus to increase solubility and allow MBP affinity chromatography. In addition, E6 is a

cysteine-rich protein that prone to aggregation due to the formation of disulfide bridges. Therefore, we introduced mutations to all the non-conserved surfaced exposed cysteines (C80S, C97S, C111S, C140S for 16E6) and (C97S, C111S for 31E6) to reduce the risk of oxidation and aggregation. The LxxLL motif of E6AP alone is sufficient in binding and stabilizing high-risk E6 proteins [5, 45, 148, 149]. Thus, to increase the stability of E6 proteins, the LxxLL motif sequence of E6AP (ESSELTLQELLGEER) was fused to the C-terminus of E6, mimicking the partial binding to E6AP. For the following experiment, it is crucial to know if the LxxLL motif plays a role in the interaction. Thus, the E6 of HPV16, the most carcinogenic HPV and the main focus of this part of the thesis, was cloned with and without the LxxLL motif sequences. We expressed all E6 proteins from *E. coli BL21(DE3)* in Terrific Broth (TB) media in a flask overnight at 16 °C, selected with 30 µg/mL kanamycin, and induced with 1 mM Isopropyl β- d-1-thiogalactopyranoside (IPTG) and 100 µM zinc chloride ($ZnCl_2$) as described [5]. The expression growth curves and the corresponding reducing SDS-PAGE can be found in ***Appendix 2*** - ***Appendix 3*****.**

For purification of E6 proteins, the crude lysates were subjected to MBP affinity chromatography (a self-packed amylose column) followed by overnight ultracentrifugation (UC) at 25, 000 rpm at 4 °C with an SW28 rotor to remove the large molecular weight oligomers. The supernatants of all E6 proteins were concentrated, and 4 mL of 15 – 20 mg/mL E6 proteins were loaded onto a HiLoad 16/600 Superdex 200pg column to separate the monomers from oligomers. All purified E6 proteins showed a pre-dominant peak for monomers at ~85.5 mL except MBP-16E6_4C4S at ~86.5 mL due to its slightly smaller size (***Figure 11***). Different oligomeric species are present during purification and this phenomenon has been described previously [150]. However, MBP-16E6_4C4SF47R-LxxLL show a higher oligomeric species ratio than other E6 proteins, probably due to the lower centrifugal force applied overnight ultracentrifugation, whereby 18, 000 rpm instead of 25, 000 rpm was applied due to technical limitation which may be insufficient to remove most of the agglomerates. Ten micrograms of the proteins were resolved on a reducing SDS-PAGE, and the purity of each protein was determined by densitometry analysis (***Figure 11***). The protein bands that are slightly above 55 kDa are the different E6 proteins as indicated which fit to the theoretical weight of ~60kDa. The impurities that are present could be the degraded product of the respective E6 proteins. It is also possible that these impurities are either

the endogenous MBP of *E. coli* or any other proteins that bound to E6 were co-purified. The detailed expression and purification steps for each E6 protein can be found in (***Appendix 2*** - ***Appendix 7***).

Table 1 Summary of yield and purity of purified E6 proteins.

Protein (monomer)	Yield (per 10 g wet biomass)	Purity
MBP-16E6_4C4S-LxxLL	10 mg	≥ 90 %
MBP-31E6_2C2S-LxxLL	10 mg	≥ 89 %
MBP-16E6_4C4S	20 mg	≥ 95 %
MBP-16E6_4C4SF47R-LxxLL	10 mg	≥ 88 %

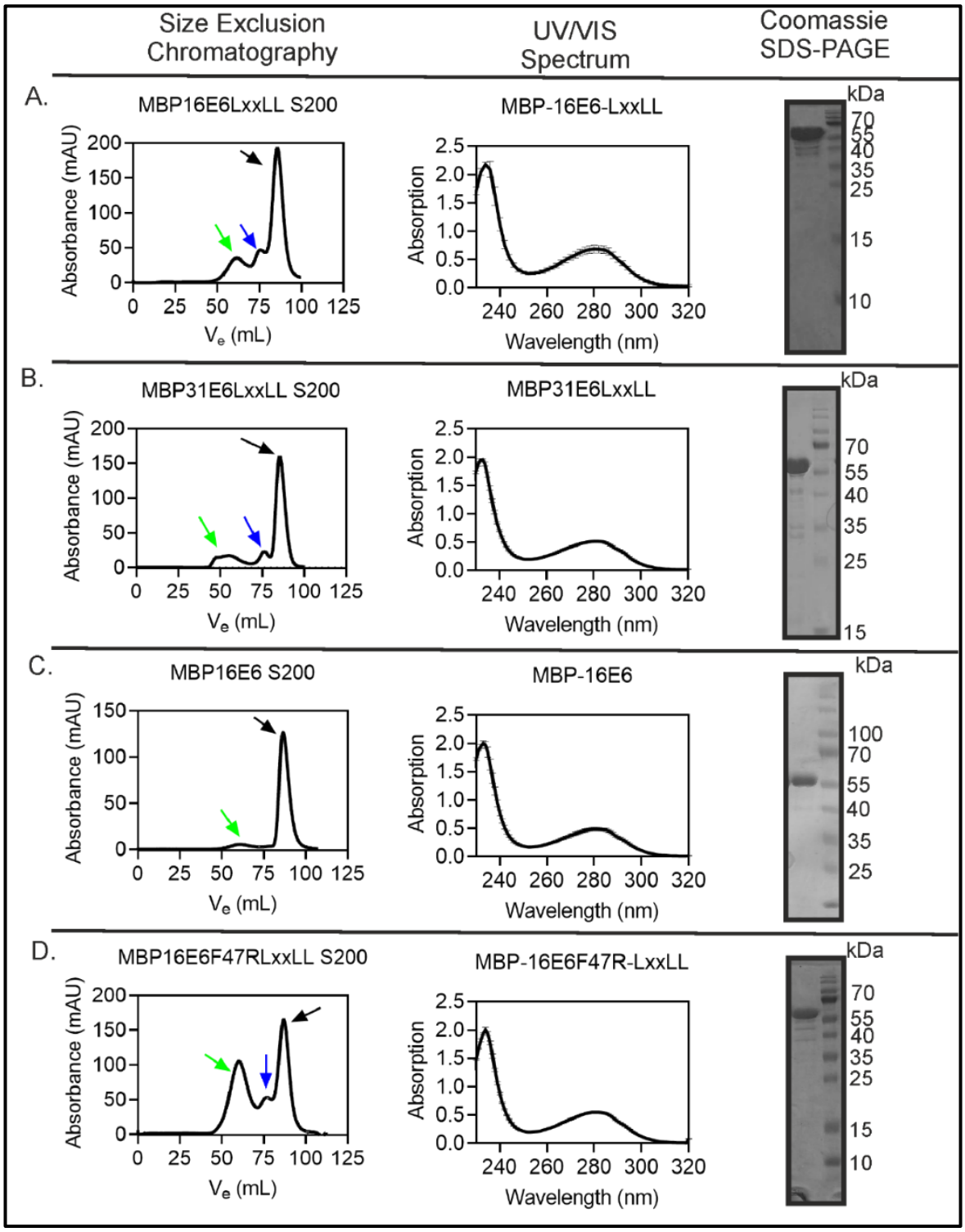

Figure 11 Summary of purified E6 proteins. The first column shows the chromatogram of SEC on HiLoad 16/600 Superdex 200pg columns of **A.** MBP-16E6_4C4S-LxxLL, **B.** MBP-31E6_2C2S-LxxLL, **C.** MBP-16E6_4C4S, and **D.** MBP-16E6_4C4SF47R-LxxLL. Chromatogram of SEC on HiLoad 16/600 Superdex 200pg column shows large molecular weight oligomers (green arrow), dimer species (blue arrow), and monomer species (black arrow). A higher proportion of oligomers that appeared for MBP-16E6_4C4SF47R-LxxLL may be the consequence of the lower centrifugation speed applied due to technical issues, which is insufficient to sediment most of the agglomerates. The second column shows the final UV/VIS spectra of the respective purified E6 proteins at a dilution of 1:150. The data plotted are the mean value and standard deviation of the three technical replicates. The third column shows the Coomassie stained reducing SDS-PAGE of the respective10 µg purified E6 protein.

3.2.2.2 Production and Purification of E7 Proteins from His_6-TEV-GGG-E7

The His_6-tag coupled with a TEV cleavage site (ENLYFQG) downstream was fused to the N-terminus of 16E7 and 31E7. These constructs were expressed from the pET28a(+) vector in *E. coli BL21(DE3)* utilizing a process-controlled fermentation in the bioreactor Labfors 5 overnight at 20°C. The expression was conducted based on an established protocol from our working group [151]. His_6-TEV-GGG-16E7 and His_6-TEV-GGG-31E7 were expressed by Nora Roos, assisted by Maximilian Feige and Desi Frecot, respectively.

The crude lysates were subjected to Ni-NTA affinity chromatography. The large oligomers of E7 proteins were removed by overnight ultracentrifugation at 25,000 rpm or 18, 000 rpm at 4 °C with an SW28 rotor. A lower rotation speed was applied due to technical issues. For His_6-TEV-GGG-31E7, the proteins extracted from NiNTA affinity chromatography were subjected to anion exchange (AEX) to remove impurities. The AEX fractions containing purified E7 proteins were pooled and applied on HiLoad 16/600 Superdex 75pg columns for SEC. Each time, 5 mL of proteins were loaded to separate dimers from the oligomers. In the case of His_6-TEV-GGG-16E7, the supernatant from overnight ultracentrifugation was loaded directly on HiLoad 16/600 Superdex 200pg columns, 5 mL each time. The AEX was omitted due to the high loss to retain a higher yield of E7 proteins. The purified His_6-TEV-GGG-E7 dimers from SEC (elution volume = ~88 mL) were pooled and concentrated in a 3 kDa MWCo spin column to 50 µM for TEV cleavage. The detailed purification steps for each His_6-TEV-GGG-E7 can be found in ***Appendix 8*** and ***Appendix 10***.

3.2.2.3 Purification of GGG-E7 And *Srt A* Labeling of Fl-E7

His_6-TEV protease (2.5 µM) was added to the 50 µM His_6-TEV-GGG-E7 at a molar ratio of 1:20 to cleave the His_6-TEV overnight with gentle stirring in the cold room (4 – 8 °C). The aggregates formed from the cleavage reaction were sedimented by ultracentrifugation (UC) at 25,000 or 18, 000 rpm at 4 °C for 1 hour with an SW28 rotor. The lower speed applied was due to technical limitations. Then, 5 mL of supernatant was loaded each time on the HiLoad 16/600 Superdex 200pg columns coupled with a 1 mL Ni-NTA affinity column upstream to separate His_6-TEV protease from the cleaved E7 proteins. The GGG-E7 dimers (elution volume = ~ 89 mL) were pooled and concentrated in 3 kDa MWCo spin columns. Ten micrograms of the

proteins were resolved on a reducing SDS-PAGE ***Figure 12***, and the purity of each protein was determined by densitometry analysis (***Table 2***). The protein bands that are slightly above the 15 kDa marker band are the GGG-E7. The band which is above the GGG-16E7 in Figure 12A, column 3 could be the remaining non-cleaved His_6-TEV-GGG-16E7.

After TEV cleavage, 5 mg of GGG-E7 has obtained for *Srt A*-based labeling. *Srt A* is a transpeptidase from *Staphylococcus aureus* that mediates the anchoring of the proteins to the cell wall through the recognition of the LPTxG motif [152]. This motif is cleaved after the threonine residues, forming an intermediate thioester coupling to an N-terminal glycine residue of the anchor [152]. The mechanism was employed to label the GGG-E7 as described earlier [153]. Therefore, The GGG-E7 proteins (at molar concentration of 50 µM) were incubated with His_6-*Srt A* (25 µM) at a molar ratio of 1:2, a 2-fold molar excess of fluorescein-LPETGGRR peptide (100 µM) overnight with gentle stirring in the cold room (4 – 8 °C). The co-factors of the *Srt A* reaction were also added (10 mM $CaCl_2$ and 5 mM $MgCl_2$). *Srt A* cleaves the fluorescein peptide after the first glycine residues and ligates the peptide to the glycine residue at the N-terminus of E7. After labeling incubation, the proteins were centrifuged at 18, 000 rpm at 4 °C for 1 hour with an SW28 rotor to remove any aggregates. Then, 5 mL of supernatant was loaded on the HiLoad 16/600 Superdex 200pg columns coupled with a Ni-NTA affinity column upstream to separate His_6-*Srt A* from the fl-E7 proteins. Notably, for GGG-16E7, GGG-31E7 and fl-31E7, the pre-dominant peak of ~88.0 mL (***Figure 12***) corresponds to the molecular weight of a tetramer based on the column calibration analysis template from our group. This phenomenon was observed previously and has been proven with multiangle light scattering that the hydrodynamic radius of the 22 kDa dimer is comparable to the hydrodynamic radius of the 44 kDa globular protein [61]. Hence, it is proposed that such behavior of E7 is due to a rather extended than globular conformation of E7 dimer. The fl-E7 proteins were pooled and concentrated in 3 kDa MWCo spin columns. Finally, fl-16E7 showed a degree of labeling (DoL) of 11 % and fl-31E7 of 36 % (***Table 2***), calculated based on the UV/VIS spectrum with the signal at 280 nm and 495 nm. Ten micrograms of the proteins were resolved on a reducing SDS-PAGE (***Figure 12***). The SDS-PAGE gel indicated fl-E7 (upper band of Coomassie gel which is aligned to the UV signal of the same gel) and the non-labeled GGG-E7 (lower band). The lower DoL in fl-16E7 might be due to the

different stock of the fluorescein dye, where the concentration may vary. Therefore, the concentration of fluorescein stock should be accessed more meticulously in the future. A higher amount of fluorescein peptide used may also achieve a higher DoL. The detailed purification steps for each GGG-E7 and *Srt A labeling* can be found in (***Appendix 9*** and ***Appendix 11***).

Table 2 Summary of yield and purity of purified E7 proteins.

Protein (monomer)	Yield (per 20 g wet biomass)	Purity	Degree of labeling (DoL)
GGG-16E7	3 mg	≥ 70 %	-
fl-16E7	-	-	11 %
GGG-31E7	8 mg	≥ 88 %	-
fl-31E7	-	-	36 %

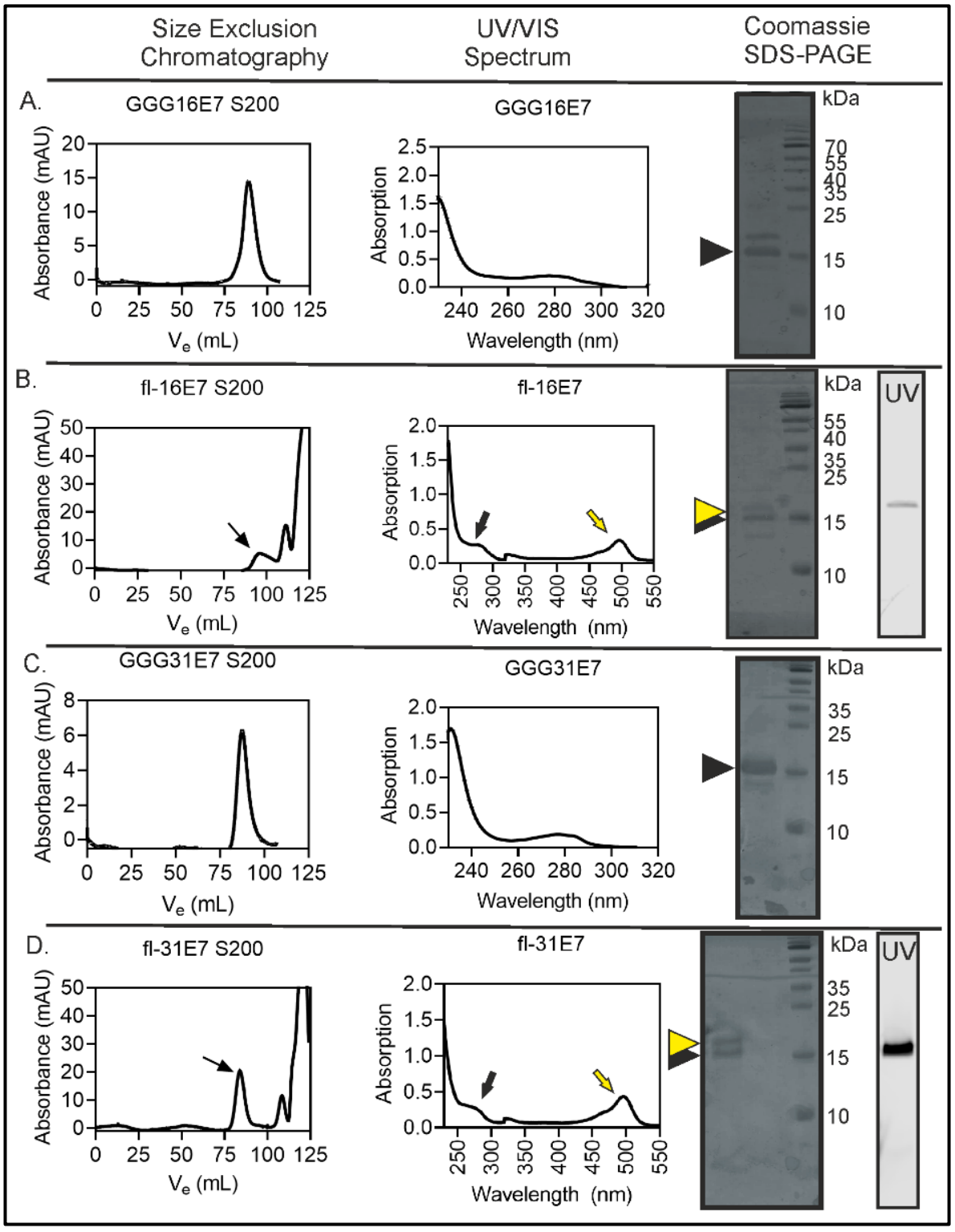

Figure 12 Summary of purified E7 proteins. The first column shows the chromatogram of SEC on HiLoad 16/600 Superdex 200pg columns of **A.** GGG-16E7, **B.** fl-16E7, **C.** GGG-31E7, and **D.** fl-31E7. The second column shows the final UV/VIS spectra of the respective purified E7 proteins at a dilution of 1:40. Data plotted are the three technical replicates. The black arrow indicates the signal of fl-E7 at 280 nm and the yellow arrow is the fl-E7 signal at 495 nm (fluorescein). The third column shows the Coomassie stained reducing SDS-PAGE (left) and the same reducing SDS-PAGE illuminated with UV light for detecting fluorescein signal before the gel was stained (right) of the respective10 µg purified fl-E7 protein. The black arrow points to the protein bands of GGG-E7 and the yellow is the fl-E7.

3.2.2.4 Stoichiometry of E6/E7 Complex

Analytical ultracentrifugation (AUC) involves two measurements, sedimentation equilibrium (AUC-SE) and sedimentation velocity (AUC-SV). Both AUC-SE and AUC-SV measure the sedimentation of a molecule over time by measuring the absorbance of the sample in a cuvette from top to bottom during ultracentrifugation. AUC-SE measures the concentration profile formed in the sedimentation equilibrium achieved by the back-diffusion occurring from the bottom (high concentration) to the top (low concentration) of the cuvette when applied centrifugal force. This sedimentation profile depends on the protein's molecular weight and allows the molecular mass calculation and subsequent stoichiometry of the molecule [154, 155]. AUC-SV provides information on the molecule's size and homogeneity [155, 156]. The larger molecules sediment faster than the smaller molecules. A sedimentation coefficient (s_{app}) can be calculated based on sedimentation velocity, buffer viscosity, centrifugal force, and temperature [157].

Therefore, AUC-SE and AUC-SV were carried out to determine the molecular mass and to understand the complex formation using MBP-16E6_4C4S-LxxLL and fl-16E7. For this purpose, the E6/E7 complex was measured at a monomeric molar ratio of 1:1 (100 µM E6:100µM E7) in SEC buffer (20 mM HEPES, 200 mM NaCl, 1 mM TCEP, pH 7.5). The controls with only E6 or E7 alone were also measured in the same buffer. We used fl-16E7 instead of GGG-16E7 for the measurement because E7 has a low extinction coefficient and makes the measurement at 280 nm at a low concentration challenging. Using fl-16E7 allows the measurement to be done at 495 nm with and without MBP-16E6_4C4S-LxxLL.

First, the AUC-SV (***Figure 13***) revealed the calculated sedimentation coefficient (s_{app}) of 4.30 for MBP-16E6_4C4S-LxxLL and 1.70 for fl-16E7. The AUC-SV analysis disclosed a s_{app} for two species of E6/E7 complexes, of which 89 % were the major species with s_{app} = 6.70 and the minor species with s_{app} = ~ 4.0. Since the complex was monitored at 495 nm, the minor species of s_{app} = 4.0 could be the intermediate species of the complex.

Next, the sedimentation equilibrium measurement revealed the molecular weight (MW_{app}) of 63.4 ± 4.9 kDa for MBP-16E6_4C4S-LxxLL, 19.7 ± 2.1 kDa for fl-16E7, and

142 kDa for the MBP-16E6_4C4S-LxxLL/fl-16E7 complex. These results fitted the theoretical molecular weight of MBP-16E6_4C4S-LxxLL (60 kDa), resembling one E6 molecule, and fl-16E7 (11 kDa), resembling two E7 molecules. Hence, the MW_{app} = 142 kDa for the complex may correlate to two fl-16E7 molecules and two MBP-16E6_4C4S-LxxLL molecules (2:2). Furthermore, MBP-16E6_4C4S-LxxLL was titrated from 0 - 150 µM against a fixed concentration of fl-16E7 (100 µM monomer) to verify the result. The amount of free fl-16E7 decreased with the increasing E6/E7 ratio. At a molar ratio of 1:1, the sedimentation coefficient was between 6.0 to 7.0, with approximately 89 % free fl-16E7 used in complex formation. These results further supported the results described above.

In short, the shift of the sedimentation coefficient for the complex verified the interaction between E6 and E7. We proposed that fl-16E7 appeared as a dimer because E7 protein is known to form a stable dimer with its unique β1β2α1β3α2 topology located in the CR3 domain and that a dimer is the most prominent oligomeric species under physiological conditions for E7 [60-62]. Therefore, we hypothesized one E7 dimer and two E6 monomers (2:2) participate in complex formation. The minor species that appeared in the complex could be the intermediate species which could be two E7 molecules and one E6 molecule (2:1).

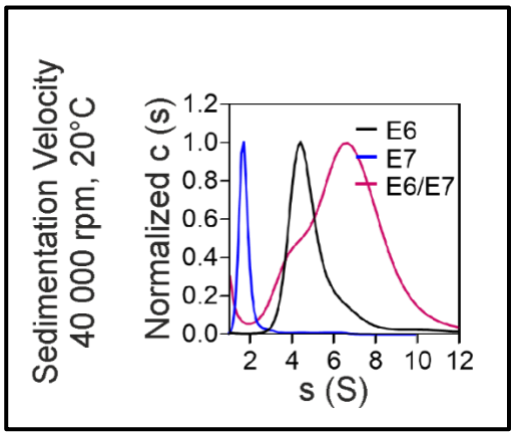

Figure 13 The sedimentation velocity revealed the sedimentation coefficient of MBP-16E6_4C4S-LxxLL(E6AP) (black), fl-16E7 (magenta), and the complex (blue) calculated with SEDFIT version 12.52. Adapted from [2].

3.2.2.5 Binding Affinity of HPV16 and HPV31 E6/E7 Complexes

A fluorescence polarization (FP) assay was employed to analyze the binding affinity of the E6/E7 complex. Fluorescence polarization depends on the mobility of ligand-receptor interactions by exciting polarized light onto a fluorescently labeled ligand with monochromatic light that passes through a polarizer. The parallel and perpendicular (to the excitation light) emitted polarized lights are detected. The ratio of the collected parallel and perpendicular light intensities is calculated to obtain a polarization value. At the unbound state, the faster rotation of a fluorescently labeled ligand would lead

to the emission of depolarized light which gives a low FP. When this ligand bind to its receptor, the increase in size would reduce the rotation speed, subsequently giving a higher FP as there is a higher amount of emission light in the same plan as the polarized excitation light [158]. Two measurements, including direct measurement and competitive measurement, were performed. The direct measurement monitors the binding between purified fl-E7 (ligand) and MBP-E6 (receptor) with or without LxxLL fusion to the C-terminus of E6 by titrating an increasing amount of E6 against the fixed concentration of fl-E7. The optimum concentrations of fl-E7 were chosen as described in ***Appendix 12***. The competitive measurement uses a non-labeled GGG-E7 to displace fl-E7 in the complex to address the reversibility of the complex formation and any artefact of fluorescein peptide. The FP values can be plotted against a range of receptor concentrations obtaining a binding curve for the calculation of the binding affinity of the complex [159].

A series of 1.5-fold serial dilutions of MBP-16E6_4C4S-LxxLL and MBP-31E6_2C2S-LxxLL was titrated against the fixed concentration of fl-16E7 and fl-31E7, respectively, for direct measurement. The clear increase in the FP indicates an interaction between the E6 and E7. The fluorescence polarization data were fitted first with the Specific binding-Hill slope model to examine for the possibility of a cooperative binding event (***Appendix 13***). However, the results obtained are non-significant to conclude such a binding event. This could be due to the limit of detection from this assay because of the fluorescence lifetime, thus limiting the discrimination of the binding events from the single or the two E6 molecules as seen in AUC. Hence, we fitted the data with the One-site-Specific binding model and the binding affinity obtained from both models were similar (***Appendix 13***). From ***Table 3***, a similar binding affinity was obtained from the One-site-Specific binding model for HPV16 (46.4 ± 0.9 µM) and HPV31 (59.4 ± 2.5 µM). The same experiments were repeated by titrating MBP with 1.5-fold serial dilution against fl-E7. No change in the FP signal indicated that the interaction seen above is not an artifact of the MBP tag.

Furthermore, to investigate if the LxxLL motif sequence is involved in the complex formation, the same experiment was repeated by substituting the MBP-16E6_4C4S-LxxLL with MBP-16E6_4C4S (no LxxLL fusion). A clear increase in the FP signal indicated the binding of E6 and E7 in the absence of the LxxLL peptide. Besides, a

21-fold difference of binding affinity (3.0 ± 0.1 µM) was revealed in ***Table 3***. The different binding affinity obtained could mean an artifact binding of the fluorescein or the LxxLL peptide impairs the binding. Therefore, the MBP-16E6_4C4S was titrated with the same dilution series against a fixed concentration of fluorescein, and we observed a slight increase in the FP signal with >100 µM MBP-16E6_4C4S. Hence, the higher affinity observed may be the synergetic effect of the fluorescein.

Next, competitive measurements were performed to investigate if the complex formation is reversible. Therefore, complexes formed at 60-80 % saturation concentration were titrated with increasing GGG-E7 dimer. The competition was carried out by competing for fl-16E7/MBP-16E6_4C4S (no LxxLL in fusion) with GGG-16E7 and fl-31E7/MBP-31E6_2C2S-LxxLL (LxxLL in fusion) with GGG-31E7. As mentioned earlier in *section 3.2.2.4* that E7 is forming the complex as a dimer. Hence, plotting the GGG-E7 with a dimer concentration is crucial for competitive measurement. We observed a clear decrease in the FP signal indicating a reversible complex formation in both cases. The binding affinity obtained from the complex of HPV16 (61.9 ± 1.3 µM) and HPV31 (54.2 ± 1.4 µM) are similar ***Table 3***.

Table 3 Binding affinity of MBP-E6 or MBP-E6-LxxLL with fl-E7.

Complex	Direct measurement	Competition
fl-16E7/MBP-16E6_4C4S	3.0 ± 0.1 µM	61.9 ± 1.3 µM
fl-16E7/MBP-16E6_4C4S-LxxLL	46.4 ± 0.9 µM	N.D
fl-16E7/MBP-31E6_2C2S-LxxLL	59.4 ± 2.5 µM	54.2 ± 1.4 µM

*Note: N.D = no data

In summary, the binding affinity based on the One-site-Specific binding model for the E6/E7 complex of HPV16 and HPV31 are similar and are in the range of ~55 - 60 µM. This is the average binding affinitz of the two binding sites. The dissociation constant is concluded from the competitive measurement as the binding affinity was obtained based on the non-labeled E7 proteins. The FP signal in the competitive measurement did not go down to zero because of the dynamic equilibrium between fl-E7 and GGG-E7 binding to E6. Therefore, it is unavoidable that there are some of the fl-E7 remain bound.

The fluorescein seems to enhance the binding between MBP-16E6_4C4S and fl-16E7, probably due to the exposure of the hydrophobic LxxLL binding pocket where fluorescein could probably bind to. Combining the binding affinity obtained from the competition FP, these results suggest that the LxxLL motif does not bind to the E7 but may impair the binding to fluorescein. In addition, the E6N and E6C domain is rather flexible [160]. The two domains are held in place by the LxxLL peptide of E6AP to facilitate the binding to p53 [45]. Therefore, we suggest that the flexibility of the E6N and E6C domains may also influence the binding. A competitive measurement using E6AP-LxxLL peptide with fl-16E7/MBP-16E6_4C4S may be conducted to verify its influence on the E6/E7 complex. The changes in the binding affinity may indicate an impact of the flexibility of the E6 and E6C domains on the E6/E7 complex.

3.2.2.6 The N-Terminus of E7 Participate in The Complex Formation

CR1 and CR2 of E7 are actively involved in cellular interactions. CR1 is the binding site of UBR4 ubiquitin ligase, which E7 acts together to bind and degrade tumor suppressor PTPN14 [65]. As mentioned earlier, the pre-dominant pRb binding motif LxCxE is located in the CR2. Hence, we analyze if E6 could interact with E7 N-terminus by titrating an increasing amount of MBP-16E6_4C4S at 1.5-fold against a constant amount of fl-16E7CR1/2 (1-44). The increase in the FP signal indicates interaction and a binding affinity of 101.3 ± 2.3 µM was obtained. Competitive measurement was conducted by titrating a 2-fold serial dilution of fl-16E7CR1/2 (1-44) against the complex formed at 60 % saturation concentration. A decrease in FP indicated a reversible complex formation and revealed a binding affinity of 128.1 ± 16.0 µM. The control measurement with MBP did not increase the FP signal indicating that the binding is not an artifact of the MBP tag. Hence, these results showed that E6 is binding to the N-terminal region of 16E7, the CR1-2 region (aa 1-44). The competition between 16E7CR1/2 with fl-16E7/MBP-16E6_4C4S was additionally conducted and revealed a binding affinity of 288.0 ± 7.8 µM, which is 5-fold lower than the binding affinity obtained with full-length 16E7. The lower binding affinity is probably due to the intrinsically disordered structure in the N-terminus, which has been shown to exert a lower affinity to their ligands [161, 162]. Another reason for the low affinity might be that 16E7CR1/2 (1-44) may not be the only binding region.

Nonetheless, these results show that 16E7 N-terminus (1-44) is binding to the 16E6 with lower affinity than the 16E7 full length.

3.2.2.7 Ongoing research

The precise binding site between E6 and E7 remains unknown. We have shown that the 16E7CR1/2 (1-44) is involved in the interaction with a lower affinity and proposed one possibility that another binding domain may exist. In fact, we investigated the interaction between E7CR1/2 (1-44) and E7CR3 (45-98) of HPV 16 and HPV31 with E6 using FACS-FRET assays. Unfortunately, no interaction could be concluded due to a low number of FRET-positive cells (***Figure 14A*** and ***Figure 14B***) as a result of low expression of EYFP tagged E7CR1/2 (1-44) and E7CR3 (45-98). However, we titrated 16E7CR3 against a fixed concentration of MBP-16E6_4C4S-LxxLL labeled with red fluorescent dye NT-647-NHS and measured the binding affinity using Microscale Thermophoresis (MST). MST instead of fluorescence polarization was conducted due to the materials' limited availability at the experiment's time. The 16E7CR3 was expressed and purified as described in ***Appendix 14*** and ***Appendix 15*****.** As a result, the MST measurement indicated a binding event between MBP-16E6_4C4S-LxxLL and 16E7CR3 (45-98) and revealed a binding affinity of 115.7 ± 3.7 µM (***Figure 14E***). Notably, fluorescence polarization measures the rotational diffusion of molecules while MST measures the movement of the molecules along with a temperature gradient. Besides, the fluorescence dye, the fluorescence detection channel, the filter, the sensitivity of the devices, the types of laser, and many other parameters could contribute to a discrepancy in the binding affinities obtained. Hence, comparing directly the binding affinity obtained from fluorescence polarization and MST should be avoided. Nevertheless, 16E7CR3 45-98 could bind to E6 in the MST measurement.

To determine if E6 and E7 may compete with their cellular targets, respectively for the same binding site in order to interact, some mutations in the E6 and E7 were generated. For 16E7, the R77A, M84A and R77A_M84A that are deficient in interacting with PTPN14 were introduced into EYP-16E7 for FACS-FRET assays. As a result, all of the mutated EYFP-16E7 remained to show a % FRET of more than 10% and more than 500 FRET-positive cells (***Figure 14C*** and ***Figure 14D***). Thus, R77 and M84 mutants could not abolish the binding of E7 to E6 and we could not conclude

these two amino acids as a potential binding sites for E6. For 16E6, the F47R mutation which is known to lead to E6 being defective in degrading the p53 tumor suppressor was introduced into mTagBFP2-16E6. The % FRET and the number of FRET-positive cells for mTagBFP2-16E6 F47R and EYFP-16E7 WT were below the threshold of 10% and 500 cells (***Figure 14C*** and ***Figure 14D***). The interaction seems to be reduced indicating that F47 despite a similar double positive population observed. However, the exact expression levels between the wild-type E6 and the F47R mutant are not assessed, hence a conclusion could not be drawn. Therefore, to verify the FACS-FRET result obtained for F47R mutant in a qualitative and quantitative way, we introduced the F47R mutation into MBP-16E6_4C4S-LxxLL for fluorescence polarization. A direct binding curve was titrated and obtained a binding affinity of 32.3 ± 2.9 µM, which is in the similar range to MBP-16E6_4C4S-LxxLL. This result indicates that the F47 may not be the binding site which contradicts the FACS-FRET data. A competition with non-labeled GGG-16E7 is required to address the reversibility of the complex and its specificity towards E7. A similar binding affinity obtained from competitive measurement would means that F47R may not be the potential binding site and the contradicting result obtained from FACS-FRET would probably due to the different expression levels of wild-type and mutant E6, which need further study. However, a lower affinity obtained with E6 mutant would indicate an artefact from fluorescein as described in *Section 3.2.2.5*. A titration of MBP-16E6_4C4SF47R-LxxLL with fluorescein may then be helpful in determining if fluorescein enhances the binding.

In summary, 16E7CR3 is involved in complex formation with 16E6 in addition to presumably unstructured N-terminus region of E7, CR1/2. The 16E6 F47R seems to impair the binding in FACS-FRET but not in the direct measurement of fluorescence polarization. The R77 and M84 in 16E7 do not seem to be a potential predominant binding site.

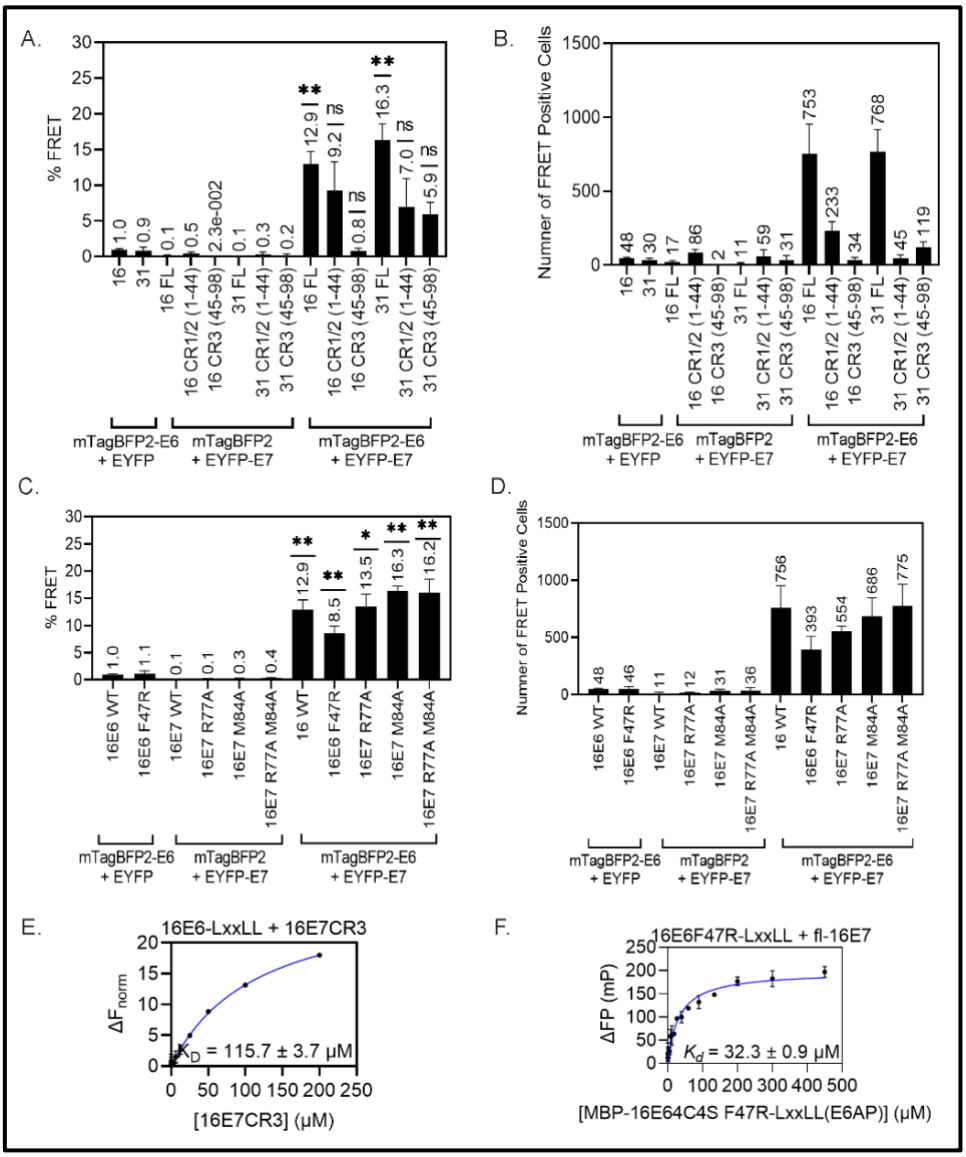

Figure 14 Potential binding sites of E6 and E7. C33A co-expressing mTagBFP2-E6 and EYFP-E7 variants were subjected to FACS-FRET. Low % FRET **(A, C)** and the number of FRET-positive cells **(B, D)** in the controls of mTagBFP-E6 + EYFP and mTagBFP2 + EYFP-E7 indicate no interaction seen. (**A, B**) The EYFP-16E7CR1/2 (1-44), EYFP-16E7CR3 (45-98), EYFP-31E7CR1/2 (1-44), and EYFP-31E7CR3 (45-98) that paired with respective mTagBFP2-16E6 and mTagBFP2-31E6 did not meet the threshold of >10% and >500 FRET positive cells to generate a significant cell population in FACS-FRET. Thus, an interaction could not be concluded. (**D, E**) mTagBFP2-16E6F47R mutant paired with EYFP-16E7 WT show % FRET and the number of FRET positive cells that are below the assay's threshold. Thus, the interaction is unclear. The EYFP-16E7 R77A, M84A and R77A + M84A mutants show % FRET and the number of FRET-positive cells above the assay's threshold indicates an interaction. Data are derived from the mean value of three independent biological replicates. The error bars are plotted to represent the standard deviation of the mean value from the three independent biological replicates. P value in **A** and **C** were calculated with one sample t-test, where ** = P >0.005, * = P >0.01, ns = P > 0.05. **E**. An increasing amount of 16E7CR3 (45-98) was titrated against a fixed concentration of MBP-16E6_4C4SF47R-LxxLL labeled with red fluorescent dye NT-647-NHS and subjected to MST measurement. An interaction has been observed with the increase of MST signal and a binding affinity of 115.7 ± 3.7 µM was determined with One Site-specific binding model using GraphPad Prism version 9.4.1 (681). **F**. Direct binding curve of purified MBP-16E6_4C4SF47R-LxxLL with fl-16E7 was monitored in fluorescence polarization by titrating fl-16E7 with an increasing amount of MBP-16E6_4C4SF47R-LxxLL. The clear increase in FP indicates a binding event has occurred. The binding affinity of 32.3 ± 0.9 µM is similar to MBP-16E6_4C4S-LxxLL (46.4 ± 0.9 µM). The binding affinities were obtained with One Site-specific binding model using GraphPad Prism version 9.4.1 (681).

4 Conclusions and Outlook

4.1 Part I: Cottontail Rabbit Papillomavirus E6 Proteins: Interaction with MAML1 and Modulation of The Notch Signaling Pathway

The work presented in this thesis shows CRPV E6 interacts with MAML1 and represses Notch signaling, as previously shown for beta HPV. Though the Notch repression seems species-specific, CRPV E6 remains a promising animal model for further investigation in cutaneous PV-associated carcinogenesis with regard to the role of Notch signaling.

The MAML1 binding sites in HPV8 E6 have been described previously [56]. However, the crystal structure of beta HPV49 E6 with MAML1 LxxLL motif (PDBID:6SMV) available on PDB revealed a different binding site than as shown for HPV8 E6 [56, 163]. HPV49 belongs to the beta genus, species-3 while HPV8 belongs to the beta genus, species-1 which could imply a phylogeny relation. Hence, structural analysis would be interesting to find out if CRPV E6 shares the same binding sites as HPV8 E6 or HPV49 E6.

In addition, affinity purification-mass spectrometry (AP-MS) may help to determine other cellular targets of CRPV E6. The functional analysis could be conducted for cellular targets found with AP-MS, especially those in common with beta HPV E6. This may further support CRPV as an extraordinary animal model in understanding cutaneous HPV-associated cancers. Moreover, the information obtained from AP-MS may also help to identify the primary cellular target of CRPV E6 to understand further not only the Notch inhibition mechanism employed by CRPV E6, but also other cellular pathways that are in relation to the viral life cycle and keratinocytes immortalization. Understanding the binding interface of the beta E6 or CRPV E6 with MAML1 and their primary target on Notch signaling may help design novel E6 inhibitors. By utilizing the triple fluorescence Notch reporter assay we established, these novel inhibitors specific for E6 may be screened by monitoring their efficiency in a rapid medium-throughput way. A promising candidate may be further tested in a rabbit model after cell culture assays are well established in keratinocytes. These studies may help to provide a novel therapy for beta HPV-associated cancers.

4.2 Part II: Human Papillomavirus E6 Proteins: Interaction with E7 Proteins and Characterization of The Complex

The interactions of E6 and E7 from HPV16, HPV31, HPV18, and HPV38 have been verified in the cell-based assay. The interaction of HPV16 E6 and E7 was confirmed further with analytical ultracentrifugation and fluorescence polarization. According to the analytical ultracentrifugation, one E7 dimer and two E6 monomers are proposed to participate in complex formation. The binding affinities of HPV16 and HPV 31 are in the same range of 55 – 60 μM, and the N-terminus region (1-44) and C-terminus region (45-98) of E7 are both involved in the binding. The E7 N-terminus (1-44) binds E6 at a lower affinity while the binding strength between E7 C-terminus (45-98) remains to be verified by fluorescence polarization. HPV16 and HPV31 belong to the high-risk alpha genus, species-9 not only shows the interaction between E6 and E7 but also a similar binding affinity. Combining the E6 and E7 interaction seen in HPV18 (high-risk alpha genus, species-7) and HPV38 (beta genus, species-2), we suggest that the interaction of E6 and E7 proteins could be a conserved phenomenon across the HPV phylogenetic tree.

Structural analysis of the E6/E7 complex is necessary to reveal the undiscovered precise interaction interface. Understanding the structure of the complex may ease the functional analysis. Indeed, we have started co-crystallization trials, but none of the tested conditions have been successful. This may be due to the μM range binding affinity that could be too low for co-crystallization. In addition, the highly disordered N-terminus of 16E7 may also make the crystallization challenging. Thus, a different approach such as high-resolution nuclear magnetic resonance (NMR) spectroscopy may be an alternative for structural analysis. However, the low yield of GGG-16E7 can made the material availability another limitation for structural analysis. To increase the yield of 16E7 for structural analysis, one may try to purify the protein from inclusion bodies for co-crystallization X-ray chromatography and NMR. Alternatively, a cross-linking mass-spectrometry that provides fast, sensitive, high-throughput analysis with much lower protein consumption could also be another good option to circumvent the difficulty faced with the low yield of GGG-16E7. Moreover, it has been mentioned in *Section 1.6* that HPV E7 proteins are highly conserved and it is more conserved among different HPV types as compared to E6. Thus, other than biophysical approaches, HPV cross-type FACS-FRET screening by pairing 16E7 with E6 of

different HPV types in combination with multiple sequence alignment to determine the specific binding sites. A similar FRET signal obtained would indicate the involvement of conserved binding sites while a loss of FRET signal would mean that non-conserved amino acid residues of the tested HPV types are participating in the complex formation.

The synergistic effect of E6 and E7 proteins in promoting and maintaining HPV-associated carcinogenesis has been described in *Section 1.7*. However, the functional role of the E6/E7 complex remains unknown. We speculate on a regulatory mechanism between E6 and E7 proteins in maintaining a network balance between free versus complexed E6 and E7 in targeting cellular proteins and pathways at different time points during the infectious cycle. Keratinocyte immortalization studies using mutants of E6 and E7 that are defective in complex formation would provide information on the tumorigenesis induced by E6 and E7. Transducing human keratinocytes with E6 or E7 alone and E6/E7 followed by AP-MS may allow the investigation of the cellular targets of the complex. This information would provide new perspectives in understanding the tumor viral strategies. In addition, it would be fascinating to find out whether E6 and E7 would facilitate, enhance or dismiss the binding to their known cellular targets upon complex formation or even allow binding to novel targets that have been missed or misinterpreted when they were investigated as single proteins. With fluorescence polarization, a competition employing the known cellular targets of E6 and E7, such as p53 and pRb tumor suppressor, respectively may also be titrated against the E6/E7 complex. A change in the affinities may indicate an interference of the complex on the role of E6 and E7, whether it is a synergistic interplay between the single activities of E6 and E7 or an interaction between E6 and E7 is essential for these activities in viral replication, immune invasion and tumorigenesis. Furthermore, the phosphorylation of E7 has been shown several times to be essential for its stability and functional roles in viral life cycles and different phases of malignant progression, though it is not clear how E7 phosphorylation changes in these processes [164-170]. Hence, studying the phosphorylation of E7 upon binding to E6 may provide a new perspective on understanding the role of E6 and E7 in HPV life cycle and its associated carcinogenesis.

Bibliography

1. Mittal, S. and L. Banks, *Molecular mechanisms underlying human papillomavirus E6 and E7 oncoprotein-induced cell transformation.* Mutat Res Rev Mutat Res, 2017. **772**: p. 23-35.
2. Lim, J., et al., *Evidence for direct interaction between the oncogenic proteins E6 and E7 of high-risk human papillomavirus (HPV).* J Biol Chem, 2023. **299**(8): p. 104954.
3. Suarez, I. and G. Trave, *Structural Insights in Multifunctional Papillomavirus Oncoproteins.* Viruses, 2018. **10**(1).
4. Yun, H.Y., et al., *Structural basis for recognition of the tumor suppressor protein PTPN14 by the oncoprotein E7 of human papillomavirus.* PLoS Biol, 2019. **17**(7): p. e3000367.
5. Conrady, M.C., et al., *Structure of High-Risk Papillomavirus 31 E6 Oncogenic Protein and Characterization of E6/E6AP/p53 Complex Formation.* J Virol, 2020. **95**(2).
6. Lim, J., et al., *An enhanced triple fluorescence flow-cytometry-based assay shows differential activation of the Notch signaling pathway by human papillomavirus E6 proteins.* Sci Rep, 2022. **12**(1): p. 3000.
7. Lim, J., et al., *Cottontail rabbit papillomavirus E6 proteins: Interaction with MAML1 and modulation of the Notch signaling pathway.* Virology, 2022. **576**: p. 52-60.
8. de Villiers, E.M., et al., *Classification of papillomaviruses.* Virology, 2004. **324**(1): p. 17-27.
9. de Villiers, E.M., et al., *Esophageal squamous cell cancer in patients with head and neck cancer: Prevalence of human papillomavirus DNA sequences.* Int J Cancer, 2004. **109**(2): p. 253-8.
10. Humans, I.W.G.o.t.E.o.C.R.t., *Human papillomaviruses.* IARC Monogr Eval Carcinog Risks Hum, 2007. **90**: p. 1-636.
11. Sung, H., et al., *Global Cancer Statistics 2020: GLOBOCAN Estimates of Incidence and Mortality Worldwide for 36 Cancers in 185 Countries.* CA Cancer J Clin, 2021. **71**(3): p. 209-249.
12. de Martel, C., et al., *Worldwide burden of cancer attributable to HPV by site, country and HPV type.* Int J Cancer, 2017. **141**(4): p. 664-670.
13. Munoz, N., et al., *Epidemiologic classification of human papillomavirus types associated with cervical cancer.* N Engl J Med, 2003. **348**(6): p. 518-27.
14. Stein, A.P., et al., *Prevalence of Human Papillomavirus in Oropharyngeal Cancer: A Systematic Review.* Cancer J, 2015. **21**(3): p. 138-46.
15. Isayeva, T., et al., *Human papillomavirus in non-oropharyngeal head and neck cancers: a systematic literature review.* Head Neck Pathol, 2012. **6 Suppl 1**: p. S104-20.
16. Michaud, D.S., et al., *High-risk HPV types and head and neck cancer.* Int J Cancer, 2014. **135**(7): p. 1653-61.
17. Plasmeijer, E.I., et al., *Epidemiology of cutaneous human papillomavirus infections.* Cancer Treat Res, 2009. **146**: p. 143-57.
18. Egawa, N., et al., *Human Papillomaviruses; Epithelial Tropisms, and the Development of Neoplasia.* Viruses, 2015. **7**(7): p. 3863-90.

19. Antonsson, A., et al., *The ubiquity and impressive genomic diversity of human skin papillomaviruses suggest a commensalic nature of these viruses.* J Virol, 2000. **74**(24): p. 11636-41.
20. Bouwes Bavinck, J.N., et al., *Multicenter study of the association between betapapillomavirus infection and cutaneous squamous cell carcinoma.* Cancer Res, 2010. **70**(23): p. 9777-86.
21. Hsu, J.Y., et al., *Shared and persistent asymptomatic cutaneous human papillomavirus infections in healthy skin.* J Med Virol, 2009. **81**(8): p. 1444-9.
22. Antonsson, A., et al., *General acquisition of human papillomavirus infections of skin occurs in early infancy.* J Clin Microbiol, 2003. **41**(6): p. 2509-14.
23. Orth, G., *Host defenses against human papillomaviruses: lessons from epidermodysplasia verruciformis.* Curr Top Microbiol Immunol, 2008. **321**: p. 59-83.
24. Ostrow, R.S., et al., *Human papillomavirus DNA in cutaneous primary and metastasized squamous cell carcinomas from patients with epidermodysplasia verruciformis.* Proc Natl Acad Sci U S A, 1982. **79**(5): p. 1634-8.
25. Orth, G., et al., *Characterization of two types of human papillomaviruses in lesions of epidermodysplasia verruciformis.* Proc Natl Acad Sci U S A, 1978. **75**(3): p. 1537-41.
26. Meyer, T., et al., *Frequency and spectrum of HPV types detected in cutaneous squamous-cell carcinomas depend on the HPV detection system: a comparison of four PCR assays.* Dermatology, 2000. **201**(3): p. 204-11.
27. Casabonne, D., et al., *A prospective pilot study of antibodies against human papillomaviruses and cutaneous squamous cell carcinoma nested in the Oxford component of the European Prospective Investigation into Cancer and Nutrition.* Int J Cancer, 2007. **121**(8): p. 1862-8.
28. Waterboer, T., et al., *Serological association of beta and gamma human papillomaviruses with squamous cell carcinoma of the skin.* Br J Dermatol, 2008. **159**(2): p. 457-9.
29. Viarisio, D., et al., *Beta HPV38 oncoproteins act with a hit-and-run mechanism in ultraviolet radiation-induced skin carcinogenesis in mice.* PLoS Pathog, 2018. **14**(1): p. e1006783.
30. Kines, R.C., et al., *The initial steps leading to papillomavirus infection occur on the basement membrane prior to cell surface binding.* Proc Natl Acad Sci U S A, 2009. **106**(48): p. 20458-63.
31. Moody, C.A. and L.A. Laimins, *Human papillomavirus oncoproteins: pathways to transformation.* Nat Rev Cancer, 2010. **10**(8): p. 550-60.
32. McBride, A.A., J.G. Oliveira, and M.G. McPhillips, *Partitioning viral genomes in mitosis: same idea, different targets.* Cell Cycle, 2006. **5**(14): p. 1499-502.
33. Munger, K., et al., *Mechanisms of human papillomavirus-induced oncogenesis.* J Virol, 2004. **78**(21): p. 11451-60.
34. Hummel, M., J.B. Hudson, and L.A. Laimins, *Differentiation-induced and constitutive transcription of human papillomavirus type 31b in cell lines containing viral episomes.* J Virol, 1992. **66**(10): p. 6070-80.
35. Bedell, M.A., et al., *Amplification of human papillomavirus genomes in vitro is dependent on epithelial differentiation.* J Virol, 1991. **65**(5): p. 2254-60.
36. Kirnbauer, R., et al., *Efficient self-assembly of human papillomavirus type 16 L1 and L1-L2 into virus-like particles.* J Virol, 1993. **67**(12): p. 6929-36.

37. Hagensee, M.E., N. Yaegashi, and D.A. Galloway, *Self-assembly of human papillomavirus type 1 capsids by expression of the L1 protein alone or by coexpression of the L1 and L2 capsid proteins.* J Virol, 1993. **67**(1): p. 315-22.
38. Wang, Q., et al., *Functional analysis of the human papillomavirus type 16 E1=E4 protein provides a mechanism for in vivo and in vitro keratin filament reorganization.* J Virol, 2004. **78**(2): p. 821-33.
39. Bryan, J.T. and D.R. Brown, *Association of the human papillomavirus type 11 E1()E4 protein with cornified cell envelopes derived from infected genital epithelium.* Virology, 2000. **277**(2): p. 262-9.
40. Middleton, K., et al., *Organization of human papillomavirus productive cycle during neoplastic progression provides a basis for selection of diagnostic markers.* J Virol, 2003. **77**(19): p. 10186-201.
41. Klaes, R., et al., *Detection of high-risk cervical intraepithelial neoplasia and cervical cancer by amplification of transcripts derived from integrated papillomavirus oncogenes.* Cancer Res, 1999. **59**(24): p. 6132-6.
42. Melsheimer, P., et al., *DNA aneuploidy and integration of human papillomavirus type 16 e6/e7 oncogenes in intraepithelial neoplasia and invasive squamous cell carcinoma of the cervix uteri.* Clin Cancer Res, 2004. **10**(9): p. 3059-63.
43. Snijders, P.J., et al., *HPV-mediated cervical carcinogenesis: concepts and clinical implications.* J Pathol, 2006. **208**(2): p. 152-64.
44. Pinidis, P., et al., *Human Papilloma Virus' Life Cycle and Carcinogenesis.* Maedica (Bucur), 2016. **11**(1): p. 48-54.
45. Martinez-Zapien, D., et al., *Structure of the E6/E6AP/p53 complex required for HPV-mediated degradation of p53.* Nature, 2016. **529**(7587): p. 541-5.
46. Nomine, Y., et al., *Domain substructure of HPV E6 oncoprotein: biophysical characterization of the E6 C-terminal DNA-binding domain.* Biochemistry, 2003. **42**(17): p. 4909-17.
47. Talis, A.L., J.M. Huibregtse, and P.M. Howley, *The role of E6AP in the regulation of p53 protein levels in human papillomavirus (HPV)-positive and HPV-negative cells.* J Biol Chem, 1998. **273**(11): p. 6439-45.
48. Kiyono, T., et al., *Binding of high-risk human papillomavirus E6 oncoproteins to the human homologue of the Drosophila discs large tumor suppressor protein.* Proc Natl Acad Sci U S A, 1997. **94**(21): p. 11612-6.
49. Glaunsinger, B.A., et al., *Interactions of the PDZ-protein MAGI-1 with adenovirus E4-ORF1 and high-risk papillomavirus E6 oncoproteins.* Oncogene, 2000. **19**(46): p. 5270-80.
50. Thomas, M., et al., *Oncogenic human papillomavirus E6 proteins target the MAGI-2 and MAGI-3 proteins for degradation.* Oncogene, 2002. **21**(33): p. 5088-96.
51. Thomas, M., et al., *The hScrib/Dlg apico-basal control complex is differentially targeted by HPV-16 and HPV-18 E6 proteins.* Oncogene, 2005. **24**(41): p. 6222-30.
52. Mesplede, T., *p53 degradation activity, expression, and subcellular localization of E6 proteins from 29 human papillomavirus genotypes.* J. Virol., 2012. **86**.
53. White, E.A., et al., *Comprehensive analysis of host cellular interactions with human papillomavirus E6 proteins identifies new E6 binding partners and reflects viral diversity.* J Virol, 2012. **86**(24): p. 13174-86.
54. Brimer, N., et al., *Cutaneous papillomavirus E6 oncoproteins associate with MAML1 to repress transactivation and NOTCH signaling.* Oncogene, 2012. **31**(43): p. 4639-4646.

55. Tan, M.J.A., et al., *Cutaneous β-human papillomavirus E6 proteins bind Mastermind-like coactivators and repress Notch signaling.* Proceedings of the National Academy of Sciences of the United States of America, 2012. **109**(23): p. E1473-80.
56. Meyers, J.M., et al., *Inhibition of TGF-β and NOTCH Signaling by Cutaneous Papillomaviruses.* Frontiers in Microbiology, 2018. **9**(389).
57. Boxman, I.L., et al., *Transduction of the E6 and E7 genes of epidermodysplasia-verruciformis-associated human papillomaviruses alters human keratinocyte growth and differentiation in organotypic cultures.* J Invest Dermatol, 2001. **117**(6): p. 1397-404.
58. Dyson, N., et al., *The human papilloma virus-16 E7 oncoprotein is able to bind to the retinoblastoma gene product.* Science, 1989. **243**(4893): p. 934-7.
59. Dahiya, A., et al., *Role of the LXCXE binding site in Rb function.* Mol Cell Biol, 2000. **20**(18): p. 6799-805.
60. Ohlenschlager, O., et al., *Solution structure of the partially folded high-risk human papilloma virus 45 oncoprotein E7.* Oncogene, 2006. **25**(44): p. 5953-9.
61. Alonso, L.G., et al., *High-risk (HPV16) human papillomavirus E7 oncoprotein is highly stable and extended, with conformational transitions that could explain its multiple cellular binding partners.* Biochemistry, 2002. **41**(33): p. 10510-8.
62. Liu, X., et al., *Structure of the human Papillomavirus E7 oncoprotein and its mechanism for inactivation of the retinoblastoma tumor suppressor.* J Biol Chem, 2006. **281**(1): p. 578-86.
63. Huh, K., et al., *Human papillomavirus type 16 E7 oncoprotein associates with the cullin 2 ubiquitin ligase complex, which contributes to degradation of the retinoblastoma tumor suppressor.* J Virol, 2007. **81**(18): p. 9737-47.
64. Roman, A. and K. Munger, *The papillomavirus E7 proteins.* Virology, 2013. **445**(1-2): p. 138-68.
65. Hatterschide, J., et al., *PTPN14 degradation by high-risk human papillomavirus E7 limits keratinocyte differentiation and contributes to HPV-mediated oncogenesis.* Proc Natl Acad Sci U S A, 2019. **116**(14): p. 7033-7042.
66. Butz, K., et al., *siRNA targeting of the viral E6 oncogene efficiently kills human papillomavirus-positive cancer cells.* Oncogene, 2003. **22**(38): p. 5938-45.
67. Yoshinouchi, M., et al., *In vitro and in vivo growth suppression of human papillomavirus 16-positive cervical cancer cells by E6 siRNA.* Mol Ther, 2003. **8**(5): p. 762-8.
68. Demers, G.W., C.L. Halbert, and D.A. Galloway, *Elevated wild-type p53 protein levels in human epithelial cell lines immortalized by the human papillomavirus type 16 E7 gene.* Virology, 1994. **198**(1): p. 169-74.
69. Jones, D.L., D.A. Thompson, and K. Munger, *Destabilization of the RB tumor suppressor protein and stabilization of p53 contribute to HPV type 16 E7-induced apoptosis.* Virology, 1997. **239**(1): p. 97-107.
70. Seavey, S.E., et al., *The E7 oncoprotein of human papillomavirus type 16 stabilizes p53 through a mechanism independent of p19(ARF).* J Virol, 1999. **73**(9): p. 7590-8.
71. Giampieri, S., et al., *Human papillomavirus type 77 E6 protein selectively inhibits p53-dependent transcription of proapoptotic genes following UV-B irradiation.* Oncogene, 2004. **23**(34): p. 5864-70.
72. Nees, M., et al., *Papillomavirus type 16 oncogenes downregulate expression of interferon-responsive genes and upregulate proliferation-associated and NF-*

kappaB-responsive genes in cervical keratinocytes. J Virol, 2001. **75**(9): p. 4283-96.
73. Li, S., et al., *The human papilloma virus (HPV)-18 E6 oncoprotein physically associates with Tyk2 and impairs Jak-STAT activation by interferon-alpha.* Oncogene, 1999. **18**(42): p. 5727-37.
74. Nishio, M., et al., *Endogenous YAP1 activation drives immediate onset of cervical carcinoma in situ in mice.* Cancer Sci, 2020. **111**(10): p. 3576-3587.
75. Gardiol, D., et al., *Oncogenic human papillomavirus E6 proteins target the discs large tumour suppressor for proteasome-mediated degradation.* Oncogene, 1999. **18**(40): p. 5487-96.
76. Nakagawa, S. and J.M. Huibregtse, *Human scribble (Vartul) is targeted for ubiquitin-mediated degradation by the high-risk papillomavirus E6 proteins and the E6AP ubiquitin-protein ligase.* Mol Cell Biol, 2000. **20**(21): p. 8244-53.
77. Messa, L., et al., *The Dimeric Form of HPV16 E6 Is Crucial to Drive YAP/TAZ Upregulation through the Targeting of hScrib.* Cancers (Basel), 2021. **13**(16).
78. Durczak, M. and P.P. Jagodzinski, *Apicidin upregulates PHD2 prolyl hydroxylase gene expression in cervical cancer cells.* Anticancer Drugs, 2010. **21**(6): p. 619-24.
79. Tang, X., et al., *Overexpression of human papillomavirus type 16 oncoproteins enhances hypoxia-inducible factor 1 alpha protein accumulation and vascular endothelial growth factor expression in human cervical carcinoma cells.* Clin Cancer Res, 2007. **13**(9): p. 2568-76.
80. Toussaint-Smith, E., D.B. Donner, and A. Roman, *Expression of human papillomavirus type 16 E6 and E7 oncoproteins in primary foreskin keratinocytes is sufficient to alter the expression of angiogenic factors.* Oncogene, 2004. **23**(17): p. 2988-95.
81. Lopez-Ocejo, O., et al., *Oncogenes and tumor angiogenesis: the HPV-16 E6 oncoprotein activates the vascular endothelial growth factor (VEGF) gene promoter in a p53 independent manner.* Oncogene, 2000. **19**(40): p. 4611-20.
82. Li, F. and J. Cui, *Human telomerase reverse transcriptase regulates vascular endothelial growth factor expression via human papillomavirus oncogene E7 in HPV-18-positive cervical cancer cells.* Med Oncol, 2015. **32**(7): p. 199.
83. Hawley-Nelson, P., et al., *HPV16 E6 and E7 proteins cooperate to immortalize human foreskin keratinocytes.* EMBO J, 1989. **8**(12): p. 3905-10.
84. Chang, J.T., et al., *Highly potent and specific siRNAs against E6 or E7 genes of HPV16- or HPV18-infected cervical cancers.* Cancer Gene Ther, 2010. **17**(12): p. 827-36.
85. Yamato, K., et al., *New highly potent and specific E6 and E7 siRNAs for treatment of HPV16 positive cervical cancer.* Cancer Gene Ther, 2008. **15**(3): p. 140-53.
86. Lee, K.A., et al., *Protein profiling and identification of modulators regulated by human papillomavirus 16 E7 oncogene in HaCaT keratinocytes by proteomics.* Gynecol Oncol, 2005. **99**(1): p. 142-52.
87. Rozenblatt-Rosen, O., et al., *Interpreting cancer genomes using systematic host network perturbations by tumour virus proteins.* Nature, 2012. **487**(7408): p. 491-5.
88. White, E.A., et al., *Systematic identification of interactions between host cell proteins and E7 oncoproteins from diverse human papillomaviruses.* Proc Natl Acad Sci U S A, 2012. **109**(5): p. E260-7.

89. Smith, S.P., et al., *Identification of host transcriptional networks showing concentration-dependent regulation by HPV16 E6 and E7 proteins in basal cervical squamous epithelial cells.* Sci Rep, 2016. **6**: p. 29832.
90. Yang, R., et al., *Combined Transcriptome and Proteome Analysis of Immortalized Human Keratinocytes Expressing Human Papillomavirus 16 (HPV16) Oncogenes Reveals Novel Key Factors and Networks in HPV-Induced Carcinogenesis.* mSphere, 2019. **4**(2).
91. Na Rangsee, N., et al., *Host proteome linked to HPV E7-mediated specific gene hypermethylation in cancer pathways.* Infect Agent Cancer, 2020. **15**: p. 7.
92. Dust, K., et al., *Human Papillomavirus 16 E6 and E7 Oncoproteins Alter the Abundance of Proteins Associated with DNA Damage Response, Immune Signaling and Epidermal Differentiation.* Viruses, 2022. **14**(8): p. 1764.
93. Gammoh, N., et al., *Regulation of human papillomavirus type 16 E7 activity through direct protein interaction with the E2 transcriptional activator.* J Virol, 2006. **80**(4): p. 1787-97.
94. Grm, H.S., et al., *Crosstalk between the human papillomavirus E2 transcriptional activator and the E6 oncoprotein.* Oncogene, 2005. **24**(33): p. 5149-64.
95. Shope, R.E. and E.W. Hurst, *Infectious Papillomatosis of Rabbits : With a Note on the Histopathology.* J Exp Med, 1933. **58**(5): p. 607-24.
96. Rous, P. and J.W. Beard, *The Progression to Carcinoma of Virus-Induced Rabbit Papillomas (Shope).* J Exp Med, 1935. **62**(4): p. 523-48.
97. Javier, R.T. and J.S. Butel, *The history of tumor virology.* Cancer Res, 2008. **68**(19): p. 7693-706.
98. Cladel, N.M., et al., *The rabbit papillomavirus model: a valuable tool to study viral-host interactions.* Philos Trans R Soc Lond B Biol Sci, 2019. **374**(1773): p. 20180294.
99. Salmon, J., et al., *Variation in the nucleotide sequence of cottontail rabbit papillomavirus a and b subtypes affects wart regression and malignant transformation and level of viral replication in domestic rabbits.* J Virol, 2000. **74**(22): p. 10766-77.
100. Selvakumar, R., et al., *Regression of papillomas induced by cottontail rabbit papillomavirus is associated with infiltration of CD8+ cells and persistence of viral DNA after regression.* J Virol, 1997. **71**(7): p. 5540-8.
101. Zhang, P., et al., *Induction of E6/E7 expression in cottontail rabbit papillomavirus latency following UV activation.* Virology, 1999. **263**(2): p. 388-94.
102. Maglennon, G.A., P. McIntosh, and J. Doorbar, *Persistence of viral DNA in the epithelial basal layer suggests a model for papillomavirus latency following immune regression.* Virology, 2011. **414**(2): p. 153-163.
103. Jeckel, S., et al., *A transactivator function of cottontail rabbit papillomavirus e2 is essential for tumor induction in rabbits.* J Virol, 2002. **76**(22): p. 11209-15.
104. Huber, E., et al., *Gene profiling of cottontail rabbit papillomavirus-induced carcinomas identifies upregulated genes directly Involved in stroma invasion as shown by small interfering RNA-mediated gene silencing.* J Virol, 2004. **78**(14): p. 7478-89.
105. Leiprecht, N., et al., *A novel recombinant papillomavirus genome enabling in vivo RNA interference reveals that YB-1, which interacts with the viral regulatory protein E2, is required for CRPV-induced tumor formation in vivo.* American journal of cancer research, 2014. **4**(3): p. 222-233.

106. Delcuratolo, M., et al., *Papillomavirus-Associated Tumor Formation Critically Depends on c-Fos Expression Induced by Viral Protein E2 and Bromodomain Protein Brd4.* PLoS Pathog, 2016. **12**(1): p. e1005366.
107. Kreider, J.W., et al., *Treatment of latent rabbit and human papillomavirus infections with 9-(2-phosphonylmethoxy)ethylguanine (PMEG).* Antiviral research, 1990. **14**(1): p. 51-58.
108. Christensen, N.D., et al., *In vivo anti-papillomavirus activity of nucleoside analogues including cidofovir on CRPV-induced rabbit papillomas.* Antiviral research, 2000. **48**(2): p. 131-142.
109. Han, R., et al., *Protection of rabbits from viral challenge by gene gun-based intracutaneous vaccination with a combination of cottontail rabbit papillomavirus E1, E2, E6, and E7 genes.* Journal of virology, 1999. **73**(8): p. 7039-7043.
110. Christensen, N.D., *Cottontail rabbit papillomavirus (CRPV) model system to test antiviral and immunotherapeutic strategies.* Antiviral chemistry & chemotherapy, 2005. **16**(6): p. 355-362.
111. Breitburd, F., et al., *Immunization with viruslike particles from cottontail rabbit papillomavirus (CRPV) can protect against experimental CRPV infection.* Journal of virology, 1995. **69**(6): p. 3959-3963.
112. Christensen, N.D., et al., *Immunization with viruslike particles induces long-term protection of rabbits against challenge with cottontail rabbit papillomavirus.* Journal of virology, 1996. **70**(2): p. 960-965.
113. Cladel, N.M., et al., *CRPV Genomes with Synonymous Codon Optimizations in the CRPV E7 Gene Show Phenotypic Differences in Growth and Altered Immunity upon E7 Vaccination.* PLOS ONE, 2008. **3**(8): p. e2947-e2947.
114. Govan, V.A., E.P. Rybicki, and A.-L. Williamson, *Therapeutic immunisation of rabbits with cottontail rabbit papillomavirus (CRPV) virus-like particles (VLP) induces regression of established papillomas.* Virology Journal, 2008. **5**(1): p. 45-45.
115. Schneider, M., et al., *Orf Virus-Based Therapeutic Vaccine for Treatment of Papillomavirus-Induced Tumors.* Journal of virology, 2020. **94**(15).
116. Rangarajan, A., *Notch signaling is a direct determinant of keratinocyte growth arrest and entry into differentiation.* EMBO J., 2001. **20**.
117. Wu, L., et al., *MAML1, a human homologue of Drosophila mastermind, is a transcriptional co-activator for NOTCH receptors.* Nature genetics, 2000. **26**(4): p. 484-489.
118. Oswald, F., et al., *p300 acts as a transcriptional coactivator for mammalian Notch-1.* Mol Cell Biol, 2001. **21**(22): p. 7761-74.
119. Krishna, B.M., *Notch signaling in breast cancer: From pathway analysis to therapy.* Cancer Lett., 2019. **461**.
120. Mittal, S., et al., *Cooperation of Notch and Ras/MAPK signaling pathways in human breast carcinogenesis.* Mol Cancer, 2009. **8**: p. 128.
121. Teodorczyk, M. and M.H.H. Schmidt, *Notching on Cancer's Door: Notch Signaling in Brain Tumors.* Front Oncol, 2014. **4**: p. 341.
122. Stylianou, S., R.B. Clarke, and K. Brennan, *Aberrant activation of notch signaling in human breast cancer.* Cancer Res, 2006. **66**(3): p. 1517-25.
123. Hayward, S.D., *Viral interactions with the Notch pathway.* Semin. Cancer Biol., 2004. **14**.
124. Ito, T., *The critical role of Notch ligand Delta-like 1 in the pathogenesis of influenza A virus (H1N1) infection.* PLoS Pathog., 2011. **7**.

125. Rizzo, P., *COVID-19 in the heart and the lungs: Could we "Notch" the inflammatory storm?* Basic Res. Cardiol., 2020. **115**.
126. Hohlfeld, R., *Myelin failure in multiple sclerosis: Breaking the spell of Notch.* Nat. Med., 2002. **8**.
127. Aparicio, E., et al., *The Notch signaling pathway: Its role in focal CNS demyelination and apotransferrin-induced remyelination.* J. Neurochem., 2013. **127**.
128. Fan, H., *Effect of Notch1 gene on remyelination in multiple sclerosis in mouse models of acute demyelination.* J. Cell Biochem., 2018. **119**.
129. Agrawal, N., et al., *Exome sequencing of head and neck squamous cell carcinoma reveals inactivating mutations in NOTCH1.* Science, 2011. **333**(6046): p. 1154-7.
130. Wang, N.J., et al., *Loss-of-function mutations in Notch receptors in cutaneous and lung squamous cell carcinoma.* Proc Natl Acad Sci U S A, 2011. **108**(43): p. 17761-6.
131. Zhang, M., et al., *Does Notch play a tumor suppressor role across diverse squamous cell carcinomas?* Cancer Med, 2016. **5**(8): p. 2048-60.
132. Zanier, K., et al., *The E6AP binding pocket of the HPV16 E6 oncoprotein provides a docking site for a small inhibitory peptide unrelated to E6AP, indicating druggability of E6.* PLoS One, 2014. **9**(11): p. e112514.
133. Brimer, N., C.M. Drews, and S.B. Vande Pol, *Association of papillomavirus E6 proteins with either MAML1 or E6AP clusters E6 proteins by structure, function, and evolutionary relatedness.* PLoS Pathog, 2017. **13**(12): p. e1006781.
134. Selvin, P.R., *The renaissance of fluorescence resonance energy transfer.* Nat Struct Biol, 2000. **7**(9): p. 730-4.
135. Lim, J., et al., *Flow cytometry based-FRET: basics, novel developments and future perspectives.* Cell Mol Life Sci, 2022. **79**(4): p. 217.
136. Banning, C., et al., *A flow cytometry-based FRET assay to identify and analyse protein-protein interactions in living cells.* PLoS One, 2010. **5**(2): p. e9344.
137. Drews, C.M., N. Brimer, and S.B. Vande Pol, *Multiple regions of E6AP (UBE3A) contribute to interaction with papillomavirus E6 proteins and the activation of ubiquitin ligase activity.* PLoS pathogens, 2020. **16**(1): p. e1008295-e1008295.
138. Mesplède, T., et al., *p53 degradation activity, expression, and subcellular localization of E6 proteins from 29 human papillomavirus genotypes.* Journal of virology, 2012. **86**(1): p. 94-107.
139. Yugawa, T., *Regulation of Notch1 gene expression by p53 in epithelial cells.* Mol. Cell Biol., 2007. **27**.
140. Yun, J., *p53 modulates notch signaling in MCF-7 Breast cancer cells by associating with the notch transcriptional complex via MAML1.* J. Cell Physiol., 2015. **230**.
141. Brimer, N., et al., *Cutaneous papillomavirus E6 oncoproteins associate with MAML1 to repress transactivation and NOTCH signaling.* Oncogene, 2012. **31**.
142. Vliet-Gregg, P.A., J.R. Hamilton, and R.A. Katzenellenbogen, *NFX1-123 and human papillomavirus 16E6 increase Notch expression in keratinocytes.* J. Virol., 2013. **87**.
143. Vliet-Gregg, P.A., J.R. Hamilton, and R.A. Katzenellenbogen, *Human papillomavirus 16E6 and NFX1-123 potentiate Notch signaling and differentiation without activating cellular arrest.* Virology, 2015. **478**.

144. Rangarajan, A., *Activated Notch1 signaling cooperates with papillomavirus oncogenes in transformation and generates resistance to apoptosis on matrix withdrawal through PKB/Akt.* Virology, 2001. **286**.
145. Ganzenmueller, T., et al., *The E7 protein of the cottontail rabbit papillomavirus immortalizes normal rabbit keratinocytes and reduces pRb levels, while E6 cooperates in immortalization but neither degrades p53 nor binds E6AP.* Virology, 2008. **372**(2): p. 313-324.
146. Muench, P., et al., *Cutaneous papillomavirus E6 proteins must interact with p300 and block p53-mediated apoptosis for cellular immortalization and tumorigenesis.* Cancer research, 2010. **70**(17): p. 6913-6924.
147. Lim, J., T. Iftner, and C. Simon, *Native Isolation of 3xHA-Tagged Protein Complexes to Characterize Protein-Protein Interactions.* Curr Protoc, 2021. **1**(2): p. e29.
148. Zanier, K., et al., *Structural basis for hijacking of cellular LxxLL motifs by papillomavirus E6 oncoproteins.* Science, 2013. **339**(6120): p. 694-8.
149. Ansari, T., N. Brimer, and S.B. Vande Pol, *Peptide interactions stabilize and restructure human papillomavirus type 16 E6 to interact with p53.* J Virol, 2012. **86**(20): p. 11386-91.
150. Zanier, K., et al., *E6 proteins from diverse papillomaviruses self-associate both in vitro and in vivo.* J Mol Biol, 2010. **396**(1): p. 90-104.
151. Roos, N., et al., *Optimized production strategy of the major capsid protein HPV 16L1 non-assembly variant in E. coli.* Protein Expr Purif, 2020. **175**: p. 105690.
152. Ton-That, H., L.A. Marraffini, and O. Schneewind, *Protein sorting to the cell wall envelope of Gram-positive bacteria.* Biochim Biophys Acta, 2004. **1694**(1-3): p. 269-78.
153. Schmohl, L. and D. Schwarzer, *Chemo-enzymatic three-fragment assembly of semisynthetic proteins.* J Pept Sci, 2014. **20**(2): p. 145-51.
154. Lebowitz, J., M.S. Lewis, and P. Schuck, *Modern analytical ultracentrifugation in protein science: a tutorial review.* Protein Sci, 2002. **11**(9): p. 2067-79.
155. Laue, T.M. and W.F. Stafford, 3rd, *Modern applications of analytical ultracentrifugation.* Annu Rev Biophys Biomol Struct, 1999. **28**: p. 75-100.
156. Howlett, G.J., A.P. Minton, and G. Rivas, *Analytical ultracentrifugation for the study of protein association and assembly.* Curr Opin Chem Biol, 2006. **10**(5): p. 430-6.
157. Cole, J.L., et al., *Analytical ultracentrifugation: sedimentation velocity and sedimentation equilibrium.* Methods Cell Biol, 2008. **84**: p. 143-79.
158. Moerke, N.J., *Fluorescence Polarization (FP) Assays for Monitoring Peptide-Protein or Nucleic Acid-Protein Binding.* Curr Protoc Chem Biol, 2009. **1**(1): p. 1-15.
159. Radek, J.T., et al., *Association of the A subunits of recombinant placental factor XIII with the native carrier B subunits from human plasma.* Biochemistry, 1993. **32**(14): p. 3527-34.
160. Zanier, K., et al., *Solution structure analysis of the HPV16 E6 oncoprotein reveals a self-association mechanism required for E6-mediated degradation of p53.* Structure, 2012. **20**(4): p. 604-17.
161. Dyson, H.J. and P.E. Wright, *Intrinsically unstructured proteins and their functions.* Nat Rev Mol Cell Biol, 2005. **6**(3): p. 197-208.
162. Vreven, T., et al., *Prediction of protein-protein binding free energies.* Protein Sci, 2012. **21**(3): p. 396-404.

163. Suarez, I.P., et al. *Structure of HPV49 E6 protein in complex with MAML1 LxxLL motif*. 2019; Available from: https://www.rcsb.org/structure/6smv.
164. Firzlaff, J.M., B. Luscher, and R.N. Eisenman, *Negative charge at the casein kinase II phosphorylation site is important for transformation but not for Rb protein binding by the E7 protein of human papillomavirus type 16.* Proc Natl Acad Sci U S A, 1991. **88**(12): p. 5187-91.
165. Massimi, P. and L. Banks, *Differential phosphorylation of the HPV-16 E7 oncoprotein during the cell cycle.* Virology, 2000. **276**(2): p. 388-94.
166. Liang, Y.J., et al., *DYRK1A stabilizes HPV16E7 oncoprotein through phosphorylation of the threonine 5 and threonine 7 residues.* Int J Biochem Cell Biol, 2008. **40**(11): p. 2431-41.
167. Nogueira, M.O., et al., *Monitoring HPV-16 E7 phosphorylation events.* Virology, 2017. **503**: p. 70-75.
168. Zine El Abidine, A., et al., *A naturally occurring variant of HPV-16 E7 exerts increased transforming activity through acquisition of an additional phospho-acceptor site.* Virology, 2017. **500**: p. 218-225.
169. Basukala, O., et al., *The HPV-18 E7 CKII phospho acceptor site is required for maintaining the transformed phenotype of cervical tumour-derived cells.* PLoS Pathog, 2019. **15**(5): p. e1007769.
170. Basukala, O., V. Sarabia-Vega, and L. Banks, *Human papillomavirus oncoproteins and post-translational modifications: generating multifunctional hubs for overriding cellular homeostasis.* Biol Chem, 2020. **401**(5): p. 585-599.

Appendix
Appendix 1

Dual-luciferase Notch Reporter Assay

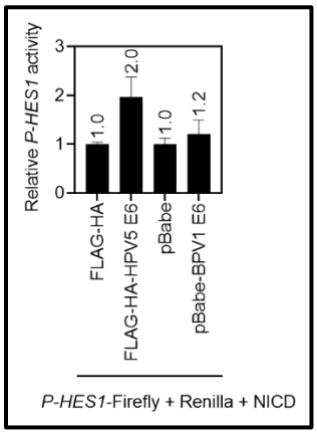

Figure 15 Dual-luciferase Notch activity. On day 1, C33A cells were seeded in a 96-wells plate, each well with 12,000 cells. The cells were co-transfected with 20 ng *P-HES1*-Luc (Notch reporter, Firefly), 10 ng pCiNeo-Rluc (Renilla), 20 ng NICD (Notch activator), 50 ng control plasmid or the respective E6 plasmid as indicated (modulator) on day 2 using jetPRIME transfection reagent, following manufacturer's protocol. After 48 hours post-transfection incubation, cells were washed in 100 µL pre-cooled PBS and lysed in 40 µL lysis buffer with gentle shaking in the cold room (4 – 8 °C) for 20 minutes before proceeding for luminescence measurement to access the *P-HES1* activity in the absence and presence of E6. The measurement was carried out with the Tecan microplate reader by first injecting 50 µL Firefly luciferase assay buffer [100 mM KH_2PO_4, 15 mM $MgSO_4$, 5 mM ATP, 1:50 luciferin] to 20 µL cell lysates, applying 1s integration to measure Firefly expression in response to *P-HES1* promotor activity. Then, another 50 µL Renilla luciferase assay buffer [Gaussia/Renilla Juice, 70 mM EDTA, 1:50 coelenterazine] was injected into each well immediately by applying 10s of waiting time for the quenching of Firefly reaction before 5s integration time to measure Renilla signal. The firefly to Renilla luciferase activity ratio was calculated and normalized to the respective control groups (FLAG-HA or pBabe). No expected repression activity was observed but rather a slight increase in the *P-HES1* promotor activity by HPV5 E6 and no impact with BPV1 E6.

Appendix 2

Expression of MBP-E6-LxxLL Proteins

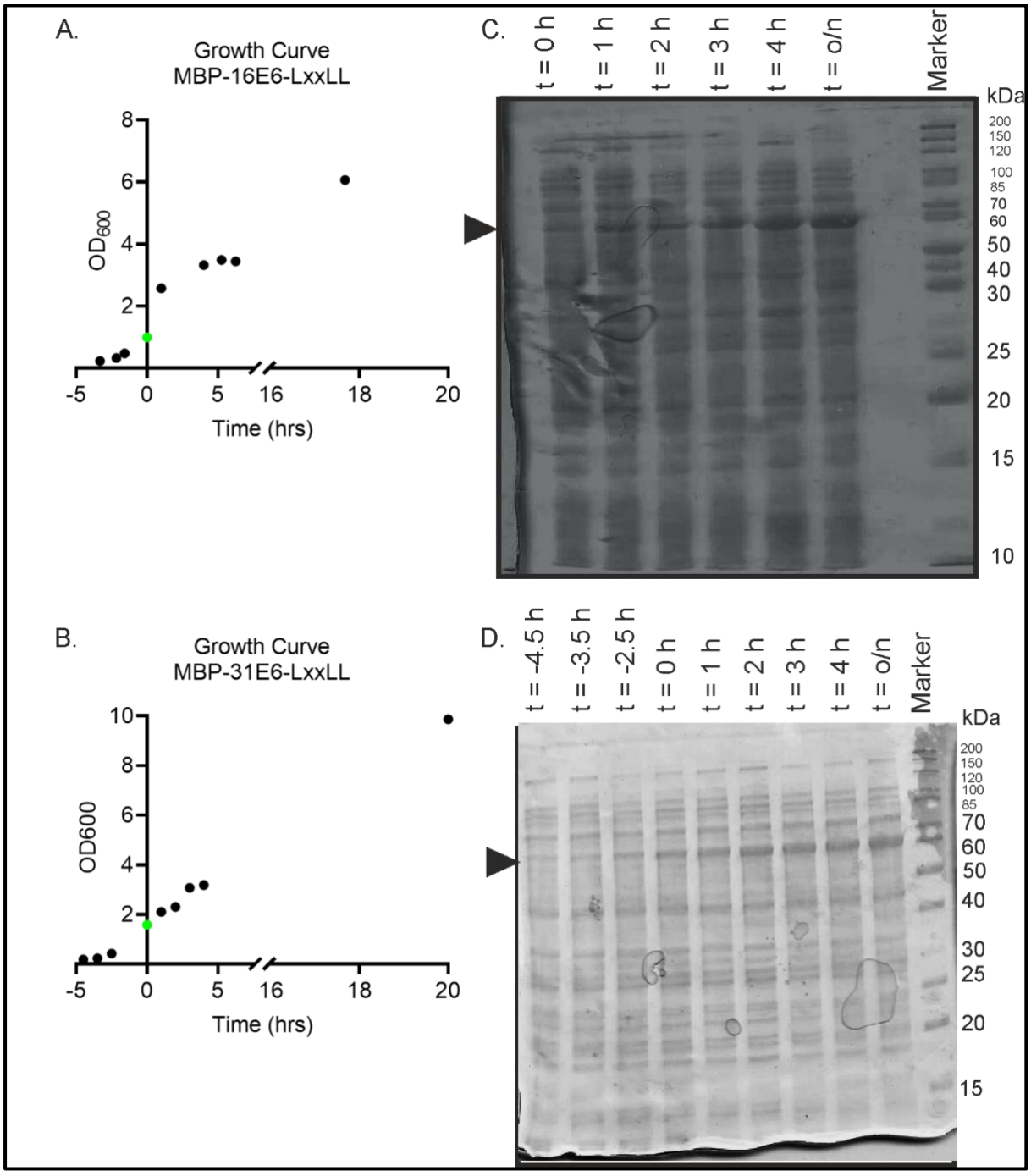

Figure 16 Expression of MBP-E6-LxxLL proteins. The bacterial growth curve of *E. coli BL21(DE3)* during expression of **A.** MBP-16E6_4C4S-LxxLL and **B.** MBP-31E6_2C2S-LxxLL with optical density measured at 600 nm plotted against the time in hours before and after induction with IPTG (green point, t = 0). The equal amount of biomass was resolved on 15 % SDS-PAGE to monitor the expression of **C.** MBP-16E6_4C4S-LxxLL and **D.** MBP-31E6_2C2S-LxxLL over time. The increase in the intensity of the protein bands at ~60 kDa upon induction indicates the expression of the protein of interest. The t = 0 is the induction timepoint.

Appendix 3

Expression of MBP-16E6_4C4S and MBP-16E6_4C4SF47R-LxxLL Proteins

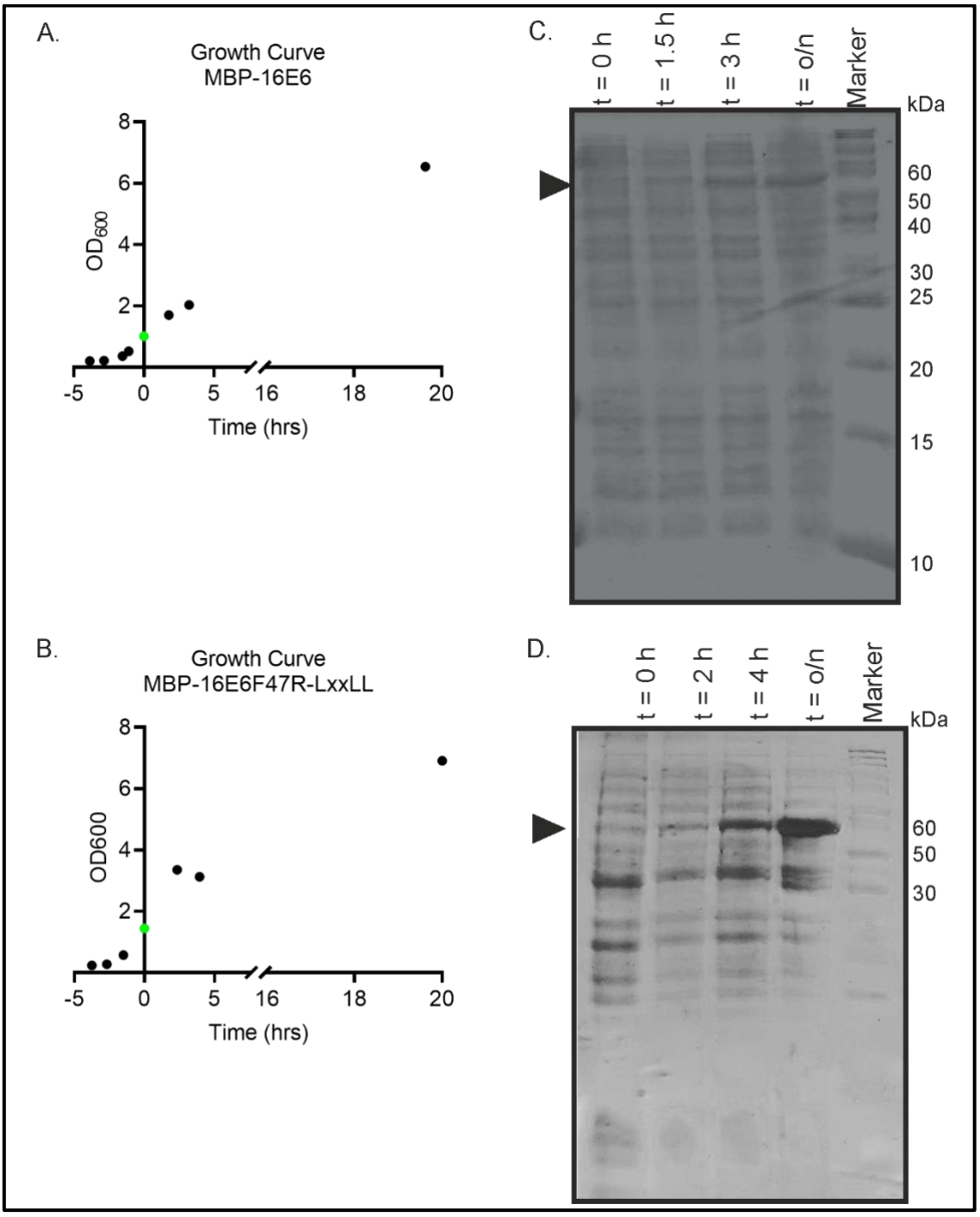

Figure 17 Expression of MBP-16E6_4C4S and MBP-16E6_4C4SF47R-LxxLL proteins. The bacterial growth curve of *E. coli BL21(DE3)* during expression of **A.** MBP-16E6_4C4S and **B.** MBP-16E6_4C4SF47R-LxxLL with optical density measured at 600 nm plotted against the time in hours before and after induction with IPTG (green point, t = 0). The equal amount of biomass was resolved on 15 % SDS-PAGE to monitor the expression of **C.** MBP-16E6_4C4S-LxxLL and **D.** MBP-16E6_4C4SF47R-LxxLL over time. The increase in the intensity of the protein bands at ~60 kDa upon induction indicates the expression of the protein of interest. The t = 0 is the induction timepoint.

Appendix 4

Purification of MBP-16E6_4C4S-LxxLL

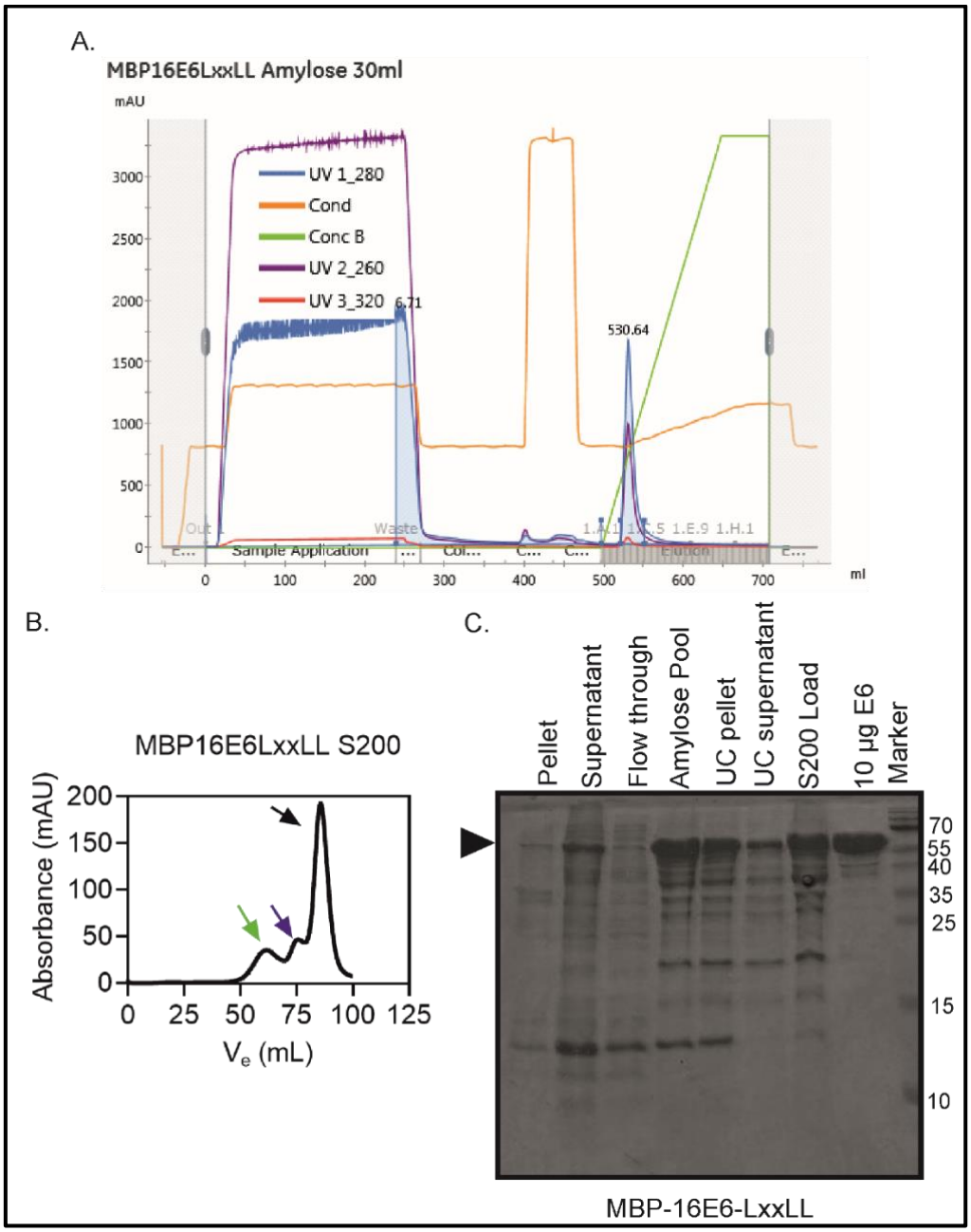

Figure 18 Purification of MBP-16E6_4C4S-LxxLL. The crude lysates were subjected to MBP affinity chromatography followed by overnight ultracentrifugation and size exclusion chromatography. **A.** Chromatogram of MBP affinity chromatography through self-packed amylose column. **B.** Chromatogram of SEC on HiLoad 16/600 Superdex 200pg column shows large molecular weight oligomers (green arrow), dimer species (purple arrow), and monomer species (black arrow). MBP-16E6_4C4S-LxxLL monomers were eluted at ~ 85.5 mL. **C.** The 8-20 % reducing SDS-PAGE shows proteins from each step of the purification. From left to the right: pellet from cell lysis, supernatant from cell lysis/load of MBP affinity chromatography, flow through from MBP affinity chromatography, fractions pool from affinity chromatography, pellet from overnight ultracentrifugation, supernatant from overnight ultracentrifugation, the load of HiLoad 16/600 Superdex 200pg column for SEC, 10 µg MBP-16E6_4C4S-LxxLL monomer and pre-stained protein ladder.

Appendix 5

Purification of MBP-31E6_2C2S-LxxLL

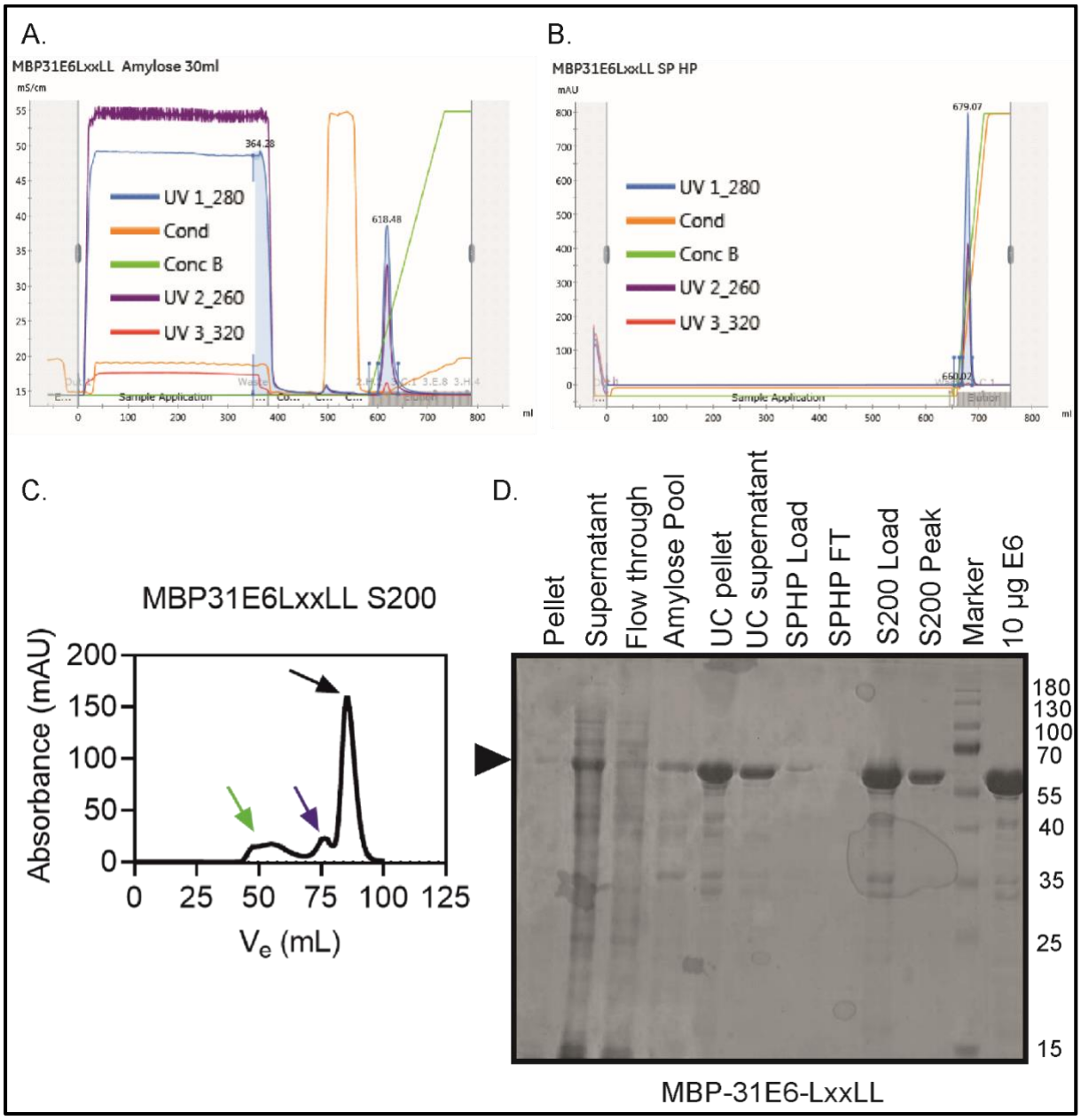

Figure 19 Purification of MBP-31E6_2C2S-LxxLL. The crude lysates were subjected to MBP affinity chromatography followed by overnight ultracentrifugation and size exclusion chromatography. **A.** Chromatogram of MBP affinity chromatography through self-packed amylose column. **B.** Chromatogram of cation exchange (SPHP). **C.** Chromatogram of SEC on HiLoad 16/600 Superdex 200pg column shows large molecular weight oligomers (green arrow), dimer species (purple arrow), and monomer species (black arrow). MBP-31E6_2C2S-LxxLL monomers were eluted at ~ 85.5 mL. **D.** The 15 % reducing SDS-PAGE shows proteins from each step of the purification. From left to the right: pellet from cell lysis, supernatant from cell lysis/load of MBP affinity chromatography, flow through from MBP affinity chromatography, fractions pool from affinity chromatography, pellet from overnight ultracentrifugation, supernatant from overnight ultracentrifugation, the load of SPHP, flow through from SPHP, the load of S200 prep SEC, the monomer peak from HiLoad 16/600 Superdex 200pg column, the pre-stained protein ladder, and 10 µg MBP-31E6_2C2S-LxxLL.

Appendix 6

Purification of MBP-16E6_4C4S

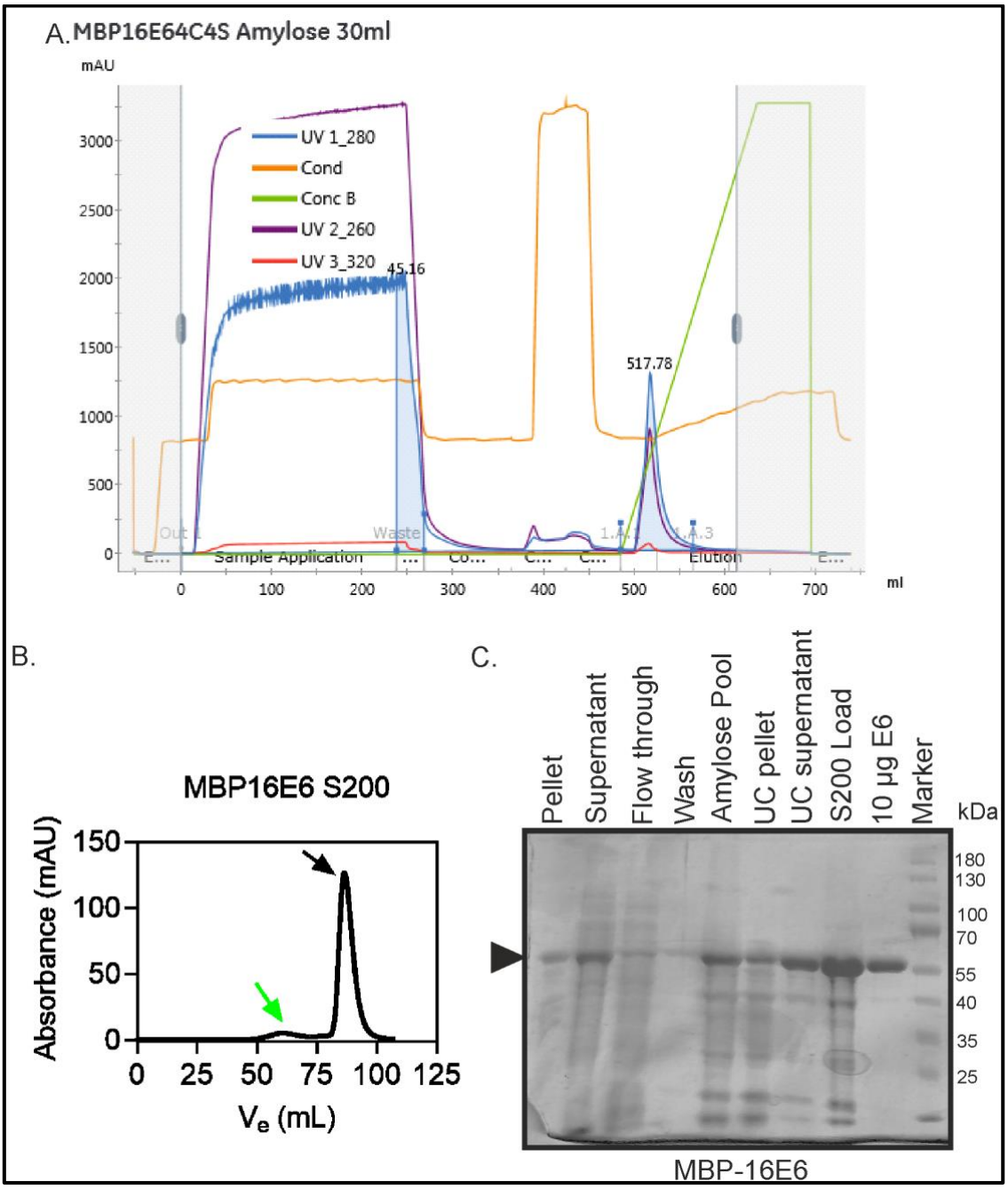

Figure 20 Purification of MBP-16E6_4C4S. The crude lysates were subjected to MBP affinity chromatography followed by overnight ultracentrifugation and size exclusion chromatography. **A.** Chromatogram of MBP affinity chromatography through self-packed amylose column. **B.** Chromatogram of SEC on HiLoad 16/600 Superdex 200pg column shows large molecular weight oligomers (green arrow) and monomer species (black arrow). MBP-16E6_4C4S monomers were eluted at ~ 86.5 mL. **C.** The 8-20 % reducing SDS-PAGE shows proteins from each step of the purification. From left to the right: pellet from cell lysis, supernatant from cell lysis/load of MBP affinity chromatography, flow through from MBP affinity chromatography, fractions pool from affinity chromatography, pellet from overnight ultracentrifugation, supernatant from overnight ultracentrifugation, the load of HiLoad 16/600 Superdex 200pg column SEC, 10 µg MBP-16E6_4C4S and pre-stained protein ladder.

Appendix 7

Purification of MBP-16E6_4C4SF47R-LxxLL

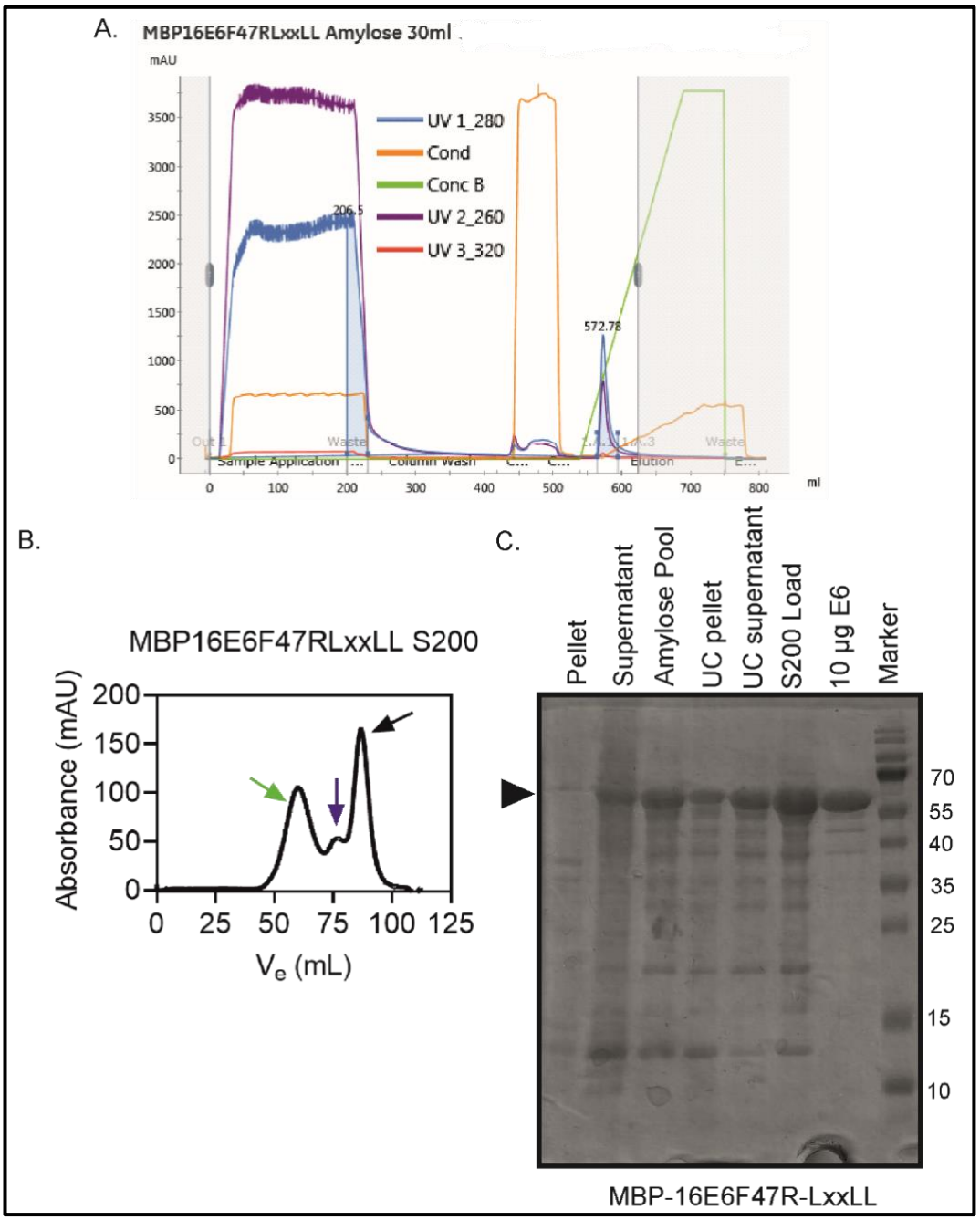

Figure 21 Purification of MBP-16E6_4C4SF47R-LxxLL. The crude lysates were subjected to MBP affinity chromatography followed by overnight ultracentrifugation and size exclusion chromatography. **A.** Chromatogram of MBP affinity chromatography through self-packed amylose column. **B.** Chromatogram of SEC on HiLoad 16/600 Superdex 200pg column shows large molecular weight oligomers (green arrow), dimer species (purple arrow), and monomer species (black arrow). MBP-16E6_4C4SF47R-LxxLL monomers eluted at ~ 85.5 mL. **C.** The 8-20 % reducing SDS-PAGE shows proteins from each step of the purification. From left to the right: pellet from cell lysis, supernatant from cell lysis/load of MBP affinity chromatography, fractions pool from affinity chromatography, pellet from overnight ultracentrifugation, supernatant from overnight ultracentrifugation, the load of HiLoad 16/600 Superdex 200pg column SEC, 10 µg MBP-16E6_4C4SF47R-LxxLL and pre-stained protein ladder. A higher proportion of oligomers that appeared for MBP-16E6_4C4SF47R-LxxLL because it was centrifuged at a lower rotation speed of 17, 000 rpm due to unsolved technical issues at the time of purification.

Appendix 8

Purification of His_6-TEV-GGG-16E7

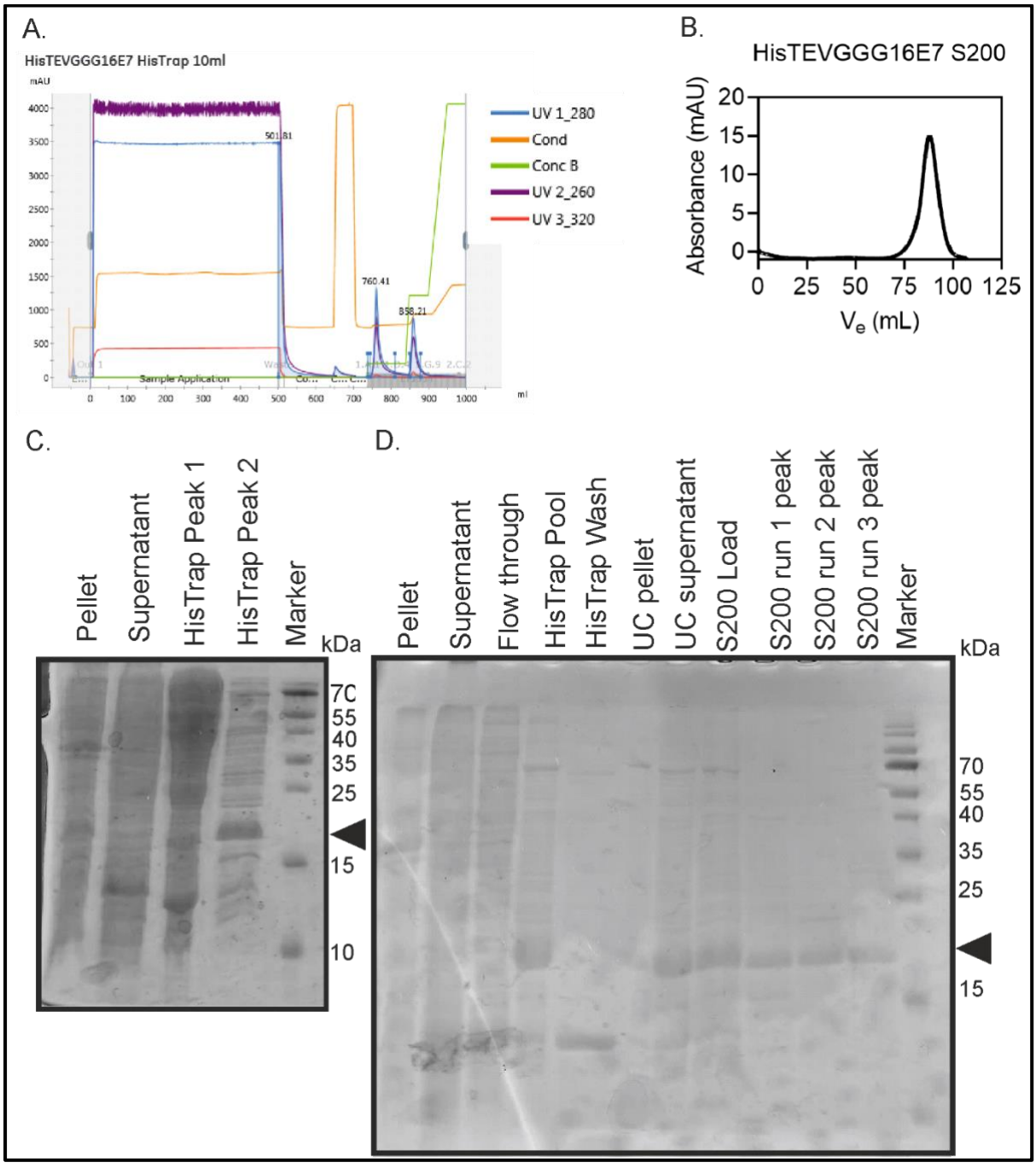

Figure 22 Purification of His_6-TEV-GGG-16E7. **A.** Chromatogram of the Ni-NTA affinity chromatography. **B.** Chromatogram of SEC on the HiLoad 16/600 Superdex 200pg column. His_6-TEV-GGG-16E7 dimers eluted at around ~88 mL. **C.** The 8-20 % reducing SDS-PAGE of His_6-TEV-GGG-16E7 from cell lysis and Ni-NTA run. From left to right: pellet from cell lysis, supernatant from cell lysis, impurities eluted with 5 % Ni-NTA buffer B (Peak 1), proteins eluted with 30 % Ni-NTA buffer B (peak 2, contains E7 proteins), and pre-stained marker. His_6-TEV-GGG-16E7 is pointed with the black arrow (between 15-25 kDa marker bands). Most of the impurities have been washed off with 25 mM imidazole (HisTrap Peak 1). **D.** The 8-20 % reducing SDS-PAGE of His_6-TEV-GGG-16E7 purification. From left to right: pellet from cell lysis, supernatant from cell lysis, flow through from Ni-NTA, fractions pooled from Ni-NTA, Ni-NTA high-salt buffer wash, pellet from overnight ultracentrifugation, supernatant from overnight ultracentrifugation, the load of S200 prep SEC, and the peak of HiLoad 16/600 Superdex 200pg column SEC. His_6-TEV-GGG-16E7 is pointed with the black arrow (between 15-25 kDa).

Appendix 9

Purification of GGG-16E7 and *Srt A* Labeling

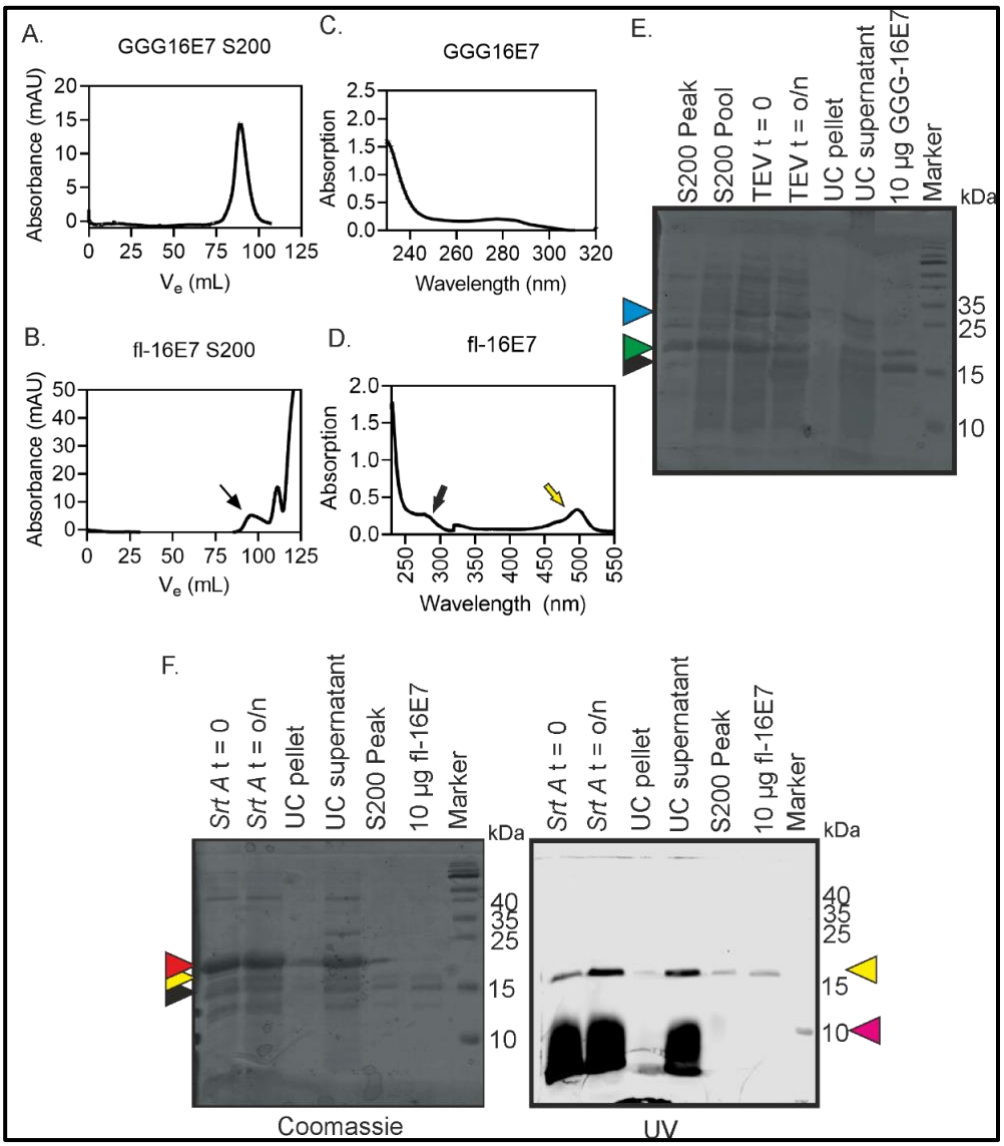

Figure 23 Purification of GGG-16E7 and fl-16E7. A, B. Chromatogram of SEC for GGG-16E7 and fl-16E7 on the HiLoad 16/600 Superdex 200pg column, respectively. GGG-16E7 dimer eluted at ~88 mL and fl-16E7 eluted at ~95 mL. Black arrow in B indicates the elution peak of fl-16E7. **C, D.** The final UV/VIS spectra of the respective purified E7 proteins at a dilution of 1:40. Data plotted are the three technical replicates. Black arrow in **D.** indicates the signal of fl-16E7 at 280 nm and yellow arrow is the fl-16E7 signal at 495 nm. **E.** The 22 % reducing SDS-PAGE shows the purification of GGG-16E7. From left to right: His_6-TEV-GGG-16E7 S200 prep peak fraction, His_6-TEV-GGG-16E7 S200 prep pool fractions, TEV cleavage at time point 0, TEV cleavage at the overnight time point, pellet from ultracentrifugation after TEV cleavage, supernatant from ultracentrifugation after TEV cleavage/load for S200 prep, 10 µg GGG-16E7, pre-stained protein ladder. The cyan arrow is the TEV protease, the green arrow is the His_6-TEV-GGG-16E7 and the black arrow is the GGG-16E7. **F.** The 22 % reducing SDS-PAGE shows labeling of fl-16E7. From the left to right: *Srt A* labeling reaction at time point 0, *Srt A* labeling reaction at the overnight time point, pellet from ultracentrifugation after *Srt A* reaction, supernatant from ultracentrifugation after *Srt A* reaction/load for HiLoad 16/600 Superdex 200pg column, S200 peak for fl-16E7, 10 µg fl-16E7, pre-stained protein ladder. The coomassie stained reducing SDS-PAGE (left) and the same reducing SDS-PAGE illuminated with UV light for detecting fluorescein signal before the gel was stained (right) show the protein bands of 16E7 before and after the *Srt A* labeling. The red arrow is the *Srt A*, the yellow arrow is the fl-16E7, the black arrow is the GGG-16E7, and the magenta arrow is the free fluorescein.

Appendix 10

Purification of His_6-TEV-GGG-31E7

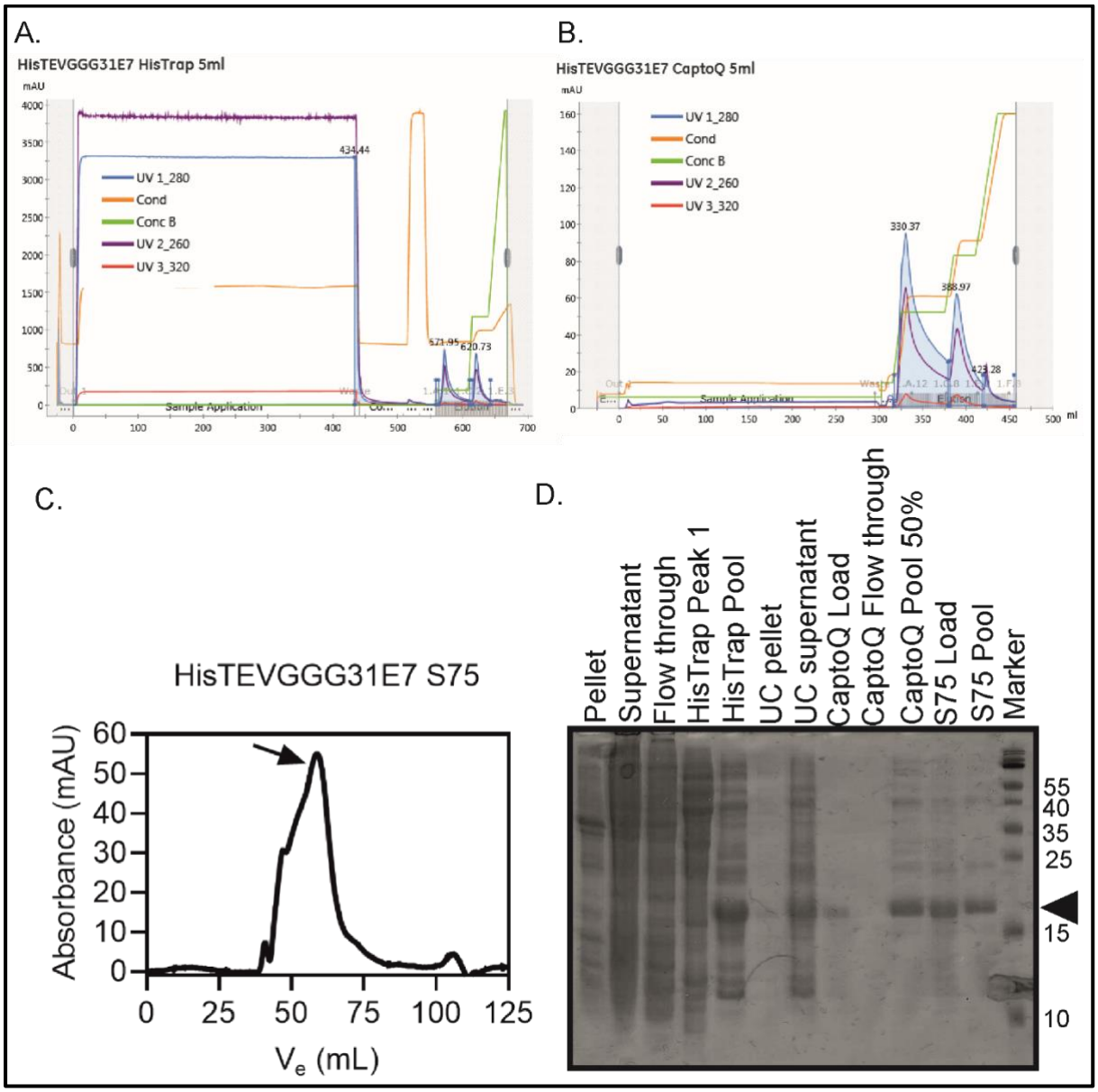

Figure 24 Purification of His_6-TEV-GGG-31E7. **A.** Chromatogram of the Ni-NTA affinity chromatography. **B.** Chromatogram of anion exchange (Capto Q). **C.** Chromatogram of SEC on the HiLoad 16/600 Superdex 75pg column. The black arrow pointed the His_6-TEV-GGG-31E7 dimer which eluted at ~60 mL. **D.** The 18 % reducing SDS-PAGE of His_6-TEV-GGG-31E7. From left to right: pellet from cell lysis, supernatant from cell lysis, flow through from Ni-NTA, impurities eluted with 5 % Ni-NTA buffer B (Peak 1), proteins eluted with 30 % Ni-NTA buffer B (peak 2, contains E7 proteins, the pool), pellet from overnight ultracentrifugation, supernatant from overnight ultracentrifugation, load for AEX CaptoQ, flow through from AEX Capto Q, fractions pool from AEX Capto Q, the load of S75 prep SEC, and the pool fractions of S75 prep SEC, pre-stained protein ladder. His_6-TEV-GGG-31E7 is pointed with the black arrow (between 15-25 kDa).

Appendix 11

Purification of GGG-31E7 and *Srt A* Labeling

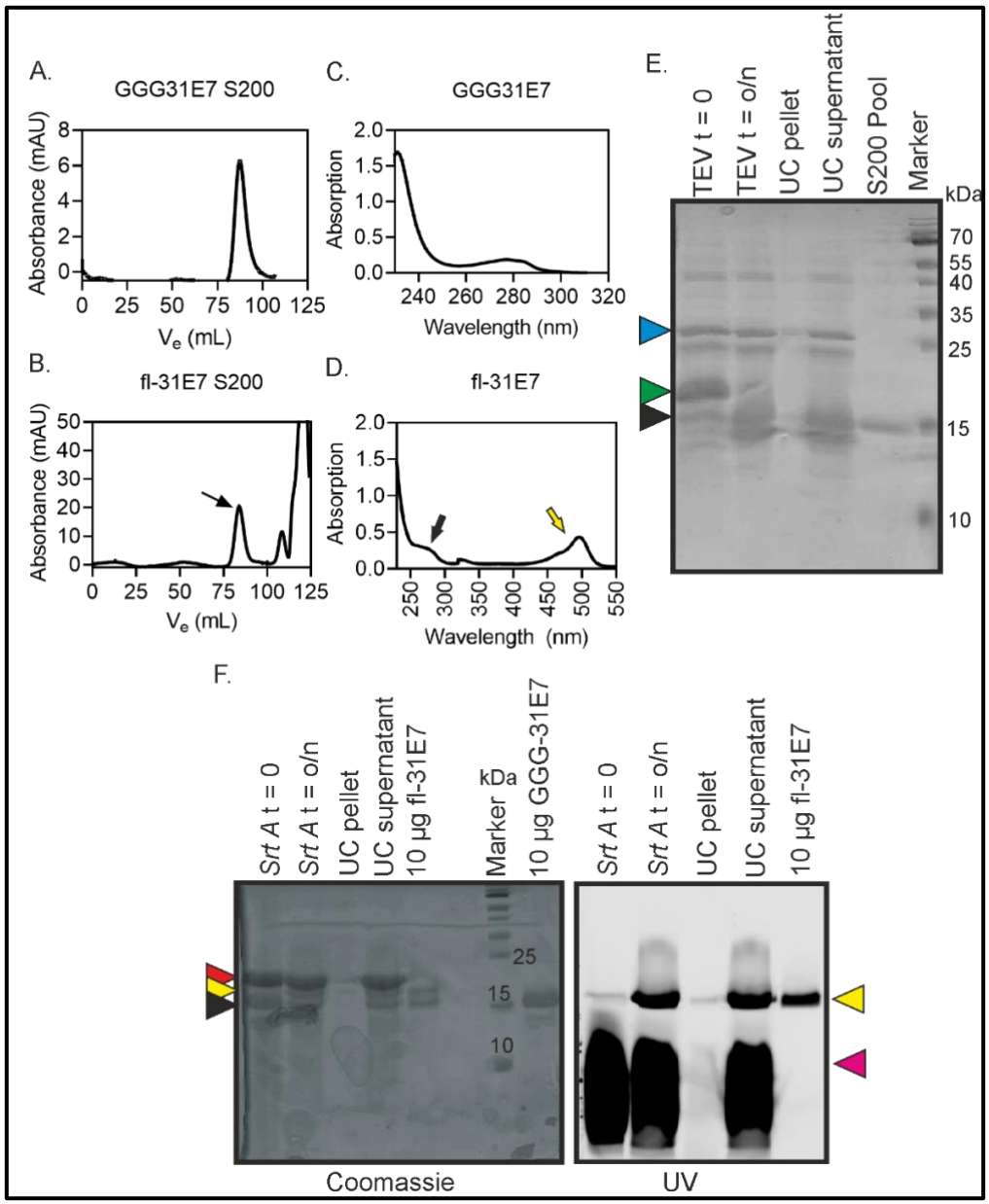

Figure 25 A, B. Chromatogram of SEC for GGG-31E7 and fl-31E7 on the HiLoad 16/600 Superdex 200pg column, respectively. Black arrow in B indicates the elution peak of fl-31E7. **C, D.** The final UV/VIS spectra of the respective purified E7 proteins at a dilution of 1:40. Data plotted are the three technical replicates. Black arrow in **D.** indicates the signal of fl-16E7 at 280 nm and yellow arrow is the fl-16E7 signal at 495 nm. **E.** The 18 % reducing SDS-PAGE shows the purification of GGG-31E7. From left to right: His_6-TEV-GGG-31E7 TEV cleavage at time point 0, TEV cleavage at the overnight time point, pellet from ultracentrifugation after TEV cleavage, supernatant from ultracentrifugation after TEV cleavage/load for S200 prep, pre-stained protein ladder. The cyan arrow is the TEV protease, the green arrow is the His_6-TEV-GGG-31E7 and the black arrow is the GGG-31E7. **F.** The 18 % reducing SDS-PAGE shows labeling of fl-31E7. From the left to right: *Srt A* labeling reaction at time point 0, *Srt A* labeling reaction at the overnight time point, pellet from ultracentrifugation after *Srt A* reaction, supernatant from ultracentrifugation after *Srt A* reaction/load for S200 prep, 10 µg fl-31E7, empty well, pre-stained protein ladder, 10 µg GGG-31E7. The coomassie stained reducing SDS-PAGE (left) and the same reducing SDS-PAGE illuminated with UV light for detecting fluorescein signal before the gel was stained (right). The red arrow is the *Srt A*, the yellow arrow is the fl-31E7, the black arrow is the GGG-31E7, and the magenta arrow is the free fluorescein.

Appendix 12

Determination of the Optimal Concentration for fl-E7

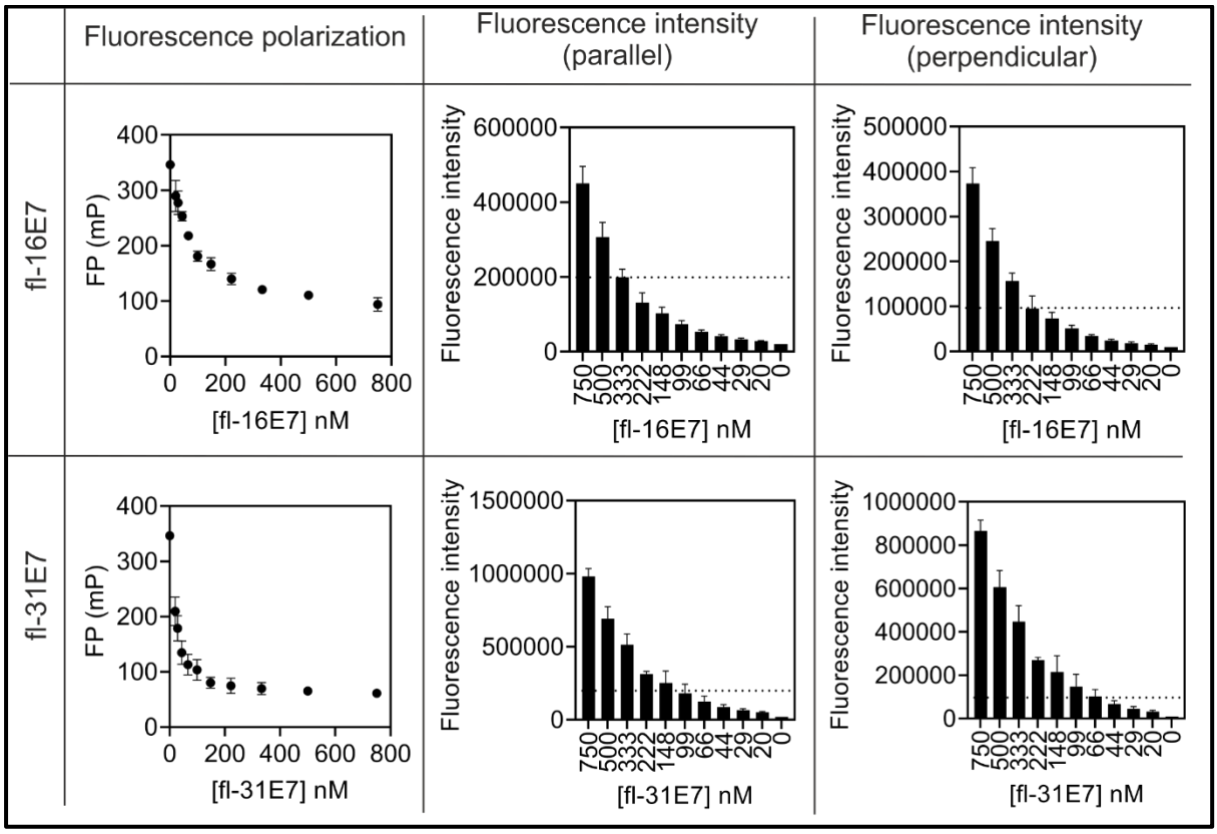

Figure 26 Titration of fl-E7 for fluorescence polarization. The fl-16E7 (top) and fl-31E7 (bottom) were titrated 1.5-fold from 750 nM. The fluorescence polarization signal (column 1), the fluorescence intensity of the parallel (column 2) and perpendicular (column 3) emitted polarized lights were assessed to determine the lowest optimum concentration of fl-E7 that exert a low FP signal. Therefore, at least 333 nM of fl-16E7 and 148 nM of fl-31E7 gave the lowest basal FP signal. The lowest concentrations that gave a fluorescence intensity (parallel and perpendicular) that are 10-fold higher than buffer signals (dotted line) were considered for the optimum condition to ensure a low signal-to-noise ratio. Finally, 350 nM of fl-16E7 and 200 nM of fl-31E7 were chosen for the fluorescence polarization experiment.

Appendix 13

Fluorescence Polarization Fitted with Specific Binding – Hill Slope

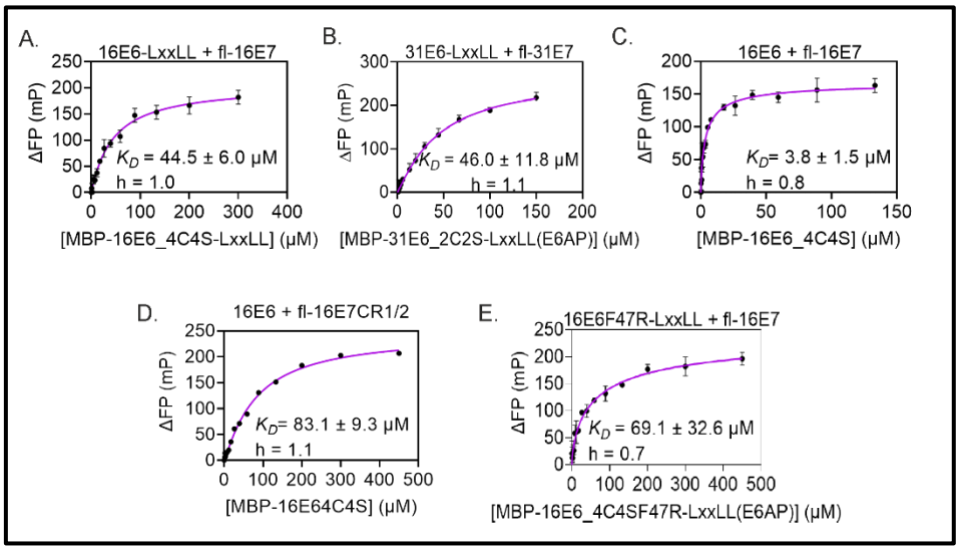

Figure 27 Fluorescence polarization data fitted with Specific binding-Hill slope model. All direct measurement data were fitted with the Specific binding-Hill slope model to calculate the binding affinities. A hill coefficient (h) of 1.0 indicates a monomer bind with no cooperativity to one site. When h > 0 with a sigmoidal curve indicates the receptor or ligand exerts multiple binding sites with positive cooperativity. An h that is less than 0 indicates the presence of multiple binding sites with different affinities for ligand or negative cooperativity is present. **A**. The h = 1.0 indicate no cooperative binding. **B** and **D** show h = 1.1 but they may not be significant to indicate a positive cooperative binding as the sigmoidal patterns were not observed with the fit. **C** and **E** show an h < 0 with binding affinity exert variation of more than 40 % thus they are not significant to conclude a negative cooperative binding. Thus, the cooperative binding in all complexes could not be concluded with Specific binding with Hill slope model.

Table 4 The summary of binding affinity (K_D), hill coefficient and coefficient of determination of each FP dataset obtained from Specific binding with the Hill slope model. The binding affinity obtained from all different complexes are similar to the binding affinity calculated from the One site-Specific binding model.

Model	One site-Specific	Specific binding with Hill slope		
Complex	K_D (μM)	K_D (μM)	Hill coefficient (h)	Coefficient of Determination (R^2)
fl-16E7/MBP-16E6_4C4S-LxxLL	46.4 ± 0.9	44.5 ± 6.0	1.0	0.97
fl-16E7/MBP-31E6_2C2S-LxxLL	59.4 ± 2.5	46.0 ± 11.8	1.1	0.97
fl-16E7/MBP-16E6_4C4S	3.0 ± 0.1	3.8 ± 1.5	0.8	0.91
fl-16E7CR1/2/MBP-16E6_4C4S-LxxLL	101.3 ± 2.3	83.1 ± 9.3	1.1	0.97
fl-16E7/MBP-16E6_4C4SF47R-LxxLL	32.3 ± 0.9	69.1 ± 32.6	0.7	0.96

Appendix 14

Expression of 16E7CR3 (45-98) Proteins

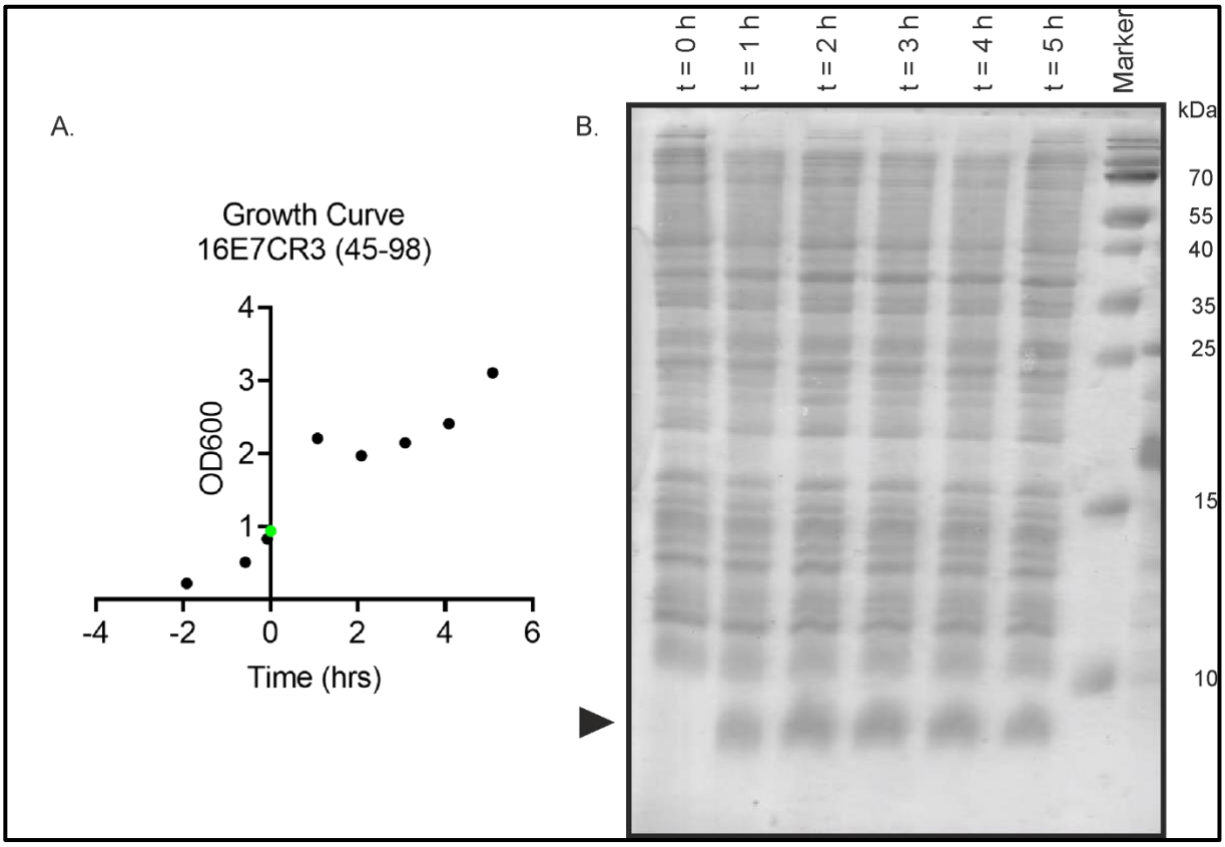

Figure 28 Expression of 16E7CR3 (45-98) proteins. The bacterial growth curve of *E. coli BL21(DE3)* during expression of 16E7CR3 (45-98) in M9 medium with optical density measured at 600 nm plotted against the time in hours before and after induction with IPTG (green point, t = 0). Proteins was expressed at 37 °C for 5 hours. B. The equal amount of biomass was resolved on 22 % SDS-PAGE to monitor the expression of 16E7CR3 (45-98) over time. The increase in the intensity of the protein bands slightly below the 10 kDa marker band upon induction indicates the expression of the protein of interest. The t = 0 is the induction timepoint.

Appendix 15

Purification of 16E7CR3 (45-98) Proteins

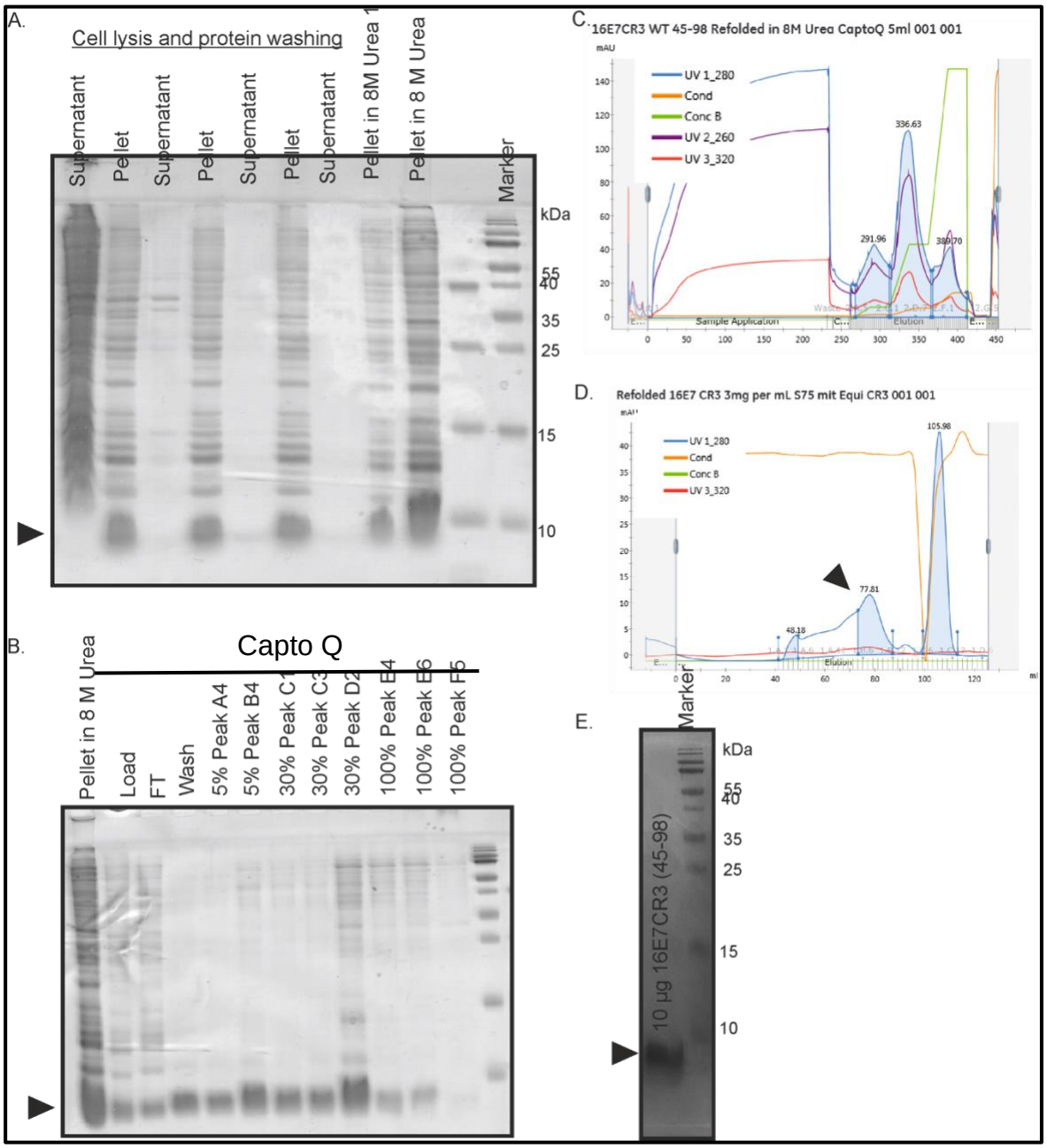

Figure 29 Purification of 16E7CR3 (45-98). **A.** The 22% reducing SDS-PAGE of 16E7CR3 (45-98) from washing steps in lysis buffer (50 mM Tris-HCl pH 8 at 8 °C, 300 mM NaCl, 3 mM $MgCl_2$, 10 µM $ZnCl_2$, 5 % (v/v) glycerol, 1 mM TCEP. From left to right: supernatant and pellet from cell lysis followed by the pellet and supernatant obtained from the three times washing steps. The cleaned inclusion bodies were solubilized in a buffer containing 20 mM Tris-HCl pH 8 at 8°C, 150 mM NaCl, 8M Urea, 10 µM $ZnCl_2$ and 1 mM TCEP. **B.** The 22 % reducing SDS-PAGE of 16E7CR3 (45-98) from anion exchange (Capto Q). The protein eluted in the wash, 5 % and 25% buffer B were pooled for on-column refolding using HiLoad 16/600 Superdex 75pg column. **C.** Chromatogram of anion exchange (Capto Q) run. Proteins were diluted with buffer A, 20 mM Tris-HCl pH 8 at 8 °C, 1 mM TCEP) to obtained 20 mM NaCl concentration. The proteins were eluted with gradient from 5 – 100% buffer B (Buffer A + 1M NaCl). **D.** On-column refolding of 16E7CR3 (45-98) in HiLoad 16/600 Superdex 75pg column. Each time, 3 mL of 3 mg/mL proteins were loaded. The 16E7CR3 (45-98) eluted at ~78 mL is a dimer according to our group's column calibration analysis template. **E.** Ten microgram of 16E7CR3 (45-98) showed high purity of the proteins.

Author Contribution

Lim, J., Frecot, D. I., Stubenrauch, F., Iftner, T., & Simon, C. (2022). Cottontail rabbit papillomavirus E6 proteins: Interaction with MAML1 and modulation of the Notch signaling pathway. Virology, 576, 52–60.

JL provided the conception of the project. JL designed the cloning of all constructs and cloned all constructs with DIF. JL designed, performed and analyzed data from all experiments. JL wrote the manuscript with CS. FS and TI validated the data and contributed to the writing and review of the manuscript. CS provided the conception of the project and the intellectual contribution to experimental design and data interpretation.

Lim, J., Straub, E., Stubenrauch, F., Iftner, T., Schindler, M., & Simon, C. (2022). An enhanced triple fluorescence flow-cytometry-based assay shows differential activation of the Notch signaling pathway by human papillomavirus E6 proteins. Scientific Reports, 12(1), 1–13.

JL provided the conception of the project. JL designed and performed the cloning of all constructs. JL designed, performed and analyzed data from all experiments. ES contributed to the protocol and assisted with the immunofluorescence and RT-PCR during manuscript revision. JL wrote the manuscript with CS. FS, TI and MS validated the data and contributed to the writing and review of the manuscript. CS provided the conception of the project and the intellectual contribution to experimental design and data interpretation.

Lim, J., Iftner, T., & Simon, C. (2021). Native Isolation of 3×HA-Tagged Protein Complexes to Characterize Protein-Protein Interactions. *Current Protocols*, *1*(2), 1–20.

JL designed, performed and analyzed data from all experiments. JL wrote the manuscript with CS. TI validated the data and contributed to the writing and review of the manuscript. CS provided the conception of the project and the intellectual contribution to experimental design and data interpretation.

Lim, J., Lilie, H., Kalbacher, H., Roos., N, Frecot, D. I., Feige. M., Conrady, M., Votteler, T., Cousido-Siah, A., Corradini Bartoli, G., Iftner, T., Trave, G., & Simon, C. Evidence for direct interaction between the oncogenic proteins E6 and E7 of high-risk human papillomavirus (HPV). J Biol Chem, 2023. **299**(8): p. 104954.

JL provided the conception of the project. JL designed the constructs used in FACS-FRET and cloned them together with TV. JL cloned all 16E6 constructs used in *E.coli* expression. JL expressed all E6 proteins. NR expressed E7 full-length proteins, assisted by DIF and MF. JL purified all E6 and E7 proteins. HK synthesized 16E7 CR1/2 peptide. NR expressed *Sortase A* and DIF purified *Sortase A*. TV expressed and purified TEV proteases. MC expressed and purified MBP proteins. ACS contributed to the purification protocol and the professional guidance and advice for E6 purification as well as reviewed the manuscript. JL designed, performed and analyzed data for FACS-FRET, CoIP, and fluorescence polarization. HL performed and analyzed AUC data. GCB, MC, DIF and TV conducted some preliminary experiments. JL wrote the manuscript with CS. TI validated the data and contributed to the review and writing of the manuscript. CS provided the conception of the project. GT and CS provided the intellectual contribution to data interpretation as well as review and writing the manuscript.

Ongoing research

JL and CS provided the conception of the project. JL designed, performed and analyzed data from all experiments. CS provided the intellectual contributions to data interpretation.

Acknowledgments

I would like to thank **Prof. Iftner** for the opportunity studying my Ph.D. at the Institute of Medical Virology, being there especially the last year to support. A big thanks to **Dr. Claudia Simon** for her never-ending guidance, advice, encouragement, and confidence to achieve all my goals. This journey wouldn't have been possible without her unconditional support, trust, and patience. I would like to extend my appreciation to **Dr. Nora Roos** for her assistance in the lab, especially at the ÄKTA and the fermenter, and **Desiree Frecot**, **Maximillian Feige**, **Marcel Conrady**, and **Tobias Votteler** for contributing to the project of E6/E7 complex.

I thank **Prof. Stehle** for being one of my supervisors, and not to forget his post-doc, **Dr. Christoph Schall**, for his assistance at the fermenter. I thank **Elke Straub** and **Franziska Kühner** for taking care of my cells whenever I am absent from any unexpected event. I thank **Prof. Schindler** and his students, **Maximillian Bunz** and **Dr. Ramona Businger**, for their advice and discussion on the flow-cytometry data. I want to thank **Dr. Iwan Grin**, **Dr. Fabian Renscheler**, and **Dr. Karolin Leibiger**, who always supply me with materials in urgent need. I thank **Prof. Schwarzer** for providing me with fluorescein dye and **Prof. Hubert Kalbacher**, who gave all out to synthesize the peptides I used in the FP assays at zero cost. I would also like to thank **Prof. Hauke Lilie** for the AUC data. A special thanks to **Prof. Gilles Trave** for all the advice and discussion on the E6/E7 complex, **Alexandra Cousido-Siah**, who worked on the X-ray crystallography for E6/E7 complex, and **Dr. Gergo Gogl** for his valuable comments on the FP data. I would also like to thank **Dr. Murielle Masson** for the cells she provided in two publications. I also thank **Prof. Scott vande Pol** for his advice on the dual-luciferase Notch assay. I thank **Prof Jörg Matin** and **Astrid Ursinus** for the MST and CD measurement, **Dr. Marcus Hartmann** for the possibility to use their HiLoad 16/600 Superdex 30 pg, and **Prof. Roberta Pieratelli** for the 16E7CR3 plasmid. Though the following experiment didn't work, I would like to take still this opportunity to thank **Prof. Charlotte Uetrecht** and **Kira Schamoni** for their effort on the native MS;

A special thanks to all former members of AG Simon, in addition to all that I have mentioned above, **Anna Ohmayer**, **Bastian Breiner**, **Christine Zarges**, **Domenic Ebert**, **Laura Pfeiffer**, as well as **Karin Kegreiß**, **Silke Endres** for all the support and the great memories we created in the last few years.

I want to acknowledge my family, especially my parents, for their enduring support of me during my Ph.D. studies. Furthermore, I thank all my friends for their support and understanding throughout these years, especially **Kim Mei Loh** who proofread part of this work. I would like to mention **the late Jian Bor Lew**, my best friend for 20 years, and **the late Jin Tong Lim**, my wonderful cousin for the last 21 years, who both I lost recently, for all the fond memories and wishes I have with them in the past years.

scientific reports

Check for updates

OPEN

An enhanced triple fluorescence flow-cytometry-based assay shows differential activation of the Notch signaling pathway by human papillomavirus E6 proteins

JiaWen Lim, Elke Straub, Frank Stubenrauch, Thomas Iftner, Michael Schindler & Claudia Simon✉

Human papillomaviruses are DNA tumor viruses. A persistent infection with high-risk HPV types is the necessary risk factor for the development of anogenital carcinoma. The E6 protein is a viral oncoprotein that directly interacts with different cellular regulatory proteins mainly affecting the cell cycle, cellular differentiation and polarization of epithelial cells. In dependency of the phylogenetic classification of HPV different interaction partners of E6 have been described. The Notch pathway seems to be one common target of HPV, which can be up or down regulated by different E6 proteins. Our novel triple fluorescence flow-cytometry-based assay allows a semi-quantitative comparison of the E6 proteins´ effect on the Notch pathway using a Notch-responsive reporter plasmid. As a result, all E6 proteins of beta-HPV repressed the Notch reporter expression, of which HPV38 E6 showed the greatest repression potential. In contrast, alpha-HPV E6 of HPV16, activates the reporter expression most significantly, whereas E6 of HPV31 and low-risk HPV6b showed significant activation only in a p53-null cell line. Interestingly, HPV18 E6, with the second highest carcinogenic risk, shows no effect. This high divergence within different genus of HPV is important for targeting the Notch pathway regarding a potential HPV therapy.

Promotor activity assays are indispensable to study the regulation of gene expression. Commonly, the gene of interest is replaced by a reporter gene, whose expression is then under the control of regulatory region of the original gene of interest resulting in a reporter plasmid. Reporter genes are usually enzymes such as luciferases for bioluminescence, beta-galactosidases or beta-glucuronidase for absorbance or fluorescence; or fluorescent proteins (FP). Commonly, dual reporter systems, such as dual luciferase assay, dual FPs or combinations are applied in order to account for promotor activity and variations in transfection efficiency. Cell lysis is required in most dual luciferase-based assays prior to measurement, i.e. lysis efficiency is a further variable in these assays. Compared with luciferase enzymes, FPs do not require co-factors or substrates for their fluorescence activity and can be monitored in living cells. On the other hand, modulatory proteins, which affect the expression of the gene of interest, are co-transfected with the reporter plasmid. However, the expression level of modulatory proteins can differ from experiment to experiment and between different modulatory proteins. With flow-cytometry, the expression level of the modulatory protein genetically fused to a specific fluorescent protein could be easily identified and examined with an appropriate laser. The application of flow-cytometry combined with FPs allows to monitor single cells, excludes dead cells as well as non-transfected cells and can significantly lower the background.

Proteins are expressed at different amounts and have different turnover rates in cells meaning that just transfecting the same amount of DNA does not result in same protein levels of different proteins or protein variants. In order to compare the effect of different modulatory proteins on reporter gene expression, a quantitative assessment of the amount of modulatory protein is necessary. Concomitant western blot analysis can determine the protein amount of modulatory proteins. This analysis is offline to the promotor activity measurement, necessitates Western Blot validations of each target for quantitative analysis and is time consuming. Further, low

Institute of Medical Virology and Epidemiology of Viral Diseases, University Hospital Tuebingen, Tuebingen, Germany. ✉email: Claudia.simon@med.uni-tuebingen.de

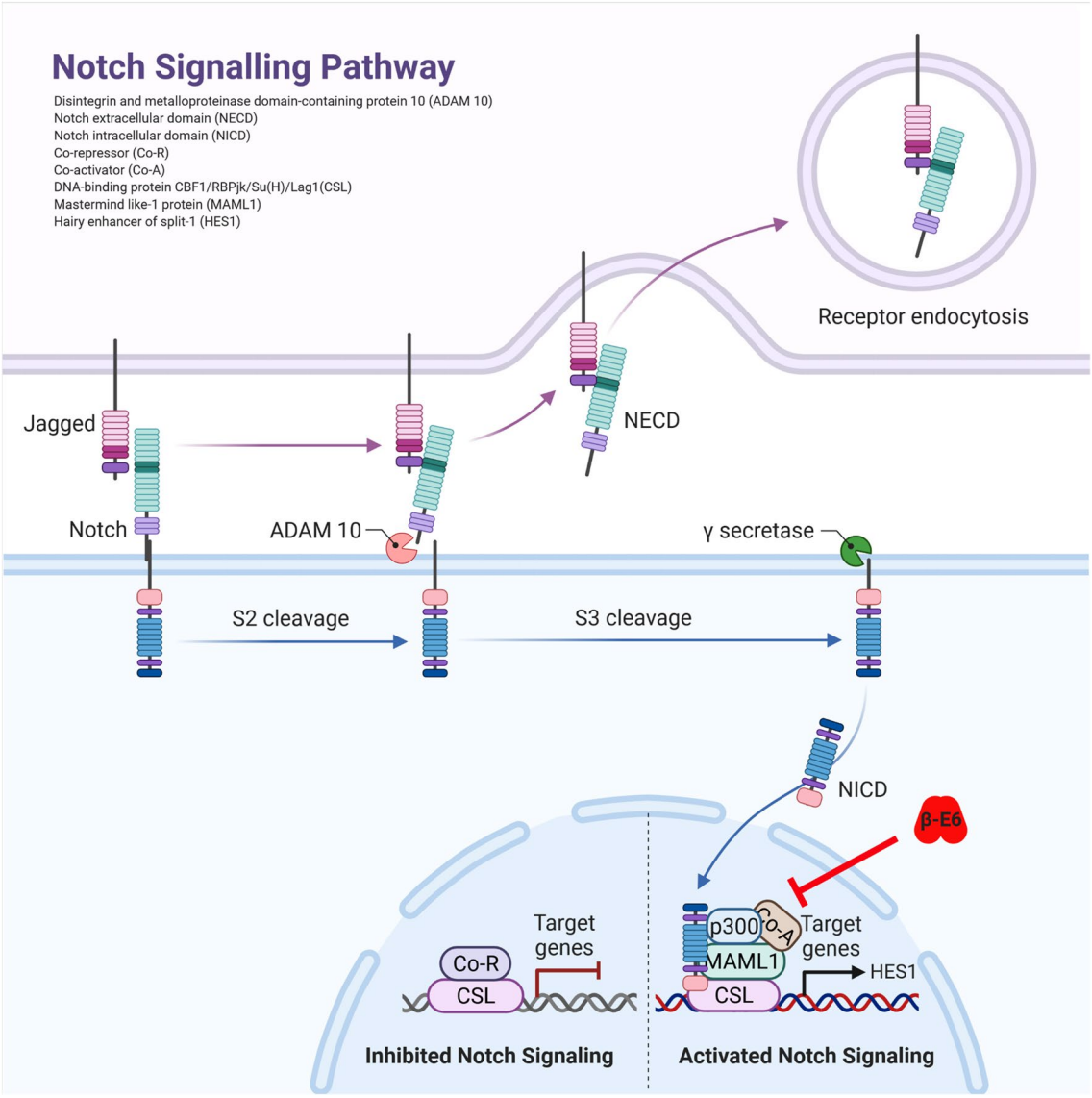

Figure 1. Scheme of the Notch signaling pathway. The Notch receptor is cleaved at S2 cleavage site by ADAM 10 protease upon binding to Notch ligand, Jagged from neighboring cells. Thus, releasing Notch extracellular domain (NECD) for receptor endocytosis. Cleavage of Notch intracellular domain (NICD) at S3 cleavage site by γ secretase leads to the translocation of NICD into nucleus. NICD then recruits MAML1, p300, CSL and other co-activators to activate the expression of Notch target gene, *HES1*. Beta HPV E6 protein associates with MAML1 and inhibits Notch Signaling. Adapted from "Notch Signaling Pathway", by BioRender.com (2020). Retrieved from https://app.biorender.com/biorender-templates.

co-transfection efficiency of plasmid DNA or low expression yields and high turnover rates of the modulatory proteins can deteriorate the signal-to-noise ratio of the reporter assay because of e.g. the high number of cells negative for the modulatory protein. To reduce this background, flow-cytometry is feasible to identify cells, which express the modulatory protein genetically fused to FPs, and monitor the reporter activity only in these positive cells.

The highly conserved Notch signaling pathway plays an important role in cell proliferation and differentiation[1]. Miss-signaling is associated with cancer progression[3], several diseases as e.g. multiple sclerosis[4–6], as well as viral infections[7–10]. Therefore, the Notch signaling pathway is considered as a potential drug target to treat associated diseases. The signaling is triggered by direct cell-to-cell contact (Fig. 1). The activated Notch-receptor undergoes proteolytic cleavage resulting in the release of the Notch intracellular domain (NICD) to the nucleus[11]. The NICD binds to other cellular proteins (MAML1, p300, Co-Activator) recruiting the initiation complex of e.g. *HES1* gene transcription. The effect of modulatory factors such as drugs, viral or cellular proteins on the Notch signaling pathway can be monitored by measuring the *HES*1 promotor activity (*P-HES1*). In cell culture, Notch signaling pathway can be triggered by either co-culturing jagged cells, expressing the jagged protein as a Notch-receptor ligand on the cell surface (Fig. 1), or co-transfecting the NICD as an exogenous activator[12]. The second approach, however, does not allow monitoring effects upstream of NICD cleavage by gamma-secretase[13]. There are over 200

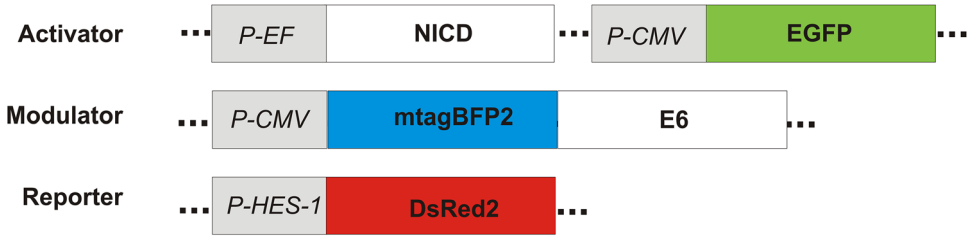

Figure 2. Constructs of triple fluorescence flow-cytometry-based assay to analyze *P-HES1* activity. Three plasmids are co-transfected: (I) activator plasmid with two open reading frames encoding the Notch intracellular domain (NICD) as the activator of the Notch pathway and the EGFP as transfection control for the activator plasmid. (II) the modulator plasmid, encoding the modulator protein of interest E6, which is N-terminally fused to mTagBFP2 to monitor E6 expression. (III) the reporter plasmid encoding for the reporter DsRed2. The expression of DsRed2 is under control of the *HES1* promotor which is regulated by the Notch pathway. Picture was created with CorelDRAW X7, version 17.5.0.907.

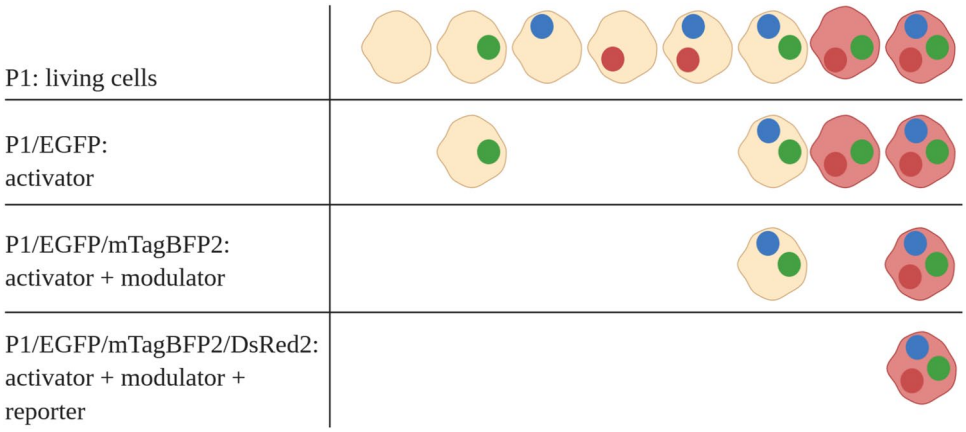

Figure 3. Schematic triple gating strategy. Living cells are first identified by FSC/SSC gating followed by specific inclusions of cells that are transfected with the activator plasmid (EGFP + cells). Next step is to gate on EGFP/mTagBFP2 to only monitor cells that have been transfected with the activator and the modulator (EGFP + /mTagBFP2 + cells). Then, Notch-activation is assessed in this population by measuring the DsRed2 expression (EGFP + /mTagBFP2 + /DsRed2 + cells). Picture was created with BioRender.com.

types of human papillomaviruses (HPV), of which only some repress the Notch pathway. Types of the beta genus interfere with Notch signaling via the interaction of the viral protein E6 with proteins of the transcription initiation complex for Notch-responsive expression as of *HES1*[12,14–16]. In contrast, it has been reported, that HPV16 found in 50% of all cervical cancer[17], shows an upregulation of HES1 and Notch in cervical cancer cells[3,18–20]. This indicates, that E6 proteins of different HPV types can either up- or downregulate the Notch signaling pathway. E6 proteins of different HPV types are conserved in their amino acid sequence and structure. However, it has been shown, that the E6 proteins of different HPVs differ in their intracellular level[21]. A comparison of the modulatory effect of the individual E6 proteins on the Notch signaling necessitates information about its intracellular protein amount on a single-cell level. However, this cannot be achieved by commonly employed dual luciferase-based assays measuring luciferase expression controlled by the Notch-responsive *HES1-promotor.*

To overcome this, we developed a flow-cytometry-based assay to analyze *P-HES1* activity using three different fluorescent proteins reporting (I) the transfection of the activator plasmid, human Notch 1 intracellular domain by EGFP co-expression (here NICD), (II) the intracellular amount of the modulator (here E6) by N-terminal fusion of mTagBFP2 and (III) the promotor activity (here of *P-HES1*) by DsRed2 expression (Fig. 2). This allows us to monitor *HES1*-activation on a single cell level and consider only cells which are triple positive. By this, we can reduce the background and, additionally account for different protein expression levels (Fig. 3). Using this strategy, we assess the activating or repressing potential of E6 proteins of different genera, species and types of HPV (Table 1) on the Notch signaling pathway with a semi-quantitative approach.

Results

Exogenous activation of Notch signaling pathway in C33A and H1299 cells. To verify, that the cell systems activate Notch signaling in response to exogenous NICD, we co-transfected the reporter plasmid and the control plasmid encoding for mTagBFP2 further with and without the activator plasmid and gated for

Genus	Alpha				Beta		
Species	7	9		10	1		2
Tested types	18	16	31	6	5	8	38

Table 1. Tested E6 proteins of different HPV types.

DsRed2 positive cells (Fig. 4). Without the activator plasmid, C33A and H1299 cells showed less than 0.2 ± 0.06% and 0.02 ± 0.003% DsRed2 expressing cell population, respectively (Fig. 4), indicating that the constitutive and endogenous Notch signaling is low and thereby not triggering *P-HES1* regulated reporter expression sufficiently. Additionally, the co-expression of neither mTagBFP2 nor EGFP affected the signal of DsRed2. Conversely, C33A and H1299 cells co-transfected with the activator plasmid showed a significant increase in the DsRed2 expressing cell population, which was at least tenfold above the background signal of DsRed2 expressing cell population without exogenous NICD. Hence, both cell lines clearly show an activation of the Notch pathway by exogenous NICD with very low background of endogenous *P-HES1*-activity (Fig. 4b and c).

Triple gating strategy- proof of concept. As the excitation and emission spectra of fluorescent proteins EGFP, mTagBFP2, DsRed2 overlap partially, it is important to carefully control for crosstalk in the three applied channels and compensate accordingly. As a control, we transfected cells individually with plasmids each encoding for EGFP, mTagBFP2 or DsRed2. Gates were set for each protein such as there is no crosstalk (< 0.5%) in the other channels (Fig. 5). By this, we were able to gate specifically for triple positive viable cells (P1/EGFP/mTagBFP2/DsRed2) showing EGFP (activator transfected), mTagBFP2 (modulator protein) and DsRed2 (Notch-responsive reporter) expression.

It had been shown previously that Notch signaling is activated when the NICD translocate into the nucleus and forms a Notch initiation complex with other cellular proteins. However, E6 proteins localize into the nucleus to interfere with formation of the Notch initiation complex. Thus, it would be interesting to know if mTagBFP2-E6s fusion retain ability to localize into the nucleus. Hence, we first analyze the mTagBFP2-E6s fusion constructs, of which all accumulated in the nucleus (Supplementary information SI1 – SI3).

To examine the *P-HES1* reporter activity with our triple gating strategy, an exemplary triple gating is shown for C33A co-transfected with *P-HES1* reporter plasmid, NICD activator plasmid and mTagBFP2-E6 modulator plasmid for 16E6 and 8E6 (Fig. 6). Finally, ~ 66.0 ± 1.6% cells for 16E6 and ~ 18.7 ± 4.5% cells for the E6 of the HPV8 (8E6) were DsRed2 positive in the triple gated cell population. Compared with our control (46.6 ± 4.7% cells), where we co-transfected mTagBFP2 instead of the fusion construct mTagBFP2-E6, 16E6 clearly shows an activation, while 8E6 clearly shows a repression of the *P-HES1* activity.

In parallel, we validated the results by Western Blot analysis (Fig. 7). This shows, that EGFP, mTagBFP2, mTagBFP2-E6 and DsRed2 are expressed. In accordance with the flow cytometric analyses, the *P-HES1* regulated expression of DsRed2 is activated by co-transfection of the activator plasmid (NICD), decreased for 8E6 and increased for 16E6.

Modulation of Notch signaling pathway by different HPV E6 proteins. We analyzed the effect on the Notch signaling pathway of seven different E6 proteins derived from HPVs of different genus, species and carcinogenic potential (Table 1). E6 proteins interfere with p53, especially HPV types of high-risk directly degrade p53[21]. Since there is a crosstalk between p53 and the Notch pathway, we performed the same experiments in two different cell lines: the HPV-negative cervix carcinoma cell line C33A and the p53 null lung cancer cell line H1299. Applying our triple gating strategy, we analyzed the data considering the percentage of DsRed2 positive cells and the mean fluorescence intensity (MFI) (Fig. 8). Assessing MFI considers the intracellular expression level of DsRed2 produced upon activation of *P-HES1*. Analyzing the % of DsRed2 positive cells does not account for the individual single-cell level of DsRed2 expression, but rather focuses on changes on cell population levels. Nevertheless, both, % cells and MFI should change accordingly in case of repression or activation.

The E6 proteins of beta HPV 5, 8 and 38 showed a significant repression of DsRed2 + % cells and MFI in C33A and H1299 cells. In H1299 cells, repression was so potent, that the total cell numbers in the final triple-gated DsRed2 + population was below 500 cells. In contrast, the alpha-7 HPV 16E6 showed a highly significant activation of reporter expression in both cell lines.

The E6 of alpha-7 HPV 31 and alpha-10 HPV 6b show a low activation of *P-HES1* activity in C33A cells, in which activation by HPV 31 is not significant for the MFI of the DsRed2. In the p53-null H1299 cells the activation of Notch pathway by 31E6 and 6bE6 seems increased, especially for 31E6. Regarding the effect of alpha-7 HPV 18E6, in % cell-signal 18E6 shows a slight repression, whereas this effect was less clear and not significant for the MFI of the DsRed2 in both cell lines. Altogether, our triple gating strategy is suitable to monitor the modulation of the Notch signaling pathway by different E6, which show repression for all beta-HPV E6, activation for HPV16, cell-line dependent activation for HPV31 and 6b and rather no effect for HPV18.

Semi-quantitative analysis of E6 activities. Both signals of mTagBFP2-E6 for % cells and MFI, , vary between the different E6 proteins (Fig. 9) indicating that the intracellular protein amount of the mTagBFP2-E6 variants differs between the different HPV types. Principally, the MFI per cell of a FP is equivalent to the amount of the respective FP per cell. Thereby, the MFI of mTagBFP2 equals to the amount of the modulator mTagBFP2-E6 and the MFI of DsRed2 equals the amount of DsRed2 as the reporter of *P-HES1* activity.

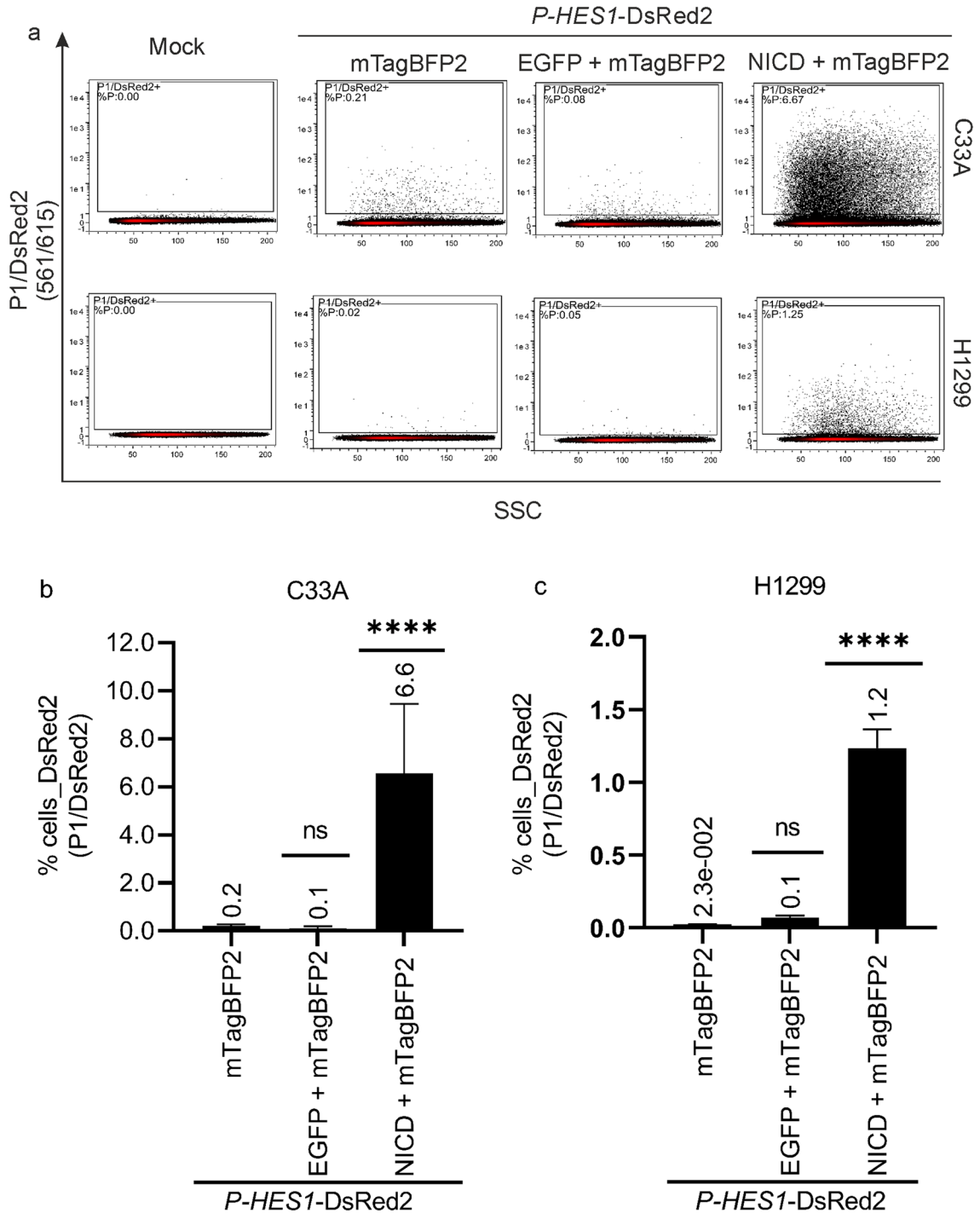

Figure 4. Notch activation by exogenous NICD. C33A and H1299 cells were co-transfected with 250 ng *P-HES1*-DsRed2 reporter plasmid, 250 ng EGFP or 250 ng NICD activator plasmid and 125 ng mTagBFP2 plasmid as indicated. C33A and H1299 cells were harvested for FACS measurement 48 h or 36 h post transfections, respectively. Living cells (P1) were gated for DsRed2 signal reporting the Notch pathway activity. (**a**)**.** Representative FACS plots show that the endogenous NICD is unable to activate the expression of the Notch target *HES1* gene (Column2 and Column3) sufficiently. Upon co-transfection of NICD (Column4), the increased cell population of DsRed2 positive cells clearly indicates the exogenous activation of Notch signaling. (**b, c**)**.** Three independent biological replicates were conducted. A significant cell population of DsRed2 positive cells was detected in C33A (b) and H1299 (c), respectively in presence of exogenous NICD (*P-HES1*-DsRed2 + mTagBFP2 + NICD). In contrast, the endogenous NICD does not activate *P-HES1*-DsRed2 expression sufficiently (*P-HES1*-DsRed2 + mTagBFP2), independent of the co-transfection of EGFP control plasmid (*P-HES1*-DsRed2 + mTagBFP2 + EGFP). The mean % cells of DsRed2 expressing cell populations as gated for each sample is stated above each bar and the error bars plotted indicate the standard deviation of the mean from the three independent biological replicates. P-values were calculated using One-Way ANOVA with Fischer's LSD test by comparing the mean of each sample with mean of *P-HES1*-DsRed2 + mTagBFP2. **** = $P \leq 0.0001$, ns = $P > 0.05$.

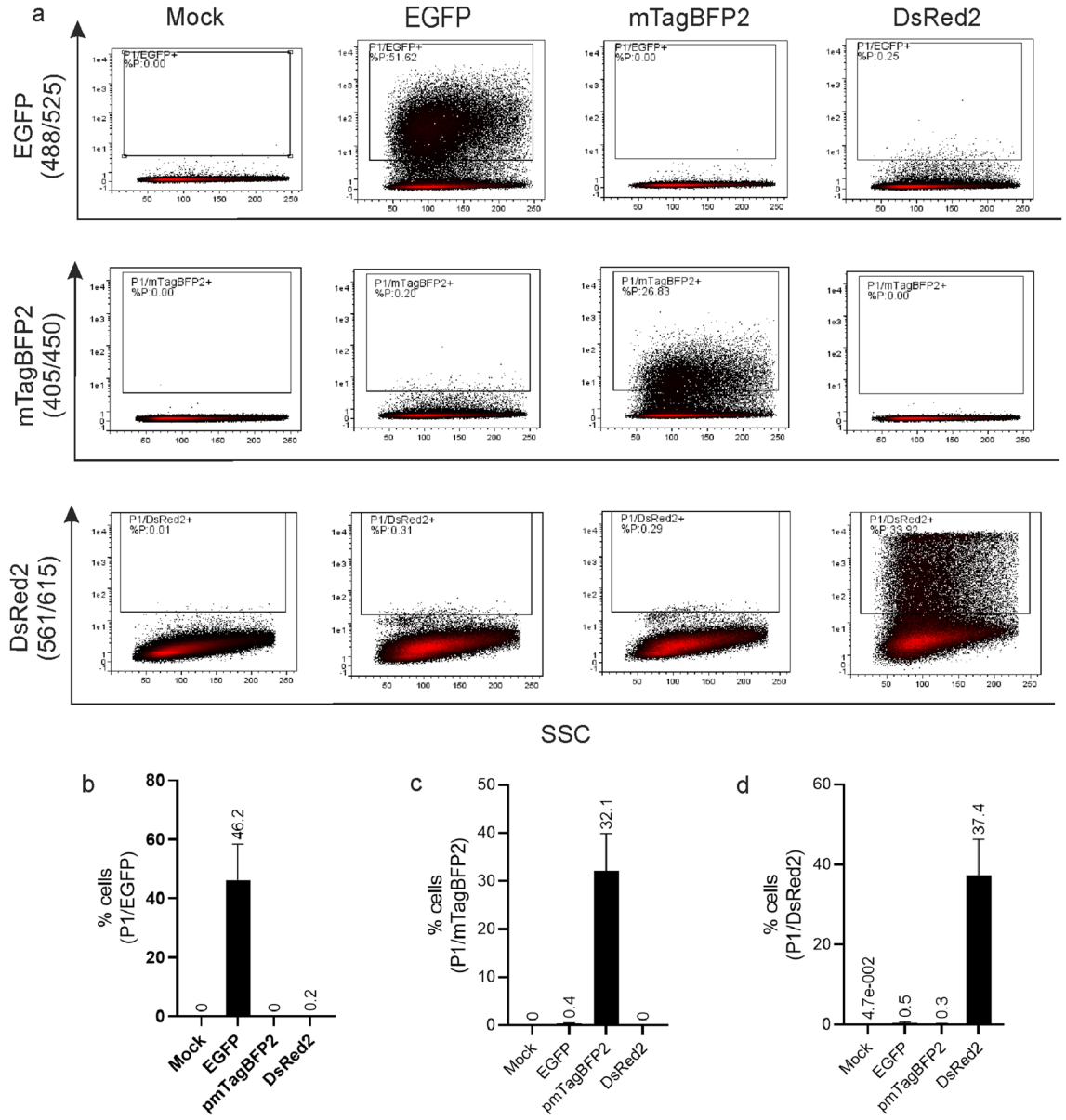

Figure 5. Cross talk of fluorescent proteins. (**a**). Representative FACS plots showing the crosstalk level of the three fluorescence proteins after compensation. C33A cells were transfected with control plasmid 250 ng EGFP, 125 ng mTagBFP2 or 125 ng DsRed2 individually. FACS measurement was carried out 48 h post transfection. Living cells (P1) were gated for EGFP, mTagBFP2 and DsRed2 separately to monitor the crosstalk of each fluorescence proteins in respective channel showing cell populations in % cells. EGFP showed a compensable crosstalk signal in the channel of mTagBFP2 and DsRed2. Crosstalk levels were always kept below 0.5% of cell populations in each experiment. (**b, c, d**). The experiment was repeated three times. The mean % cells of cell populations as gated of three independent biological experiments are plotted in b, c and d with the mean value stated above each bar. The error bars plotted are indicating the standard deviation of mean value from the three independent biological replicates.

Assuming no effect of unfused mTagBFP2, its DsRed2 MFI was set to zero. Subsequently, as expected, normalized MFI < 0 show repression, whereas MFI > 0 show activation of *P-HES1*. We then calculated the ratio of normalized MFI DsRed2 to the MFI of mTagBFP2-E6 including triple positive cells only. This ratio then resembles the specific activity of each E6 protein in this assay (Fig. 10) accounting for the different E6 expression levels (Fig. 9). A step to step analysis guide can be found in Supplementary information SI 5. As a result, the repressing activities of the beta-HPV 5E6 and 8E6 proteins are comparable, whereas 38E6 shows a 2-times and 4-times higher potential in repressing *P-HES1* regulated transcription of DsRed2 in H1299 and C33A cells, respectively. 16E6 shows a 5–7-times higher activation potential than the other E6 proteins of alpha-HPV 6bE6, 31E6, 18E6, which showed no significant impact on *P-HES1* activity in C33A cells. Surprisingly, a higher and more significant activation of the Notch pathway was observed in the p53-null H1299 cells for E6 of HPV 31 and 6b. Here the activity of 31E6 is even similar to the activity of 16E6. In principle, the trend of these semi-quantitative results

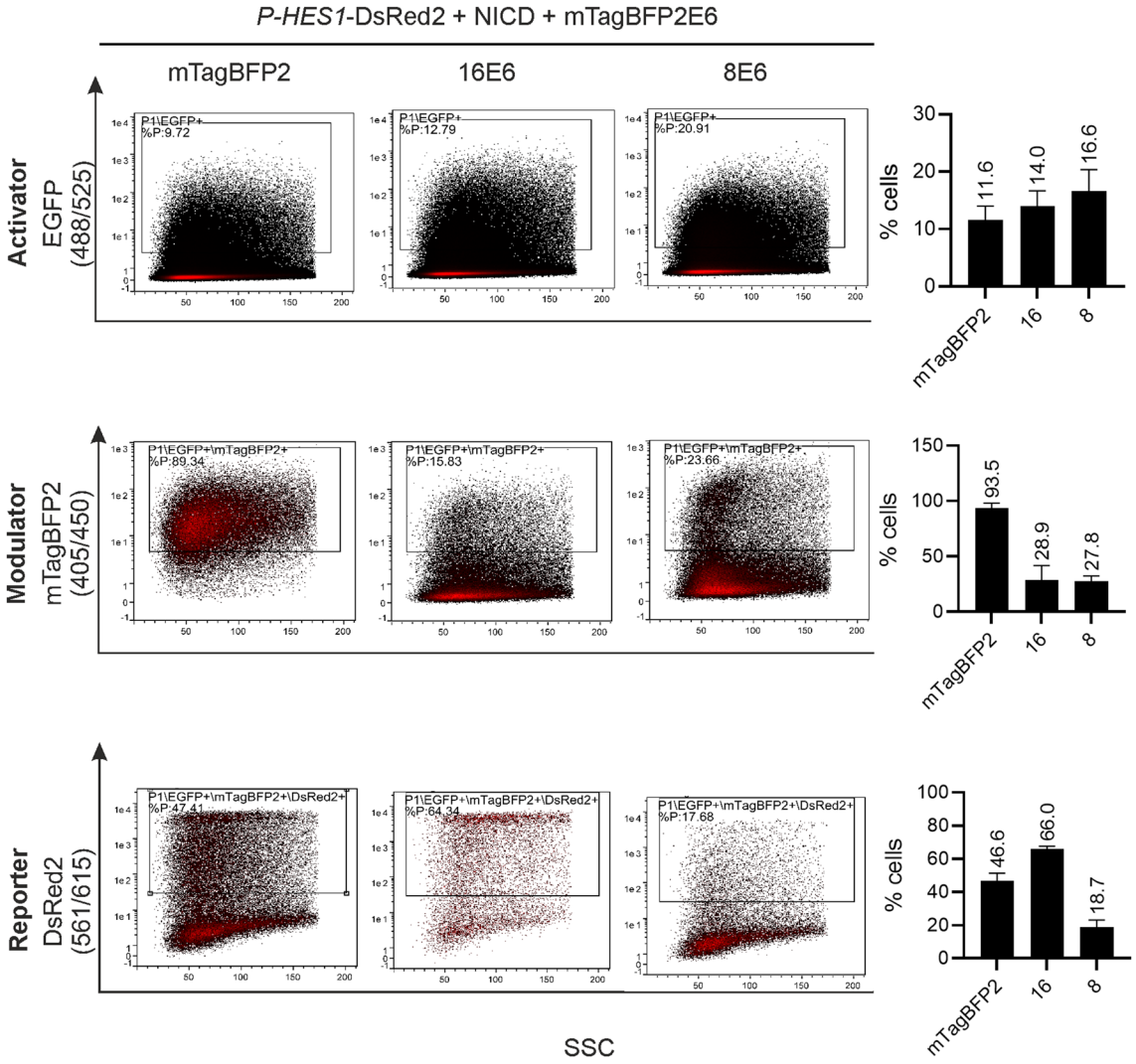

Figure 6. Experimental triple gating strategy, exemplary for Notch activation (16E6) and repression (8E6). C33A cells were co-transfected with 250 ng *P-HES1*-DsRed2 reporter plasmid, 250 ng NICD activator plasmid, 500 ng mTagBFP2-E6 modulator plasmid respectively or 125 ng of mTagBFP2 as a control. Cells were harvested for FACS measurement 48 h post transfection. Living cells were gated for P1/EGFP > P1/EGFP/mTagBFP2 > P1/EGFP/mTagBFP2/DsRed2 to monitor the activity of *P-HES1*. The mean % cells of cell population as gated for three independent biological replicates were plotted to the right of the representative FACS plots. The mean values were stated above each bar and the error bars indicate the standard deviation of the mean value from the three independent biological replicates.

is in line with the results above (Fig. 8). An additional accounting for the different E6 expression shows, that the individual activities of E6 proteins diverge largely in modulating the Notch pathway and are cell line dependent.

Discussion

Notch signaling pathway plays an important role in cell fate determination and cell proliferation[1]. Dysregulation of Notch signaling is often observed in the progression of carcinoma[2,3]. Hence, it is extensively studied as a potential drug target to counter for treatment of its associated diseases. Numerous studies have shown the dysregulation of Notch signaling in HPV associated cancer progression by employing dual-luciferase assay[14–16]. However, the disadvantages of this luciferase reporter assay include the needs of the expensive commercial dual luciferase kit containing exogeneous substrates and cell lysis, disrupting the compartmentation of cells. The main limitation of luciferase assays is the comparison of the effect of different modulators on the reporter gene expression based on the expression of these modulatory proteins. To overcome these drawbacks, we established a triple fluorescence flow-cytometry-based reporter assay to analyze the effect of different HPV E6 proteins on Notch signaling pathway. The advantage of this flow-cytometry-based reporter assay is the triple gating strategy, which allows to monitor exclusively living cells that express the modulatory protein as well as the reporter and the activator. Reducing the background is especially advantageous if potential modulatory proteins show low transfection efficiencies and/or low steady-state expression levels. In addition to that, fluorescently labeled

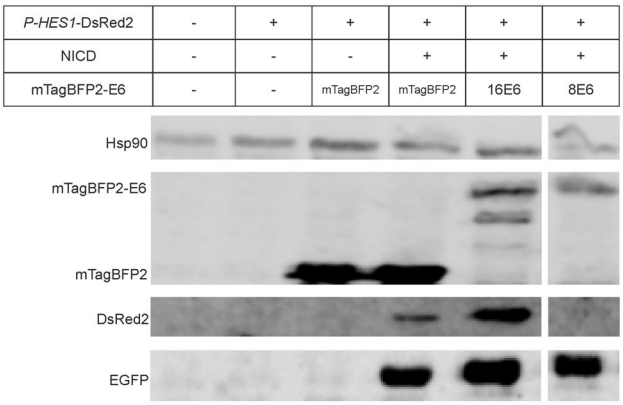

Figure 7. Expression of proteins by Western blot analysis. Expression level of mTagBFP2-E6, DsRed2, and EGFP were assessed by loading 70 µg of total proteins on reducing 8–20% SDS-PAGE gel. HSP90 serves as a loading control. DsRed2 protein signal is increased for 16E6 but absent for 8E6. In line with the FACS assay, these results indicate an activation by 16E6 and a repression for 8E6 of the Notch pathway. Please find full blot and detailed blot information in Figure SI4.

modulatory proteins allows quantification via flow-cytometry, possibly also in spatial localization which could give further insight into their modulating effect on gene regulation based on protein activity and protein amount.

Concerning the background of endogenous Notch signaling, which is tenfold lower than of the exogenously activated cells (Fig. 4). We expected that the E6 proteins also modulate the endogenous NICD. Indeed, we conducted experiments by co-transfecting C33A and H1299 cells with only *P-HES1*-DsRed2 reporter plasmid and mTagBFP2-E6 or mTagBFP2 (control) to examine the modulation effect of *P-HES1* activity by HPV16 and 8 E6 with endogenous NICD. In this case, a double fluorescence gating strategy was applied whereby the viable cells were gated for mTagBFP2 followed by DsRed2 (P1 > P1/mTagBFP2 > P1/mTagBFP2/DsRed2). Despite a similar overall trend, without heterologous expression of NICD, the % cells expressing DsRed2 in mTagBFP2-E6 cell population are too low to find a statistically relevant population to quantify differences (Supplementary information SI 6).

The effect of modulatory proteins on gene regulation can be influenced by protein activity (the more active the protein, the higher the effect) and the protein amount (the more protein, the higher the effect). In our assay, the expression level of mTagBFP2-E6 varies among the different HPV types. Different intracellular levels of E6 have been reported previously[21] affecting the gene regulation by different E6 amounts. The expression levels of E6 are unknown in its native environment, during infection or cell transformation. Of course, the assay conditions do not fully resemble the native environment, especially with regard to the levels of E6, NICD and *P-HES1*. Nevertheless, and therefore allows a comparison of their activity this assay provides information about the specific activity of individual E6 proteins, which allow a comparison of each E6 protein potential in the context of dysregulating the Notch signaling pathway by HPVs. Our semi-quantitative analysis allows the comparison of different modulatory proteins, e.g. the different HPV E6 proteins, or mutants accounting for their individual variations in their expression levels. Overall, the triple fluorescence assay can be easily transferred to other genes of interest or signaling pathways by cloning the respective promotor, activator and modulatory protein into respective plasmids. Further it can be used to screen specific inhibitors of the modulatory proteins, here the HPV E6 proteins, and monitor their efficiency on the target gene expression in a fast way as well as in medium throughput.

Concerning the HPV E6 proteins and their biological functions, we could show that E6 proteins of different genus differentially manipulate the Notch signaling pathway. (I) all tested E6 proteins of beta-HPV repress the Notch pathway. This is in line with their reported interaction with MAML1 as a co-factor of the initiation complex of *HES1* transcription[2,12,14–16]. The repression potential is highest for 38E6, and lower for 5E6 and 8E6. 5E6 and 8E6 show a similar repression potential. HPV 38 belongs to beta-2 HPV, whereas HPV 5 and 8 belong to beta-1 HPV, indicating an association between function and phylogeny. (II) E6 of alpha-HPV do marginally interact with MAML1 and do not repress Notch signaling, as previously proposed for e.g. 16E6[12,14]. Indeed, the activity of the tested alpha-HPV E6 proteins is highly divergent. In C33A only 16E6 showed a clear activation. Higher levels of Notch signaling were previously reported for HPV16-positive keratinocytes and high-grade lesions [19,20,22–24]. 18E6, 31E6 and 6bE6 showed no significant impact in C33A cells. (III) It is known, that E6 proteins of high-risk alpha-HPV 16, 18 and 31 lead to the degradation of the tumor suppressor p53[25–29]. Since there is a crosstalk between p53 and the Notch pathway[30,31] we applied the same experiment in H1299 cells, which are p53 deficient. Here, the overall trend looks similar, beta-HPV E6 proteins repress and 16E6 activates the activity of the *P-HES1* reporter. Remarkably, the repressing effect in H1299 was so strong, that the triple positive cell population consisted of less than 500 cells. Nevertheless, the repressing effect of beta-HPV is clear and the tendency of the potentials of the different beta-HPV E6 proteins resembles the results measured in C33A. Whereas 18E6 again shows no effect on Notch signaling. H1299 31E6 and 6bE6 show a clear tendency to activate the Notch pathway in the p53-null cell line. Especially HPV 31E6, a high-risk type of the same species as 16E6, shows a strong activation similar to the activity of 16E6 and over two-fold stronger than the low-risk HPV 6bE6.

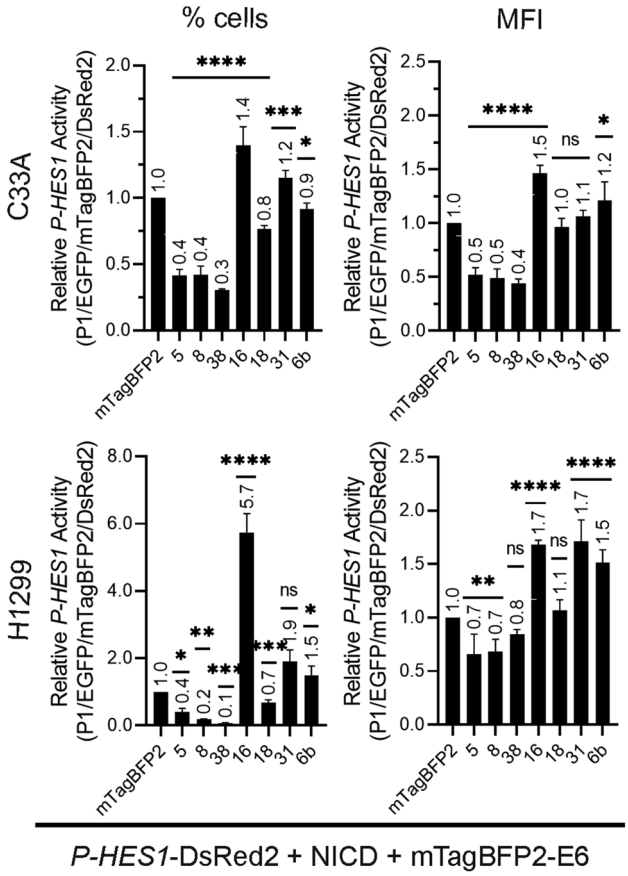

Figure 8. HPVE6 influence on *P-HES1* promotor activity. The influence on *P-HES1* promotor activity was analyzed by the triple gating strategy and signals for % cells (left) and mean fluorescence intensities of DsRed2 per cell (MFI, right) were plotted. Cell were co-transfected with 250 ng *P-HES1*-DsRed2 reporter plasmid, 250 ng activator NICD plasmid and 125 ng mTagBFP2 or 500 ng of respective mTagBFP2-E6. FACS measurement was carried out 48 h or 36 h post transfection for C33A and H1299 cells, respectively. Compared to the negative control (mTagBFP2 not fused to E6), E6 of beta HPV types 5, 8 and 38 inhibit DsRed2 expression in both cell lines. E6 of the alpha HPV type 16 clearly upregulates expression of DsRed2 in both cell lines. E6 of the alpha-HPV31 and 6 show a slight activation in C33A and a more pronounced activation in p53-null cell line H1299. 18E6 shows no significant effect, rather slight repressing effect in % cells in both cell lines. Data plotted are the mean values of three independent biological replicates. The number above bars are the respective mean value. The error bars plotted are the standard deviation of the mean value from three independent biological replicates. P-values were calculated using One-Way ANOVA with Fischer's LSD test by comparing the mean of each activation and repression sample with the control activation sample from three independent experiments where * = $P \leq 0.05$, ** = $P \leq 0.01$, *** = $P \leq 0.005$, **** = $P \leq 0.0001$, ns = $P > 0.05$.

Why 31E6 is more active in the p53-null cell line H1299 than in C33A, whereas the activity of the closely related 16E6 seems similar in both cell lines, is unknown. Both cell lines certainly differ in more than just the presence of p53. However, a speculative relation might be the lower potential of 31E6 interacting with[32] and degrading p53[21] than 16E6. E6 of HPV18, as the second most carcinogenic HPV type, surprisingly shows no significant effect on the Notch signaling in both cell lines. However, this approach focused only on the *P-HES1* promotor which is downstream of the Notch signaling pathway. To our knowledge, the effect of HPV18 on Notch signaling pathway has not been investigated so far. One speculation might be that HPV18 E6 is interfering with Notch signaling in a different way. Besides, to dysregulate cell proliferation many options exist despite Notch signaling.

It was previously reported that the HPV-related activation of the Notch pathway is driven by the transcription factor NFX123[22], which is upregulated by 16E6. Presumably, the activation observed here depends on NICD downstream of gamma-secretase cleavage and impacts the formation of the transcription initiation complex (Fig. 1) directly or indirectly.

In conclusion, the triple fluorescence flow-cytometry-based assay is a novel suitable method to investigate the influence of exogenous proteins on the Notch pathway utilizing a Notch-responsive reporter plasmid. The possibility for semi-quantification allows a comparison of multiple modulatory proteins. Here, we utilized the assay to establish the differential regulation of the Notch-pathway by different HPV E6 proteins. In line with previous data, beta-1-HPV 5, 8 and beta-2-HPV 38 E6 proteins repress Notch, with 38E6 being the most potent repressor. Alpha-7 (16, 31) and alpha-10 (6b) HPV E6 proteins seem to activate the Notch pathway. Especially in the p53-null H1299 cell line both high-risk alpha-7 HPV 16E6 and 31E6 show a strong activation on *P-HES1* activity. E6

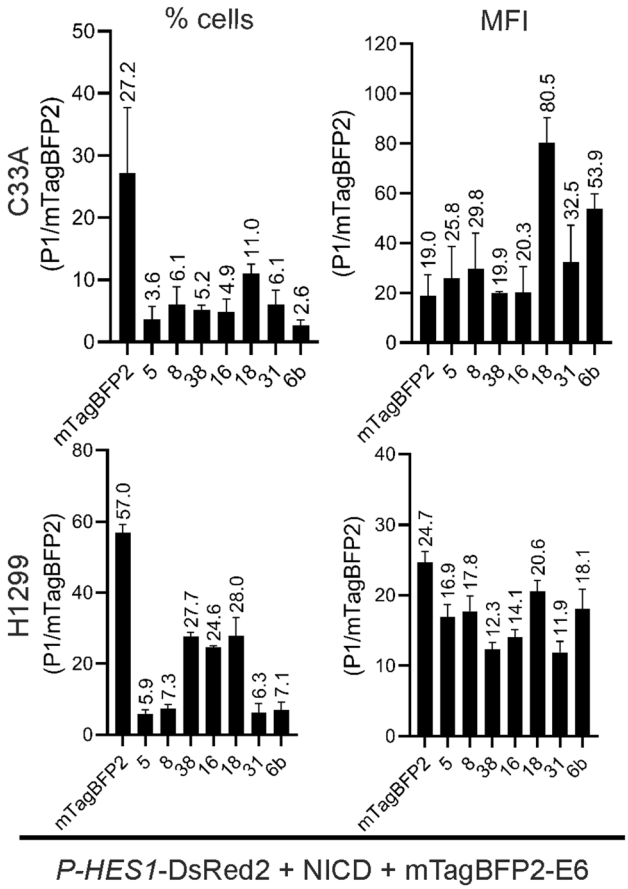

Figure 9. Different expression levels of mTagBFP2-E6. E6 proteins are expressed in different amounts. Cells were co-transfected with 250 ng *P-HES1*-DsRed2 reporter plasmid, 250 ng activator NICD plasmid and 125 ng mTagBFP2 or 500 ng of respective mTagBFP2-E6. FACS measurement was carried out 48 h or 36 h post transfection for C33A (top) and H1299 (lower) cells, respectively. Living cells transfected with activator, modulator and reporter plasmid were gated for mTagBFP2 signal (P1/mTagBFP2) with respect to % cells (change in population, left) and their mean fluorescence intensity per cell (intracellular level, right). Both values vary between different E6 proteins indicating that different intracellular amounts of E6 were expressed in different number of cells. Data are derived from the mean value of three independent biological replicates with the mean value stated above each bar. The error bars plotted represent the standard deviation of the mean value from the three independent biological replicates.

of alpha-9 HPV18, which is the second most carcinogenic HPV after HPV16, had no effect on the Notch pathway. In summary the potency of the E6 proteins of HPV influencing the Notch pathway is highly variable even within the same genera but also between high-risk HPV types. Targeting the Notch pathway for HPV therapy requires an HPV-typing and individual adaption with respect to the HPV type.

Materials and methods

Plasmid DNA. Fluorescence based reporter plasmid *P-HES1*-DsRed2 (Addgene #13,767,[33]) and the Notch activation plasmid EF.ICN1.CMV.GFP (Addgene #17,623,[34]) were obtained from Addgene. HPV 16E6, 31E6, 18E6, 6bE6, 5E6, 8E6 and 38E6 (PAVE or GenBank protein reference numbers HPV16REF.1/GI:333,031, HPV31REF.1/GI:333,048, HPV18REF.1/GI:60,975, HPV6REF.1/GI:60,955, GenBank: CAA52689.1, HPV8REF.1/GI:333,074, HPV38REF.1/GI:1,020,234) constructs were cloned in pmTagBFP-C1 via restriction cloning or Gibson cloning obtaining an N-terminal Fusion of E6 with mTagBFP2.

Cell culture. HPV negative cervical cancer cell line C33A and p53 null non-small cell lung carcinoma cell line H1299 were cultured in DMEM (Gibco, 41,965–062) supplemented with 10% fetal bovine serum (FBS) (Gibco, 10,270–106) and gentamicin (50 µg/mL) (Gibco, 157,710,049) at 37 degree Celsius, 95% humidity and 5% carbon dioxide. One day before transfection, 250 000 of C33A cells or 180 000 of H1299 cells were seeded in 12-wells sterile cell culture plate (Thermo Scientific, 150,628). Both cells were transfected with respective plasmid DNA using jetPRIME following manufacturer's instructions on day 2. Control plasmid was always added to keep total amount of plasmid DNA transfected constant. Cells were trypsinized with Trypsin–EDTA (0.25%),

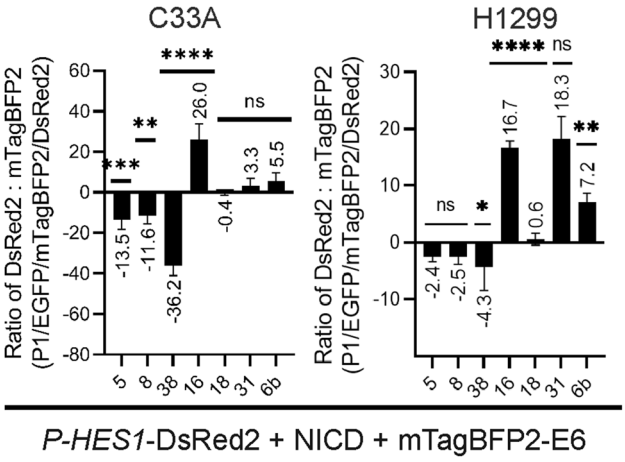

Figure 10. E6 activity on *P-HES1* regulated genes. The ratio of mean fluorescence intensity (MFI) of DsRed2 and mTagBFP2 were calculated for each mTagBFP2-E6 based on the triple gating strategy as described in Fig. 6 and normalized to the control mTagBFP2, which has no effect on *P-HES1* controlled DsRed2 expression (ratio set to zero). The more negative or positive the value the higher the repressing or activating activity of the respective E6. Data are derived from the average of three independent biological replicates with the mean value labelled above each bar. The error bars plotted are the standard deviation of the mean from the three independent biological replicates. P value were calculated using One-Way ANOVA with Fischer's LSD test by comparing the mean of each activation and repression sample with the control activation sample where * = $P \leq 0.05$, ** = $P \leq 0.01$, *** = $P \leq 0.005$, **** = $P \leq 0.0001$, ns = $P > 0.05$.

phenol red (Gibco, 25,200,072) for FACS measurements or immunoblotting 48 h post-transfection for C33A cells or 36 h post-transfection for H1299 cells.

FACS based reporter assay. For flo- cytometry, cells were harvested and washed in 500 µL precooled Dulbecco's phosphate-buffered saline (DPBS) (Gibco, 14,190–169) containing 1% FBS. After washing, cells were resuspended in 200 µL precooled DPBS containing 1% FBS. FACS measurements were performed using MACSQuant VYB Flow Cytometer (Miltenyi Biotec) and analyzed with Flowlogic version 7.2.2 (Miltenyi–Inivai). Cells expressing the fluorescent proteins mTagBFP2, EGFP or DsRed2 were detected in channel V1 [405/450(50)] nm, B1 [488/450(50)] nm or channel Y2 [561/615(20)] nm, respectively. Three biological replicates were carried out for all experiments. For statistical analysis, we carried out Ordinary One-Way ANOVA with Fischer's LSD test, comparing always all samples (E6) to the control (mTagBFP2) in Prism 9, version 9.1.2 (226). All figures presented in results and supplementary information were prepared using CorelDRAW X7, version 17.5.0.907. Example of the analysis method could be found in Supplementary information.

Immunoblotting. Cells were lysed in lysis buffer [10% (v/v) Glycerol (MP Biomedicals, 4,800,689); 50 mM HEPES, pH 7.5 (Carl Roth, 9105.4); 3 mM Magnesium Chloride (Merck, 105,833); 0.1% (v/v) IGEPAL CA-630 (Merck, 18,896); 150 mM Sodium Chloride (Carl Roth, 3957.2); 1 mM Tris(2-carboxyethyl)phosphine (TCEP) (Alfa Aesar, J60316); 200 µM Zinc Chloride (Carl Roth, 3533); supplemented with Benzonase Endonuclease (Merck, 101,656), PhosSTOP (Roche, PHOSSRO) and cOmplete EDTA-free Protease Inhibitor Cocktail (Roche, COEDTAF-RO)]. The total protein concentration of the crude lysates was determined by Bradford assay and 70 µg total protein of the cell lysate were resolved on 8–20% SDS-PAGE gel. Proteins were electrotransfered onto nitrocellulose membrane (GE Healthcare) via wet blotting using blotting buffer (10 mM 3-(Cyclohexylamino)-1-propanesulfonic acid (CAPS) (Sigma, C2632), 0.001% (w/v) SDS (Carl Roth, 2326.2), 10% (v/v) methanol (Honeywell, 32,213), pH 10.3 at room temperature) for one hour at 70 V (constant). The membrane was blocked with 5% (w/v) Albumin Bovine Fraction V (Serva, 11,930) in phosphate buffer saline (PBS) one hour at room temperature and probed with appropriate primary antibodies overnight at 4 °C. Primary antibodies used at dilution of 1:1000 include anti-tRFP (Evrogen, AB233) for detection of mTagBFP2 and Living Colors A.v. Monoclonal Antibody (JL-8) (Takara Bio, 632,381) for detection of EGFP. DsRed2 was detected using Anti-DsRed (E-8) (sc-390909) and as a loading control HSP90 was detected by anti-HSP90 (4F10) (sc-69703) from Santa Cruz Biotechnology, both at a dilution of 1:200. Membrane was washed three times with PBS-T (0.05% v/v Tween 20). Secondary antibodies IRDye 680RD Goat anti-Rabbit IgG (H + L), IRDye 680RD Goat anti-Mouse IgG (H + L) or IRDye 800CW Goat anti-Mouse IgG (H + L) (LI-COR Biotechnology GmbH) were used at dilution of 1:10 000 and incubated for 30 min at room temperature. Membrane was again washed three times with PBS-T. The signal of respective protein was then visualized using LI-COR Odyssey Fc and analyzed with Image Studio Lite Software.

Received: 25 March 2021; Accepted: 27 January 2022
Published online: 22 February 2022

References

1. Rangarajan, A. *et al.* Notch signaling is a direct determinant of keratinocyte growth arrest and entry into differentiation. *EMBO J.* **20**, 3427–3436. https://doi.org/10.1093/emboj/20.13.3427 (2001).
2. BeLow, M. & Osipo, C. Notch signaling in breast cancer: A role in drug resistance. *Cells* https://doi.org/10.3390/cells9102204 (2020).
3. Krishna, B. M. *et al.* Notch signaling in breast cancer: From pathway analysis to therapy. *Cancer Lett.* **461**, 123–131. https://doi.org/10.1016/j.canlet.2019.07.012 (2019).
4. Aparicio, E., Mathieu, P., Pereira Luppi, M., Almeira Gubiani, M. F. & Adamo, A. M. The Notch signaling pathway: Its role in focal CNS demyelination and apotransferrin-induced remyelination. *J. Neurochem.* **127**, 819–836. https://doi.org/10.1111/jnc.12440 (2013).
5. Hohlfeld, R. Myelin failure in multiple sclerosis: Breaking the spell of Notch. *Nat. Med.* **8**, 1075–1076. https://doi.org/10.1038/nm1002-1075 (2002).
6. Fan, H. *et al.* Effect of Notch1 gene on remyelination in multiple sclerosis in mouse models of acute demyelination. *J. Cell Biochem.* **119**, 9284–9294. https://doi.org/10.1002/jcb.27197 (2018).
7. Rizzo, P. *et al.* COVID-19 in the heart and the lungs: Could we "Notch" the inflammatory storm?. *Basic Res. Cardiol.* **115**, 31. https://doi.org/10.1007/s00395-020-0791-5 (2020).
8. Ito, T. *et al.* The critical role of Notch ligand Delta-like 1 in the pathogenesis of influenza A virus (H1N1) infection. *PLoS Pathog.* **7**, e1002341. https://doi.org/10.1371/journal.ppat.1002341 (2011).
9. Hayward, S. D. Viral interactions with the Notch pathway. *Semin. Cancer Biol.* **14**, 387–396. https://doi.org/10.1016/j.semcancer.2004.04.018 (2004).
10. Vazquez-Ulloa, E., Lizano, M., Sjoqvist, M., Olmedo-Nieva, L. & Contreras-Paredes, A. Deregulation of the Notch pathway as a common road in viral carcinogenesis. *Rev. Med. Virol.* **28**, e1988. https://doi.org/10.1002/rmv.1988 (2018).
11. De Strooper, B. *et al.* A presenilin-1-dependent gamma-secretase-like protease mediates release of Notch intracellular domain. *Nature* **398**, 518–522. https://doi.org/10.1038/19083 (1999).
12. Tan, M. J. *et al.* Cutaneous beta-human papillomavirus E6 proteins bind Mastermind-like coactivators and repress Notch signaling. *Proc. Natl. Acad. Sci. USA* **109**, E1473-1480. https://doi.org/10.1073/pnas.1205991109 (2012).
13. de Martel, C., Plummer, M., Vignat, J. & Franceschi, S. Worldwide burden of cancer attributable to HPV by site, country and HPV type. *Int. J. Cancer* **141**, 664–670. https://doi.org/10.1002/ijc.30716 (2017).
14. Brimer, N., Lyons, C., Wallberg, A. E. & Vande Pol, S. B. Cutaneous papillomavirus E6 oncoproteins associate with MAML1 to repress transactivation and NOTCH signaling. *Oncogene* **31**, 4639–4646. https://doi.org/10.1038/onc.2011.589 (2012).
15. Meyers, J. M., Spangle, J. M. & Munger, K. The human papillomavirus type 8 E6 protein interferes with NOTCH activation during keratinocyte differentiation. *J. Virol.* **87**, 4762–4767. https://doi.org/10.1128/JVI.02527-12 (2013).
16. Meyers, J. M., Uberoi, A., Grace, M., Lambert, P. F. & Munger, K. Cutaneous HPV8 and MmuPV1 E6 Proteins Target the NOTCH and TGF-beta tumor suppressors to inhibit differentiation and sustain keratinocyte proliferation. *PLoS Pathog* **13**, e1006171. https://doi.org/10.1371/journal.ppat.1006171 (2017).
17. IARC. Human papillomaviruses. *IARC Monographs on the evaluation of carcinogenic risks to humans* **90**, 1–636 (2007).
18. Tripathi, R. *et al.* HES1 protein modulates human papillomavirus-mediated carcinoma of the uterine Cervix. *J. Glob. Oncol.* **5**, 1–10. https://doi.org/10.1200/JGO.18.00141 (2019).
19. Weijzen, S., Zlobin, A., Braid, M., Miele, L. & Kast, W. M. HPV16 E6 and E7 oncoproteins regulate Notch-1 expression and cooperate to induce transformation. *J. Cell Physiol.* **194**, 356–362. https://doi.org/10.1002/jcp.10217 (2003).
20. Vliet-Gregg, P. A., Hamilton, J. R. & Katzenellenbogen, R. A. NFX1-123 and human papillomavirus 16E6 increase Notch expression in keratinocytes. *J. Virol.* **87**, 13741–13750. https://doi.org/10.1128/JVI.02582-13 (2013).
21. Mesplede, T. *et al.* p53 degradation activity, expression, and subcellular localization of E6 proteins from 29 human papillomavirus genotypes. *J. Virol.* **86**, 94–107. https://doi.org/10.1128/JVI.00751-11 (2012).
22. Vliet-Gregg, P. A., Hamilton, J. R. & Katzenellenbogen, R. A. Human papillomavirus 16E6 and NFX1-123 potentiate Notch signaling and differentiation without activating cellular arrest. *Virology* **478**, 50–60. https://doi.org/10.1016/j.virol.2015.02.002 (2015).
23. Henken, F. E. *et al.* The functional role of Notch signaling in HPV-mediated transformation is dose-dependent and linked to AP-1 alterations. *Cell Oncol. (Dordr.)* **35**, 77–84. https://doi.org/10.1007/s13402-011-0062-4 (2012).
24. Rangarajan, A. *et al.* Activated Notch1 signaling cooperates with papillomavirus oncogenes in transformation and generates resistance to apoptosis on matrix withdrawal through PKB/Akt. *Virology* **286**, 23–30. https://doi.org/10.1006/viro.2001.0867 (2001).
25. Hiller, T., Poppelreuther, S., Stubenrauch, F. & Iftner, T. Comparative analysis of 19 genital human papillomavirus types with regard to p53 degradation, immortalization, phylogeny, and epidemiologic risk classification. *Cancer Epidemiol. Biomark. Prev.* **15**, 1262–1267. https://doi.org/10.1158/1055-9965.EPI-05-0778 (2006).
26. Fu, L. *et al.* Degradation of p53 by human Alphapapillomavirus E6 proteins shows a stronger correlation with phylogeny than oncogenicity. *PLoS ONE* https://doi.org/10.1371/journal.pone.0012816 (2010).
27. Talis, A. L., Huibregtse, J. M. & Howley, P. M. The role of E6AP in the regulation of p53 protein levels in human papillomavirus (HPV)-positive and HPV-negative cells. *J. Biol. Chem.* **273**, 6439–6445. https://doi.org/10.1074/jbc.273.11.6439 (1998).
28. Zanier, K. *et al.* Solution structure analysis of the HPV16 E6 oncoprotein reveals a self-association mechanism required for E6-mediated degradation of p53. *Structure* **20**, 604–617. https://doi.org/10.1016/j.str.2012.02.001 (2012).
29. Martinez-Zapien, D. *et al.* Structure of the E6/E6AP/p53 complex required for HPV-mediated degradation of p53. *Nature* **529**, 541–545. https://doi.org/10.1038/nature16481 (2016).
30. Yun, J. *et al.* p53 modulates notch signaling in MCF-7 Breast cancer cells by associating with the notch transcriptional complex via MAML1. *J. Cell Physiol.* **230**, 3115–3127. https://doi.org/10.1002/jcp.25052 (2015).
31. Yugawa, T. *et al.* Regulation of Notch1 gene expression by p53 in epithelial cells. *Mol. Cell Biol.* **27**, 3732–3742. https://doi.org/10.1128/MCB.02119-06 (2007).
32. Conrady, M. C. *et al.* Structure of high-risk Papillomavirus 31 E6 oncogenic protein and characterization of E6/E6AP/p53 complex formation. *J. Virol.* https://doi.org/10.1128/JVI.00730-20 (2020).
33. Matsuda, T. & Cepko, C. L. Controlled expression of transgenes introduced by in vivo electroporation. *Proc. Natl. Acad. Sci. USA* **104**, 1027–1032. https://doi.org/10.1073/pnas.0610155104 (2007).
34. Yu, X. *et al.* HES1 inhibits cycling of hematopoietic progenitor cells via DNA binding. *Stem Cells* **24**, 876–888. https://doi.org/10.1634/stemcells.2005-0598 (2006).
35. Tao, M., Kruhlak, M., Xia, S., Androphy, E. & Zheng, Z. M. Signals that dictate nuclear localization of human papillomavirus type 16 oncoprotein E6 in living cells. *J. Virol.* **77**, 13232–13247. https://doi.org/10.1128/jvi.77.24.13232-13247 (2003).

Acknowledgements
This work was supported by a grant from the Wilhelm Sander-Stiftung **2020.141.1** to CS and TI. We gratefully thank Scott vande Pol supplying us the plasmid EF.ICN1.CMV.GFP and constructive discussions on the dual-luciferase based *P-HES1* activity assay. We kindly thank Murielle Masson supplying us the H1299 cell line. We appreciate Daniel Sauter for the discussion on the fluorescence microscopy images.

Author contributions
J.W.L. experimental setup and performance. C.S. experimental setup, supervision. E.S. experimental setup. F.S. experimental setup, supervision. M.S. experimental setup, supervision. T.I. funding, supervision. J.W.L. and C.S. wrote the main manuscript text and prepared figures. All authors reviewed the manuscript.

Funding
Open Access funding enabled and organized by Projekt DEAL.

Competing interests
The authors declare no competing interests.

Additional information
Supplementary Information The online version contains supplementary material available at https://doi.org/10.1038/s41598-022-06922-0.

Correspondence and requests for materials should be addressed to C.S.

Reprints and permissions information is available at www.nature.com/reprints.

Publisher's note Springer Nature remains neutral with regard to jurisdictional claims in published maps and institutional affiliations.

Supplementary Information

An enhanced triple fluorescence flow-cytometry-based assay shows differential activation of the Notch signaling pathway by Human Papillomavirus E6 proteins

JiaWen Lim[1], Elke Straub[1] Frank Stubenrauch[1] Thomas Iftner[1], Michael Schindler[1], Claudia Simon[1]*

Supplementary Information SI 1: Fluorescence microscopy

C33A and H1299 cells were grown on coverslip and transfected with 375 ng mTagBFP2 or 1500 ng of respective mTagBFP2-E6 and mounted on microscopy slide. Control plasmid was always added to keep total amount of plasmid DNA transfected constant. In order to have a clear differentiation between nucleus and cytoplasm, both cells were stained with HCS NuclearMask Red stain (Thermo Scientific) that for unknown reasons in our cell lines accumulated in the cytosol around the nucleus as evident by co-staining with DAPI (Thermo Scientific) (see Fig. SIa). Nevertheless, in co-staining with HCS NuclearMask Red stain it is evident that only mTagBFP2 is distributed all over the cells whereas mTagBFP2-E6 fusion is localized in the nucleus, except 6bE6 which is in the nucleus and cytosol (This is in line with literature data[35]). Please see Fig. SIb. All images are visualized with Zeiss Axio Observer Z1 Inverted Phase Contrast Fluorescence Microscope equipped with Apotome.2 under Plan-Apochromat 63x/1.40 oil immersion objective. Images were acquired using Axiocam 503 and Zen2 (blue edition), version 2.0.14283.302. Acquisition information and the dimension of the images are shown in Table SI2 and Table SI3.

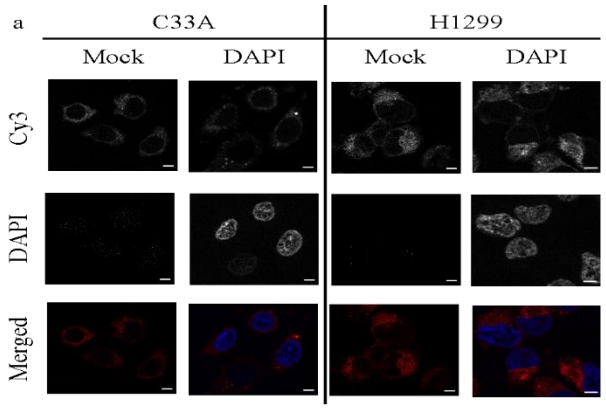

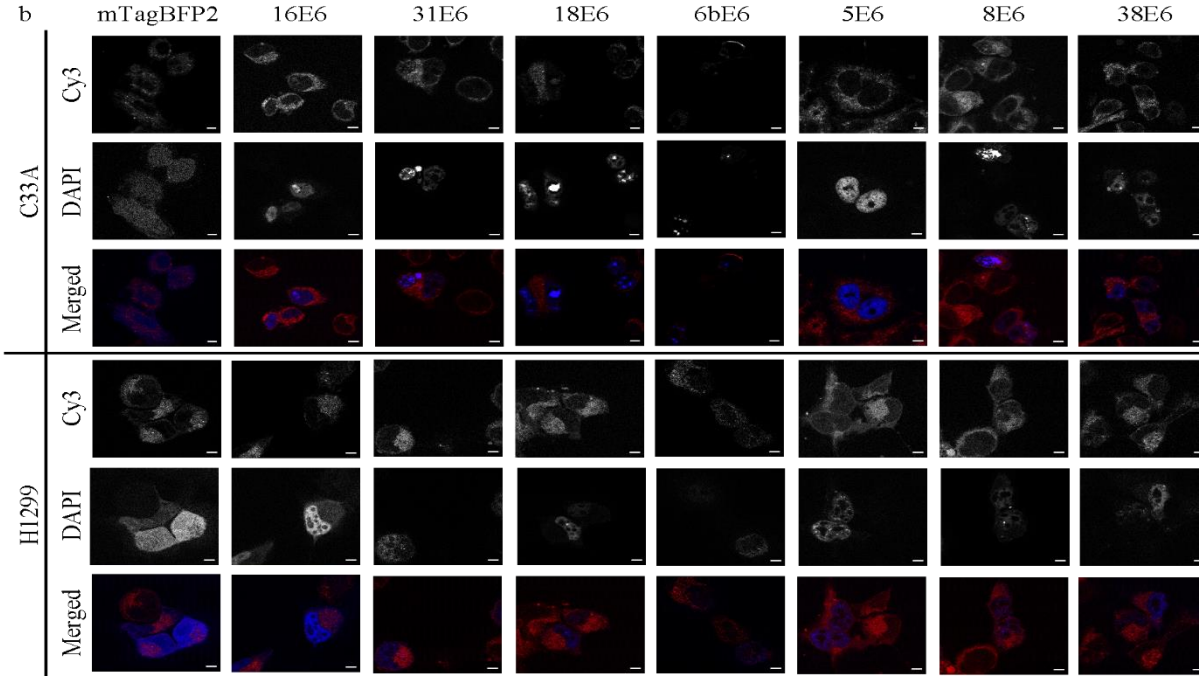

Figure SI1 Nuclear localization of mTagBFP2-E6.
C33A and H1299 cells were grown on coverslip and transfected with 375 ng mTagBFP2 or 1500 ng of respective mTagBFP2-E6. Control plasmid was always added to keep amount of total plasmid DNA transfected constant. After 48 hours post-transfection, cells were fixed with paraformaldehyde and nuclei were stained with HCS NuclearMask Red stain alone or co-stained with DAPI before mounted on microscopy slide. All images are visualized with Zeiss Axio Observer Z1 Inverted Phase Contrast Fluorescence Microscope equipped with Apotome.2 under 63x oil immersion objective. DAPI nuclear stained in a (exposure time = 15.3 ms) and mTagBFP2 or mTagBFP2-E6 in b (exposure time = 144.8 ms) were detected with DAPI channel while HCS NuclearMask Red stain was detected with Cy3 channel. a. HCS NuclearMask Red stain accumulates around the nucleus while DAPI shows a clear nucleus staining. b. mTagBFP2 alone localized everywhere in the cells while mTagBFP2-E6 localized in the nucleus. 18E6 and 6bE6 are expressed in the nucleoli whereas the other E6 are excluded from the nucleoli. 6bE6 localized in both nucleus and cytosol. All images were processed in Zen2 (blue edition) by cropped in the cells expressing mTagBFP2-E6 as shown. Scale bar = 5 µm.

Supplementary Information SI 2: Acquisition information of microscopy images

Table SI2 Acquisition information of microscopy images for C33A and H1299 cells.

Acquisition Information	HCS NuclearMask Red stain	mTagBFP2 / DAPI stain
Channel	Cy3	DAPI
Reflector	43 HE DsRed	49 DAPI
Beam splitter	570	395
Filter Ex. Wavelength	538-562	335-383
Filter Em. Wavelength	570-640	420-470

Supplementary Information SI 3: Image dimension of microscopy images

Table SI3 Image dimension of microscopy images during acquisition and export.

	C33A	H1299
Acquisition		
Image Size (Pixels)	968 x 728	968 x 728
Bit Depth	14 Bit	14 Bit
Exported		
Image size (Pixels)	448 x 448	455 x 425
Bit Depth	24 Bit	24 Bit

Supplementary Information SI 4: Full blot

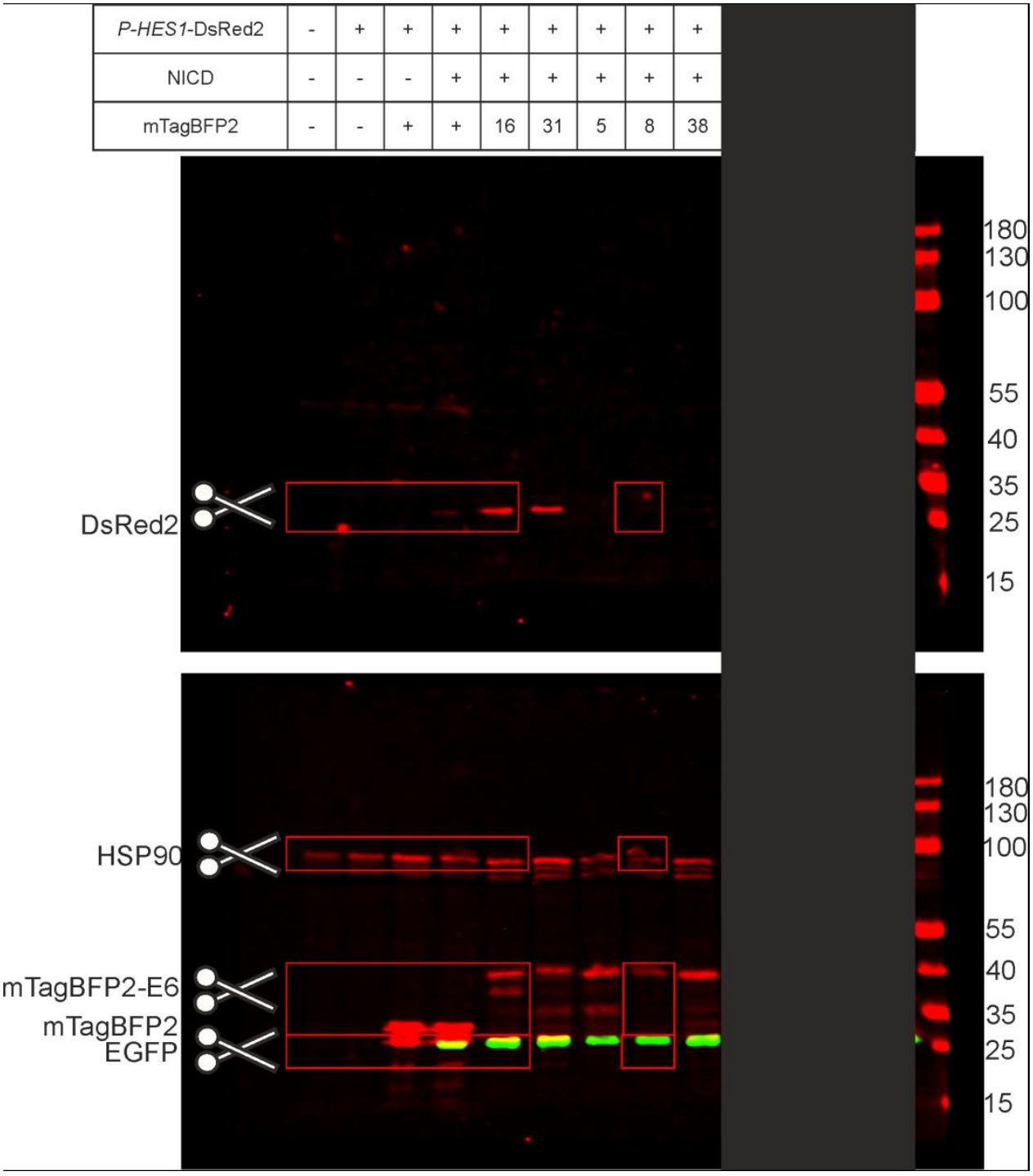

Figure SI4: Full length membrane blot of Figure 7 – Expression of proteins by Western blot analysis. Expression level on mTagBFP2 (27 kDa), mTagBFP2-E6 (~44kDa), DsRed2 (26kDa), and EGFP (27 kDa) were assessed by loading 70 µg total proteins on reducing 8-20% SDS-PAGE gel. HSP90 serves as a loading control. The blot was first incubated with anti-DsRed2 followed by IRDye 680RD Goat anti-Mouse (red). After visualization, the same blot was cut in between 55 kDa and 100 kDa marker band. The upper part of the blot was incubated with anti-HSP90 while the lower part was incubated with anti-tRFP to detect mTagBFP2

and mTagBFP2-E6. Then, upper part of the blot was incubated with IRDye 680RD Goat anti-Mouse (red) while the lower part with IRDye 680RD Goat anti-Rabbit (red). After visualization, the lower part of the same blot was incubated with Living Colors A.v. Monoclonal Antibody (JL-8) followed by IRDye 800RD Goat anti-Mouse (green) to detect EGFP. DsRed2 protein signal is increased for 16E6 but absent for 8E6. In line with FACS assay, these results indicate an activation by 16E6 and a repression for 8E6 of the Notch pathway. The cropped areas were highlighted with red boxes as shown above. Delineation of EGFP that shown in Figure 7 was cropped only in the green channel.

Supplementary Information SI 5: Guide to data analysis for triple fluorescence flow-cytometry-based assay

This supplementary information provides the step to step guide for the analysis of triple fluorescence flow-cytometry-based assay as shown in Fig. 8 and Fig. 10.

First, gate cells with the triple gating strategy as described in Fig. 6 to obtain data required for the following analysis.

➔ For the analysis shown in Fig. 8:

1. Import FACS data, either **% cells representing DsRed2 positive cell population** or **mean fluorescence intensity (MFI) that shows the intracellular expression level** of DsRed2 and mTagBFP2 from the **triple gated cells (P1/EGFP/mTagBFP2/DsRed2)**. Examples given below are calculated based on **mean MFI of three independent biological replicates**:

Table 1	Mean MFI P1/EGFP/mTagBFP2/DsRed2	
FPs	DsRed2	mTagBFP2
mTagBFP2	1239.6	40.7
8E6	632.2	57.7
16E6	1934.7	26.8

2. Calculate **relative promotor activity** as below:

$$\frac{\%\ cells\ or\ MFI\ of\ DsRed2\ obtained\ by\ modulator\ (E6)}{\%\ cells\ or\ MFI\ of\ DsRed2\ obtained\ by\ control\ (mTagBFP2)}$$

Table 2	*P-HES1* activity
mTagBFP2	1.0
8E6	0.5
16E6	1.6

➔ For the analysis shown in Fig. 10:

To calculate **Ratio of MFI of DsRed2: MFI of mTagBFP2**

First, set MFI of the control in to zero [called as delta DsRed2 (ΔDsRed2) from now on] by subtracting MFI of DsRed2 of modulator from Table 1 with MFI of DsRed2 of control from Table 1

MFI of DsRed2 of modulator (E6) – MFI of DsRed2 of control (mTagBFP2)

Table 3	ΔDsRed2
8E6	-607.5
16E6	695.1

Then, calculate Ratio of MFI of DsRed2 : MFI of mTagBFP2 as below:

$$\frac{\Delta DsRed2\ (from\ Table\ 3)}{MFI\ of\ mTagBFP2\ (from\ Table\ 1)}$$

Table 4	Ratio of MFI of DsRed2 : MFI of mTagBFP2
8E6	-11.1
16E6	25.7

Supplementary Information SI 6: Endogenous NICD is insufficient in activating *P-HES1* promotor

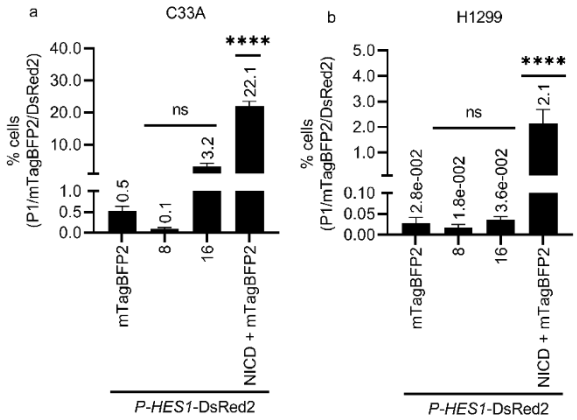

Figure SI6 DsRed2 positive cell population with/without exogenous NICD in C33A and H1299 cells. C33A and H1299 cells were transfected with 250 ng *P-HES1*-DsRed2, 125 ng mTagBFP2 or 500 ng mTagBFP2-E6, with or without 250 ng NICD as indicated. C33A cells were harvested 48 hours whereas H1299 cells were harvested 36 hours post transfection for FACS measurement. Living cells (P1) were double gated for mTagBFP2 followed by DsRed2 to examine the DsRed2 cell population activated with endogenous or exogenous NICD. A clear activation was observed in both cell line when NICD was co-transfected while endogenous NICD seemed to be insufficient to activate Notch activity. Co-transfection of modulator proteins mTagBFP2-E6 shows a similar trend as in mTagBFP2 without exogenous NICD. Three biological replicates were conducted in both cell lines with the mean value of % cells plotted and labelled above each bar. The error bars indicate the standard deviation of the mean value from the three independent replicates. P- values were calculated using One-Way ANOVA with Fischer's LSD test by comparing the mean each sample with mean of *P-HES1*-DsRed2 + mTagBFP2. **** = $P \leq 0.0001$, ns = $P > 0.05$.

Virology 576 (2022) 52–60

Contents lists available at ScienceDirect

Virology

journal homepage: www.elsevier.com/locate/virology

Cottontail rabbit papillomavirus E6 proteins: Interaction with MAML1 and modulation of the Notch signaling pathway

JiaWen Lim, Desiree Isabella Frecot, Frank Stubenrauch, Thomas Iftner **, Claudia Simon *

Institute of Medical Virology and Epidemiology of Viral Diseases, University Hospital Tuebingen, Tuebingen, Germany

ARTICLE INFO

Keywords:
Notch signaling pathway
Human papillomavirus
Cottontail rabbit papillomavirus

ABSTRACT

Animal models are necessary to study how cutaneous human papillomaviruses (HPVs) are associated with carcinogenesis. The cottontail rabbit papillomavirus (CRPV) induces papilloma in the -cutaneous skin of rabbits and serves as an established animal model for HPVlinked carcinogenesis where viral E6 proteins play crucial roles. Several studies have reported the dysregulation of the Notch signaling pathway by cutaneous beta HPV, bovine PV and mouse PV E6 via their association with Mastermind-like 1 protein (MAML1), thus interfering with cell proliferation and differentiation. However, the CRPV E6 gene encodes an elongated E6 protein (long E6, LE6) and an N-terminally truncated product (short E6, SE6) making it unique from other E6 proteins. Here, we describe the interaction between both CRPV E6 proteins and MAML1 and their ability to downregulate the Notch signaling pathway which could be a way CRPV infection induces carcinogenesis similar to beta HPV.

1. Introduction

Papillomaviruses (PVs) are small, non-enveloped, doublestranded DNA tumor viruses infecting epithelia in humans and animals. Infection with PVs may be asymptomatic or may progress into benign or malignant tumors upon persistent infection in the latter case. More than 210 human PV types are grouped into five genera (alpha, beta, gamma, mu, nu) based on the sequence of the major L1 capsid proteins and subdivided into different species (Bzhalava et al., 2015). Cutaneous beta HPVs (as e.g. HPV5, HPV8, HPV38, HPV49) are believed to be involved in non-melanoma skin cancer (NMSC) in cooperation with the ultraviolet (UV) radiation (Orth et al., 1978; Viarisio et al., 2011, 2018; Uberoi et al., 2016). The cutaneous cottontail rabbit papillomavirus (CRPV), which is also known as *Sylvilagus floridanu* papillomavirus 1 (SfPV1), belongs to the genus kappa and is the first papillomavirus described to be associated with malignant progression (Shope and Hurst, 1933). CRPV-induced lesions can either regress or develop into carcinoma, depending on the host. The CRPV-rabbit tumor model has been an important model for the investigation of latent infection (Selvakumar et al., 1997; Zhang et al., 1999; Maglennon et al., 2011), development of prophylactic and therapeutic vaccines (Breitburd et al., 1995; Christensen et al., 1996; Cladel et al., 2008; Govan et al., 2008; Schneider et al., 2020), anti-viral therapy (Kreider et al., 1990; Christensen et al., 2000; Han et al., 1999; Christensen, 2005), immunotherapy (Christensen et al., 2000; Han et al., 1999; Christensen, 2005) and the mechanism of carcinogenesis by cutaneous PV (Jeckel et al., 2002; Huber et al., 2004; Ganzenmueller et al., 2008; Muench et al., 2010; Leiprecht et al., 2014; Delcuratolo et al., 2016).

The viral regulatory proteins encoded by PV are crucial for developing and maintaining PV-associated carcinomas, with E6 as one of the important carcinogenic HPV proteins. E6 is highly conserved among PVs in structure and sequence. It consists of four zinc-binding motifs CxxC, resulting in two E6 domains, E6N and E6C. The open reading frame (ORF) of CRPV E6 encodes an elongated E6 protein (Fig. 1a), long E6 (LE6). The N-terminus of CRPV LE6 shares the conserved region with the other E6 proteins. However, the C-terminal elongation, the so-called tail, is not conserved and makes the CRPV E6 protein unique compared to other PV E6 proteins (Giri et al., 1985). The LE6 ORF also gives rise to an N-terminally truncated version of LE6, called short E6 (SE6). The function of SE6 is primarily unknown and proof of its expression in rabbit tumors is still lacking (Meyers et al., 1992).

Generally, E6 proteins bind to LxxLL motifs of cellular proteins. The LxxLL-peptides are bound in the cleft between the E6N and E6C domains. The best-studied model is the recruitment of the E3 ubiquitin ligase, E6AP by HR alpha HPV16 E6 to form a ternary complex with the tumor suppressor p53, leading to its degradation via the proteasomal

* Corresponding author.
** Corresponding author.
E-mail addresses: Thomas.iftner@med.uni-tuebingen.de (T. Iftner), Claudia.simon@med.uni-tuebingen.de (C. Simon).

https://doi.org/10.1016/j.virol.2022.08.014
Received 23 May 2022; Received in revised form 22 August 2022; Accepted 22 August 2022
Available online 11 September 2022

pathway (Talis et al., 1998; Mesplède et al., 2012; White et al., 2012; Martinez-Zapien et al., 2016; Conrady et al., 2020). As previously reported, cutaneous beta HPV E6s, e.g. HPV8 E6, bind the LxxLL motif of the Master-mind like 1 (MAML1) protein and by this are predicted to downregulate the Notch signaling (Brimer et al., 2012; Tan et al., 2012; Meyers et al., 2017, 2018).

Notch signaling plays crucial roles in cell fate determination and cell proliferation (Rangarajan et al., 2001). It is initiated by cell-to-cell contacts. The jagged2 cell surface proteins bind to the extracellular domain of Notch receptors triggering the proteolytic cleavage of the extracellular Notch domain by ADAM metalloproteases and the cleavage of the intracellular Notch domain (NICD) by the tetrameric ϒ-secretase complex. NICD translocates to the nucleus and forms a Notch activation complex with the DNA-binding protein CBF-1/RBPjk/Su(H)/Lag1, MAML1, p300, and other co-activators to activate transcription of the Notch target genes, e.g. *HES-1* (De Strooper et al., 1999; Lim et al., 2022). In addition to beta HPV E6 proteins, several studies have shown that also E6s encoded by bovine PV 1 (BPV-1) and Mus musculus 1 PV (MmuPV1) were able to associate with MAML1 and repress Notch transactivation activity (White et al., 2012; Brimer et al., 2012; Tan et al., 2012; Meyers et al., 2017).

For CRPV LE6, only interaction with p300 has been shown to be necessary in inhibiting p53-mediated apoptosis to facilitate the immortalization of keratinocytes and the tumor induction (Muench et al., 2010). CRPV LE6 does not interact with E6AP (Ganzenmueller et al., 2008). However, the association of CRPV E6 protein with MAML1 and its role in Notch signaling remains unknown.

Hence, we investigated if CRPV LE6 or SE6 can bind to LxxLL-motifs, target MAML1 and affect the Notch signaling pathway by combining sequence similarity analysis and *in cellulo* protein interaction studies as well as Notch-signaling pathway reporter assays. This will allow to understand the mechanism of CRPV-induced carcinogenesis better and generally of cutaneous PVs in carcinogenesis.

2. Material and methods

2.1. Structure predictions, sequence alignments and phylogenetic analysis

Structure predictions were carried out with LE6 and SE6 protein sequences using Jpred4 (Jnet version 2.3.1) (Drozdetskiy et al., 2015). Sequence alignments and sequence analysis were performed using JalView (version 2.11.1.4) (Waterhouse et al., 2009) with extracted PAVE E6 protein sequences as indicated.

2.2. Cell culture

HPV negative cervical cancer cells C33A were cultivated in Dulbecco's Modified Eagle Medium (DMEM) (Gibco, 41965-062) supplemented with 10% fetal bovine serum (FBS) (Gibco, 10270-106) and 50 μg/mL gentamycin (Gibco, 157710049) at 37 °C, 5% CO2, and 95% humidity. Immortalized rabbit keratinocyte RK1-16E7/ras were cultured in supplemented keratinocyte serum-free medium (K-SFM, Invitrogen) as described previously (Leiprecht et al., 2014). One day before transfection, 200 000 C33A or 180 000 RK1-16E7/ras cells were seeded in 12-well plates (Thermo Scientific, 150628) or 6 000 000 C33A cells in 150 mm plates (Thermo Scientific, 168381). On day 2, C33A cells were transfected with the respective plasmid DNAs using jetPRIME® (Polypus, #114-15), whereas RK1-16E7/ras were transfected using Polyethylenimine (PEI) (Polysciences, #26008) following manufacturer's instructions. C33A were harvested by trypsinization for FACS experiments or in lysis buffer for co-immunoprecipitation 48 h post-transfection, respectively. RK1-16E7/ras cells were harvested by trypsinization for FACS experiments 24 h post-transfection.

2.3. Plasmids and transfections

Plasmids used for co-immunoprecipitation assays include pNCMV vectors with FLAG-hemagglutinin epitopes (FLAG-HA) (a kind gift from Professor Karl Munger) (Spangle and Münger, 2010) fused to the amino termini of HPV5 E6 (GenBank: CAA52689.1), CRPV LE6M98S and CRPV SE6 (UniProtKB: AEG21063.1) via EcoRV and BamHI restriction site. All CRPV LE6 constructs were used as M98S to avoid SE6 expression starting at M98 (Meyers et al., 1992). MAML1 plasmid, pHAGE-N-V5-hMAML1-FL (Addgene #37048) (Tan et al., 2012) and pHAGE-N-V5-hMAML1 (1–990) (Addgene plasmid #37049) (Tan et al., 2012) were used for co-immunoprecipitation. For flow cytometry-based assays, HPV5 and 8 E6 (HPV8REF.1/GI:333 074), CRPV LE6 M98S, CRPV SE6 constructs were cloned in pmTagBFP2-C1 as described previously, obtaining an N-terminal fusion of E6 with mTagBFP2 (Lim et al., 2022). The same constructs were also used in triple fluorescence flow-cytometry-based Notch reporter assay.

For flow-cytometry-based-FRET (FACS-FRET) experiments, human MAML1 (hMAML1) full-length (1–1016), hMAML1full-length S1007 N mimicking the LxxLL motif of rabbit MAML1 (rMAML1), C-terminally truncated hMAML1 (1–990) with a deletion of the LxxLL motif were cloned into pEYFP-C1 obtaining an N-terminal fusion of hMAML1 with EYFP. C-terminal hMAML1 (759–1016) and C-terminal hMAML1 (759–990) with deletion of LxxLL motif were also cloned into pEYFP-C1 with nuclear localization sequence (NLS) of hMAML1 (PGHKKTRR) inserted downstream of EYFP and upstream of MAML1 (Fig. 3). C-

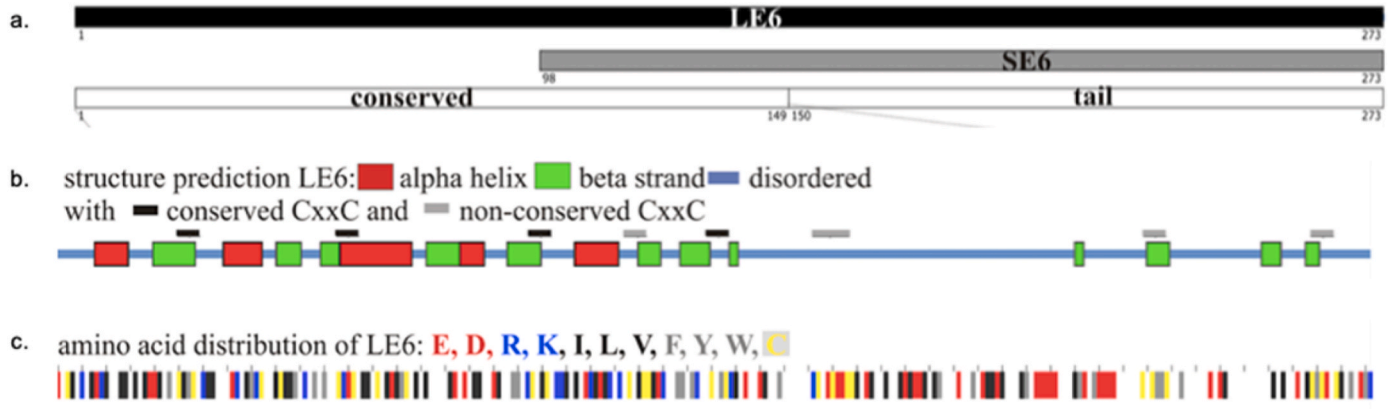

Fig. 1. The unique schematic structure of CRPV E6. a. Schematic structure of CRPV E6 shows the N-terminus (1–149) of CRPV E6 conserved with other E6 proteins of papillomaviruses. b. Structure prediction and CxxC motif of CRPVE6. The additional non-conserved CxxC motifs are in grey while the conserved CxxC motifs are in black. The tail region (150–273) is highly disordered. c. The amino acid composition of CRPV E6 shows that the tail region is highly acidic.

terminal fusions of MAML1-EYFP were not expressed sufficiently (data not shown). Plasmids used in triple fluorescence FACS-based Notch reporter assay including *P-HES1*-DsRed2 (Addgene #13767) (Matsuda and Cepko, 2007) and Notch signaling activator plasmid EF.ICN1.CMV.GFP (Addgene #17623) (Brimer et al., 2012) was a kind gift from Scott Vande Pol.

2.4. Co-immunoprecipitation

Human influenza hemagglutinin (HA) immunoprecipitation was performed with extracts from C33A cells that co-expressed FLAG-HA tagged E6 proteins and full-length hMAML1 (1–1016) or hMAML1 1–990. Four 150 mm plates with 90% confluent cells co-expressing FLAG-HA E6 and hMAML1 were harvested 16 h after treatment with 3 μM MG132 proteasome inhibitor in 3 mL of lysis buffer [10% (v/v) glycerol (MP Biomedicals, 4800689); 50 mM HEPES, pH 7.5 (Carl Roth, 9105.4); 3 mM magnesium chloride (Merck, 105833); 0.1% (v/v) IGEPAL CA-630 (NP-40) (Merck, 18896); 150 mM sodium chloride (Carl Roth, 3957.2); 1 mM Tris(2-carboxyethyl)phosphine (TCEP) (Alfa Aesar, J60316); 200 μM zinc chloride (Carl Roth, 3533); supplemented with Benzonase® Endonuclease (Merck, 101656), PhosSTOP™ (Roche, PHOSSRO) and cOmpleteTM EDTA-free Protease Inhibitor Cocktail (Roche, COEDTAF-RO)]. Cell lysates were incubated on a shaker at 4 °C for 1 h before centrifuging at 18 000 *xg* at 4 °C for 10 min. The total protein concentration of the cleared crude lysates was determined by the Bradford assay. Each time, 4500 μg of total proteins of the cleared crude lysates were incubated with 50 μL of anti-HA Microbeads (μMACS HA Isolation Kits (Miltenyi Biotec, #130-091-122) for 2 h at 4 °C. Then, the suspension was loaded on μColumns (Miltenyi Biotec, #130-042-701) that were attached to a μMACS Separator (Miltenyi Biotec, #130-042-602). Proteins of interest were eluted with reducing SDS-sample buffer after 5 times of column washing with 500 μL lysis buffer each time. Each eluted protein sample was heated at 95 °C for 10 min before further analysis by immunoblotting.

2.5. FACS-FRET

C33A cells co-expressing N-terminally fused mTagBFP2-E6 with different variants of EYFP-hMAML1 were used in FACS-FRET measurements. Cells expressing mTagBFP2-EYFP fusion were included as positive control while negative controls include the pairs of i) mTagBFP2 + EYFP, ii) mTagBFP2-E6s + EYFP or iii) EYFP-hMAML1 variants + mTagBFP2. All cells were washed in pre-cooled DPBS supplemented with 1% FBS (FACS buffer). Cells were then resuspended in 250 μL of FACS buffer followed by FACS measurement using MACSQuant® VYB Flow Cytometer (Miltenyi Biotec). FACS-FRET measurement was conducted as described previously (Banning et al., 2010). Cells expressing fluorescent proteins mTagBFP2 and EYFP were detected in channel V1 [405/450(50)] nm and B1 [488/529(50)] nm, respectively. FRET signal was assessed in channel V2 [405/525(50)] nm. FACS and statistical analysis were conducted using Flowlogic version 7.2.2 (Miltenyi–Inivai) and GraphPad Prism version 9.1.2 (226), respectively. All figures presented were prepared using CorelDraw®X7, version 17.5.0.907.

2.6. Immunoblotting

All proteins were resolved on reducing SDS-PAGE gradient gel (8% to 20%) at 4 °C and electrotransferred onto nitrocellulose membrane via wet blotting with blotting buffer (10 mM 3-(Cyclohexylamino)-1-propanesulfonic acid (CAPS), 10% (v/v) methanol, 0.1% (w/v) SDS, pH 10.3). The membrane blots were then blocked with 5% albumin (Carl Roth, 3737) in phosphate-buffered saline (PBS). Each blot was incubated with the following primary antibodies respectively: 1:200 Hsp 90 (4F-10) mouse monoclonal antibody (Santa Cruz Biotechnology, #sc-69703), 1:1000 HA-Tag (C29F4) rabbit monoclonal antibody (Cell signaling, #3724) and 1:1000 MAML1 rabbit polyclonal antibody (Cell Signaling, #4608) overnight at 4 °C. After three washing steps with PBS-Tween 20 (0.05% v/v), each blot was incubated with respective secondary antibodies (1:10 000 IRDye® 680RD goat anti-mouse IgG (LI-COR Biotechnology – GmbH, #926–68070) or 1:10 000 IRDye® 680RD goat anti-rabbit IgG (LI-COR Biotechnology – GmbH, #926–68071) followed by visualization with Licor Odyssey® Fc Imaging System and analyzed with Licor Image Studio™ Lite, version 5.2.5. All figures presented were prepared using CorelDraw®X7, version 17.5.0.907.

2.7. Triple fluorescence FACS-based Notch reporter assay

The FACS-based Notch reporter assay has been described previously (Lim et al., 2022). In short, C33A and RK1-16E7/ras were co-transfected with 250 ng reporter plasmid *P-HES1*-DsRed2, 250 ng activator plasmid encoding for NICD (activator) co-expressing EGFP as a transfection control, and 500 ng modulator plasmid mTagBFP2-E6. The cells were washed in pre-cooled DPBS supplemented with 1% FBS (FACS buffer). After that, cells were resuspended in 250 μL of FACS buffer. FACS measurement was carried out using MACSQuant® VYB Flow Cytometer (Miltenyi Biotec) with 200 μL taken for measurement. Cells expressing EGFP (Notch activator co-expressing EGFP) were first gated in channel B1 [488/525(50)] nm followed by mTagBFP2 (modulators which are the mTagBFP2 fusion E6s) in V1 [405/450(50)] nm and finally DsRed2 (*P-HES-1* reporter) in channel Y2 [561/615(20)] nm, thus resulting in triple fluorescence expressing cells (P1/EGFP/mTagBFP2/DsRed2) for the investigation of Notch transactivation activity. FACS analysis and statistical analysis were conducted using Flowlogic version 7.2.2 (Miltenyi–Inivai) and GraphPad Prism version 9.1.2 (226), respectively. Statistical analyses of three independent biological experiments are always conducted with One-way ANOVA with Fischer's LSD test. All figures presented were prepared using CorelDraw®X7, version 17.5.0.907.

3. Results

3.1. in silico analysis of CRPV E6 protein and the potential to interact with MAML1

HPV16 and 31 as well as HPV5 and 8 that come from the same alpha or beta species, respectively, share a sequence identity of more than 65% (Table 1). CRPV E6 is unique among E6 proteins due to its elongated tail structure (Fig. 1a). It consists of an N-terminal region that is conserved with other E6s (sequence identity of LE6 (1–149) to 8E6 and 16E6 is 27% and 26%, respectively (clustalX) (Table 1)). The E6 of the animal PVs MmuPV1 and BPV1 share sequence identity within the same range of 20–30% to the human PV alpha and beta E6 as to CRPV E6. In contrast, the tail region is neither conserved with any E6 protein nor shares similarities with other HPV E6 proteins nor any other protein (LE6 aa 150–276) present in the swiss protein database. This tail region is predicted to be largely unstructured (Jpred4, Fig. 1b) and is highly acidic with low complexity (Fig. 1c). The common E6N-E6C domain organization including the four CxxC motifs, which are important for zinc binding, are conserved in CRPV LE6 N-terminus (Fig. 1b). However, CRPV E6 full-length harbors five additional CxxC motifs: one in the

Table 1
Pairwise sequence alignments show the percentage identity of different pairs of E6. (kappa CRPV = LE6 (1–149) as the conserved N-terminal region.

	ID (%)		
	Kappa CRPV	Alpha HPV16	Beta HPV5
Kappa CRPV	NA	NA	NA
Alpha HPV16	26	NA	NA
Alpha HPV31	24	66	NA
Beta HPV5	27	23	NA
Beta HPV8	27	23	70
Pi MMuPV1	27	21	29
Delta BPV1	28	27	24

conserved region of E6C and four CxxC motifs in the tail region (Fig. 1b). The N-terminally truncated variant SE6 contains the conserved CxxC motifs of the E6C domain and the tail region of LE6. Notably, LE6 harbors 26 cysteines in total (Fig. 1c) limiting recombinant production due to oxidation of cysteines and unspecific oligomerization and aggregation during purification (data not shown), hampering structural analysis.

With regard to LxxLL binding, we aligned LE6 conserved region to beta HPV 8 or 5 E6 and alpha HPV 16 or 31 E6 (Fig. 2a). The amino acids L1, L4 and L5 of the LxxLL motif (Fig. 2b) are bound in a hydrophobic pocket of E6, which was shown to allow variability in the positions of the hydrophobic amino acids of E6 (Conrady et al., 2020). However, 16E6 L50, which is conserved among HPV, was shown to be crucial for LxxLL-binding. In addition, 16E6 R102, conserved among HPV E6 proteins, is a keystone amino acid because it bridges the E6N and E6C and the LxxLL motif. Notably, 16E6L50 and R102 are conserved in CRPV LE6 (Fig. 2a).

It has been shown that the E6 of the cutaneous beta HPV8, BPV1 and MmuPV1 can bind MAML1 and repress the Notch signaling (Brimer et al., 2012; Tan et al., 2012; Meyers et al., 2017). Mutants of HPV8 E6 have revealed that K64 in E6N and K142 in E6C are important for the interaction with hMAML1 (Meyers et al., 2017) as a predominant binding site and for the repressing activity of Notch transactivation. In 16E6 and 31E6, the analogous R55 (Martinez-Zapien et al., 2016; Conrady et al., 2020) which is conserved among alpha HPV, was shown to bind to the negatively charged E3 of the E6AP LxxLL-motif, which corresponds to the negatively charged D3 in the hMAML1 and rMAML1 LxxLL-motif (Fig. 2b). Notably, the position of 8E6 K64 is partially conserved in beta HPV (60% identity, JalView2). In CRPV LE6, WHK (51/52/53) instead of 8E6 WK (63/64) can be found. Here, either the protonated histidine or the positively charged lysine could contribute to the interaction with the negatively charged D3 of the LxxLL-motif. The other crucial amino acid for MAML1 binding and repressing Notch activity, 8E6 K142 is conserved among all beta HPV as "WKG" or "WRG" (W + G in Fig. 2A) but not in alpha HPV E6 proteins. It remains elusive if HPV 8E6 K142 participates in the interaction with the MAML1 directly or if it is essential for the integrity of the E6 protein. Nevertheless, W + G is also conserved as amino acid sequence "WRG" in CRPV LE6 and CRPV SE6.

In addition to the aa D3 in the MAML1 LxxLL motif that is conserved with regard to the binding to E6, the hydrophobic residue at position −3 upstream of LxxLL as well as the acidic side chain at position 2 and position −1 had also been reported to be required in the MAML1 binding (Brimer et al., 2012). These amino acids are conserved in hMAML1 and rMAML1 (Fig. 2b). Though the amino acid at position −2 upstream of rMAML1(N) is not conserved with the aa "S" in hMAML1, it is however conserved with position −2 of canine and murine MAML1 (Brimer et al., 2012). It was shown that human-dog or human-mouse MAML1, in which the last 12 amino acids of the human MAML1 sequence containing the LxxLL E6 binding site were replaced with the canine or murine LxxLL sequences, are able to bind to CPV2 and MnPV1 E6 proteins, respectively as well as to BPV1 E6 (Brimer et al., 2012).

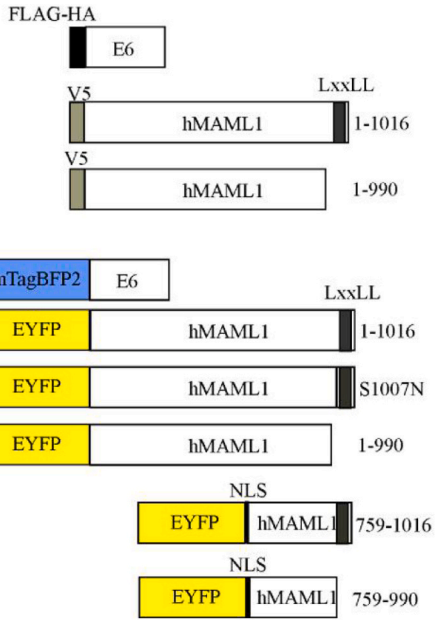

Fig. 3. E6 and MAML1 constructs.
In co-immunoprecipitation, E6s are N-terminally tagged with FLAG-HA while hMAML1 obtained from Addgene are N-terminally tagged with V5. All E6s and hMAML1 variants constructs used in FACS-FRET are N-terminally tagged with mTagBFP2 or EYFP, respectively as described. The figure is generated from CorelDraw®X7, version 17.5.0.907.

a.

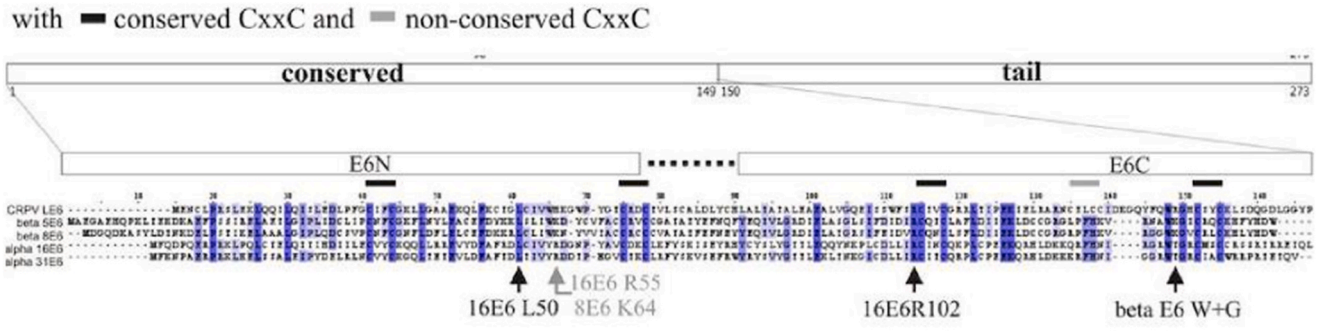

b.

genus	type	LxxLL	-3	-2	-1	1	2	3	4	5	+1	+2	+3	+4
kappa	CRPV	rMAML1	M	N	D	L	D	D	L	L	G	S	Q	/
beta	HPV8	hMAML1	M	S	D	L	D	D	L	L	G	S	Q	/
alpha	HPV16	hE6AP	E	L	T	L	Q	E	L	L	G	E	E	R
						L	x	x	L	L				

Fig. 2. Multiple sequence alignment of different E6 proteins. A. The sequences of E6 proteins are aligned with the conserved CxxC (blue) Zinc binding motif. The sequences are aligned with the program T-coffee and colored with the Clustal X color scheme in Jalview. B. LxxLL peptide sequences of rMAML1, hMAML1 and hE6AP that interact with HPV E6.

Hence, with these sequence similarities, we hypothesized that CRPV LE6 could interact with MAML1 because LE6 (I) shares N-terminally the primary structure necessary for the common two-domain structure E6N and E6C of the E6 proteins, and (II) harbors key amino acids for LxxLL-motif interaction and MAML1-LxxLL binding. In contrast, CRPV SE6 only contains the conserved E6C region, including the "WRG" motif.

3.2. CRPV E6 association with hMAML1

As a proof of concept, we conducted co-immunoprecipitation assays to pull down hMAML1 with FLAG-HA-E6 proteins in C33A cells. We could not co-immunoprecipitate endogenous hMAML1 for all tested E6 proteins due to the low endogenous expression level and detection limit of the applied antibodies already in the input (data not shown). Thus, we decided to carry out the experiment by co-transfecting C33A cells with FLAG-HA-E6 and pHAGE-V5-hMAML1full-length (1–1016). As hypothesized, HPV5 E6 which is closely related to HPV8 E6, and CRPV LE6M98S bind to hMAML1full-length (1–1016), while CRPV SE6 only showed a very weak signal in the pull-down (Fig. 4a). It was known that the binding of cutaneous beta HPV E6s to MAML1 predominantly requires the LxxLL motif (Brimer et al., 2012, 2017; Meyers et al., 2017). Hence, we repeated the experiment by co-transfecting C33A cells with FLAG-HA-E6 and pHAGE-V5-hMAML1 dLxxLL (1–990). Interestingly, hMAML1 dLxxLL (1–990) was pulled down by HPV5 E6 and CRPV LE6M98S but not CRPV SE6 (Fig. 4b). These data show that CRPV LE6 M98S is able to interact with hMAML1, whereas SE6 interacted only weakly. For CRPV LE6 M98S and 5E6, the interaction is not limited to the LxxLL motif indicating that other domains in hMAML1 may contribute.

To further investigate the association of CRPV LE6 M98S and CRPV SE6 with MAML1, we screened the interaction via FACS-FRET by co-transfecting mTagBFP2-E6s with different variants of MAML1 that are all N-terminally tagged with EYFP in C33A cell. A genetic fusion of mTagBFP2-EYFP served as a positive control. Negative controls include EYFP + mTagBFP2-E6 and mTagBFP2 + EYFP-hMAML1s. The beta mTagBFP-HPV8 and -HPV5 E6 served as biological positive controls. Notably, no FRET signal was observed for N-terminal truncations of hMAML1 with the positive controls (data not shown) unless the natural

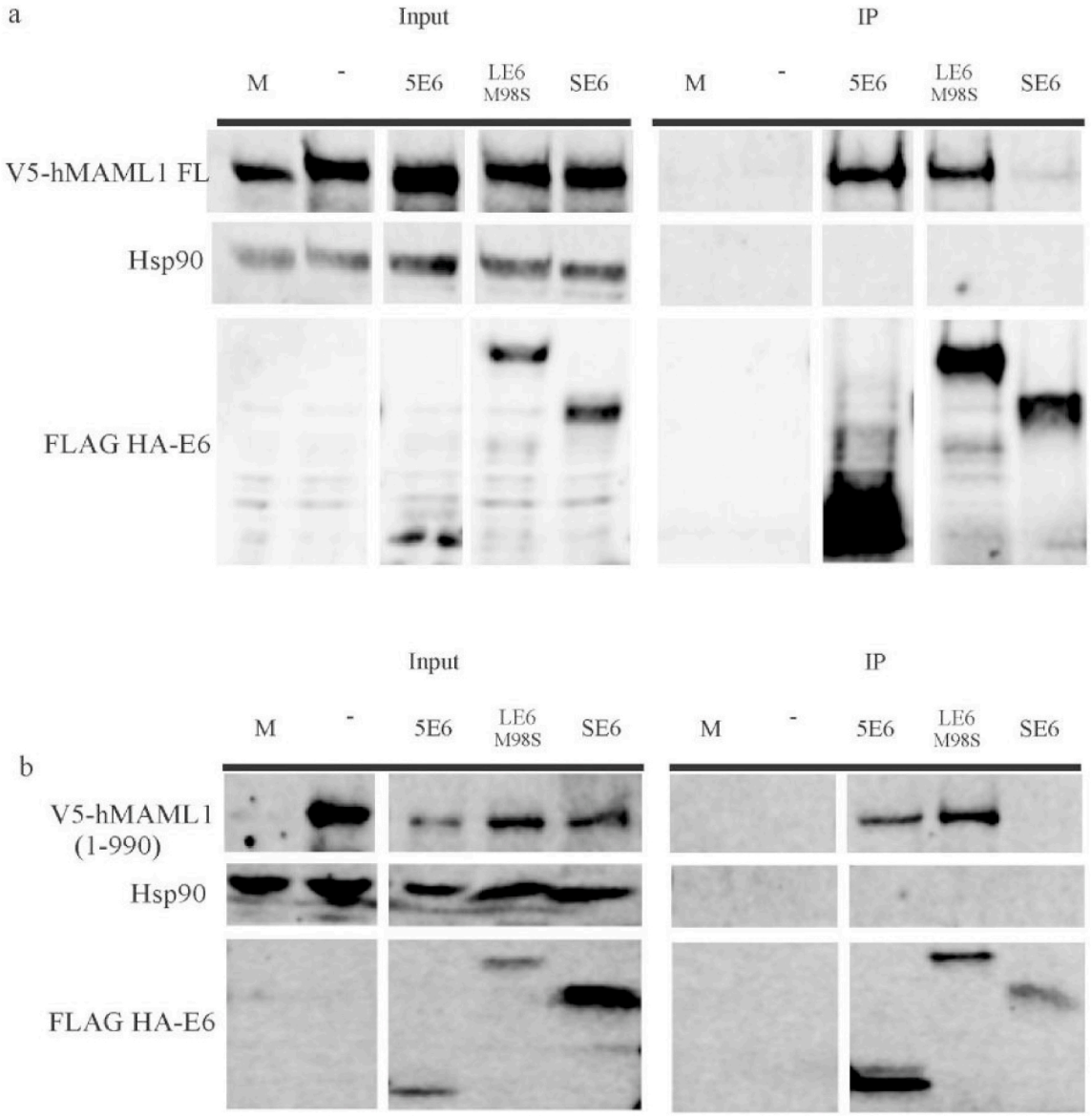

Fig. 4. CRPV E6 co-immunoprecipitated hMAML1.
The interaction between E6 and hMAML1. The HA co-immunoprecipitation shows a) hMAML1 1–1016 and b) 1–990 are pulled down by HPV5 E6 and CRPV LE6M98S. CRPV SE6 only co-immunoprecipitated hMAML1 1–1016 weakly but not hMAML1 1–990. M indicates a mock sample. Please see SI3 for the full blot.

NLS sequence of hMAML1 (aa 135 to 142) was cloned directly upstream of the variant sequence to allow the nuclear localization.

Interaction between E6s and hMAML1-FL: Here, HPV5 and HPV8 E6 show %FRET signals with MAML1 full-length (1–1016) of 45.4 ± 10.4% and 44.0 ± 10.4%, respectively (Fig. 5), and CRPV LE6 M98S with 82.0 ± 3.7% and CRPV SE6 with 32.7 ± 6.1%. However, it should be noted that the number of FRET-positive cells for CRPV SE6 is <500 cells (SI 1) which is below the threshold of a statistically significant cell population in this assay (Banning et al., 2010).

Interaction between E6s and hMAML1-FL with rabbit LxxLL-motif: We generated a mutant of hMAML1 by substituting S1007 to N to mimic the rabbit-MAML1-LxxLL motif. HPV5 E6 and HPV8 E6 co-expressed with hMAML1-FL S1007N showed a clear but twice lower % FRET signal (24.9 ± 1.5% and 26.6 ± 1.5%) while the %FRET signal of CRPV LE6 M98S remained similar (83.3 ± 1.4%) (Fig. 5). CRPV SE6 showed a FRET Signal of 21.3 ± 1.3%. However, again, the number of positive FRET cells with SE6 is < 500 (SI 1).

Alternative binding sites at MAML1: The same experiments were conducted with C-terminally LxxLL truncated hMAML1 (named as hMAML1 1–990 from now on). The depletion of the LxxLL-motif reduced the %FRET signal for HPV5 E6 and HPV8 E6 up to two-fold (27.4 ± 4.8% and 22.6 ± 5.8% for HPV5 and 8 E6, respectively) and the cell numbers of these are lower than the threshold of at least 500 cells (SI1), as compared to the full-length (Fig. 5). Hence, an interaction cannot be verified. Interestingly, the %FRET signal of 81.5 ± 7.0% for CRPV LE6 M98S and hMAML1 1–990, comparable to full-length hMAML1, clearly indicates binding. In contrast, CRPV SE6 gives a % FRET signal of 31.1 ± 10.3% (Fig. 5), but again fewer than 500 FRET-positive cells (SI 1). These results indicated that there might be a strong binding site in the N-terminus of hMAML1 for CRPV LE6M98S.

Consequently, we deleted residues 1–758 while retaining the NLS sequence of hMAML1 resulting in EYFP-NLS-hMAML1 759–1016 and EYFP-NLS-hMAML1 759–990 to investigate if the association between CRPV LE6 and MAML1 could be LxxLL independent. HPV5 and 8 E6 resulted in a %FRET signal of 52.5 ± 8.0% and 60.4 ± 7.6%, respectively with hMAML1 759–1016 while no FRET signal was detected with hMAML1 759–990 (Fig. 5). In contrast, CRPV LE6 M98S and CRPV SE6 show reduced %FRET signals of less than 20% with extremely low FRET positive cell number of fewer than 35 cells (SI 1), indicating that besides the MAML1 LxxLL motif, an additional binding site in hMAML1 seems to exist for CRPV LE6M98S.

In summary, the FACS-FRET data show that CRPV LE6 is capable of binding hMAML1, whereby the binding of SE6 seems to remain elusive (Table 2). In contrast to HPV5 and 8 E6, the binding seems not only dependent on the LxxLL-motif but instead depends on the N-terminal part of hMAML1 (1–758). The mutation of the hMAML1 LxxLL to the rabbit LxxLL (S1007 N) motif reduced the binding of HPV 5 and 8 E6 but did not affect the binding of CRPV E6.

Table 2
Summary of FACS-FRET results (%) for the interaction of E6 proteins with the different MAML1 variants (* indicates results with FRET positive cells below the threshold of 500 cells (Banning et al., 2010) which are statistically not relevant).

	LE6	SE6	5E6	8E6
hMAML1	82.0 ± 3.7	32.7 ± 6.1*	45.5 ± 10.4	44.0 ± 10.4
hMAML1 S1007 N	83.3 ± 1.3	21.3 ± 1.3*	24.9 ± 1.5	26.6 ± 1.5
hMAML1 1–990	81.5 ± 7.0	31.1 ± 10.3*	27.4 ± 4.8*	22.6 ± 5.8*
hMAML1 759–1016	11.5 ± 6.1*	7.0 ± 3.7	52.5 ± 8.0	60.4 ± 7.6
hMAML1 759–990	16.5 ± 7.7*	11.7 ± 7.3*	0.7 ± 0.4	0.3 ± 0.3

3.3. CRPV E6 repressed Notch signaling in rabbit keratinocytes but not in human cells

Beta HPV E6s were previously shown to repress Notch signaling via their association with MAML1 (Brimer et al., 2012; Tan et al., 2012; Meyers et al., 2017). To investigate if CRPV E6 could repress Notch signaling, we used the previously described triple fluorescence FACS-based Notch reporter assay. C33A (HPV negative human cervix cell line) and RK1 16E7/ras (rabbit keratinocytes immortalized by 16E7/ras) cells were co-transfected with a Notch responsive reporter plasmid *P-HES1*-DsRed2, an activator plasmid NICD, and the modulator plasmid mTagBFP2-E6. Viable cells co-expressing reporter, activator and modulator were sorted with a triple gating strategy (P1/EGFP/m-TagBFP2/DsRed2) as described earlier (Lim et al., 2022) to monitor the *P-HES1* transactivation activity. As expected for the Notch-repressing HPVs, a lower DsRed2-positive signal indicated a smaller cell population expressing the reporter DsRed2 was observed (Fig. 6, left) for beta HPV E6 in C33A cells (0.4 ± 0.1 and 0.4 ± 0.1 in HPV5 and 8E6, respectively).

Surprisingly, CRPV LE6 M98S and CRPV SE6 show no impact on the reporter activity in C33A cells despite a clear interaction with hMAML1 as shown above. However, in the rabbit keratinocytes, RK1 16E7/ras Notch responsive *P-HES1* reporter expression population was repressed by HPV5 E6 (0.4 ± 0.02), 8 E6 (0.3 ± 0.04) as well as by CRPV LE6M98S (0.4 ± 0.05) significantly, while CRPV SE6 showed only weak repression (Fig. 6).

Hence, these results demonstrate that CRPV LE6 M98S is able to downregulate the expression of Notch target gene *HES1* only in rabbit

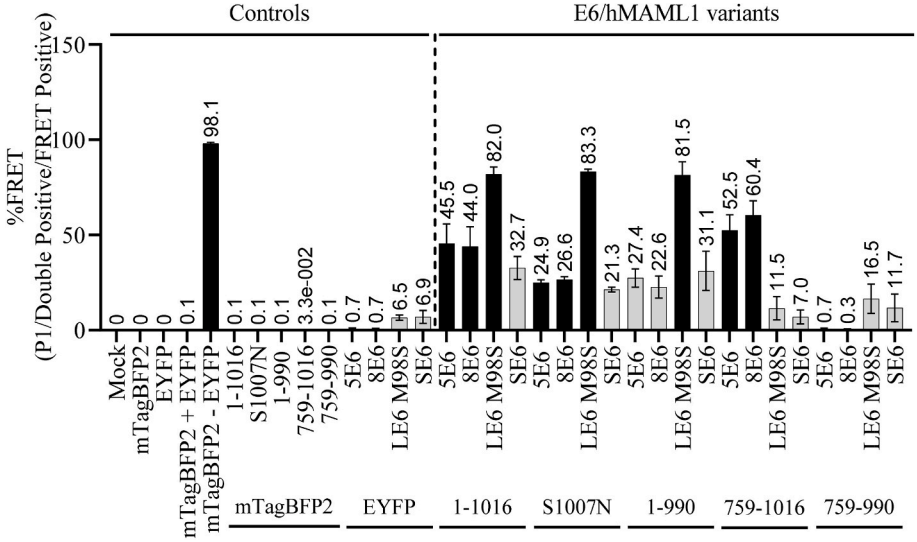

Fig. 5. CRPV E6 binding to hMAML1 is independent of the LxxLL motif. C33A co-expressing the different EYFP-hMAML1 variants and mTagBFP2-E6s, as indicated, are subjected to FACS-FRET measurement. Samples with cell numbers lower than 500 are in grey, always considered as negative FRET. In contrast, the black bars with more than 500 FRET-positive cells and %FRET of >10% are positive, indicating an observed interaction. HPV5 and 8 E6 bind hMAML1 1–1016, S1007 N, 1–990 and 759–1016 while CRPV LE6M98S showed only positive FRET signal with hMAML1 1–1016, S1007 N and 1–990. CRPV SE6 did not fulfill the threshold that concludes a positive FRET signal. No FRET was observed for all E6s with hMAML1 759–990. Data were derived from the mean value of three independent biological replicates with the mean value stated above each bar. The error bars were plotted to represent the standard deviation of the mean value from the three independent biological replicates.

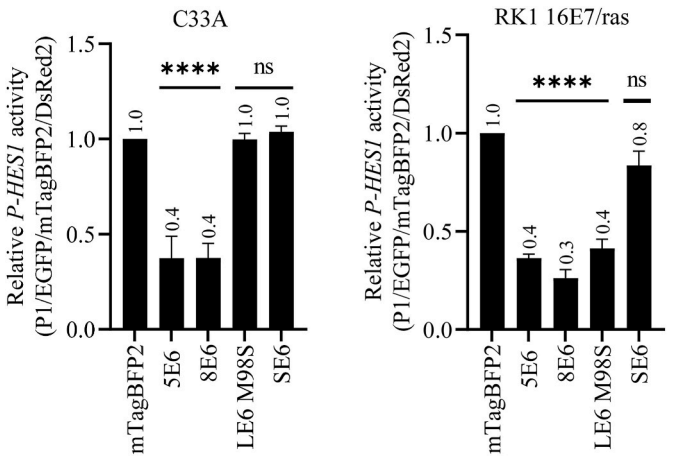

Fig. 6. CRPV E6 inhibits Notch in rabbit keratinocytes.
Viable cells co-expressing Notch activator (NICD) with EGFP, mTagBFP2-E6 and *P-HES1*-DsRed2 are triple gated (P1/EGFP/mTagBFP2/DsRed2) as described. a. In C33A cells, HPV 5 and 8 E6 inhibit *P-HES1* promotor activity. CRPV E6 activates the *P-HES1* promotor weakly and has no impact on *P-HES1* activity. b. In RK1 16E7/ras keratinocyte, HPV5 and 8 E6, as well as CRPV LE6M98S, repress *P-HES1* promotor activity while CRPV SE6 weakly represses the activity. Data were derived from three independent biological replicates with the mean value plotted and labeled on top of each bar. The error bars were the standard deviation of the mean value. P values were calculated using One-Way ANOVA with Fischer's LSD test by comparing the mean value of each sample to the control sample, where **** = $P \leq 0.0001$, ns = $P > 0.05$.

keratinocytes but not in the human cell line C33A. CRPV SE6 showed no impact on *P-HES1* regulated transcription of DsRed2.

4. Discussion

HPV5 and HPV8 were the first cutaneous beta HPV types isolated from the skin of EV patients (Orth et al., 1978). Organ transplant recipients and immunocompetent patients are believed to be a high-risk group of individuals in acquiring HPV infection which may then progress into non-melanoma skin carcinoma upon UV exposure. Viarisio et al. showed that the oncoproteins E6 and E7 of beta HPV38 cooperate with UV and significantly contribute to the development of actinic keratosis-like lesions and squamous cell carcinoma in mice (Viarisio et al., 2011). Later on, they found that HPV38 oncogenic proteins play a role in initiating UV radiation-mediated skin tumorigenesis but are not required for its maintenance in mice (Uberoi et al., 2016).

One of the largest obstacles faced in papillomavirus research is the lack of an animal model for studying pathogenesis associated with beta HPV. The multiple sequence alignment of E6s from MmuPV1, BPV1 or CRPV to human alpha or beta PV revealed that their percentage sequence identity to HPV E6 are within a similar range (Table 1). They also share the crucial CxxC motifs as described earlier (Fig. 1b). MmuPV1 has been suggested to be a suitable animal model to study the pathogenesis of cutaneous HPV infection as MmuPV1 E6 shares similar cellular targets with beta HPV E6s including MAML1 and Notch repression (Meyers et al., 2017, 2018) as well as the risk factor UV exposure that promotes malignant progression of MmuPV1 induced warts (Uberoi et al., 2018). BPV1 and CRPV models have been used for decades and CRPV has been proven to be one of the best models to study the infection and carcinogenesis caused by high-risk PV (Breitburd et al., 1995; Christensen et al., 1996, 2000, 2017; Cladel et al., 2008; Govan et al., 2008; Schneider et al., 2020; Kreider et al., 1990; Han et al., 1999; Christensen, 2005; Hu et al., 2007). Hence, CRPV which only infects cutaneous skin is a suitable animal model to study the mechanism of carcinogenesis of beta HPV.

Here we examined if CRPV E6 associates with MAML1, a conserved target for beta HPV E6 by co-immunoprecipitation and FACS-FRET analyses. Notably, FACS-FRET analysis can only be evaluated qualitatively due to the different expression levels of the MAML1 variants and the different E6 proteins (SI2). This limits the comparison of the FRET signals between the different E6 proteins and the MAML1 variants. Advantageously, FACS-FRET analysis detects transient interactions in living cells, which co-immunoprecipitation experiments might not detect. Our results showed that CRPV LE6 M98S is able to interact with hMAML1 as shown for HPV8, MmuPV1 and BPV1 (Brimer et al., 2012; Tan et al., 2012; Meyers et al., 2017) while CRPV SE6 seems to interact only weakly with hMAML1, (Figs. 4 and 5). We also showed for the first time *in cellulo* the interaction between hMAML1 and HPV5 E6 which belongs to the same species as HPV8 E6. All E6s bind to S1007 N hMAML1 mutants mimicking the C-terminus of the rMAML1 LxxLL motif which suggests that all tested E6 may also bind to rMAML1. However, while HPV5 and 8E6 do repress Notch signaling in the human cell line C33A and the rabbit keratinocyte RK1 16E7/ras, CRPV LE6 only represses Notch signaling in rabbit RK1 16E7/ras cells and does not in human cells indicating that a species-specific factor plays a crucial role in Notch repression.

It was reported previously that the C-terminus acidic domain of MAML1 (DLIDSLLKNRTSEEWMSD**L**DD**LL**GSQ) is crucial for the binding to beta HPV, BPV1 and MmuPV1 E6 and that the interaction stabilizes E6 (Brimer et al., 2012; Meyers et al., 2017). This was confirmed with our FACS-FRET analysis. Although FRET signals for HPV5 and 8 E6 with hMAML1 759–1016 were detected, a weaker signal with hMAML1 1–990 was observed that was lost with hMAML1 759–990. It should be noted that the number of double positive cells (E6+/MAML1+) was so low when CRPV LE6M98S was co-expressed with N-terminally truncated hMAML1 (SI2) that no conclusions could be drawn. Nevertheless, our results show that the association of CRPV LE6M98S with hMAML1 may not only depend on the LxxLL motif (Fig. 5) but additional binding sites within the MAML1 protein.

To date, it is unclear how E6 interacts with MAML1 and consequently dysregulates the Notch pathway. CRPV E6 consists of four conserved CxxC motifs that create an E6N and E6C domain in its N-terminus. E6 proteins are known to interact with LxxLL motifs in several cellular proteins via their E6N and E6C domain (Martinez-Zapien et al., 2016; Conrady et al., 2020; Zanier et al., 2013). However, an additional CxxC motif is found in-between the conserved CxxC motif that makes up the E6C domain (Fig. 1) whose function is so far unclear. Recently, Drews *et al* reported the interactions of E6 proteins from several human PVs and animal PVs with E6AP and characterized these interactions into two different types, namely, Type I interaction in which E6 proteins such as HPV16 and SsPV1 E6, that are able to interact directly with the LxxLL peptide of E6AP to recruit p53 fall in this group; while Type II interaction refers to E6 proteins like HPV11 and MmPV1 E6 that require either the N-terminus or the C-terminus HECT domain to associate with the LxxLL motif of E6AP (Drews et al., 2020). From these data, one could speculate that a similar mechanism might be involved in the interaction between CRPV E6 and MAML1. It would be interesting to further characterize the E6/MAML1 complex in the future to unravel how these two proteins interact.

We previously showed that CRPV E6 like HPV38 (Muench et al., 2010), HPV5 and 8 E6 (Howie et al., 2011) is able to interact with p300, another co-activator of Notch. Interestingly, MmuPV1 E6 which does not bind to p300 is able to repress the Notch activity (Meyers et al., 2017). CRPV with an E6 protein that is able to interact with both MAML1 and p300, like the beta HPV E6s, therefore seems an interesting model system to study the pathogenesis of cutaneous HPV in relation to the Notch signaling pathway as a potential drug target for HPV-related carcinogenesis.

Notch signaling plays a crucial role as a tumor suppressor in squamous epithelial cells. It was reported previously that the NICD translocates to the nucleus upon cleavage by gamma-secretase and forms a Notch initiation complex with other cellular proteins (De Strooper et al.,

1999). However, the formation of the Notch initiation complex is inhibited by the E6 proteins from HPV5, 8, 38, BPV1, and MmuPV1 via their association with MAML1 (Brimer et al., 2012; Tan et al., 2012; Meyers et al., 2017; Lim et al., 2022). Thus, we further investigated the effect of CRPV LE6M98S and CRPV SE6 on the Notch responsive *HES1* promoter, focusing only on the pathway downstream of NICD translocation. The repression of Notch responsive *HES-1* activity by beta HPV E6s is consistent in both C33A and RK1 16E7/ras with similar fold change in the repression activity (SI4) despite a different transfection efficiency observed in the two cell types (SI5), which supports the reported data (Brimer et al., 2012; Tan et al., 2012; Meyers et al., 2017; Lim et al., 2022). Surprisingly, the Notch responsive *P-HES-1* activity was repressed by CRPV LE6M98S only in rabbit keratinocytes but not in human cells, indicating species-specific effects. Interestingly, our group previously described another species-specific function of CRPV E6 and E7 that immortalized primary rabbit keratinocytes, while primary human keratinocytes could not be immortalized (Ganzenmueller et al., 2008). If we combine these findings, it appears that the species-specific restriction of hampering Notch transactivation is the same as the ability to immortalize primary cells. It should be noted that the Notch initiation complex is formed with the DNA-binding protein CBF-1/RBPjk/Su (H)/Lag1, MAML1, p300, and other co-activators to activate transcription of the Notch target genes, e.g., *HES-1* (De Strooper et al., 1999; Lim et al., 2022). Hence, it is plausible that the inhibition is mediated through other E6 binding partners such as p300, shown previously in our group (Muench et al., 2010), or some other not-yet-defined partners. Future investigations should therefore investigate which component of the Notch initiation complex is the primary target of CRPV E6 in dysregulating the Notch signaling and if the Notch pathway is directly involved in the immortalization of primary rabbit cells and the carcinogenesis in the rabbit animal model system.

5. Conclusion

The results shown in this study provide evidence that CRPV E6 interacts with MAML1 and represses the Notch signaling pathway, which is in alignment with beta HPV. Surprisingly Notch signaling repression was found to be species-dependent and worked only in rabbit cells, similar to the species-specific immortalization of CRPV E6/E7 that also was restricted to rabbit cells found earlier. Hence, the CRPV animal model keeps great promise for more in-depth investigations on cutaneous PV-associated carcinogenesis with respect to the role of Notch signaling.

Ethics approvals and consent to participate

Not applicable.

Consent for publication

Not applicable.

Funding

This work was supported by a grant from the Wilhelm Sander-Stiftung 2020.141.1 to CS and TI.

CRediT authorship contribution statement

JiaWen Lim: Data curation, Methodology, Formal analysis, Investigation, Visualization, Writing - original draft, Writing - review & editing. **Desiree Isabella Frecot:** Data curation. **Frank Stubenrauch:** Supervision, Writing - review & editing. **Thomas Iftner:** Conceptualization, Funding acquisition, Supervision, Validation, Project administration, Resources, Writing - review & editing. **Claudia Simon:** Conceptualization, Methodology, Data curation, Funding acquisition, Methodology, Project administration, Resources, Software, Supervision, Validation, Visualization, Writing - original draft, Writing - review & editing.

Declaration of competing interest

The authors declare that they have no known competing financial interests or personal relationships that could have appeared to influence the work reported in this paper.

Acknowledgements

We gratefully thank Scott Vande Pol for supplying us with the plasmid EF.ICN1.CMV.GFP and constructive discussions on the dual-luciferase-based *P-HES1* activity assay. We would like to acknowledge funding from Wilhelm Sander-Stiftung 2020.141.1 to CS and TI.

List of abbreviations

BPV1	bovine papillomavirus 1
CPV2	canine papillomavirus 2
CRPV	cottontail rabbit papillomavirus
D	aspartic acid
FACS	Fluorescence-activated cell sorting
FRET	Förster resonance energy transfer
H	histidine
HA	human influenza hemagglutinin amino acids 98-106
HPV	human papillomavirus
HR	high-risk
K	lysine
LR	low risk
MAML1	Mastermind-like 1 protein
MmPV1	Macaca mulata papillomavirus 1
MmuPV1	Mus musculus papillomavirus 1
MnPV 1	Mastomys natalensis papillomavirus 1
N	asparagine
NICD	notch intracellular domain
ORF	open reading frame
R	arginine
S	serine
SDS-PAGE	sodium dodecyl sulfate polyacrylamide gel electrophoresis
SsPV1	Sus scrofa papillomavirus 1
UV	ultraviolet
W	tryptophan

Appendix A. Supplementary data

Supplementary data to this article can be found online at https://doi.org/10.1016/j.virol.2022.08.014.

References

Banning, C., et al., 2010. A Flow Cytometry-Based FRET Assay to Identify and Analyse Protein-Protein Interactions in Living Cells, vol. 5.
Breitburd, F., et al., 1995. Immunization with viruslike particles from cottontail rabbit papillomavirus (CRPV) can protect against experimental CRPV infection. J. Virol. 69 (6), 3959–3963.
Brimer, N., et al., 2012. Cutaneous papillomavirus E6 oncoproteins associate with MAML1 to repress transactivation and NOTCH signaling. Oncogene 31 (43), 4639–4646.
Brimer, N., Drews, C.M., Vande Pol, S.B., 2017. Association of papillomavirus E6 proteins with either MAML1 or E6AP clusters E6 proteins by structure, function, and evolutionary relatedness. PLoS Pathog. 13 (12) e1006781-e1006781.
Bzhalava, D., Eklund, C., Dillner, J., 2015. International standardization and classification of human papillomavirus types. Virology 476, 341–344.
Christensen, N.D., 2005. Cottontail rabbit papillomavirus (CRPV) model system to test antiviral and immunotherapeutic strategies. Antivir. Chem. Chemother. 16 (6), 355–362.

Christensen, N.D., et al., 1996. Immunization with viruslike particles induces long-term protection of rabbits against challenge with cottontail rabbit papillomavirus. J. Virol. 70 (2), 960–965.
Christensen, N.D., et al., 2000. In vivo anti-papillomavirus activity of nucleoside analogues including cidofovir on CRPV-induced rabbit papillomas. Antivir. Res. 48 (2), 131–142.
Christensen, N.D., et al., 2017. Recent advances in preclinical model systems for papillomaviruses. Virus Res. 231, 108–118.
Cladel, N.M., et al., 2008. CRPV genomes with synonymous codon optimizations in the CRPV E7 gene show phenotypic differences in growth and altered immunity upon E7 vaccination. PLoS One 3 (8) e2947-e2947.
Conrady, M.C., et al., 2020. Structure of high-risk papillomavirus 31 E6 oncogenic protein and characterization of E6/E6AP/p53 complex formation. J. Virol. 95 (2).
De Strooper, B., et al., 1999. A presenilin-1-dependent gamma-secretase-like protease mediates release of Notch intracellular domain. Nature 398 (6727), 518–522.
Delcuratolo, M., et al., 2016. Papillomavirus-associated tumor formation critically depends on c-fos expression induced by viral protein E2 and bromodomain protein Brd4. PLoS Pathog. 12 (1), e1005366.
Drews, C.M., Brimer, N., Vande Pol, S.B., 2020. Multiple regions of E6AP (UBE3A) contribute to interaction with papillomavirus E6 proteins and the activation of ubiquitin ligase activity. PLoS Pathog. 16 (1) e1008295-e1008295.
Drozdetskiy, A., et al., 2015. JPred4: a protein secondary structure prediction server. Nucleic Acids Res. 43 (W1), W389–W394.
Ganzenmueller, T., et al., 2008. The E7 protein of the cottontail rabbit papillomavirus immortalizes normal rabbit keratinocytes and reduces pRb levels, while E6 cooperates in immortalization but neither degrades p53 nor binds E6AP. Virology 372 (2), 313–324.
Giri, I., Danos, O., Yaniv, M., 1985. Genomic structure of the cottontail rabbit (Shope) papillomavirus. Proc. Natl. Acad. Sci. U. S. A 82 (6), 1580–1584.
Govan, V.A., Rybicki, E.P., Williamson, A.-L., 2008. Therapeutic immunisation of rabbits with cottontail rabbit papillomavirus (CRPV) virus-like particles (VLP) induces regression of established papillomas. Virol. J. 5 (1), 45-45.
Han, R., et al., 1999. Protection of rabbits from viral challenge by gene gun-based intracutaneous vaccination with a combination of cottontail rabbit papillomavirus E1, E2, E6, and E7 genes. J. Virol. 73 (8), 7039–7043.
Howie, H.L., et al., 2011. Beta-HPV 5 and 8 E6 promote p300 degradation by blocking AKT/p300 association. PLoS Pathog. 7 (8) e1002211-e1002211.
Hu, J., et al., 2007. Impact of genetic changes to the CRPV genome and their application to the study of pathogenesis in vivo. Virology 358 (2), 384–390.
Huber, E., et al., 2004. Gene profiling of cottontail rabbit papillomavirus-induced carcinomas identifies upregulated genes directly Involved in stroma invasion as shown by small interfering RNA-mediated gene silencing. J. Virol. 78 (14), 7478–7489.
Jeckel, S., et al., 2002. A transactivator function of cottontail rabbit papillomavirus e2 is essential for tumor induction in rabbits. J. Virol. 76 (22), 11209–11215.
Kreider, J.W., et al., 1990. Treatment of latent rabbit and human papillomavirus infections with 9-(2-phosphonylmethoxy)ethylguanine (PMEG). Antivir. Res. 14 (1), 51–58.
Leiprecht, N., et al., 2014. A novel recombinant papillomavirus genome enabling in vivo RNA interference reveals that YB-1, which interacts with the viral regulatory protein E2, is required for CRPV-induced tumor formation in vivo. Am J.Cancer Res. 4 (3), 222–233.
Lim, J., et al., 2022. An enhanced triple fluorescence flow-cytometry-based assay shows differential activation of the Notch signaling pathway by human papillomavirus E6 proteins. Sci. Rep. 12 (1), 3000.
Maglennon, G.A., McIntosh, P., Doorbar, J., 2011. Persistence of viral DNA in the epithelial basal layer suggests a model for papillomavirus latency following immune regression. Virology 414 (2), 153–163.
Martinez-Zapien, D., et al., 2016. Structure of the E6/E6AP/p53 complex required for HPV-mediated degradation of p53. Nature 529 (7587), 541–545.
Matsuda, T., Cepko, C.L., 2007. Controlled expression of transgenes introduced by in vivo electroporation. Proc. Natl. Acad. Sci. U. S. A 104 (3), 1027–1032.
Mesplède, T., et al., 2012. p53 degradation activity, expression, and subcellular localization of E6 proteins from 29 human papillomavirus genotypes. J. Virol. 86 (1), 94–107.
Meyers, C., et al., 1992. Identification of three transforming proteins encoded by cottontail rabbit papillomavirus. J. Virol. 66 (3), 1655–1664.
Meyers, J.M., et al., 2017. Cutaneous HPV8 and MmuPV1 E6 proteins target the NOTCH and TGF-β tumor suppressors to inhibit differentiation and sustain keratinocyte proliferation. PLoS Pathog. 13 (1) e1006171-e1006171.
Meyers, J.M., et al., 2018. Inhibition of TGF-β and NOTCH signaling by cutaneous papillomaviruses. Front. Microbiol. 9 (389).
Muench, P., et al., 2010. Cutaneous papillomavirus E6 proteins must interact with p300 and block p53-mediated apoptosis for cellular immortalization and tumorigenesis. Cancer Res. 70 (17), 6913–6924.
Orth, G., et al., 1978. Characterization of two types of human papillomaviruses in lesions of epidermodysplasia verruciformis. Proc. Natl. Acad. Sci. U. S. A 75 (3), 1537–1541.
Rangarajan, A., et al., 2001. Notch signaling is a direct determinant of keratinocyte growth arrest and entry into differentiation. EMBO J. 20 (13), 3427–3436.
Schneider, M., et al., 2020. Orf virus-based therapeutic vaccine for treatment of papillomavirus-induced tumors. J. Virol. 94 (15).
Selvakumar, R., et al., 1997. Regression of papillomas induced by cottontail rabbit papillomavirus is associated with infiltration of CD8+ cells and persistence of viral DNA after regression. J. Virol. 71 (7), 5540–5548.
Shope, R.E., Hurst, E.W., 1933. Infectious papillomatosis of rabbits : with a note on the histopathology. J. Exp. Med. 58 (5), 607–624.
Spangle, J.M., Münger, K., 2010. The human papillomavirus type 16 E6 oncoprotein activates mTORC1 signaling and increases protein synthesis. J. Virol. 84 (18), 9398–9407.
Talis, A.L., Huibregtse, J.M., Howley, P.M., 1998. The role of E6AP in the regulation of p53 protein levels in human papillomavirus (HPV)-positive and HPV-negative cells. J. Biol. Chem. 273 (11), 6439–6445.
Tan, M.J.A., et al., 2012. Cutaneous β-human papillomavirus E6 proteins bind Mastermind-like coactivators and repress Notch signaling. Proc. Natl. Acad. Sci. U. S. A 109 (23), E1473–E1480.
Uberoi, A., et al., 2016. Role of ultraviolet radiation in papillomavirus-induced disease. PLoS Pathog. 12 (5) e1005664-e1005664.
Uberoi, A., Yoshida, S., Lambert, P.F., 2018. Development of an in vivo infection model to study Mouse papillomavirus-1 (MmuPV1). J. Virol Methods 253, 11–17.
Viarisio, D., et al., 2011. E6 and E7 from beta HPV38 cooperate with ultraviolet light in the development of actinic keratosis-like lesions and squamous cell carcinoma in mice. PLoS Pathog. 7 (7), e1002125.
Viarisio, D., et al., 2018. Beta HPV38 oncoproteins act with a hit-and-run mechanism in ultraviolet radiation-induced skin carcinogenesis in mice. PLoS Pathog. 14 (1) e1006783-e1006783.
Waterhouse, A.M., et al., 2009. Jalview Version 2—a multiple sequence alignment editor and analysis workbench. Bioinformatics 25 (9), 1189–1191.
White, E.A., et al., 2012. Comprehensive analysis of host cellular interactions with human papillomavirus E6 proteins identifies new E6 binding partners and reflects viral diversity. J. Virol. 86 (24), 13174–13186.
Zanier, K., et al., 2013. Structural basis for hijacking of cellular LxxLL motifs by papillomavirus E6 oncoproteins. Science (New York, N.Y.) 339 (6120), 694–698.
Zhang, P., et al., 1999. Induction of E6/E7 expression in cottontail rabbit papillomavirus latency following UV activation. Virology 263 (2), 388–394.

Supplementary Information 1 (SI1): Number of FRET positive cells

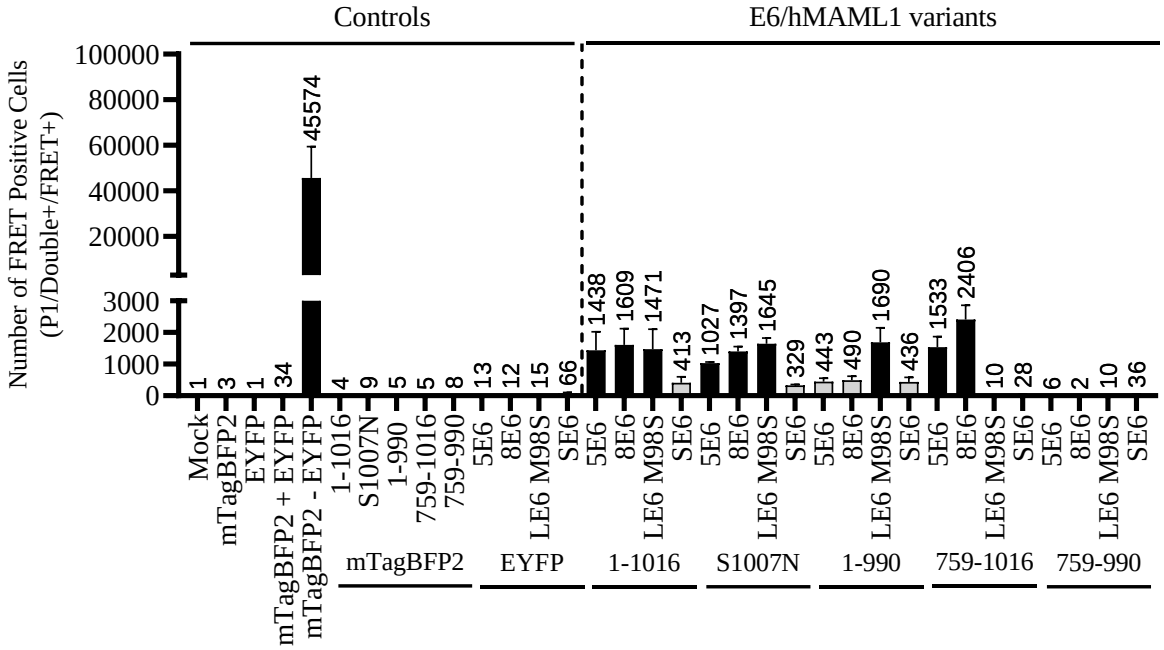

Figure SI1. Number of FRET-positive cells.
The number of FRET-positive cells corresponds to the % FRET signal in Figure 3a. C33A co-expressing the different EYFP-MAML1 variants and mTagBFP2-E6s as indicated are subjected to FACS-FRET measurement. Samples with cell numbers lower than 500 are grey, while the black bars have more than 500 FRET-positive cells. Data are derived from the mean value of three independent biological replicates with the mean value stated above each bar. The error bars are plotted to represent the standard deviation of the mean value from the three independent biological replicates.

Supplementary Information 2 (SI2): % signal and number of double positive cells for FACS-FRET

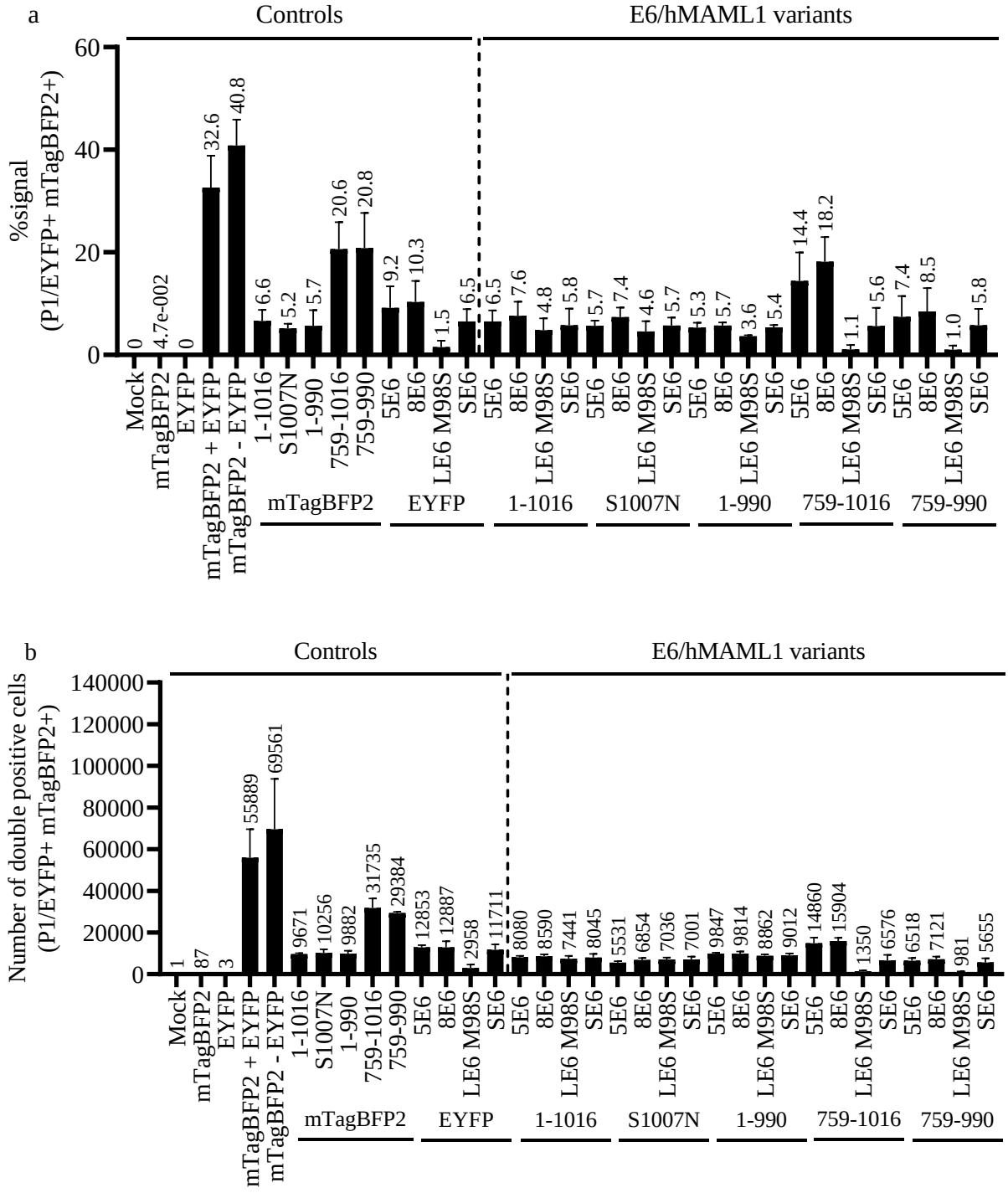

Figure SI2. % signal and the number of double positive cells.
C33A co-expressing the different EYFP-hMAML1 variants and mTagBFP2-E6s as indicated are subjected to FACS-FRET measurement. Viable cells are gated for EYFP and mTagBFP2 to examine cells expressing both mTagBFP-E6 and EYFP-hMAML1 variants. Data are derived from the mean value of three independent biological replicates with the mean value stated above each bar. The error bars are plotted to represent the standard deviation of the mean value from the three independent biological replicates.

Supplementary information 3 (SI3): Full blot

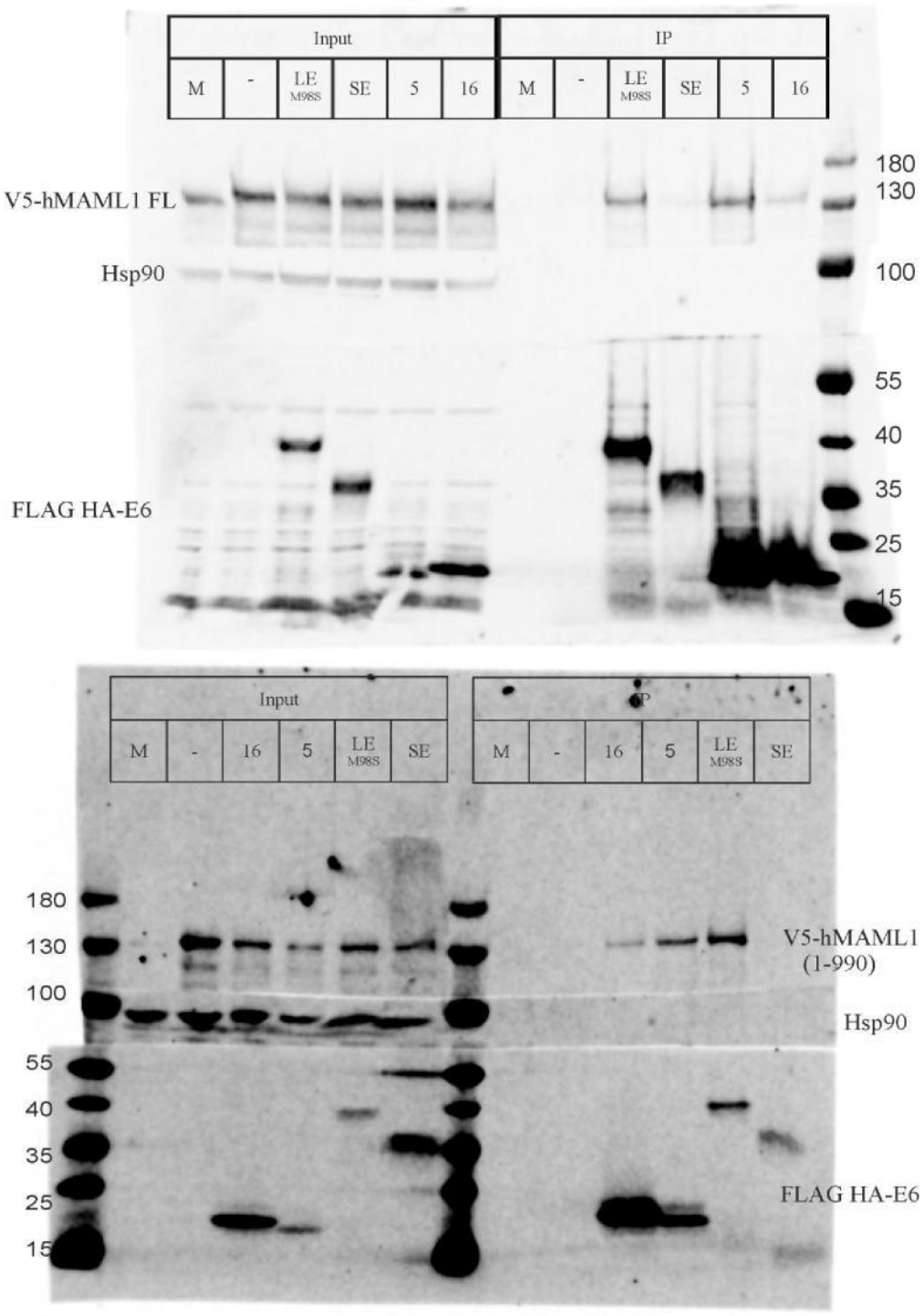

Figure SI3 Co-immunoprecipitation of MAML1 by FLAG-HA-E6
Full western blot. The HA co-immunoprecipitation show hMAML1 1-1016 and 1-990 are pulled down by HPV16, 5 E6, and CRPV LE6M98S. CRPV SE6 only co-immunoprecipitated hMAML1 1-1016 slightly but not hMAML1 1-990. The M indicates mock. The blot was cut between 55 and 100 kDa and between 100 and 130kDa and incubated with different antibodies. Membrane blot 15 – 55 kDa was incubated with anti-HA antibodies followed by IRDye® 680RD Goat anti-Rabbit IgG; 55 -100 kDa membrane was incubated with anti-Hsp90 (as loading control) followed by IRDye® 680RD Goat anti-Mouse IgG; and finally, the 100 – 180 kDa membrane blot was incubated with anti-MAML1 followed by IRDye® 680RD Goat anti-Rabbit IgG.

Supplementary information 4 (SI4): Notch inhibition by E6 proteins (non-normalized data)

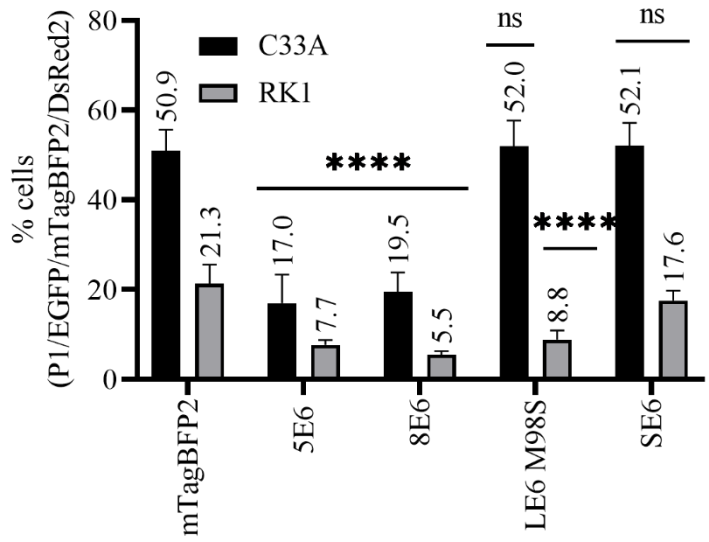

CRPV E6 inhibits Notch in rabbit keratinocytes. Viable cells co-expressing Notch activator (NICD) with EGFP, mTagBFP2-E6 and *P-HES1*-DsRed2 are triple gated (P1/EGFP/mTagBFP2/DsRed2) as described. In C33A cells, HPV5 and 8 E6 inhibit *P-HES1* promotor activity. CRPV E6 activates the *P-HES1* promotor weakly and has no impact on *P-HES1* activity. In RK1 16E7/ras keratinocyte, HPV5 and 8 E6, as well as CRPV LE6M98S, repress *P-HES1* promotor activity while CRPV SE6 weakly represses the activity. Though a higher activation was shown in C33A cells, the repression activity in the two different cell types was in a similar fold change of approximately 2.5-fold to 3-fold. Data were derived from three independent biological replicates with the mean value plotted and labeled on top of each bar. The error bars are the standard deviation of the mean value. P values were calculated using One-Way ANOVA with Fischer's LSD test by comparing the mean value of each sample to the control sample, where **** = $P \leq 0.0001$, ns = $P > 0.05$.

Supplementary information 5 (SI5): Transfection efficiency in C33A and RK1

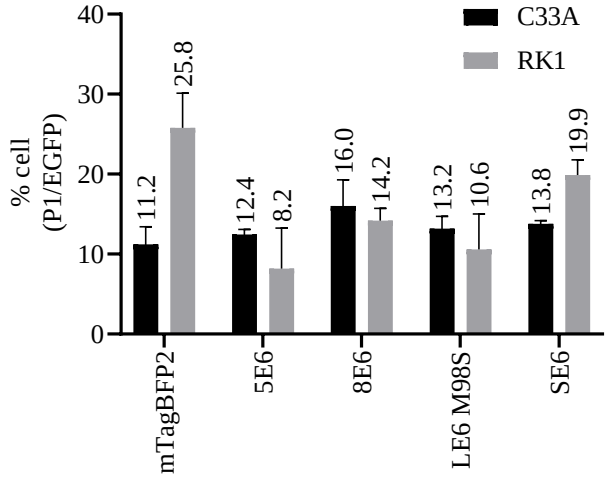

Transfection efficiency in C33A and RK1. Viable cells co-expressing Notch activator (NICD) with EGFP, mTagBFP2-E6, and *P-HES1*-DsRed2 were gated for EGFP signal (P1/EGFP) in C33A and RK1, assuming EGFP signal was not interfered by the expression of other recombinant proteins. Different % cell populations were observed in C33A and RK1, indicating the different transfection efficiency. Data were derived from three independent biological replicates with the mean value plotted and labeled on top of each bar. The error bars are the standard deviation of the mean value.

Native Isolation of 3×HA-Tagged Protein Complexes to Characterize Protein-Protein Interactions

JiaWen Lim,[1] Thomas Iftner,[1] and Claudia Simon[1,2]

[1]Institute of Medical Virology, Medical Faculty, Eberhard-Karls-University, Tuebingen, Germany

[2]Corresponding author: *Claudia.simon@med.uni-tuebingen.de*

Co-immunoprecipitation (Co-IP) is a straightforward method that is widely used in studying direct protein-protein interactions in physiological environments. This technique is based on the antigen-antibody interaction: the protein of interest (bait) is captured by a specific antibody, followed by antibody-bait precipitation. The proteins interacting with the bait protein (prey) co-precipitate with the antibody-bait complex from a cell lysate as an antibody-bait/prey complex. Nowadays, a variety of surface-functionalized materials with antibodies immobilized on agarose or magnetic beads are available, replacing the precipitation of antibodies and simplifying the application. However, unspecific binding of cellular proteins to matrix surfaces and/or antibodies has become a common issue. Unspecific binding that leads to false-positive signals and a high background can hamper further analysis. Our protocol describes a strategy to tremendously reduce unspecific background when isolating native proteins and protein complexes. Instead of eluting our samples under denaturing conditions, we elute triple hemagglutinin (3×HA)-tagged bait/prey complexes in their native form with a competitive peptide simulating the 3×HA tag of the bait protein. Matrix-unspecific interacting proteins and Co-IP antibodies remain on the matrix instead of being eluted under conventionally applied denaturing conditions. We optimized the elution by altering incubation time, eluent concentration, and temperature. These improvements result in more pure proteins. This strategy not only reduces background in SDS-PAGE and western blot but also allows complex characterization in vitro. © 2021 Wiley Periodicals LLC.

This article was corrected on 19 July 2022. See the end of the full text for details.

Keywords: co-immunoprecipitation • native elution • native protein complexes • protein interaction • pull down

How to cite this article:
Lim, J., Iftner, T., & Simon, C. (2021). Native isolation of 3×HA-tagged protein complexes to characterize protein-protein interactions. *Current Protocols*, *1,* e29. doi: 10.1002/cpz1.29

The study of protein-protein interactions is one of the most important steps to understand the maintenance and regulation of biological activities in cells. There are numerous approaches to investigate protein-protein interactions in which co-immunoprecipitation (Co-IP) is used to analyze stable and strong protein complexes. For definition, the protein of interest is called bait protein. Proteins that interact with the bait protein and are

BASIC PROTOCOL

CURRENT PROTOCOLS
A Wiley Brand

Current Protocols e29, Volume 1
Published in Wiley Online Library (wileyonlinelibrary.com).
doi: 10.1002/cpz1.29

co-precipitated are called prey proteins. Advantageous prey proteins can be unknown and are identified by Co-IP by analyzing the precipitates by mass spectrometry to identify novel interaction partners.

Formerly, protein-protein complexes were precipitated from cell lysates as large antibody-protein complexes. This strategy necessitates validated antibodies raised against each individual bait protein. Co-IP has been eased by fusing epitope tags to the bait protein at either the N- or the C-terminus, which facilitates the precipitation of a broad range of tagged bait proteins and their bound prey proteins with commercial high-affinity antibodies that bind to the fused epitope tag (Fig. 1). Another advantage of using tagged proteins is the fact that the epitopes that antibodies bind to are not always characterized. Antibody binding might compete with the bait/prey interaction, interfering with bait/prey binding by steric hindrance, if the antibody epitope is close to the bait/prey interface. Antibodies binding to the fused terminal epitopes are less likely to interfere with bait/prey binding.

Alternatively, antibody-protein complexes can be isolated by applying a Protein G or A affinity matrix. Proteins G and A have high affinity for the constant region (Fc) of most antibody classes, ensuring no interference with antigen binding to the variable site (Fab) of antibody molecules (Kaboord & Perr, 2008; Lin & Lai, 2017). Furthermore, the isolation of the antibody-bait/prey complex is simplified by direct, covalent coupling of antibodies to magnetic beads or agarose beaded support (Fig. 1). In combination with epitope tagging of the bait protein, this allows automation of the Co-IP. These alternative methods of isolating the antibody-bait/prey complex are not classical precipitations; rather, they are called pull downs.

Antibody interactions are very strong. Proteins can be eluted by a drop in pH or denaturing conditions such as in the presence of sodium dodecyl sulfate (SDS), urea, or guanidinium hydrochloride. Commonly, reducing SDS sample buffer is used, followed by SDS-PAGE and western blot analysis. All elution methods include the unfolding of proteins and disintegration of the protein complexes. Another disadvantage of denaturing elution is the co-elution of unspecific binders, immunoglobulin (Ig), or Ig light chains, which can cause problems in the downstream application, such as giving unspecific and false-positive signals or high background in western blots and mass spectrometry. Unspecific binding occurs due to binding of proteins to the antibodies or the surface of beads. Blocking the surface of the beads with bovine serum albumin (BSA) is described in many troubleshooting protocols to minimize unspecific binding of cellular proteins. However, this results in high BSA contamination after denaturing elution and interferes with mass spectrometry analysis. In addition, denaturing elution hinders further characterization of the eluted proteins, such as structural analysis, crosslinking/native mass spectrometry, or activity analysis. In order to tackle this problem, native elution of the protein complex, which does not elute unspecific binders, is necessary.

In this protocol, we describe a strategy for the elution of bait proteins under native conditions without loss of the proteins' biological activities by employing the established 16E6/E6AP/p53 ternary complex as our experimental model. The method is based on the competitive elution of the triple hemagglutinin (3×HA)-tagged bait protein 3×HA-E6AP by applying 3×HA-peptide as an eluent. We analyzed eluted samples with respect to their protein content and purity by SDS-PAGE and western blot.

Overview and Principle

Co-IP is a direct method that is commonly used to study protein-protein interactions under physiological conditions. Antibodies bind to proteins of interest called bait proteins and facilitate co-purification of the interacting partners, called prey proteins, from cellular lysates (Fig. 1). Antibody-antigen interactions are one of the strongest reversible

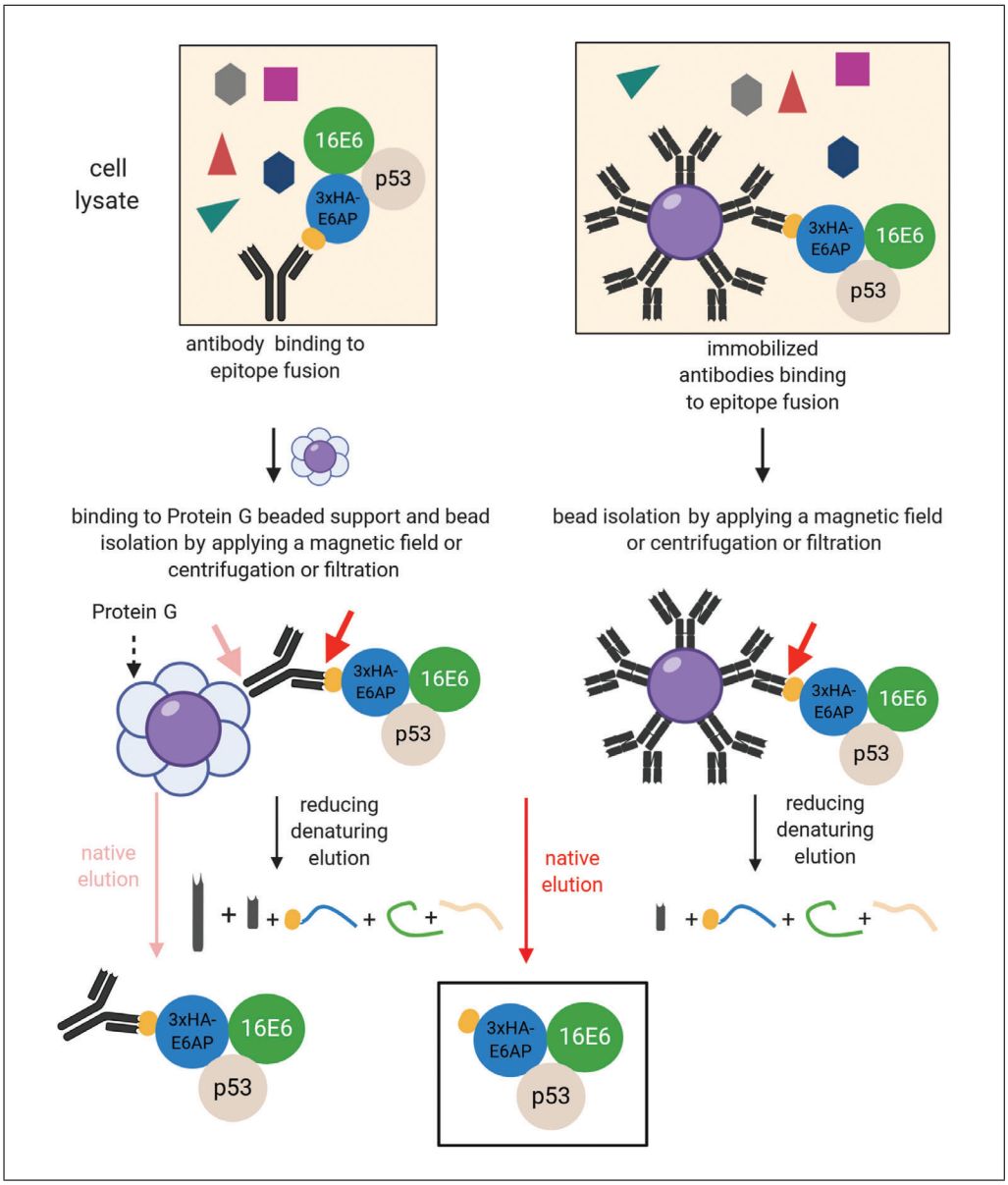

Figure 1 Schematic overview of bead-assisted co-immunoprecipitation of 3×HA-E6AP/16E6/p53 ternary complex. The antibody captures the 3×HA-E6AP/16E6/p53 ternary complex by binding to the epitope fusion tag (yellow) of the 3×HA-E6AP. The antibody complex is then isolated by binding to a Protein G beaded support (left) or antibody directly immobilized on magnetic beads or agarose beaded support (right). Denatured complex proteins and antibodies (heavy and light chains) as well as proteins nonspecifically bound to the bead surface and antibodies (not shown) elute from the isolated beads under denaturing conditions. Protein G (left) and the heavy chain (right) are covalently coupled to the beads and do not co-elute. The red arrows indicate the possible site of native elution, which competes with the binding of the antibody to the epitope fusion tag. The pink arrow (left only) indicates the possibility to elute the complex by competing with the Protein G–antibody interaction. Here, the eluted antibody remains bound to the complex. Our strategy involves E6AP with N-terminal 3×HA fusion as an epitope for an anti-HA antibody, which is immobilized on magnetic beads. Native elution is triggered by a 3×HA-peptide competing with the antibody for fusion epitope binding, as indicated by the red arrow (right). The figure was created with BioRender.com.

biological interactions. Most antibodies have a high avidity due to polyvalent epitope-binding sites. The dissociation constant (K_d) of an antibody-antigen interaction is usually in the picomolar (pM) range, demonstrating a high functional affinity. Furthermore, antibodies are highly specific regarding antigen binding. Consequently, antibodies can bind to their antigens even at low antigen concentrations in crude extracts, making them preferable candidates for affinity purification. However, for a successful Co-IP, it is important to maintain the integrity of proteins and protein complexes during the Co-IP procedure. Thus, gentle lysis and appropriate washing conditions are required (see Strategic Planning).

The antibody-bait/prey complex can be isolated by different approaches, including direct precipitation, binding to Protein G or A, or direct covalent coupling of the bait-specific antibody to a beaded support (Fig. 1). Proteins G and A are bacterial cell membrane proteins that bind to Ig heavy chains, preferring IgG and IgA, respectively. Commonly, Proteins G and A are covalently coupled to a beaded support. Usually, this strategy is used if the bait is not fused to an epitope tag. Consequently, the Co-IP needs to involve a bait protein–specific antibody.

Magnetic beads with immobilized antibodies are commonly used for Co-IP of proteins with epitope fusions, such as HA, FLAG, c-myc, or V5 tags.

Affinity Epitope Tagging

Fusing epitope tags to a bait protein is commonly used in detecting proteins in vitro and in cell culture. These epitopes are relatively short and have very specific primary antibodies that are commercially available for most tags. These short tags also rarely affect the properties of the heterologous protein of interest. HA peptide (YPYDVPDYA) derived from human influenza virus HA protein is one of the fusion protein tags widely used in recombinant protein expression and immunodetection in mammalian cells. We choose the multimeric HA tag (3×HA) because it was previously shown by Ranawakage, Takada, & Kamachi (2019) that this trimeric tag can significantly improve the affinity toward an anti-HA antibody, specifically six-fold. In the case of bait proteins that show low expression levels, this trimeric tag can be a key means of improving Co-IP. Commercially, several anti-HA antibodies that are pre-immobilized on magnetic beads or agarose resin beads are available, allowing isolation of HA-tagged protein complexes from cell lysate.

Native Elution Improves Specificity and Purity of Protein Complexes

Cell lysates are a complex mixture of macromolecules such as nucleic acids, proteins, and lipids. These macromolecules can bind nonspecifically to the Fc region of an antibody or to the surface of functionalized beads. Importantly, antibodies are highly specific, but cross-reactivity might occur toward proteins with similar epitopes. Unspecific binding can result in false-positive signals and increase the background and therefore hamper further analysis dramatically. Denaturing elution of protein complexes, commonly with reducing SDS sample buffer, not only elutes the bait/prey complex but also elutes nonspecifically bound macromolecules and antibodies. To overcome these common issues in Co-IP, it is more desirable to recover proteins or protein complexes in their native form. Previously, several peptide reagents have been reported to be successful in natively eluting protein complexes containing Protein A–tagged baits. These peptides are able to competitively bind to the hinge region on the Fc domain of IgG, thus releasing Protein A–tagged bait/prey complexes (Strambio-de-Castillia, Tetenbaum-Novatt, Imai, Chait, & Rout, 2005; LaCava, Chandramouli, Jiang, & Rout, 2013; LaCava, Fernandez-Martinez, Hakhverdyan, & Rout, 2016). Applying these peptides for native elution after Co-IP as illustrated in Figure 1, the complex would theoretically remain in its native form, but the antibody targeting the bait would still be bound to the eluted complex (see Fig. 1).

In this article, we describe Co-IP of the known ternary complex E6/E6AP/p53. Ubiquitin-protein ligase E3A, also known as E6AP, is N-terminally fused to a 3×HA-peptide (H-YPYDVPDYA YPYDVPDYA YPYDVPDYA-OH) as a bait. After Co-IP, we elute 3×HA-E6AP by competing with the binding of anti-HA monoclonal antibodies to 3×HA-tagged baits using a synthetic 3×HA-peptide, and we expect E6 and p53 to co-elute. In order to optimize this native elution, we consider several factors influencing the yield of elution: (i) Temperature: Temperature affects protein stability. In general, the higher the temperature, the more unstable the protein is. Even though mammalian cell culture is performed at 37°C, isolated proteins are not in their natural environment after cell lysis. Researchers always try to mimic physiological conditions; however, the stability of isolated proteins is usually lower. In vitro, experimental temperatures should always be evaluated with care to avoid protein aggregation and artifacts. In addition, the temperature has a kinetic effect on chemical reactions. According to the Arrhenius equation and van't Hoff's law, a general rule of thumb is that if the temperature is increased by 10 Kelvin (K), the reaction is 2 to 3 times faster. In summary, the temperature influences protein stability and elution time. (ii) Elution time: The time that the competition needs is dependent on the rate of dissociation of the antibody-3×HA-bait complex and the rate of formation of the antibody-3×HA-peptide complex. Both rates depend on the temperature, as described above. It is desirable to find a balance between protein stability and fast and complete reaction to optimize the yield of native elution. (iii) Eluent concentration: The 3×HA-tagged bait/prey complexes are eluted from the anti-HA antibody competitively by addition of 3×HA-peptide. The affinity of the anti-HA antibody for 3×HA-epitope is very high, with a K_d in the pM range. The excess of the 3×HA-peptide must be high enough for it to compete with the 3×HA-bait and depends on the antibody concentration, the 3×HA-bait concentration, and buffer conditions. (iv) Co-factors: To isolate native proteins and complexes, it is necessary to employ all co-factors that the proteins and complexes need. Otherwise, the complexes may dissociate, and the proteins may aggregate.

Strategic Planning

In general, it is recommended to perform a conventional Co-IP with denaturing elution to verify the proof of principle and to verify the parameters for strategic planning before starting a native elution experiment.

Selection of an epitope tag

There are two factors that one should consider in selecting an epitope tag for the bait protein: cross-reactivity of the tag with cellular proteins and whether or not the tag would hinder biological activity of the bait. If the N-terminus of a bait participates in prey binding, one may consider fusing the epitope at the C-terminus and vice versa.

Selection of bait

If one wants to purify a native complex of proteins that one already knows to interact, which component of the complex is chosen as the bait might be critical. In general, one should consider the expression level of the 3×HA-bait, the expression levels of endogenous preys, and protein stability.

To pull down the ternary complex E6/E6AP/p53, we choose E6AP as bait because the endogenous expression of E6AP is too low for detection and heterologous expression is necessary. The endogenous expression level of p53 is already high enough. 16E6, as a viral protein, also needs to be expressed heterologously. However, we did not choose to use 16E6 as the bait because both p53 and E6AP proteins directly bind to 16E6, and we intended to show whether native elution is suitable to isolate complexes even with indirect interaction partners, as is supposed for E6AP and p53. It is very important to

perform test expression in intended experimental cell lines to ensure good expression of the 3×HA-bait protein and prey proteins (if known) for an efficient pull down.

If protein stability is an issue due to proteasomal degradation, proteasome inhibitor can be applied in cell culture. We need the addition of proteasome inhibitor (MG132) because we know that HPV16E6 recruits E6AP, forming a ternary complex with p53 that then leads to the proteasomal degradation of p53. Addition of MG132 can prevent the degradation of p53.

Buffer design

Components of lysis buffers, washing buffers, and elution buffers should always be questioned with respect to protein complex demands. For example, ethylenediaminetetraacetic acid (EDTA), as a chelator of bivalent cations, is commonly used to block metalloproteases during cell lysis. When a protein complex requires bivalent cations, EDTA should be avoided. For isolation of the ternary complex E6/E6AP/p53, we know that E6 and p53 are zinc-finger proteins, i.e., they bind zinc ions via cysteines of their thiol groups. As a consequence, we do not use EDTA in any buffer, and we always supplement buffers with 1 mM Tris(2-carboxyethyl)phosphine (TCEP) as a reducing agent. Dithiothreitol (DTT) and β-mercaptoethanol (b-ME) could also be used as reduction agents. They are less bulky but also less stable than TCEP. Generally, unspecific oxidation of cysteine-rich proteins should be avoided by adding reducing agents because this can lead to false-positive interaction signals. Notably, if disulfide formations are crucial for protein structure and stability, reducing agents should be omitted. Additionally, Benzonase® should always be included in lysis buffer, as it could reduce viscosity caused by nucleic acids and prevents cell clumping by rapidly hydrolyzing all forms of DNA and RNA. An appropriate amount of bivalent magnesium ions must be included to allow an optimal level of Benzonase® activity.

Cell lysis

Cell lysis is a critical step. All cellular compartments are mixed, resulting in accessibility to phosphatases, proteases, and pH shifts. Phosphorylation can be important for protein interactions. Proteases can degrade the proteins of interest, and pH shifts can result in loss of function. Consequently, lysis buffers should be supplemented with a buffer reagent maintaining the demanded pH and containing protease inhibitors and phosphatase inhibitors. Additionally, it is important to consider cell lysis agents. Detergents, depending on the type and concentration, might interfere with the protein structure, leading to aggregation or denaturation, but may solubilize the protein. This can lead to low efficiency of the pull down due to a loss of function of bait or prey proteins. We carry out all lysis steps on ice to avoid any protein aggregation because this might lead to co-aggregation of the proteins of interest.

Necessary controls

Bait and prey proteins can also nonspecifically interact with matrix surfaces and antibodies. Though unspecific interactions are minimized by applying native elution, it is recommended to include the following controls, depending on if the prey is an endogenous protein or overexpressed:

Bait-only control: cells transfected with bait only (3×HA-E6AP) → Co-IP signal for bait only (3×HA-E6AP, no signal for p53 and E6)

Overexpressed-prey control: cells transfected with prey only (E6) → no Co-IP signal for bait and prey

Endogenous-prey control: cells transfected with empty plasmid (mock) → no Co-IP of endogenous proteins

Please note that we do not include the mock to check unspecific binding of p53 because p53 does not bind to E6AP; it binds to E6 if complexed with E6AP. Consequently, a negative Co-IP signal for p53 in the bait-only control is adequate to check for unspecific binding of p53.

Eluent

In analogy to the 3×HA fusion epitope, a 3×HA-peptide is used. The 3×HA-peptide (H-YPYDVPDYA YPYDVPDYA YPYDVPDYA-OH) is a synthetic peptide of 27 amino acid residues used to competitively elute HA-tagged fusion proteins that bind to anti-HA antibodies conjugated on magnetic beads or agarose resin beads. It is necessary to synthesize this peptide with purity of >90% in order to obtain a specific elution of target native protein complexes with high yields.

Elution conditions

It is very important to optimize the elution procedure for maximal efficiency. With respect to the described elution parameters, the temperature, elution time, and eluent concentration were set as variables for optimization. To screen these various conditions, we always loaded the magnetic beads with the same amount of cell lysate according to the total protein content. This allowed a comparable load for each experimental setup assuming similar expression of the proteins. The total protein content was determined by a Bradford measurement in triplicate for each sample.

For temperature tests, it is important that all steps (incubation and elution) are carried out at the respective temperature. Otherwise, the kinetic experiment will be misinterpreted and be less reproducible.

Native Isolation of 3×HA-Bait Protein Complex

Cells co-transfected with 3×HA-E6AP and HPV16E6 are lysed, followed by affinity capture with anti-HA microbeads using a μMACS HA Isolation Kit. Bound proteins are loaded onto μColumns that are placed in the magnetic field of a μMACS Separator. Unbound proteins are washed away before 3×HA-peptide is applied for native elution. Denaturing elution is applied to elute residual proteins that are retained on the anti-HA microbeads to determine elution efficiency for further optimization processes. Figure 2 summarizes the workflow of this protocol.

Materials

HEK293T cells (for our work, kind gift from Dr. Murielle Masson, IGMBC)
Dulbecco's modified Eagle's medium (DMEM; Gibco® by Life Technologies, #41965-062) supplemented with 10% (v/v) fetal bovine serum (FBS; Gibco® by Life Technologies, #10270-106) and 50 μg/ml gentamicin (Gibco® by Life Technologies, #157710049), 37°C
3×HA-E6AP plasmid DNA (GenScript)
HPV16E6 pcDNA3.1 (+) plasmid DNA (GenScript)
Polyethyleneimine 25K (PEI 25K; Polysciences, #23966-1)
Opti-MEM™ Reduced Serum Medium with GlutaMAX Supplement (Opti-MEM™; Gibco® by Life Technologies, #51985034)
10 mM MG132 proteasome inhibitor (AdipoGen Life Sciences, #AG-CP3-0011)
3×HA-peptide (Intavis Peptide Services)
Peptide buffer (see recipe)
10 M NaOH
Liquid nitrogen
Dulbecco's phosphate-buffered saline (DPBS; Gibco® by Life Technologies, #14190-169), 4°C
Lysis buffer (see recipe), 4°C

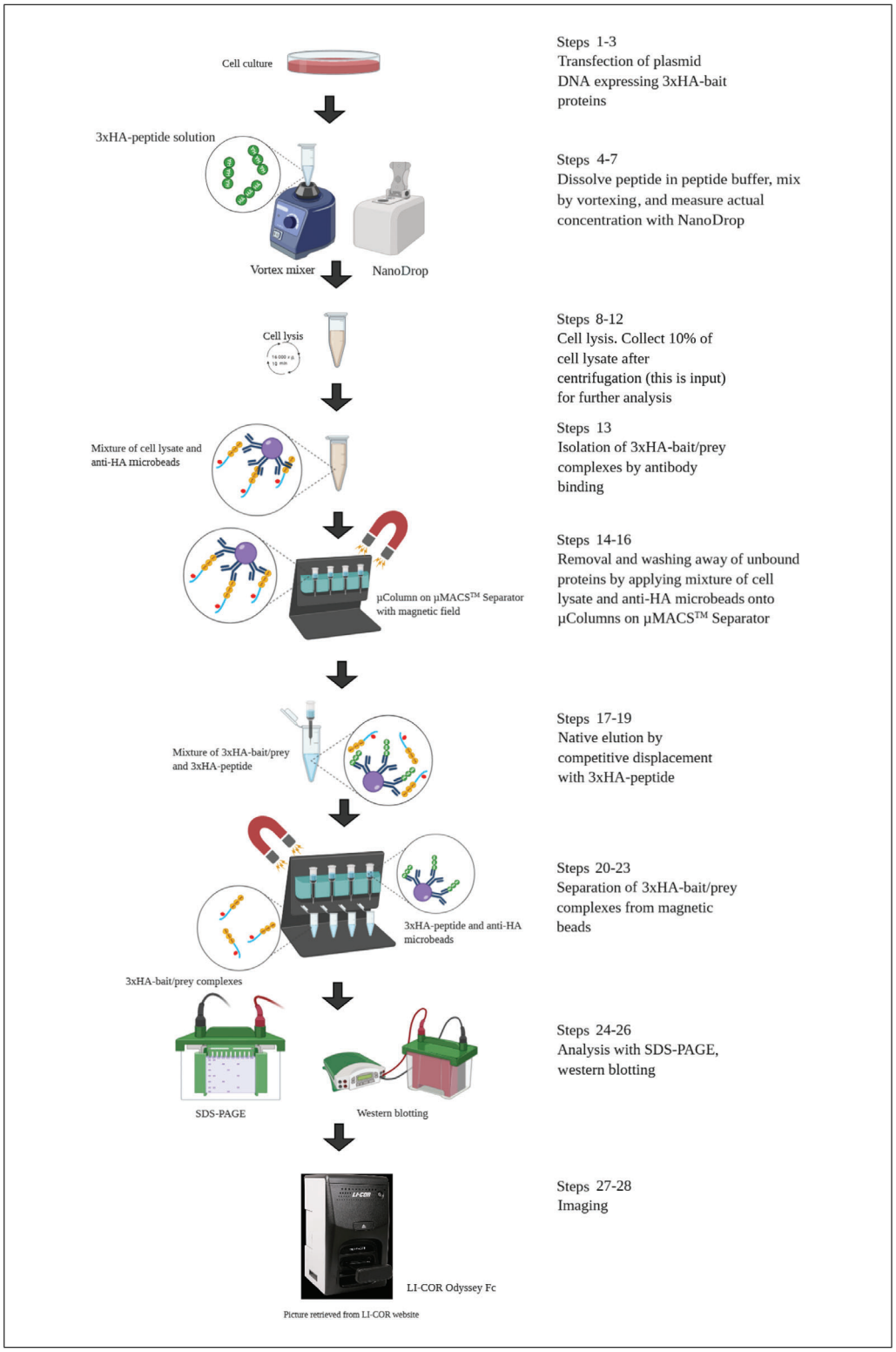

Figure 2 Schematic diagram illustrating the steps of native isolation of 3×HA-bait protein complex. Lyse transfected cells that express 3×HA-bait protein. Isolate 3×HA-bait protein (yellow-blue) and its interacting proteins (prey in red) with magnetic beads (purple) conjugated with anti-HA antibody (dark blue) and wash away unbound protein in a magnetic field. Elute 3×HA-bait/prey complex from the antibody-conjugated beads by applying 3×HA-peptide (green). The 3×HA-peptide concentration, elution temperature, and elution time need to be optimized (steps 4 to 7). Eluted complexes are analyzed by SDS-PAGE, western blot, or mass spectrometry or other biophysical methods (not shown) to analyze the structure and function of the complex. The figure was created with BioRender.com.

Bradford reagent (see recipe)
Anti-HA microbeads (from μMACS HA Isolation Kit, Miltenyi Biotec, #130-091-122), 4°C
1× reducing SDS sample buffer (from 5× reducing SDS sample stock buffer; see recipe), 95°C
8% to 20% SDS-PAGE gel
1× SDS running buffer (from 5× SDS running stock buffer; see recipe)
Coomassie staining solution (see recipe)
De-staining solution (see recipe)
Western blot transfer buffer (make fresh; see recipe)
5% (w/v) bovine serum albumin (BSA; Serva, #9048-46-8) in 1× phosphate-buffered saline (PBS; from 10× PBS; see recipe)
0.05% (v/v) and 0.1% (v/v) Tween 20 in 1× PBS (from 10× PBS; see recipe) (PBS-T)
Primary antibodies:
- Anti-glyceraldehyde 3-phosphate dehydrogenase (GAPDH) antibody (6C5; mouse; Santa Cruz Biotechnology, #sc32233)
- Anti-HA monoclonal antibody (C29F4; rabbit; Cell Signaling, #3724)
- Anti-HPV16E6 antibody (mouse; for our work, kind gift from Arbor Vita Corporation)
- Anti-p53 antibody (DO-1; mouse; BioLegend, #645702)

Secondary antibodies:
- IRDye® 680RD goat anti-mouse antibody (LI-COR Biotechnology GmbH, #926-68070)
- IRDye® 680RD goat anti-rabbit antibody (LI-COR Biotechnology GmbH, #926-68071)

100- and 150-mm sterile cell culture dishes (Thermo Scientific)
37°C, 95% humidity, and 5% CO_2 incubator
Vortex mixer
NanoDrop spectrophotometer
Eppendorf microtubes
15-ml conical centrifuge tubes (Falcon™), 4°C
Refrigerated centrifuge, 4°C
Shaker
μColumns (Miltenyi Biotec, #130-042-701)
μMACS Separator (Miltenyi Biotec, #130-042-602)
Microcentrifuge
Nitrocellulose membranes (GE Healthcare, #10600001)
LI-COR Odyssey Fc or equivalent imaging system
ImageJ 1.47v

Additional reagents and equipment for Bradford assay (see Current Protocols article; Simonian & Smith, 2006), SDS-PAGE and Coomassie blue staining (see Current Protocols article; Gallagher & Sasse, 2001), and western blotting (see Current Protocols article; Gallagher, Winston, Fuller, & Hurrell, 2008)

NOTE: All solutions and equipment coming into contact with cells must be sterile, and proper sterile technique should be used accordingly.

Transfection of plasmid DNA expressing 3×HA-bait protein

1. Culture HEK293T cells in 10 ml DMEM supplemented with 10% FBS and 50 μg/ml gentamicin in 100-mm sterile cell culture dishes at 37°C, 95% humidity, and 5% CO_2. One day before transfection, seed 8×10^6 HEK293T cells in 25 ml medium in 150-mm sterile cell culture dishes, with four dishes for each sample.

2. Replace medium with 25 ml fresh medium (same as in step 1) before transfection starts. Then, transfect cells with 12 μg of 3×HA-E6AP plasmid DNA and 8 μg HPV16E6 pcDNA3.1 (+) plasmid DNA using PEI 25K in Opti-MEMn^{TM} at a DNA/PEI 25K ratio of 1:3 following the manufacturer's instructions.

3. Treat cells with 3 μM MG132 proteasome inhibitor (from 10 mM stock) 8 hr post-transfection.

Preparation of 3×HA-peptide

4. Prepare a 5 mM stock concentration of 3×HA-peptide by dissolving peptide in peptide buffer and adjust pH to 7.0 with 10 M NaOH.

   Steps 4 to 7 should be carried out 1 day before use in step 17 or during the incubation time in step 13.

5. Vortex vigorously to ensure that the peptide is completely dissolved and measure final concentration of peptide at an absorbance of 280 nm using a NanoDrop spectrophotometer, with peptide buffer as a blank.

6. Calculate concentration of the dissolved peptide based on the Beer's Law equation, $A_{280} = \varepsilon_{280} lc$, where

   A_{280} = absorbance (AU);
   E_{280} = molar extinction coefficient, in this case 13 410 $M^{-1}cm^{-1}$ (retrieved from ExPASy ProtParam tool);
   l = length of the path that light must travel in the solution in cm (usually 1 cm); and
   c = concentration of the peptide solution [molar (M)].

7. Aliquot peptide stock solution in Eppendorf microtubes, freeze in liquid nitrogen, and store at −80°C for long-term storage to avoid hydrolysis of the peptide.

Cell lysis

8. Twenty-four hours post-transfection, harvest transfected cells by flushing the cells directly with 3 ml cold DPBS per dish, transferring cells to a pre-cooled 15-ml conical centrifuge tube, and centrifuging 10 min at 500 × *g*, 4°C.

   IMPORTANT NOTE: *Starting here, all steps should be carried out on ice or in a cold room.*

9. Discard supernatant and wash cell pellet once again in 10 ml cold DPBS followed by centrifugation for 10 min at 500 × *g*, 4°C.

10. Resuspend cell pellets in 3 ml cold lysis buffer and incubate cell lysate on a shaker for 1 hr in a cold room.

11. Centrifuge cell lysate for 10 min at 16,000 × *g*, 4°C, to remove cell debris.

12. Determine total protein concentration of the cell lysate using Bradford reagent (see Current Protocols article; Simonian & Smith, 2006). Save an aliquot of cell lysate for analysis by western blot (input; see step 24).

Isolation of 3×HA-bait/prey complexes by antibody binding

13. Add 50 μl cold anti-HA microbeads to cell lysate and incubate on shaker for 4 hr in the cold room.

14. After incubation, place a μColumn in magnetic field of a μMACS Separator and equilibrate column with 1 ml cold lysis buffer.

15. Apply cell lysate onto the μColumn and allow to run through.

Flow-through could be collected for further analysis by western blot. This step is recommended if the pull-down efficiency is not known or has low reproducibility.

16. Rinse column three times, each time with 500 µl cold lysis buffer. Proceed immediately to step 17.

Native elution by competitive displacement with 3×HA-peptide

17. Prepare 3×HA-peptide (see step 7) at appropriate working concentration (see Understanding Results section) and then apply 120 µl to the µColumn and immediately remove column from the µMACS Separator.
18. Collect flow-through in Eppendorf microtubes.
19. Reapply peptide solution onto µColumn 10 times before incubating solution on a shaker at 300 rpm in the cold room (see Understanding Results section for incubation time). Keep µColumn for use in step 20.
20. After incubation, equilibrate µColumn with 500 µl cold peptide buffer on the µMACS Separator. Then, apply peptide solution onto the µColumn, 60 µl at a time, and allow it to run through into a new Eppendorf microtube. Keep an aliquot for western blotting analysis.
21. Add 60 µl pre-heated 1× reducing SDS sample buffer onto µColumn and immediately remove column from the magnetic field to elute residual proteins retained on the µColumn.
22. Incubate µColumn at room temperature for 5 min before adding another 60 µl pre-heated 1× reducing SDS sample buffer.
23. Spin down µColumn in a new Eppendorf microtube for 20 s at 250 × *g* at room temperature in a microcentrifuge (denaturing elution).

SDS-PAGE and western blot

24. Resolve all protein samples on a 8% to 20% SDS-PAGE gel with 1× SDS running buffer and stain gel with Coomassie staining solution for 30 min on a shaker at room temperature followed by de-staining solution (see Current Protocols article; Gallagher & Sasse, 2001) or transfer protein onto a nitrocellulose membrane using for 1 hr at 70 V or 90 min at 90 V depending on the Western blot transfer buffer used (see recipe) (see Current Protocols article; Gallagher et al., 2008). For de-staining, change de-staining solution every hour, until blue bands and a clear background are obtained.
25. Block membrane with 5% BSA in 1× PBS on a shaker for 1 hr at room temperature.
26. Incubate membrane with primary antibodies in 0.1% PBS-T overnight on a shaker in the cold room (or according to the manufacturer's recommendation) and then wash three times with 0.05% PBS-T before applying secondary antibodies in 0.1% PBS-T for 30 min on a shaker at room temperature.

    Antibodies should be diluted according to the manufacturer's instructions. We dilute all primary and secondary antibodies in this protocol with 0.1% PBS-T.

27. Wash membrane three times with 0.05% PBS-T and visualize for respective signals on a LI-COR Odyssey Fc or equivalent imaging system.
28. Analyze densitometry of the protein signals using ImageJ 1.47v. Calculate elution efficiency using the equation given below:

$$\textit{Native elution efficiency}\ (\%) = \frac{\text{signal of native elution}}{\text{signal of native elution} + \text{signal of denaturing elution}} \times 100\%$$

REAGENTS AND SOLUTIONS

Bradford reagent

Dissolve Coomassie Brilliant Blue G-250 in 5% (v/v) methanol to 0.05 g/L. Slowly add 85% (v/v) phosphoric acid to this solution mix to 10%. Then, slowly add this acid solution mix to 500 ml water and mix with a magnetic stirrer. Add water to 1 L. Store ≤1 year at 4°C in the dark.

IMPORTANT NOTE: *Do NOT add water to the acid solution. The solution should be filtered through Whatman paper (GE Healthcare, #10426890) to remove any precipitate.*

CAPS buffer

10 mM 3-(cyclohexylamino)-1-propanesulfonic acid (CAPS)
0.001% (w/v) SDS
10% (v/v) methanol
Adjust to pH 10.3

Coomassie staining solution

10% (v/v) acetic acid
0.05% (w/v) Coomassie Brilliant Blue R-250
25% (v/v) propan-2-ol
Store ≤6 months at room temperature

This is an in-house Coomassie staining solution commonly used in our lab. Commercially available staining solution could also be used following the manufacturer's instructions.

De-staining solution

10% (v/v) acetic acid
10% (v/v) ethanol
80% (v/v) deionized water
Store ≤6 months at room temperature

This is an in-house de-staining solution commonly used in our lab after Coomassie staining. Commercially available de-staining solution could also be used following the manufacturer's instructions.

Lysis buffer

10% (v/v) glycerol
50 mM HEPES, pH 7.5
3 mM magnesium chloride ($MgCl_2$)
0.1% (w/v) Nonidet P-40 or IGEPAL CA-630 (NP-40)
150 mM sodium chloride (NaCl)
1 mM TCEP
200 μM zinc chloride ($ZnCl_2$)
Store ≤1 month at 4°C
Supplement with Benzonase®, phosphatase inhibitor, and protease inhibitors immediately prior to cell lysis

This buffer recipe was proven to be useful for zinc-finger proteins in our lab, but it is not universally useful and may require modification, such as use of a different buffer agent, pH, redox state, or detergent according to the protein of interest. Substitution of HEPES with Tris should be avoided if mass spectrometry is involved in the downstream process. Besides, one must be aware that the pH of Tris-based buffer is temperature dependent. We recommend the PhosSTOP™ tablet and cOmplete™ EDTA-free Protease Inhibitor Cocktail from Roche and Benzonase® endonuclease with purity grade II (>90%) from Merck. Use of EDTA-free protease inhibitors is crucial for protein binding bivalent cations as the presence of EDTA, even in limited amount, would lead to chelation of bivalent ions present in the solution.

Peptide buffer

10% (v/v) glycerol
50 mM HEPES, pH 7.5
150 mM NaCl
Store ≤1 month at 4°C

Phosphate-buffered saline (PBS), 10×

2 g/L potassium chloride (KCl)
2 g/L potassium dihydrogen phosphate (KH_2PO_4)
80 g/L NaCl
11.5 g/L sodium dibasic phosphate (Na_2HPO_4)
Adjust pH to pH 7.2 with 85% (v/v) phosphoric acid
Store ≤6 months at room temperature

Reducing SDS sample stock buffer, 5×

5% (v/v) b-ME
0.005% (w/v) bromophenol blue
50% (w/v) glycerol
5% (w/v) SDS
0.25 M Tris·HCl, pH 8
Make 950-µl aliquots from 50 ml stock buffer
Store aliquots ≤6 months at −20°C
Add 50 µl b-ME to aliquot immediately before use

This should be used at 1× concentration in the final sample. Commercially available reducing SDS sample buffer could also be used following the manufacturer's instructions.

SDS running stock buffer, 5×

960 mM glycine
1% (w/v) SDS
125 mM Tris·HCl, pH 8.3
Store ≤6 months at room temperature

This should be used at 1× concentration.

Western blot transfer buffer

Option 1:
1.2 g/L CAPS buffer (see recipe)
10% (v/v) methanol
1 g/L SDS
Adjust pH to 10.3 with 10 M NaOH
Prepare fresh immediately before use
Option 2:
11.26 g/L glycine
10% (v/v) methanol
0.2 g/L SDS
2.44 g/L Tris·HCl, pH 8.2
Prepare fresh immediately before use

There are several different formulations of western blot transfer buffer available. Above, we provide two formulations that are commonly used in our lab. For option 1, run the transfer at 70 V for 60 min, as optimized for the detected proteins. For option 2, run the transfer at 90 V for 90 min, as optimized for the detected proteins. In both cases, these parameters might be changed with respect to the protein of interest.

Table 1 Troubleshooting Guide for Native Isolation of Protein Complexes

Problem	Possible cause	Solution
Poor peptide solubility	Peptide solution is too acidic	Adjust pH of peptide carefully with 10 M sodium hydroxide and dissolve at neutral pH (∼7)
Low elution efficiency: first perform Co-IP under denaturing conditions for proof of principle: **Positive result**: problem caused by native elution → continue troubleshooting **Negative result**: problem is principally Co-IP problem: refer to Current Protocols article Brizzard & Chubet (1997)	Proteins are unstable due to improper buffer components	Refer to Strategic Planning (Buffer design and Cell lysis) and annotation to recipe for lysis buffer
	Proteins are temperature sensitive	Carry out all steps at low temperature (4-8°C)
	Proteins are unstable over time	Optimize incubation time for native elution
	Poor peptide quality	Use only peptide with purity >90%
	Insufficient amount of peptide used	Titrate peptide carefully and work with saturated concentration. Re-check peptide concentration spectroscopically.
	Peptide was hydrolyzed due improper storage and handling	Freeze peptide solution in liquid nitrogen and store at −80°C. Store lyophilized peptide at −20°C. Aliquot peptide solution to avoid repeated freeze-thaw cycles.
Low signal of prey	Low amount of prey in cell lysate	Overexpress prey for complex isolation

COMMENTARY

Background Information

Please see the Overview and Principle section above for background information.

Critical Parameters

First of all, make sure that the 3×HA-peptide has purity of >90%, and the concentration of the dissolved peptide should always be verified spectroscopically because this value directly influences the yield of native protein elution.

The incubation and elution temperatures and times should always be optimized based on the stability of the proteins of interest. Appropriate buffer conditions, especially pH and use of an appropriate detergent for cell lysis or required co-factors, ensure the stability and functionality of the proteins of interest.

Troubleshooting

Please refer to Table 1 for a troubleshooting guide for natively eluting protein complexes.

Please note that Co-IP including the presented native elution requires multiple steps and that variations can occur, starting from plasmid preparation, transfection, and peptide solubilization down to protein transfer to nitrocellulose membranes and protein probing. Variations influence the input, elution, and protein detection. Hence, Co-IP is not a quantitative method. As a consequence, semiquantitative comparisons between different experiments are questionable. From our experience, the most reproducible results can be obtained by splitting cell extracts for elution tests and running all samples of interest on one SDS-PAGE gel and blot membrane. Freezing of cell lysates and eluents affects elution efficiency and western blot analysis, respectively.

Understanding Results

3×HA-peptide stock solution

Peptide was dissolved to get a theoretical 5 mM stock concentration, as described above, in peptide buffer. A final concentration of 4.71 mM, which is equivalent to 94.2% of solubility, was obtained. This is a reasonable yield, and it indicates high solubility of the applied peptide under the described conditions. However, one should always verify the peptide concentration spectroscopically because the yield of dissolved peptide directly influences the yield of native protein elution.

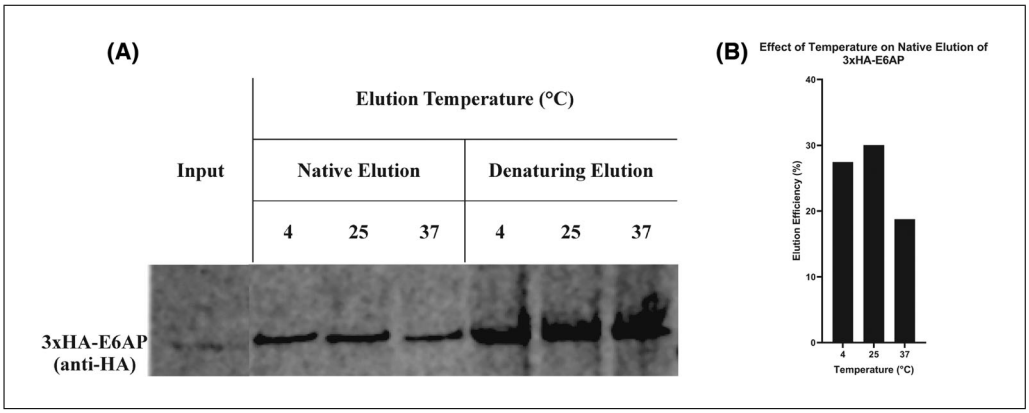

Figure 3 Effect of temperature on native elution of 3×HA-E6AP. (**A**) Cell lysates of HEK293T cells overexpressing 3×HA-E6AP were divided equally, corresponding to 2500 μg/ml total protein. Each was incubated with 50 μl magnetic anti-HA microbeads. The bead solution was transferred to a μColumn, a magnetic field was applied, and unbound proteins were washed away as described above (Fig. 2). 3×HA-E6AP complex was eluted (step 9, Fig. 2) with 120 μl of 1200 μM 3×HA-peptide at 4°C, 25°C, or 37°C for 2 hr on a shaker at 300 rpm. Residual proteins that were retained on the microbeads were eluted under denaturing conditions with 120 μl reducing SDS sample buffer. All protein samples were resolved on a 8% to 20% SDS-PAGE gel and analyzed by western blot. 3×HA-E6AP was probed with an anti-HA antibody at a dilution of 1:1000 overnight in a cold room, followed by incubation with IRDye® 680RD goat anti-rabbit secondary antibody at a dilution of 1:10,000 for 30 min at room temperature. The signal of respective protein was then visualized using a LI-COR Odyssey Fc fluorescence imaging system. (**B**) Western blot signals were quantified densitometrically using ImageJ 1.47v, and elution efficiency was calculated as described in the protocol (see step 28). The chart was plotted with GraphPad Prism 8 version 8.4.0 (671). Native elution of 3×HA-E6AP was found to be temperature dependent. At 37°C, the efficiency decreases, indicating instability at higher temperature. To avoid instability problems, an elution temperature of 4°C was chosen for further experiments.

Optimizing elution conditions

As described above, the native elution (steps 17 to 19, Fig. 2) was optimized with regard to optimal temperature, elution time, and eluent concentration. For optimization, the analysis was based on the bait protein 3×HA-E6AP only, assuming that bound prey protein does not interfere with the competitive elution of the epitope fusion tag. As a reminder, first, we performed a native elution and then applied the same beads for denaturing elution in order to analyze the bait protein that remains on the beads. The elution efficiency was analyzed by (a) performing a western blot of the samples eluted under the different conditions, (b) detecting the eluted protein 3×HA-E6AP using a fluorescently labeled anti-HA-antibody and a fluorescence imaging system, and (c) quantifying signal bands densitometrically (Fig. 3).

To identify temperature dependence on the elution efficiency, we first carried out an experiment by incubating 3×HA-E6AP bound to the anti-HA microbeads with 3×HA-peptide at 4°C, 25°C, or 37°C on a shaker at 300 rpm for 2 hr. If the elution does not depend on the elution temperature, the signal of 3×HA-E6AP should be constant at the tested temperatures, as is observed for denaturing elution. In principle, one would expect that the higher the temperature, the more the proteins are eluted because the reaction is faster at higher temperatures. We observed that the efficiency of the native elution was slightly higher when it was carried out at 25°C compared to 4°C but reduced at 37°C (Fig. 3). This indicates that the bait protein 3×HA-E6AP is not stable at 37°C under the given conditions, thus decreasing the yield of Co-IP. Furthermore, the prey protein HPV16E6 is known to be a temperature-sensitive protein. Because of these stability issues, the subsequent experiments were carried out at 4°C.

Next, the optimal concentration of peptide required for maximum elution efficiency was investigated. The higher the eluent concentration, the higher the amount of eluted protein, until a maximal efficiency is reached. This efficiency might then be limited by other factors, such as the kinetic parameter, i.e., elution time. For this test, 3×HA-E6AP bound to anti-HA microbeads was competitively displaced with increasing amounts of 3×HA-peptide (0, 50, 75, 150, 500, and 1000 μM) for 2 hr at 4°C on a shaker at 300 rpm as shown in Figure 4A. Under the given conditions, the

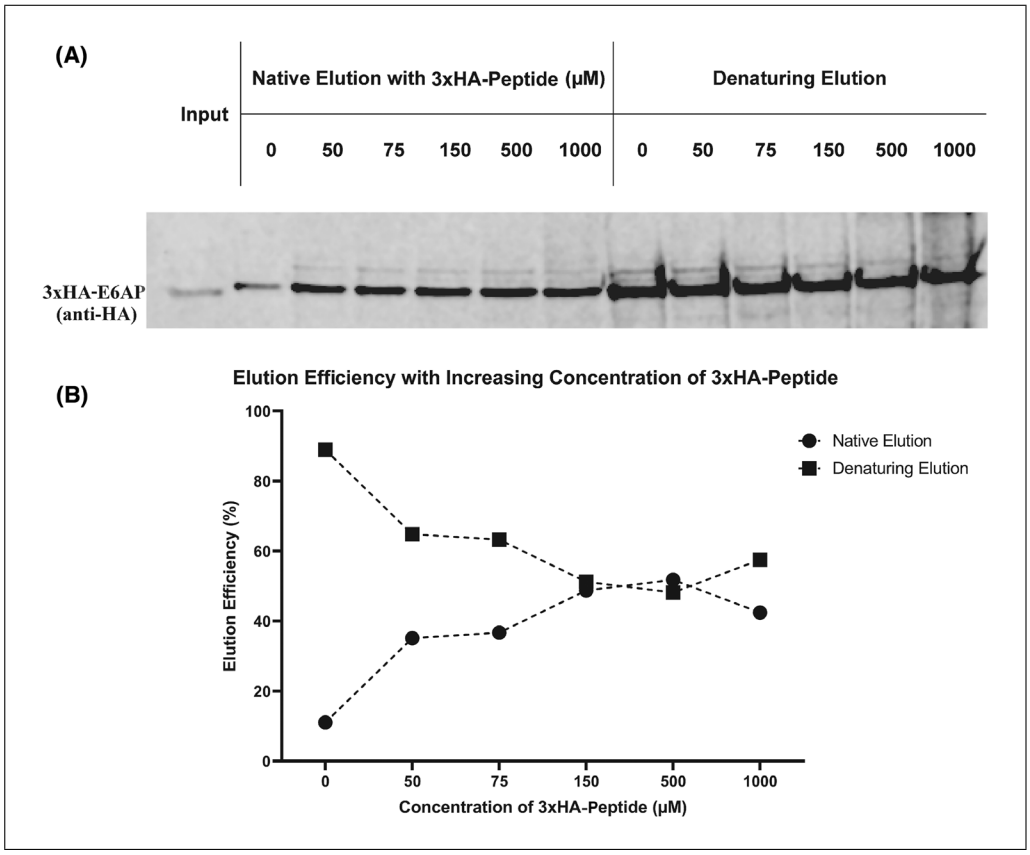

Figure 4 Elution efficiency with increasing concentration of 3×HA-peptide. (**A**) Cell lysates of HEK293T cells overexpressing 3×HA-E6AP were divided equally, corresponding to 2500 μg/ml total protein. Each was incubated with 50 μl anti-HA microbeads. The bead solution was transferred to a μColumn, a magnetic field was applied, and unbound proteins were washed away as described above (Fig. 2). 3×HA-E6AP complex was eluted with 120 μl of different concentrations of 3×HA-peptide at 4°C for 2 hr on shaker at 300 rpm. Residual proteins that were retained on the microbeads were eluted under denaturing conditions with 120 μl reducing SDS sample buffer. All protein samples were resolved on a 8% to 20% SDS-PAGE gel and analyzed by western blot. 3×HA-E6AP was probed with an anti-HA antibody at a dilution of 1:1000 overnight in a cold room, followed by incubation with IRDye® 680RD goat anti-rabbit secondary antibody at a dilution of 1:10,000 for 30 min at room temperature. The signal of respective protein was then visualized using a LI-COR Odyssey Fc fluorescence imaging system. (**B**) Western blot signals were quantified densitometrically using ImageJ 1.47v, and elution efficiency was calculated as described in the protocol (see step 28). The chart was plotted with GraphPad Prism 8 version 8.4.0 (671). The amount of eluted 3×HA-E6AP increases with higher amounts (higher eluent concentrations) of 3×HA-peptide. A maximum of ∼50% was achieved starting at an eluent concentration of 150 μM 3×HA-peptide. As a consequence, a 250 μM eluent concentration was chosen for further experiments.

elution efficiency was maximal at ∼50% starting at an eluent concentration of 150 μM 3×HA-peptide. This can be seen in Figure 4B, where the signals reach a plateau at ∼50%. In further experiments, we used a 250 μM eluent concentration to maintain a high yield of elution.

To investigate the time course of the performance of 3×HA-peptide elution, we incubated 3×HA-E6AP-saturated anti-HA microbeads with 250 μM 3×HA-peptide for different lengths of time, as indicated in Figure 5A, at 4°C on a shaker at 300 rpm. Over time, the amount of the eluted protein 3×HA-E6AP should increase until the reaction completes and reaches a plateau. In Figure 5B, indeed, the protein signals increased over time, indicating that the longer the incubation time, the more the 3×HA-E6AP was eluted. An overnight incubation allowed the elution of ∼60% 3×HA-E6AP. We did not want to prolong the incubation time further in order to avoid artifacts caused by protein aggregation or degradation.

We never reached 100% elution efficiency when applying the 3×HA-peptide. This might

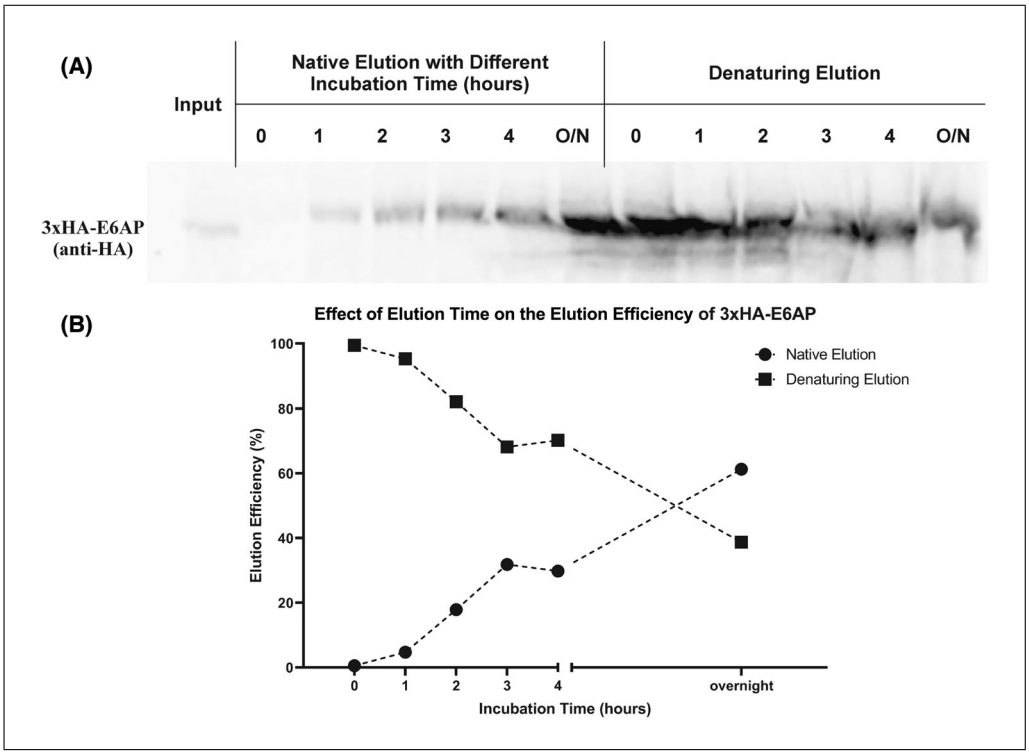

Figure 5 Effect of elution time on the elution efficiency of 3×HA-E6AP. (**A**) Cell lysates of HEK293T cells overexpressing 3×HA-E6AP were divided equally, corresponding to 2500 μg/ml total protein. Each was incubated with 50 μl anti-HA microbeads. The bead solution was transferred to a μColumn, a magnetic field was applied, and unbound proteins were washed away as described above (Fig. 2). 3×HA-E6AP complex was eluted with 120 μl of 250 μM 3×HA-peptide at 4°C and incubated for different numbers of hours on a shaker at 300 rpm. Residual proteins that were retained on the microbeads were eluted under denaturing conditions with 120 μl reducing SDS sample buffer. All protein samples were resolved on a 8% to 20% SDS-PAGE gel and analyzed by western blot. 3×HA-E6AP was probed with an anti-HA antibody at a dilution of 1:1000 overnight in a cold room, followed by incubation with IRDye® 680RD goat anti-rabbit secondary antibody at a dilution of 1:10,000 for 30 min at room temperature. The signal of respective protein was then visualized using a LI-COR Odyssey Fc fluorescence imaging system. (**B**) Western blot signals were quantified densitometrically using ImageJ 1.47v, and elution efficiency was calculated as described in the protocol (see step 28). The chart was plotted with GraphPad Prism 8 version 8.4.0 (671). The elution efficiency increases over time and is highest after overnight incubation. Consequently, an overnight incubation of the washed magnetic beads was performed in subsequent experiments.

be for several reasons. First of all, the kinetic test did not reach a plateau and could be prolonged. However, this should be analyzed carefully because the proteins are still in a rather crude environment and prone to degradation and stability issues. Second, the bait protein might also bind nonspecifically to the bead matrix; elution with the 3×HA-peptide is simply not possible in this case.

Co-elution of prey proteins of the ternary complex

With this experiment, we wanted to address two questions: (i) Is it possible to pull down the ternary complex? (ii) Can we reduce the protein background by native elution?

(i) It is known that HPV16E6 oncoprotein recruits E6AP to form a ternary complex with tumor suppressor p53 and leads to the ubiquitination and proteasomal degradation of p53 (Martinez-Zapien et al., 2016). This is a quite complicated complex because the binding of E6AP is required for conformational changes in 16E6 that enable binding of p53. Whether there is a direct interaction of p53 with E6AP within the complex is not known. We used this example to demonstrate that the natively eluted 3×HA-E6AP maintains its biological function during the isolation process and to show that our strategy allows us to isolate multimeric complexes of proteins even with indirect interactions, here p53 and E6AP. The bait protein 3×HA-E6AP

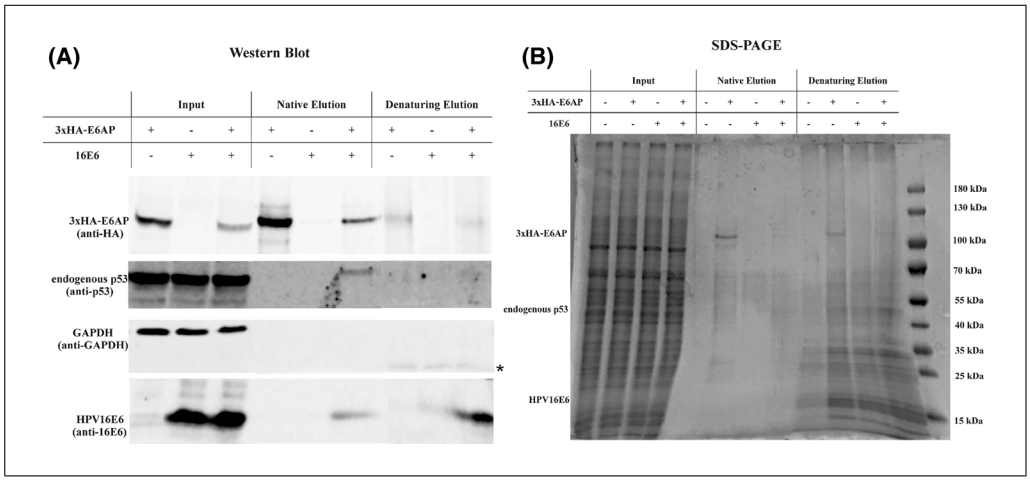

Figure 6 Co-immunoprecipitation of 3×HA-E6AP/16E6/p53 ternary complex under native conditions. (**A**) Cells overexpressing 3×HA-E6AP or 16E6 or both, with a total protein concentration of 2500 μg/ml, were prepared. Each was incubated with 50 μl anti-HA microbeads. The bead solution was transferred to a μColumn, a magnetic field was applied, and unbound proteins were washed away as described above (Fig. 2). 3×HA-E6AP that was bound on anti-HA microbeads was incubated with 120 μl of 250 μM 3×HA-peptide overnight at 4°C with gentle shaking at 300 rpm. Residual proteins that were retained on the microbeads were eluted under denaturing conditions with 120 μl reducing SDS sample buffer. All protein samples were resolved on a 8% to 20% SDS-PAGE gel and analyzed by western blot. Proteins of interest were bound to respective antibodies overnight in a cold room: anti-HA antibody at a dilution of 1:1000, anti-p53 (DO-1) antibody at a dilution of 1:1000, anti-GAPDH antibody at a dilution of 1:500 as a loading control, or anti-16E6 antibody at a dilution of 1:10,000. This was followed by incubation with IRDye® 680RD goat anti-rabbit secondary antibody or IRDye® 680RD goat anti-mouse secondary antibody at a dilution of 1:10,000 for 30 min at room temperature. The signal of respective protein was then visualized using a LI-COR Odyssey Fc fluorescence imaging system. The input samples resembled the cell lysate loaded on the magnetic beads, and signals here verified the expression of the proteins of interest 3×HA-E6AP, p53, and 16E6. The native and denaturing elutions showed that 3×HA-E6AP alone cannot pull down p53 and that 16E6 and p53 in the absence of 3×HA-E6AP do not bind and elute nonspecifically. In the presence of 3×HA-E6AP and 16E6, a co-elution of p53 and 16E6 occurs, as demonstrated by the signals for all three proteins in the native and denaturing elutions. (**B**) The samples from (A) were resolved on another 8% to 20% SDS-PAGE gel, followed by Coomassie R-250 staining in order to analyze the total protein content. Lysates of non-transfected cells were additionally applied to the SDS-PAGE gel and resembled nonspecific binders only (without heterologous 3×HA-E6AP or 16E6). The input samples resembled the overall protein content loaded on the magnetic beads. The samples of the native elution contained significantly less overall protein content compared to the denaturing elution, i.e., the native elution with 3×HA-peptide was able to avoid elution of almost all nonspecifically bound proteins as well as the light chain of anti-HA antibody [indicated with * in (A)].

and the viral protein 16E6 (first targeting prey protein) were heterologously expressed in the mammalian cell line HEK293T. Endogenous p53 was the second prey protein, with all three proteins together forming the ternary complex. As a control, the same experiment was conducted without co-expression of 16E6 or 3×HA-E6AP. We applied the optimized native elution strategy by competitively displacing 16E6/E6AP/p53 ternary complex with 250 μM 3×HA-peptide overnight. The input samples, which corresponded to the cell lysate, verified the expression of the proteins of interest and the equal loading of cell lysate on the magnetic beads, as shown by the similar signal of endogenous GAPDH as a loading control (input, Fig. 6A). Regarding the controls, 3×HA-E6AP in the absence of 16E6 did not pull down p53. The second control, the heterologous expression of 16E6 only, showed a signal neither for p53 nor for 16E6 in the natively eluted samples. This meets expectations because there was no HA-tagged protein to be pulled down with the anti-HA magnetic beads, and this verifies that there was no unspecific signal caused by unspecific binding of p53 or 16E6. Expressing 3×HA-E6AP together with 16E6, we could pull down the ternary complex from crude cell lysate, demonstrated by the clear signals for p53 and 16E6 in the western blots both in the native elution and under denaturing elution (Fig. 6A). This means that

we could pull down p53 as an indirect binder of E6AP.

(ii) Western blotting only allows the visualization of proteins specifically recognized by the applied antibodies. In order to analyze the entire protein content of the sample, meaning the purity of the sample and detection of nonspecific binders, we additionally performed Coomassie staining of a reducing SDS-PAGE gel (Fig. 6B) in analogy to the western blot. Here, we could detect a protein band corresponding to 3×HA-E6AP. The sensitivity of the Coomassie staining was too low to detect 16E6 or p53. However, higher purity and less background were clearly visible in protein samples natively eluted with 3×HA-peptide compared with the residual proteins that were eluted under denaturing conditions. All residual proteins that are commonly co-eluted under denaturing conditions gave a high background in further analysis, e.g., mass spectrometry, which is often applied after Co-IP. One of the common problems in pull-down assays is the co-elution of IgG antibodies or the heavy and light chains of antibodies, which leads to high background or smearing for the pulled-down proteins. Protein bands of heavy and light chains from the antibody could hamper detection of the signal of bait or prey of interest if they have similar molecular weights (∼50 kDa for heavy chain and ∼25 kDa for light chain, indicated with * in Fig. 6A). Given that the anti-HA antibody immobilized on the microbeads is from mouse, incubation of the blot membrane with goat anti-mouse secondary antibody will detect these antibodies. In native elution, no signals for co-eluted antibody light chains were detected. This clearly shows that this common issue could be solved easily by applying native elution. Furthermore, in the denaturing elution of residual proteins, a lot of E6 remained bound to the column, which can also be seen for the control sample E6 only (Fig. 6B). This indicates that E6 binds nonspecifically to the anti-HA microbeads. We did not observe a signal for E6 in the native elution of controls, indicating that this elution strategy could overcome the unspecific binding of the prey.

These experiments showed that this method is useful in preparing functional protein samples for protein-protein interaction studies.

Variations

The isolation procedure for the antibody-bait/prey complex can alternatively be performed by using agarose beads or Protein A/G beads.

The same strategy could also be applied when other short tags, such as V5 or FLAG, are fused to the bait protein. Native elution with commercially available single or triple FLAG peptide was reported before (see Current Protocols article; Brizzard & Chubet, 1997; Hernan, Heuermann, & Brizzard, 2000).

Time Considerations

Cell culturing, Co-IP, and overnight incubation with the peptide for native elution take 2 days. Western blot analysis takes another 1 day. In sum, the entire protocol takes 3 days. Of course, individual applications, e.g., with other cell lines or antibodies with different optimal requirements, can shorten or prolong this experiment. Notably, preparing the 3×HA-peptide stock solution can take 1 to 2 hr because the pH needs to be carefully titrated to neutral pH.

Acknowledgments

We would like to acknowledge the Wilhelm Sander-Stiftung for funding. We are grateful to Dr. Murielle Masson for providing us with the HEK293T cells. Anti-HPV16E6 antibody was generously provided by Arbor Vita Corporation. Open access funding enabled and organized by Projekt DEAL.

Author Contributions

JiaWen Lim: Data curation; Methodology; writing-original draft. **Thomas Iftner:** Funding acquisition; Supervision. **Claudia Simon:** Conceptualization; methodology; Data curation; Formal analysis; Funding acquisition; Investigation; Methodology; Project administration; Resources; Software; Supervision; Validation; Visualization; writing-original draft; writing-review & editing.

Conflict of Interest

The authors declare no conflict of interest.

Data Availability Statement

Data sharing not applicable–no new data generated.

Literature Cited

Brizzard, B., & Chubet, R. (1997). Epitope tagging of recombinant proteins. *Current Protocols in Neuroscience*, *00*(1), 5.8.1–5.8.10. doi: 10.1002/0471142301.ns0508s00.

Gallagher, S., & Sasse, J. (2001). Protein analysis by SDS-PAGE and detection by Coomassie blue or silver staining. *Current Protocols in Pharmacology*, *2*, A.3B.1–A.3B.10. doi: 10.1002/0471141755.pha03bs02.

Gallagher, S., Winston, S. E., Fuller, S. A., & Hurrell, J. G. R. (2008). Immunoblotting and immunodetection. *Current Protocols in Molecular Biology*, *83*, 10.8.1–10.8.28. doi: 10.1002/0471142727.mb1008s83.

Hernan, R., Heuermann, K., & Brizzard, B. (2000). Multiple epitope tagging of expressed proteins for enhanced detection. *BioTechniques*, *28*(4), 789–793. doi: 10.2144/00284pf01.

Kaboord, B., & Perr, M. (2008). Isolation of proteins and protein complexes by immunoprecipitation. *Methods in Molecular Biology*, *424*, 349–364. doi: 10.1007/978-1-60327-064-9_27.

LaCava, J., Chandramouli, N., Jiang, H., & Rout, M. P. (2013). Improved native isolation of endogenous protein a-tagged protein complexes. *BioTechniques*, *54*(4), 1–7. doi: 10.2144/000114012.

LaCava, J., Fernandez-Martinez, J., Hakhverdyan, Z., & Rout, M. P. (2016). Optimized affinity capture of yeast protein complexes. *Cold Spring Harbor Protocols*, *2016*(7), 615–619. doi: 10.1101/pdb.prot087932.

Lin, J.-S., & Lai, E.-M. (2017). Protein–protein interactions: Co-immunoprecipitation. In *Methods in Molecular Biology* (Vol. 1615*, pp. 211–219). New York, NY: Humana Press. doi: 10.1007/978-1-4939-7033-9_17*.

Martinez-Zapien, D., Ruiz, F. X., Poirson, J., Mitschler, A., Ramirez-Ramos, J., Forster, A., … Zanier, K. (2016). Structure of the E6/E6AP/p53 complex required for HPV-mediated degradation of p53. *Nature*, *529*(7587), 541–545. doi: 10.1038/nature16481.

Ranawakage, D. C., Takada, T., & Kamachi, Y. (2019). HiBiT-qIP, HiBiT-based quantitative immunoprecipitation, facilitates the determination of antibody affinity under immunoprecipitation conditions. *Scientific Reports*, *9*(1), 6895. doi: 10.1038/s41598-019-43319-y.

Simonian, M. H., & Smith, J. A., 2006. Spectrophotometric and colorimetric determination of protein concentration. *Current Protocols in Molecular Biology*, *76*, 10.1A.1–10.1A.9. doi: 0471142727.mb1001as76.

Strambio-de-Castillia, C., Tetenbaum-Novatt, J., Imai, B. S., Chait, B. T., & Rout, M. P. (2005). A method for the rapid and efficient elution of native affinity-purified protein A tagged complexes. *Journal of Proteome Research*, *4*(6), 2250–2256. doi: 10.1021/pr0501517.

Key References

Free, R. B., Hazelwood, L. A., & Sibley, D. R. (2009). Identifying novel protein-protein interactions using co-immunoprecipitation and mass spectroscopy. *Current Protocols in Neuroscience*, *46*(1), 139–148. doi: 10.1002/0471142301.ns0528s46.

Discusses some important criteria that need to be considered during optimization of Co-IP.

LaCava, J., Molloy, K. R., Taylor, M. S., Domanski, M., Chait, B. T., & Rout, M. P. (2015). Affinity proteomics to study endogenous protein complexes: Pointers, pitfalls, preferences and perspectives. *BioTechniques*, *58*(3), 103–119. doi: 10.2144/000114262.

Defines some effective procedures for the isolation of protein complexes, highlighting the best practices and common issues that could arise.

CORRECTIONS

In this publication, author's conflict of interest and data availability statement have been added.

The current version online now includes this information and may be considered the authoritative version of record.

JBC RESEARCH ARTICLE

Evidence for direct interaction between the oncogenic proteins E6 and E7 of high-risk human papillomavirus (HPV)

Received for publication, January 30, 2023, and in revised form, June 18, 2023 Published, Papers in Press, June 23, 2023,
https://doi.org/10.1016/j.jbc.2023.104954

JiaWen Lim[1], Hauke Lilie[2], Hubert Kalbacher[3], Nora Roos[1], Desiree Isabella Frecot[1], Maximilian Feige[1], Marcel Conrady[1], Tobias Votteler[1], Alexandra Cousido-Siah[4], Giada Corradini Bartoli[1], Thomas Iftner[1,*], Gilles Trave[4], and Claudia Simon[1,*]

From the [1]Institute of Medical Virology and Epidemiology of Viral Diseases, University Hospital Tuebingen, Tuebingen, Germany; [2]Institute of Biochemistry and Biotechnology, Martin-Luther-University Halle-Wittemberg, Halle-Wittemberg, Germany; [3]Interfaculty Institute of Biochemistry, Eberhard-Karls-University Tuebingen, Tuebingen, Germany; [4]Equipe Labellisée Ligue 2015, Department of Integrative Biology, Institut de Génétique et de Biologie Moléculaire et Cellulaire, CNRS, INSERM, UdS, Illkirch, France

Reviewed by members of the JBC Editorial Board. Edited by Craig Cameron

Human papillomaviruses (HPVs) are DNA tumor viruses that infect mucosal and cutaneous epithelial cells of more than 20 vertebrates. High-risk HPV causes about 5% of human cancers worldwide, and the viral proteins E6 and E7 promote carcinogenesis by interacting with tumor suppressors and interfering with many cellular pathways. As a consequence, they immortalize cells more efficiently in concert than individually. So far, the networks of E6 and E7 with their respective cellular targets have been studied extensively but independently. However, we hypothesized that E6 and E7 might also interact directly with each other in a novel interaction affecting HPV-related carcinogenesis. Here, we report a direct interaction between E6 and E7 proteins from carcinogenic HPV types 16 and 31. We demonstrated this interaction *via* cellular assays using two orthogonal methods: coimmunoprecipitation and flow cytometry–based FRET assays. Analytical ultracentrifugation of the recombinant proteins revealed that the stoichiometry of the E6/E7 complex involves two E7 molecules and two E6 molecules. In addition, fluorescence polarization showed that (I) E6 binds to E7 with a similar affinity for HPV16 and HPV31 (in the same micromolar range) and (II) that the binding interface involves the unstructured N-terminal region of E7. The direct interaction of these highly conserved papillomaviral oncoproteins may provide a new perspective for studying HPV-associated carcinogenesis and the overall viral life cycle.

To date, there are more than 200 types of human papillomaviruses (HPVs) known, which have been classified into five genera (alpha, beta, gamma, mu, and nu) based on their L1 nucleotide sequences (1). HPVs from the alpha genus are further divided into high risk and low risk by the International Agency for Research on Cancer based on their potential carcinogenic properties (2). High-risk HPV (HPV 16, 18, 31, 33, 35, 39, 45, 51, 52, 56, 58, 59, 66, and 68) causes approximately 5% of cancers worldwide, with HPV16 being the most carcinogenic (3, 4). The viral proteins E6 and E7 are crucial in targeting many cellular proteins and a wide range of cellular processes to develop and maintain carcinogenesis, as reviewed (5, 6).

E7 proteins are highly conserved. E7 consists of three conserved regions, namely CR1, CR2, and CR3 (7). CR1 and CR2 are highly acidic and presumably disordered (8), whereas CR3 consists of two CxxC zinc-binding motifs (9, 10). CR1 and CR2 play critical roles in cellular transformation and immortalization, with CR2 exhibiting an LxCxE motif, the dominant binding site for the retinoblastoma protein (pRb) (11, 12). CR3 of E7 triggers the formation of stable dimers (9, 13, 14), and it binds protein tyrosine phosphatase nonreceptor type 14 (PTPN14) (15). Most E7 proteins target the two tumor suppressors pRb and PTPN14 for proteasomal degradation *via* the recruitment of cullin 2 and UBR4 ubiquitin ligase, respectively, leading to uncontrolled cell cycle progression and mediating carcinogenesis (15–20). An elevation of the p53 expression level in the presence of E7 proteins that could lead to apoptosis has been reported previously (21). However, this is overcome by the expression of the E6 protein.

E6 is less conserved among papillomaviruses as compared with E7. However, all E6 consists of four CxxC zinc-binding motifs forming two domains, the E6N and E6C (22, 23). It is known that E6 targets LxxLL motifs of several cellular proteins with affinities in the micromolar range and binds the LxxLL motif at the cleft between E6N and E6C (22, 23). The most extensively studied model is the recruitment of E3 ubiquitin ligase E6–associated protein (E6AP) by E6; the complex binds tumor suppressor p53 resulting in ubiquitination and degradation of p53 (22–24). This, in turn, interferes with p53-dependent apoptosis and cell cycle arrest (25). In addition, a unique PDZ-binding domain found only at the C terminus of E6 from high-risk alpha HPV types allows these E6s to target PDZ-containing proteins such as DLG-1 and MAGI-1, dysregulating the cellular polarity (26–29).

E6 and E7 cooperate to drive cellular transformation and immortalization of human keratinocytes (30–32). This was

* For correspondence: Claudia Simon, Claudia.simon@med.uni-tuebingen.de; Thomas Iftner, Thomas.Iftner@med.uni-tuebingen.de.

observed with the indefinite growth of keratinocytes in the presence of both E6 and E7, whereas E6 alone does not immortalize human keratinocytes (30). A direct interaction between E6 and E7 has not been described so far. Here, we demonstrate an interaction between E6 and E7 proteins of several HPV types in flow cytometry–based FRET assays (fluorescence-activated cell sorting [FACS]–FRET) and *in vitro* using analytical ultracentrifugation and fluorescence polarization (FP).

Results

Evidence supporting interaction between E6 and E7 in cellular assays

To screen the interactions between E6 and E7 *via* FACS–FRET, C33A cells were cotransfected with plasmids encoding mTagBFP2-E6 and enhanced YFP (EYFP)-E7 (Fig. 1*A*) of the same HPV type for all HPV types tested. Furthermore, we verified the interaction of E6 and E7 from two high-risk HPVs, 16 and 31, by coimmunoprecipitation (co-IP). A percent FRET signal of at least 10% and at least 500 FRET-positive cells indicates an interaction. Negative controls (EYFP + mTagBFP2-E6, mTagBFP2 + EYFP-E7) and positive control (fusion of mTagBFP2-EYFP) were always included. Most of these controls showed less than 1.0% FACS–FRET signal for each HPV tested (Fig. 2*A* and Table S2*A*), indicating no binding event. The mTagBFP2-6E6 and mTagBFP2-38E6 coexpressed with EYFP show percent FRET signal of more than 1.0%. However, this signal could be neglected because of the low number of less than 50 FRET-positive cells (Fig. S2 and Table S2*B*). Finally, positive FRET signals were observed for alpha high-risk HPV16 (13.0 ± 1.7%), HPV31 (16.3 ± 2.3%), HPV18 (15.0 ± 1.2%), and beta HPV38 (17.9 ± 2.5%) with more than 750 FRET-positive cells (Fig. S2 and Table S2*B*). Because of the different expression levels of mTagBFP2-E6 and EYFP-E7 (Fig. S3 and Table S3, *A* and *B*), only qualitative evaluation could be applied. Hence, comparing the signals of various FRET pairs quantitatively should be avoided. Notably, the expression of HPV6 E6 proteins was extremely low (Fig. S3 and Table S3, *A* and *B*), leading to a low percent FRET of 8.6 ± 3.4% (Fig. 2*A*) and low FRET-positive cells of 126 cells (Fig. S2), below the threshold applied for the analysis.

Next, we performed hemagglutinin (HA) co-IP with 3XHA-E7 and E6 (Figs. 1*B* and S4) proteins coexpressed in C33A *via* plasmid DNA transfection to validate the result of the FACS–FRET. It was seen that the HPV16 E6 proteins bind nonspecifically to the HA magnetic beads but not HPV31 E6 proteins (data not shown). Hence, for HPV16, we employed a 3xHA peptide to conduct native elution of the complex to eliminate the nonspecific-bound 16E6 protein in the coelution as described (33). Figure 2, *B* and *C* showed that both untagged HPV16 E6 and HPV31 E6 bind to 3xHA-tagged HPV16 E7 and HPV31 E7, respectively.

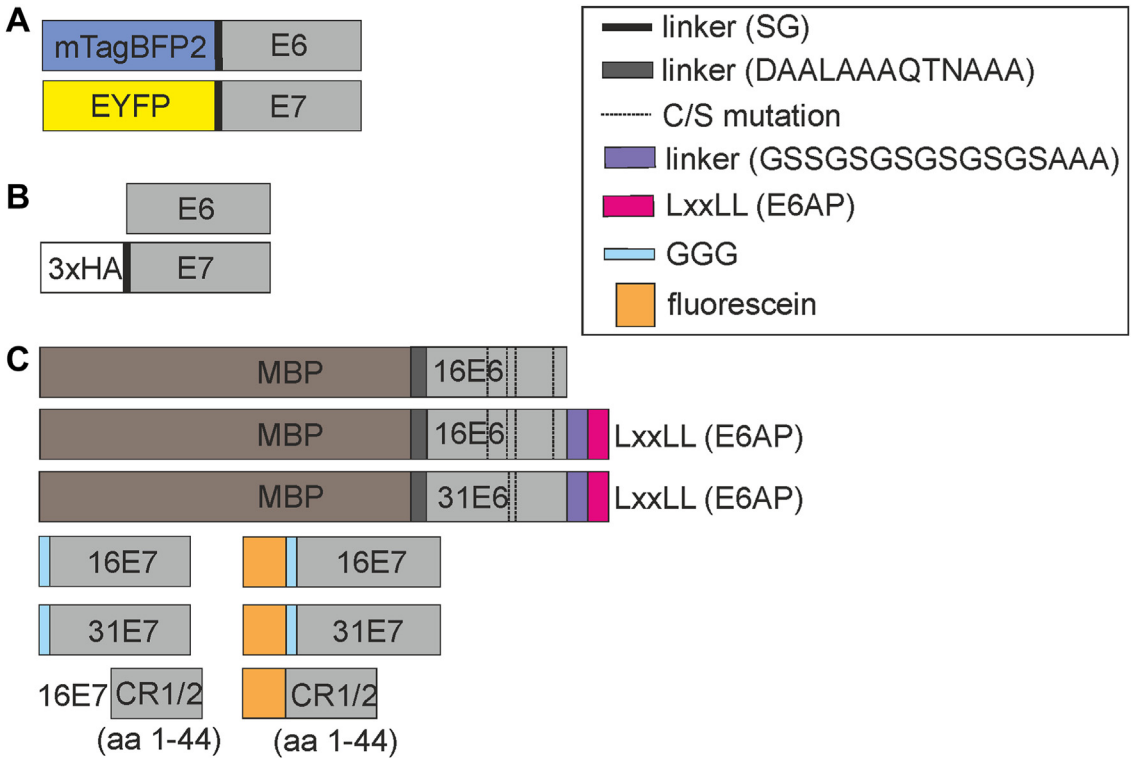

Figure 1. HPV E6 and E7 constructs used in the respective experiments. *A*, the E6 and E7 of HPV 16, 18, 31, 8, 38 used in the FACS–FRET assay were N-terminally fused with mTagBFP2 and EYFP, respectively. *B*, the untagged E6 and the N-terminally 3xHA-tagged E7 constructs of HPV 16 and HPV 31 were used in coimmunoprecipitation. *C*, the various constructs of HPV 16 and HPV 31 were used to produce purified recombinant proteins for analytical ultracentrifugation and fluorescence polarization. EYFP, enhanced YFP; FACS, fluorescence-activated cell sorting; HA, hemagglutinin; HPV, human papillomavirus.

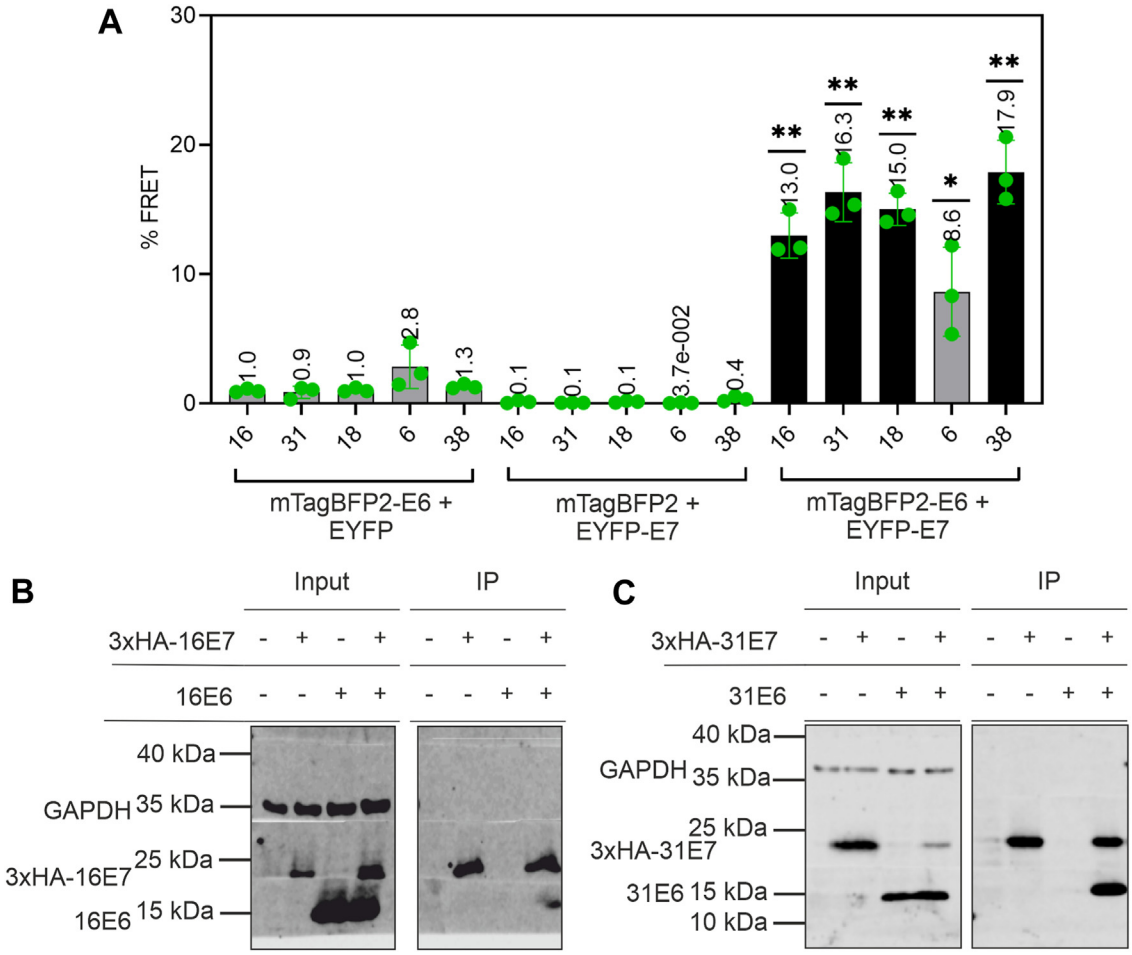

Figure 2. E6 interacts with E7 in cell-based assays. *A*, C33A coexpressing mTagBFP2-E6 and EYFP-E7 of each HPV type were subjected to FACS–FRET and revealed a positive FACS–FRET signal for E6 and E7 proteins from high-risk alpha HPV16, HPV31, HPV18, and beta HPV38, indicating an interaction. The signal for HPV6 is below the threshold; thus, the interaction is unclear. Data are derived from the mean value of three independent biological replicates. The error bars are plotted to represent the standard deviation of the mean value from the three independent biological replicates. The *green dots* represent the scatter dot plot of the three independent biological replicates. *p* Value was calculated with one-sample *t* test, where ** = $p > 0.005$ and * = $p > 0.01$. Please see Supporting information SI2 for detailed statistical data (Table S2*A*) and the number of FRET-positive cells (Fig. S2 and Table S2*B*). *B* and *C*, 70 μg cell lysates from C33A cells (*input*) or 25 μl of proteins precipitated with α-HA antibody (IP) were subjected to immunoblot analysis. The membrane was cut at respective marker bands (above 40 kDa, below 35 kDa, and above 15 kDa) before probing with respective antibodies. Later, the membrane strips were aligned and visualized at the same time at LI-COR Odyssey Fc. The untagged E6 of alpha high-risk HPV16 (*B*) or HPV31 (*C*) was coimmunoprecipitated with 3xHA-16E7 or 3xHA-31E7, respectively. Please see Fig. S4 in SI4 for the full blot. EYFP, enhanced YFP; FACS, fluorescence-activated cell sorting; HPV, human papillomavirus; IP, immunoprecipitation.

In summary, the data suggest that the E6 and E7 proteins of carcinogenic HPV16 and HPV31 formed a complex in cell-based assays. The interaction was not only observed for high-risk alpha HPV16 and HPV31 but also for high-risk alpha HPV18 and beta HPV38 through FACS–FRET.

Two E7 molecules recruit two E6 molecules according to analytical ultracentrifugation

To understand the stoichiometry of the complex, we carried out analytical ultracentrifugation (AUC) with purified recombinant E6 and E7 proteins. Two measurements were performed with a complex formed at a 1:1 molar ratio of monomers, including sedimentation velocity and sedimentation equilibrium. Measuring E7 at 280 nm at a lower concentration is challenging because of the low extinction coefficient. Hence, we labeled 16E7 with fluorescein dye *via sortase A* labeling technique as described in Supporting information S7 and measured the labeled E7 (fl-16E7) signal at 495 nm in the presence and absence of maltose-binding protein (MBP)-16E6_4C4S-LxxLL.

The sedimentation velocity measurement showed a shift in the sedimentation profile for the complex compared with MBP-16E6_4C4S-LxxLL and fl-16E7 alone (Fig. S6). It revealed a sedimentation coefficient (Fig. 3*A*) for two species of s_{app} = 6.70 (major species, ∼89%) and s_{app} = approximately 4.0 (minor species, ∼11%). The sedimentation coefficients of MBP-16E6_4C4S-LxxLL and fl-16E7 alone were s = 4.30 and s = 1.70, respectively. The shift of the sedimentation coefficient from 1.70 and 4.30 to ∼6.70 indicated the complex formation of MBP-16E6_4C4S-LxxLL and fl-16E7. In addition, the formation of a clear sedimenting species neglected the possible formation of heterogeneous agglomerates, which the high density of cysteines in both proteins may cause. Furthermore, the minor species seen in the complex with s = ∼4.0 may be the intermediate species of the complex, as this species was monitored at 495 nm for the signal from fl-16E7.

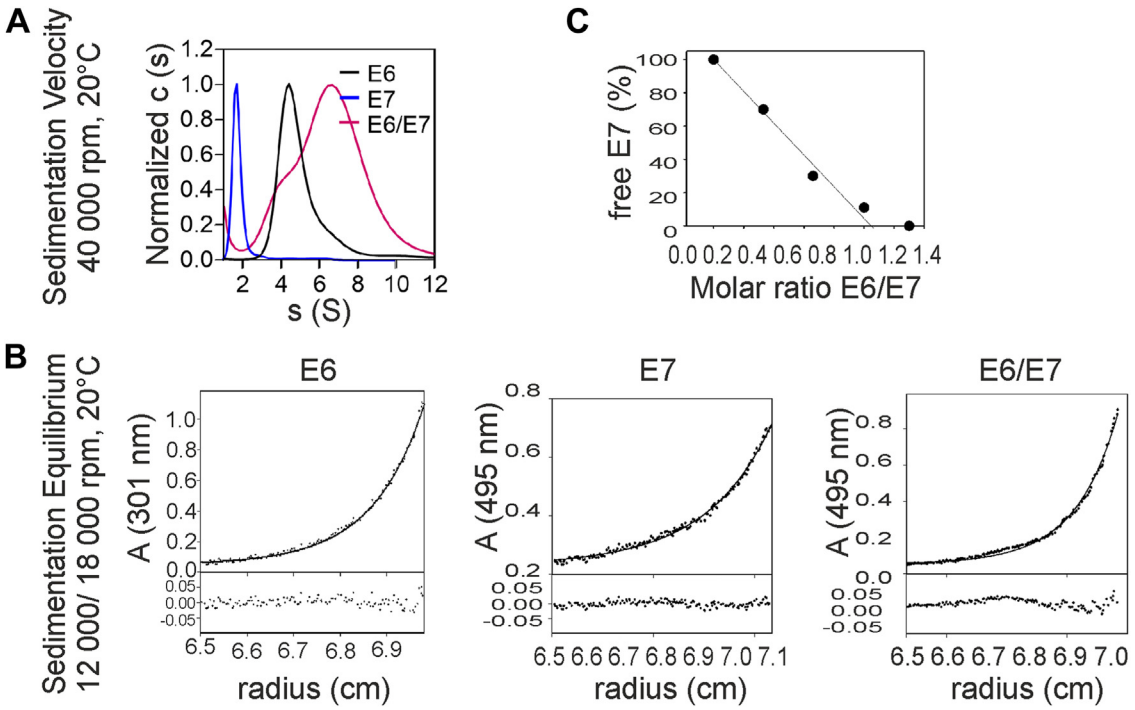

Figure 3. Stoichiometry of E6–E7 complex. *A*, the sedimentation velocity revealed the sedimentation coefficient of MBP-16E6_4C4S-LxxLL (*black*, named E6), fl-16E7 (*blue*, named E7), and the 1:1 molar ratio mixture of E6 and E7 (*magenta*, named E6/E7) calculated with SEDFIT, version 12.52. E6 was monitored at 280 nm, whereas the E7 and E6/E7 were monitored at 495 nm. *B*, the sedimentation equilibrium of MBP16E6_4C4S-LxxLL (named E6), fl-16E7 (named E7), and the 1:1 molar ratio mixture of E6 and E7 (named E6/E7). *C*, the amount of free fl-16E7 (named E7) decreased with an increasing amount of MBP16E6_4C4S-LxxLL, and it was not detected at a molar ratio of approximately 1:1. MBP, maltose-binding protein.

For further characterization, we determined the molecular weight (MW) of MBP-16E6_4C4S-LxxLL of 63.4 ± 4.9 kDa, fl-16E7 of 19.7 ± 2.1 kDa, and MBP-16E6_4C4S-LxxLL/fl-16E7 of 142.0 ± 6.5 kDa with sedimentation equilibrium runs (Fig. 3*B*). These MWs fitted the theoretical MWs of the MBP-16E6_4C4S-LxxLL monomer and fl-16E7 dimer alone (Table 1). The MW_{app} of the complex could correspond to 2× MBP-16E6_4C4S-LxxLL and 2× fl-16E7. We further titrated MBP-16E6_4C4S-LxxLL (0–150 μM) against a fixed concentration of 50 μM E7 dimer to verify this stoichiometry. The E6/E7 complex formed at a molar ratio of 1:1 in Figure 3*C* showed a sedimentation coefficient in the range of s = 6.0 to 7.0, and 89% of fl-16E7 formed a complex with ∼100 μM MBP-16E6_4C4S-LxxLL further confirmed the results obtained previously. Combining the results obtained from sedimentation velocity and sedimentation equilibrium, the broader distribution of the complex as compared with the single species might be due to the equilibrium between the 1:2 and 2:2 complex. The summary of the stoichiometry of MBP-16E6_4C4S-LxxLL, fl-16E7, and MBP-16E6_4C4S-LxxLL/fl-16E7 is shown in Table 1.

Taken together, the results indicate that the proteins of E6 and E7 from HPV16 form the complex at a molar ratio of 2:2, and the calculated MW revealed two E7 molecules and two E6 molecules in the complex.

HPV16 and HPV31 E6 and E7 proteins share a similar binding affinity according to FP assay

We performed FP to quantify the binding affinity of 16E6 and 31E6 to the 16E7 and 31E7, respectively, using recombinantly produced proteins (Fig. 1*C*) and fluorescein-labeled E7 as a probe.

For direct binding, the MBP-E6-LxxLL was titrated 1.5-fold against a fixed concentration of fl-E7, which showed an increase in the FP signal, indicating an interaction. The binding curve fitted with one-site–specific binding fit revealed a similar affinity of 46.4 ± 0.9 μM for MBP-16E6_4C4S-LxxLL (Fig. 4*A*) and 59.4 ± 2.5 μM for MBP-31E6_2C2S-LxxLL (Fig. 4*B*), respectively. The LxxLL direct fusion does stabilize E6, especially for a p53-ready conformation (22, 23). However, it does not resemble the actual situation. Hence, we repeated the same experiment using MBP-16E6_4C4S without the LxxLL peptide

Table 1
MW and sedimentation coefficient of MBP-16E6_4C4S-LxxLL, fl-16E7, and MBP-16E6_4C4S-LxxLL/fl-16E7

Proteins	MW theoretical (kDa)	MW_{app} (kDa)	Sedimentation coefficient (s_{app})	Oligomeric state
MBP-16E6_4C4S-LxxLL	62	63.4 ± 4.9	4.30	Monomer ($E6_1$)
fl-16E7	11	19.7 ± 2.1	1.70	Dimer ($E7_2$)
MBP-16E6_4C4S-LxxLL/fl-16E7	146	142.0 ± 6.5	6.70	2 × E6 + 2 × E7

MW_{app} indicates the calculated MW.

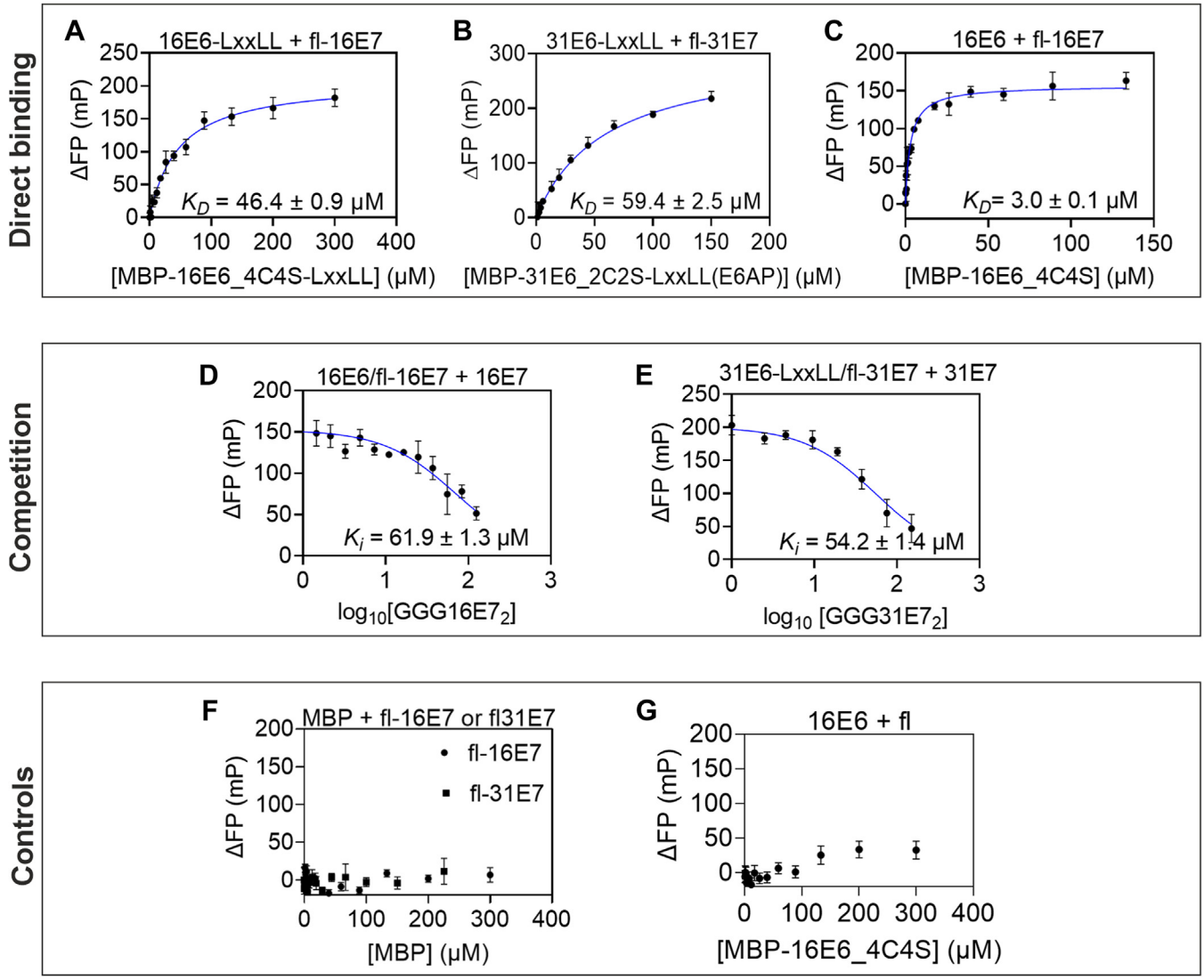

Figure 4. The binding affinity of the E6–E7 complex. *A–C*, direct binding curves of purified MBP-E6-LxxLL or MBP-E6 with fl-E7 were monitored in fluorescence polarization by titrating fl-E7 with an increasing amount of E6. All E6 proteins used above consist of C/S mutation. The clear increase in FP indicates a binding event has occurred. The binding affinity of MBP-E6-LxxLL and fl-E7 from HPV16 (*A*) and HPV31 (*B*) is similar. MBP-16E6_4C4S (*C*) shows a 15-fold higher binding affinity than MBP-16E6_4C4S-LxxLL. *D* and *E*, the reversibility of the complex formation was monitored with a competitive measurement by titrating the complex with an increasing amount of nonlabeled GGG-E7 dimer. A decrease in the FP signal indicates the reversible complex formation. Concluding from the competition measurement, HPV16 (*D*) and HPV31 (*E*) formed E6/E7 complex at a similar binding affinity, and the binding is independent of the LxxLL peptide from E6AP. *F*, an increasing amount of MBP was titrated against fl-16E7 or fl-31E7. No significant increase in the FP signal indicates that the binding between E6 and E7 is not an artifact of the MBP tag. *G*, an increasing amount of MBP-16E6_4C4S was titrated against the fluorescein peptide. A slight increase in FP signal at higher concentrations indicates the presence of artifact from fluorescein. All FP signals were subtracted with the FP signal of respective fl-E7 or fl alone and plotted against concentrations of MBP-16E6_4C4S-LxxLL, MBP-31E6_2C2S-LxxLL, MBP-16E6_4C4S, MBP, or nonlabeled GGG-E7 as indicated. The error bar plotted is the standard deviation of the mean from three technical replicates. FP, fluorescence polarization; MBP, maltose-binding protein.

of E6AP. Surprisingly, this experiment showed an affinity of 3.0 ± 0.1 μM (Fig. 4*C*).

In addition, we performed a competition assay to analyze the reversibility of the observed complex formation. For this, a two-fold dilution of unlabeled GGG-E7 dimer was prepared to compete with the E6/E7 complex formed at 60 to 80% saturation concentration. Considering the effect of the direct fusion of E6AP-LxxLL-peptide on the E6 and E7 interaction observed in direct binding, we used unlabeled GGG-16E7 dimer (titrated from 200 μM) to compete with MBP-16E6_4C4S/fl-16E7 and unlabeled GGG-31E7 dimer (titrated from 150 μM) to compete with MBP-31E6_2C2S-LxxLL/fl-31E7. We observed a decreasing FP signal in both cases, indicating a reversible complex formation of E6 and E7 (Fig. 4, *D* and *E*). In the case of MBP-31E6_2C2S-LxxLL, the direct binding and the competition showed a similar affinity of 59.4 ± 2.5 μM and 54.2 ± 1.4 μM, respectively. However, for MBP-16E6_4C4S without LxxLL fusion, the affinity obtained from direct and competitive measurement differs significantly by approximately 21-fold.

No significant binding was observed when we conducted the same experiment with the controls by substituting MBP-E6 or MBP-E6-LxxLL with MBP only (Fig. 4*F*). Because of the different affinity obtained in Figure 4, *A* and *C*, we titrated

MBP-16E6_4C4S against 42 nM unconjugated fluorescein peptide (equivalent to the fluorescein concentration in fl-16E7) to investigate the effect of fluorescein in the binding. We observed a slight increase in FP signal at concentrations higher than 100 μM of MBP-16E6_4C4S (Fig. 4*G*). This result indicates that the fluorescein may impact E6 and E7 binding without the LxxLL peptide.

Taken together (Table 2), an interaction between E6 with E7 of HPV16 and HPV31 was verified. Both HPV16 and HPV31 share a similar binding affinity between E6-LxxLL and E7. Interestingly, 16E6 without a direct LxxLL fusion seems to bind stronger to E7 in direct binding but not competition.

The CR1/2 region of E7 participates in the complex formation according to the FP assay

We synthesized 16E7CR1/2 (amino acids [aa] 1–44) peptide, labeled and unlabeled with fluorescein dye at N terminus. An increasing amount of MBP-16E6_4C4S was titrated against 350 nM fl-16E7CR1/2 (aa 1–44). An increase in FP signal was observed with MBP-16E6_4C4S again, indicating an interaction (Fig. 5*A*). Then, the nonlabeled 16E7CR1/2 (aa 1–44) was titrated against the complex formed using 200 μM MBP-16E6_4C4S and 350 nM fl-16E7CR1/2 (aa 1–44) (60% saturation) for competition. The decrease of the FP signal indicates a reversible complex formation (Fig. 5*B*) again. The affinity for direct binding and competition were similar, 101.3 ± 2.3 μM and 128.1 ± 16.0 μM (Fig. 5, *A* and *B*), respectively. No increase was observed in the FP signal when the fl-16E7 was titrated with an increasing amount of MBP up to 300 μM (Fig. 5*C*). This means that as full-length E7, the CR1/2 (aa 1–44) of E7 does not bind to MBP but E6. However, the affinity of the complex MBP-16E6_4C4S/16E7CR1-2 (aa 1–44) is approximately two-fold lower than MBP-16E6_4C4S/GGG16E7 but in the same micromolar range.

Hence, these results showed that E6 is binding to the N-terminal region of 16E7, the CR1/2 (aa 1–44).

Discussion

The direct interaction between the proteins E6 and E7 of HPVs has not been described yet. Both proteins act together to immortalize keratinocytes and are overexpressed in carcinoma cells as described earlier.

Our FACS–FRET and co-IP results showed that the E6 and E7 of HPV16 and HPV31 who are the two very closely related HPV types that belong to the alpha genus, species-9 interact with each other. Furthermore, HPV18 belongs to the alpha genus, species-7; and HPV38 belongs to the beta genus, species-2 also shows the interaction between E6 and E7 in FACS–FRET. These results indicate that the interaction between E6 and E7 might be a general phenomenon across HPV phylogenetic trees. The *in vitro* study *via* analytical ultracentrifugation and FP verified the direct interaction between E6 and E7 of HPV16 and HPV31 and revealed a binding affinity of ∼55 to 60 μM. In addition, we revealed the engagement of 16E7CR1/2 (1–44) in the complex formation.

Table 2
Binding affinity of MBP-E6 or MBP-E6-LxxLL with fl-E7

Complex	Direct measurement	Competition
fl-16E7/MBP-16E6_4C4S	3.0 ± 0.1 μM	61.9 ± 1.3 μM
fl-16E7/MBP-16E6_4C4S-LxxLL	46.4 ± 0.9 μM	ND
fl-16E7/MBP-31E6_2C2S-LxxLL	59.4 ± 2.5 μM	54.2 ± 1.4 μM

ND, no data.

It is known that E7 is a highly stable dimer and the most prominent oligomeric species under physiological conditions (9, 13, 34). Accordingly, our AUC data revealed that the fl-16E7 protein (Fig. 3) is a homogenous dimer under tested conditions, whereas MBP-16E6_4C4S-LxxLL is a monomer. In addition, the AUC complex analysis of fl-16E7 and MBP-16E6_4C4S-LxxLL revealed that two molecules of MBP-16E6_4C4S-LxxLL and two molecules of fl-16E7 are forming the predominant species at a 2:2 ratio of E6:E7. Being E7 a highly stable dimer, we propose that an fl-16E7 dimer binds two molecules of MBP-16E6_4C4S-LxxLL. The observed minor intermediate species have also appeared, which could indicate a ratio of 1:2 (1× MBP-16E6_4C4S-LxxLL and 2× fl-16E7 molecules).

Because of the observed intermediate species in AUC, we fitted the FP data with a cooperative binding model, but the results were inconclusive (data not shown). Therefore, all the binding curves and affinities shown were based on the one-site–specific binding model, which resembles the average over the two binding sites. The similar affinities observed in HPV16 and HPV31 (Fig. 4, *D* and *E*) indeed draw interest in comparing the affinities of E6/E7 from other HPV genera. However, because of inefficient material availabilities of recombinant E6 and E7, the *in vitro* analysis for the stoichiometry and affinities measurement was limited to HPV16 and HPV31.

Notably, the affinity obtained in Figure 4, *A* and *C* differs by ∼15-fold, and the fluorescein seems to exert an artifact binding with MBP-16E6_4C4S. The major difference between the two is the fusion of the LxxLL motif directly to the C terminus of 16E6, which binds to the hydrophobic LxxLL binding pocket and stabilizes the E6 (22, 23, 35). We hypothesize that the exposure of the LxxLL hydrophobic binding site in MBP-16E6_4C4S might bind to the fluorescein, thus contributing to the higher affinity in Figure 4*C*. These data also show the importance of employing a competitive measurement in verifying and concluding the binding affinities of the two proteins. The competitive measurement showed a similar affinity for GGG-16E7/MBP16E6_4C4S compared with GGG-31E7/MBP-31E6_2C2S-LxxLL (Fig. 4, *D* and *E*). These results suggest that the LxxLL peptide of E6AP may not interact with E7 but rather impair the binding to the fluorescein. Moreover, it was shown that the E6N and E6C domains are rather flexible (35) and are held in place by the E6AP LxxLL peptide to facilitate the p53 binding (22). Hence, we hypothesized that in the absence of the LxxLL fusion, the conformational flexibility of the E6N and E6C may also impact its binding to the E7.

Detailed 3D-structural information of full-length E7 is unavailable on Protein Data Bank, presumably because of its structural flexibility caused by the highly disordered N-

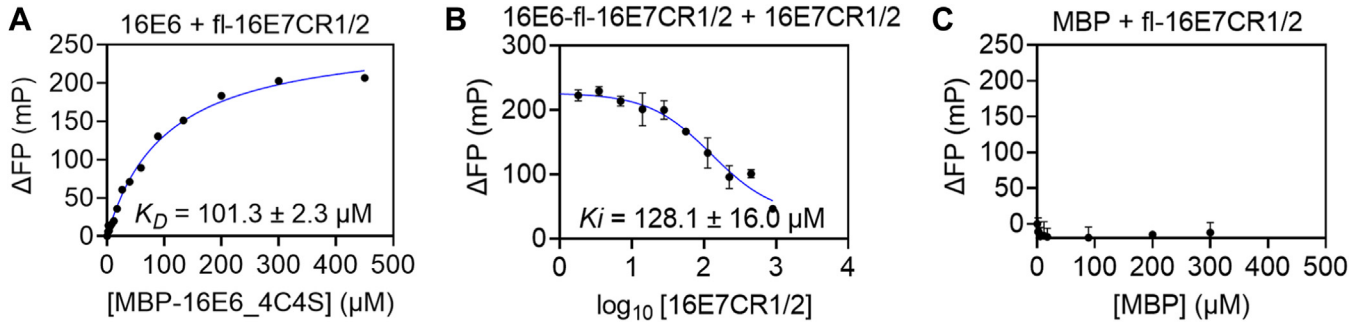

Figure 5. E6 binds N terminus of E7 protein. *A*, the direct binding curve of purified MBP-16E6_4C4S with fl-16E7CR1/2 (amino acid [aa] 1–44) was monitored in fluorescence polarization (FP) by titrating fl-16E7CR1/2 (aa 1–44) with an increasing MBP-16E6_4C4S. *B*, the reversibility of the complex formation was observed with a competitive measurement by titrating the complex with an increasing amount of nonlabeled 16E7CR1/2 (aa 1–44). A decrease in the FP signal indicates the reversible complex formation. Both direct and competitive binding show similar binding affinity. *C*, an increasing amount of MBP was titrated against fl-16E7CR1/2 (aa 1–44). No significant increase in FP signal indicates that the binding between E6 and E7CR1/2 (aa 1–44) is not an artifact of the MBP tag. MBP, maltose-binding protein.

terminal region (10). The binding affinity of the 16E7CR1/2 (aa 1–44) to MBP-16E6_4C4S is in the same range but is two-fold lower than the full-length GGG-16E7. We conducted an additional competition to compete for the fl-16E7/MBP-16E6_4C4S complex with nonlabeled 16E7CR1/2. We revealed an affinity of 288.0 ± 7.8 μM, almost a five-fold difference showing that the 16E7CR1/2 (1–44) has a lower binding affinity (Fig. S5) than full-length 16E7. These observations might be due to its intrinsically disordered properties. It has been described that a protein's intrinsically disordered proteins or regions exert low affinity to their ligands (36, 37). The idea of low affinity was derived from the coupled folding-binding process whereby the net free-energy change during the folding (free energy increases), and their binding to the ligand (free energy decreases) is smaller than in a pure binding process (37, 38). Another hypothesis for this observation is that 16E7CR1/2 (1–44) may not be the only binding region. Nevertheless, 16E7CR1/2 (1–44) is definitely one binding region for MBP-16E6_4C4S. Regarding the details of complex formation, a structural analysis would be necessary to understand the association mechanism between E6 and E7.

The synergistic effects of E6 and E7 in developing and maintaining HPV-associated carcinogenesis have been well reviewed (5, 6). HPV E7 protein does it by inhibiting pRb (11, 12), whereas HPV E6 protein does it by degrading p53 (24), in which these two models are the most studied. Moreover, E6 and E7 also interfere with cellular pathways essential for immune invasion (39). It is proposed that the inhibition effect on NF-κB activity is essential for the initial HPV infection. As soon as the transformation of epithelial cells occurs, the NF-κB is activated and might promote tumorigenesis (6). It was previously shown that the expression of E7 and both E6 and E7 downregulate the basal and tumor necrosis factor-α–induced NF-κB activity in the cervical transformation zone where most cervical cancers start to develop; the effect of E6 on tumor necrosis factor-α–induced NF-κB activity is rather mild (40, 41). On the other hand, several studies observed the upregulation of NF-κB activity in developed cervical carcinomas (42–44) where E6 and E7 are highly expressed. Besides, E6 and E7 inhibit Scrib and PTPN14, respectively to activate the Yes-association protein (YAP1), thus inducing the Hippo signaling pathway that drives cellular proliferation (45, 46). Furthermore, angiogenesis is driven by E6 and E7 by activating proangiogenic factors, oxygen-sensitive transcriptional activator hypoxia-inducible factor-1 (47) and vascular endothelial growth factor (48–50), though the mechanism is not well understood.

With the interaction of E6 with E7 observed here, it is conceivable that the complex may be formed to maintain a network balance between free *versus* complexed E6 and E7 to allow the targeting of different cellular proteins and pathways at distinct time points during the infectious cycle. It could be that the interaction between E6 and E7 may be necessary to support viral replication, immune evasion, and tumorigenesis rather than a synergistic interplay between the single activities of E6 and E7 as has been assumed so far. Further studies are required to unravel whether the complex may facilitate, enhance, or dismiss the binding to the already known cellular targets or even allow the gaining of new targets (Fig. 6). Our findings provide a new perspective for studying the molecular mechanism of E6 and E7 in the viral life cycle, cellular transformation, and carcinogenesis.

Experimental procedures

Constructs

For co-IP, HPV16 E6, HPV31 E6, HPV16 E7, and HPV31E7 (PAVE reference number HPV16REF.1/GI:333031; HPV31REF.1/GI:333048) plasmid constructs were obtained from GenScript, whereby they were cloned in pcDNA3.1 vector with E6s as untagged constructs, whereas E7s were fused to the triple human influenza HA epitopes (3xHA) at their amino (N) terminus with an SG linker. For FACS–FRET, HPV 16E6, 31E6, 18E6, 6E6, and 38E6 constructs were cloned in pmTagBFP-C1. In contrast, HPV 16E7, 31E7, 18E7, 6E7, and 38E7 were cloned into pEYFP-C1 (PAVE reference number HPV18REF.1/GI:60975, HPV6REF.1/GI:60955, HPV38REF.1/GI:1020234) *via* restriction cloning or Gibson cloning obtaining an N-terminal fusion of E6 with mTagBFP2 or N-terminal fusion of E7 with EYFP with an SG linker. For

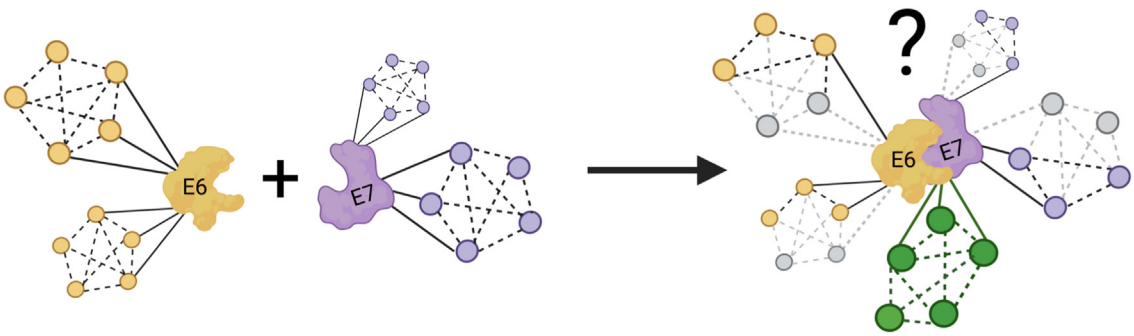

Figure 6. Schematic diagram illustrating putative roles of the complex of E6 with E7. Whether E6 or E7 may retain (*black solid and dotted lines* connecting *yellow* or *violet* interactomes), loss (*gray dotted lines* connecting *gray* interactomes), or gain (*green* interactome network) the ability to target cellular factors upon complex formation is discussed. Figure created with Biorender.com.

recombinant protein production in *Escherichia coli*, it is known that E6 exerts solubility issues, as reviewed (51). Hence, to conquer this obstacle, we fused MBP to the N terminus of E6 protein to increase the solubility and the LxxLL peptide sequence of E6AP (ESSELTLQELLGEER) to the C terminus as it is known to bind and stabilize E6 proteins. Two linkers were cloned upstream and downstream of the E6 sequences, respectively. In addition, the mutations of the nonconserved surface-exposed cysteine to serine were introduced in the E6 proteins to overcome oxidation and disulfide-mediated oligomerization, four cysteines were mutated for 16E6 (C80, C97, C111, and C140) and two for 31E6 (C97 and C111). HPV16 E7 and HPV31 E7 obtained from GenScript were cloned in the pET28a vector to obtain the N-terminally fused hexa-histidine (His_6) constructs with additional tobacco etch virus (TEV) cleavage site and a GGG linker cloned upstream of the E7 that allows tag cleavage by TEV protease followed by *sortase A*-based protein labeling. The detailed expression and purification methods for E6 and E7 full-length proteins can be found in Supplementary information SI7. HPV16E7CR1/2 (aa 1–44) was synthesized as described in Supplementary information SI7. An overview of all constructs used is shown in Figure 1. All E6 and E7 constructs mentioned are aligned with the protein sequences obtained from PAVE database unless mutations are stated (PAVE reference number HPV16REF.1/GI:333031; HPV31REF.1/GI:333048; HPV18REF.1/GI:60975, HPV6REF.1/GI:60955, and HPV38REF.1/GI:1020234). The UniProtKB accession number and protein sequences of the E6 and E7 proteins from each HPV type are also listed in Table S1 in Supporting Information SI1.

Cell culture

HPV-negative cervical cancer cell line C33A was cultured in Dulbecco's modified Eagles' medium (Gibco; catalog no.: 41965-062) supplemented with 10% fetal bovine serum (Gibco; catalog no.: 10270-106) and gentamicin (50 μg/ml) (Gibco; catalog no.: 157710049) at 37 °C, 95% humidity, and 5% carbon dioxide. One day before transfection, 200,000 cells/well were seeded in a 12-well plate (Thermo Scientific; catalog no.: 150628) or 6,000,000 cells in a 150 mm sterile cell culture plate (Thermo Scientific; catalog no.: 168381). The cells were transfected with respective plasmid DNA using jetPRIME (Polyplus; catalog no.: 101000046) following the manufacturer's instructions on day 2. Cells were trypsinized with Gibco trypsin–EDTA (Gibco; catalog no.: 25200072) for FACS measurements or lyse for co-IP 48 h post-transfection.

FACS–FRET

C33A cells coexpressing mTagBFP2-E6 and EYFP-E7 (Fig. 1) were used in FACS–FRET measurements. The positive control mTagBFP2-EYFP direct fusion and the negative controls including the pairs of (i) mTagBFP2 + EYFP, (ii) mTagBFP2-E6s + EYFP, or (iii) EYFP-E7 + mTagBFP2 were constantly employed in the measurement and analysis to ensure appropriate gating as described previously (52). All cells were washed in precooled FACS buffer (Dulbecco's PBS with 1% v/v fetal bovine serum) and resuspended in 250 μl of FACS buffer, followed by FACS measurement using MACSQuant VYB Flow Cytometer (Miltenyi Biotec). FACS–FRET measurement was performed as described earlier (52) but briefly: Cells expressing fluorescent proteins mTagBFP2 and EYFP were detected in channel V1 (405/450 (50)) nm and B1 (488/529 (50)) nm, respectively. FRET signal was assessed in channel V2 (405/525 (50)) nm. FACS and statistical analysis were conducted using FlowLogic, version 7.2.2 (Miltenyi–Inivai) and GraphPad Prism (GraphPad Software, Inc), version 9.1.2 (226), respectively. All figures presented were prepared using CorelDrawX7, version 17.5.0.907 from Alludo (formerly Corel Corporation).

Co-IP

The HA IP was performed with extracts from C33A cells that coexpressed the 3xHA-E7 and the untagged E6 proteins 48 h post-transfection. The cells were treated with 1 μM MG-132 proteasome inhibitors (AdipoGen Life Sciences; AG-CP3-0011) 16 h before harvesting. Cells from four 150 mm plates with 90% confluency were harvested in 3 ml of lysis buffer (10% [v/v] glycerol [MP Biomedicals; catalog no.: 4800689]; 50 mM Hepes, pH 7.5 [Carl Roth; catalog no.: 9105.4]; 3 mM magnesium chloride [Merck; catalog no.: 105833]; 0.1% [v/v] IGEPAL CA-630 [NP-40] [Merck; catalog no.: 18896]; 150 mM sodium chloride [NaCl] [Carl Roth; catalog no.: 3957.2]; 1 mM Tris(2-carboxyethyl)phosphine [TCEP] [Alfa Aesar;

catalog no.: J60316]; 200 μM zinc chloride [Carl Roth; catalog no.: 3533]; supplemented with 1 μl benzonase endonuclease [Merck; catalog no.: 101656] per 10 ml buffer, one tablet PhosSTOP [Roche; PHOSSRO] per 25 ml buffer, and one tablet of cOmplete EDTA-free Protease Inhibitor Cocktail [Roche; catalog no.: COEDTAF-RO] per 50 ml buffer) prior use. Cell lysates were incubated on a shaker in the cold room (4–8 °C) for 1 h before centrifuging at 18,000*g* at 4 °C for 10 min to remove cell debris and unlysed cells. Bradford assay was conducted for the supernatant to determine the total protein concentration of the cleared crude lysates. Each time, 6000 μg of total protein of the cleared crude lysates were incubated with 50 μl of anti-HA Microbeads (μMACS HA Isolation Kits [Miltenyi Biotec; catalog no.: 130-091-122]) for 2 h in the cold room (4–8 °C). Then, the suspension was loaded on μColumns (Miltenyi Biotec; catalog no.: 130-042-701), attached to a μMACS Separator (Miltenyi Biotec; catalog no.: 130-042-602), followed by five times washing steps, each time with 500 μl lysis buffer. Then, native elution with 3xHA peptide was performed to eliminate nonspecific-bound proteins as previously described (33). Proteins of interest obtained from native elution were diluted in reducing SDS-sample buffer and heated at 95 °C for 10 min before further analysis by immunoblotting.

Immunoblotting

The proteins of interest were resolved on reducing 8 to 20% gradient SDS-PAGE gel. Proteins were electro-transferred onto nitrocellulose membrane (GE Healthcare) *via* wet blotting using blotting buffer (2.2 g/l 3-(cyclohexylamino)-1-propanesulfonic acid [Sigma; catalog no.: C2632], 0.001% [w/v] SDS [Carl Roth; catalog no.: 2326.2], 10% [v/v] methanol [Honeywell; catalog no.: 32213], pH 10.3 at room temperature) for 1 h at 70 V (constant). The membrane was blocked with 5% (w/v) albumin bovine fraction V (Serva; catalog no.: 11930) in PBS for 1 h at room temperature and probed with appropriate primary antibodies, which were all diluted in PBS with 0.1% v/v Tween-20 (Sigma; catalog no.: P9416) overnight at cold room (4–8 °C). The used primary antibodies include anti-HA Rabbit (Cell Signaling; catalog no.: 3724) for detection of 3xHA-E7 at dilution of 1:1000 and anti-16E6 (AVC #G6, Lot #15) as well as anti-31E6 (AVC #C8, Lot #8) (generously provided by Arbor Vita Corporation) at dilution of 1:10,000 for detection of 16E6 and 31E6, respectively. GAPDH was used as a loading control and detected by anti-GAPDH (6C5) from Santa Cruz Biotechnology (catalog no.: sc32233) at a dilution of 1:500. All membranes were washed three times with PBS with 0.05% v/v Tween-20 after overnight incubation with primary antibodies. Secondary antibodies IRDye 680RD Goat anti-Rabbit IgG (H + L) or IRDye 680RD Goat antimouse IgG (H + L) (LI-COR Biotechnology GmbH) were used at a dilution of 1:10,000 and incubated for 30 min at room temperature. The membrane was washed three times with PBS with 0.05% v/v Tween-20. The signal of the respective protein was then visualized using LI-COR Odyssey Fc (700 nm channel) and analyzed with Image Studio Lite Software from LI-COR Biosciences.

Analytical ultracentrifugation

To analyze the molecular mass and the stoichiometry of the complex, we performed analytical ultracentrifugation in an analytical ultracentrifuge XL-I (Beckman Coulter) and an An-50 Ti rotor with double sector cells using the complex of fl-16E7 and MBP-16E6_4C4S-LxxLL (E6AP) formed in the assay buffer (20 mM Hepes [pH 7.5], 200 mM NaCl, and 1 mM TCEP). The absorbance at 495 nm, specific for fluorescein and therefore measures fl-16E7, was monitored. To determine the sedimentation velocity, the fl-16E7 and MBP-16E_64C4S-LxxLL proteins were mixed in a 1:1 molar ratio, and the sedimentation at 40,000 rpm, 20 °C, was analyzed for 5 h. Scans were taken every 10 min. The molecular mass was measured at 12,000 or 18,000 rpm in sedimentation equilibrium runs at 100 μM MBP-16E6_4C4S-LxxLL (measured at 280 and 301 nm), 100 μM of fl-16E7, and 100 μM complex (mixture of E6 and E7 at 1:1 molar ratio) in the assay buffer at 20 °C. Every sedimentation equilibrium was measured for at least 40 h until equilibrium was reached, with scans taken every 5 h. Equilibrium was proven experimentally with the final three scans being identical. The MBP-16E6_4C4S-LxxLL proteins were also titrated (0–150 μM) against 100 μM fl-16E7 proteins. The program SEDFIT version 12.52 from National Institutes of Health was used for data analysis (53).

FP

For FP direct measurements, a 1.5-fold dilution series of the MBP-E6 proteins were prepared in the FP assay buffer (20 mM Hepes [pH 7.5], 200 mM NaCl, 1 mM TCEP, and 0.005% Tween-20). For each dataset shown, three technical replicates of an identical dilution series were prepared and mixed with 350 nM or 200 nM fl-E7 of HPV16 or HPV31, respectively. Finally, 50 μl of E6/E7 complexes were transferred to 96-well microplates (nonbinding microplate, 96 wells; Greiner Bio-One; catalog no.: 655900) for measurement at the multimode reader Tristar^2 LB 942 (Berthold Technologies) equipped with a polarizer filter, with each measurement consists of 16 different protein concentrations (whereas one contained no E6 protein and corresponded to the free fl-E7). In competitive FP measurements, the E6 protein and fl-E7 were mixed in the FP assay buffer to achieve a complex formation of 60 to 80% at concentrations based on the titration of direct binding, 70 μM of MBP-31E6_2C2S-LxxLL for HPV31 and 50 μM of MBP-16E6_4C4S for HPV16, respectively. Then, a dilution series of the nonfluorescent competitor, the unlabeled HPV16 GGG-E7 and HPV31 GGG-E7 dimer proteins, were titrated against the complex. The competitive measurement was carried out identically to the direct experiment described previously. Analyses of all FP experiments were carried out in GraphPad Prism, version 9.1.2 (226). All data were fitted using the one-site–specific binding model.

Data availability

All data are contained within the article.

Supporting information—This article contains supporting information (54–58).

Acknowledgments—We thank Prof Thilo Stehle and Dr Christoph Shall for the bioreactor and the TEV protease plasmid. We acknowledge Prof Dirk Schwarzer for the fluorescein dye and the *sortase A* plasmid. We thank Dr Gergo Gogl for the extensive discussion on FP data. We thank Dr Johannes Schweizer from Arbor Vita Corporation for generously supplying us with the anti-16E6, anti-31E6, and anti-31E7 antibodies.

Author contributions—C. S. conceptualization; J. W. L., H. L., H. K., N. R., A. C.-S., G. T., and C. S. methodology; C. S. software; T. I., G. T., and C. S. validation; J. W. L. formal analysis; J. W. L. investigation; H. L., H. K., and C. S. resources; J. W. L., H. L., H. K., N. R., M. F., M. C., T. V., G. C. B., and D. I. F. data curation; J. W. L. and C. S. writing–original draft; J. W. L., H. L., H. K., N. R., D. I. F., M. F., M. C., T. V., A. C.-S., G. C. B., T. I., G. T., and C. S. writing–review & editing; J. W. L. and C. S. visualization; T. I. and C. S. supervision; C. S. project administration; T. I. and C. S. funding acquisition.

Funding and additional information—A grant supported this work from Wilhelm Sander-Stiftung 2020.141.1 (to C. S. and T. I).

Conflict of interest—The authors declare that they have no conflicts of interest with the contents of this article.

Abbreviations—The abbreviations used are: AUC, analytical ultracentrifugation; co-IP, coimmunoprecipitation; E6AP, E3 ubiquitin ligase E6–associated protein; EYFP, enhanced YFP; FACS, fluorescence-activated cell sorting; fl, fluorescein; FP, fluorescence polarization; HA, hemagglutinin; HPV, human papillomavirus; MBP, maltose-binding protein; MW, molecular weight; NaCl, sodium chloride; pRb, retinoblastoma protein; PTPN14, protein tyrosine phosphatase nonreceptor type 14; TEV, tobacco etch virus; TCEP, Tris(2-carboxyethyl)phosphine.

References

1. de Villiers, E. M., Fauquet, C., Broker, T. R., Bernard, H. U., and zur Hausen, H. (2004) Classification of papillomaviruses. *Virology* **324**, 17–27
2. IARC Working Group on the Evaluation of Carcinogenic Risks to Humans (2007) Human papillomaviruses. *IARC Monogr. Eval. Carcinog. Risks Hum.* **90**, 1–636
3. Munoz, N., Bosch, F. X., de Sanjose, S., Herrero, R., Castellsague, X., Shah, K. V., *et al.* (2003) Epidemiologic classification of human papillomavirus types associated with cervical cancer. *N. Engl. J. Med.* **348**, 518–527
4. Munoz, N., Bosch, F. X., Castellsague, X., Diaz, M., de Sanjose, S., Hammouda, D., *et al.* (2004) Against which human papillomavirus types shall we vaccinate and screen? *Inter. Perspect. Int. J. Cancer* **111**, 278–285
5. Mittal, S., and Banks, L. (2017) Molecular mechanisms underlying human papillomavirus E6 and E7 oncoprotein-induced cell transformation mutat. *Res. Rev. Mutat. Res.* **772**, 23–35
6. Vats, A., Trejo-Cerro, O., Thomas, M., and Banks, L. (2021) Human papillomavirus E6 and E7: what remains? *Tumour Virus Res.* **11**, 200213
7. Phelps, W. C., Yee, C. L., Munger, K., and Howley, P. M. (1988) The human papillomavirus type 16 E7 gene encodes transactivation and transformation functions similar to those of adenovirus. *E1A Cell* **53**, 539–547
8. Noval, M. G., Gallo, M., Perrone, S., Salvay, A. G., Chemes, L. B., and de Prat-Gay, G. (2013) Conformational dissection of a viral intrinsically disordered domain involved in cellular transformation. *PLoS One* **8**, e72760
9. Ohlenschlager, O., Seiboth, T., Zengerling, H., Briese, L., Marchanka, A., Ramachandran, R., *et al.* (2006) Solution structure of the partially folded high-risk human papilloma virus 45 oncoprotein E7. *Oncogene* **25**, 5953–5959
10. Garcia-Alai, M. M., Alonso, L. G., and de Prat-Gay, G. (2007) The N-terminal module of HPV16 E7 is an intrinsically disordered domain that confers conformational and recognition plasticity to the oncoprotein. *Biochemistry* **46**, 10405–10412
11. Dyson, N., Howley, P. M., Munger, K., and Harlow, E. (1989) The human papilloma virus-16 E7 oncoprotein is able to bind to the retinoblastoma gene product. *Science* **243**, 934–937
12. Dahiya, A., Gavin, M. R., Luo, R. X., and Dean, D. C. (2000) Role of the LXCXE binding site in Rb function. *Mol. Cell Biol.* **20**, 6799–6805
13. Alonso, L. G., Garcia-Alai, M. M., Nadra, A. D., Lapena, A. N., Almeida, F. L., Gualfetti, P., *et al.* (2002) High-risk (HPV16) human papillomavirus E7 oncoprotein is highly stable and extended, with conformational transitions that could explain its multiple cellular binding partners. *Biochemistry* **41**, 10510–10518
14. Clemens, K. E., Brent, R., Gyuris, J., and Munger, K. (1995) Dimerization of the human papillomavirus E7 oncoprotein *in vivo*. *Virology* **214**, 289–293
15. Yun, H. Y., Kim, M. W., Lee, H. S., Kim, W., Shin, J. H., Kim, H., *et al.* (2019) Structural basis for recognition of the tumor suppressor protein PTPN14 by the oncoprotein E7 of human papillomavirus. *PLoS Biol.* **17**, e3000367
16. Boyer, S. N., Wazer, D. E., and Band, V. (1996) E7 protein of human papilloma virus-16 induces degradation of retinoblastoma protein through the ubiquitin-proteasome pathway. *Cancer Res.* **56**, 4620–4624
17. Berezutskaya, E., Yu, B., Morozov, A., Raychaudhuri, P., and Bagchi, S. (1997) Differential regulation of the pocket domains of the retinoblastoma family proteins by the HPV16 E7 oncoprotein. *Cell Growth Differ.* **8**, 1277–1286
18. Gonzalez, S. L., Stremlau, M., He, X., Basile, J. R., and Munger, K. (2001) Degradation of the retinoblastoma tumor suppressor by the human papillomavirus type 16 E7 oncoprotein is important for functional inactivation and is separable from proteasomal degradation of E7. *J. Virol.* **75**, 7583–7591
19. White, E. A., Munger, K., and Howley, P. M. (2016) High-risk human papillomavirus E7 Proteins PTPN14 for degradation. *mBio* **7**, e01530-16
20. Hatterschide, J., Bohidar, A. E., Grace, M., Nulton, T. J., Kim, H. W., Windle, B., *et al.* (2019) PTPN14 degradation by high-risk human papillomavirus E7 limits keratinocyte differentiation and contributes to HPV-mediated oncogenesis. *Proc. Natl. Acad. Sci. U. S. A.* **116**, 7033–7042
21. Jones, D. L., Thompson, D. A., and Munger, K. (1997) Destabilization of the RB tumor suppressor protein and stabilization of p53 contribute to HPV type 16 E7-induced apoptosis. *Virology* **239**, 97–107
22. Martinez-Zapien, D., Ruiz, F. X., Poirson, J., Mitschler, A., Ramirez, J., Forster, A., *et al.* (2016) Structure of the E6/E6AP/p53 complex required for HPV-mediated degradation of p53. *Nature* **529**, 541–545
23. Conrady, M. C., Suarez, I., Gogl, G., Frecot, D. I., Bonhoure, A., Kostmann, C., *et al.* (2020) Structure of high-risk papillomavirus 31 E6 oncogenic protein and characterization of E6/E6AP/p53 complex formation. *J. Virol.* **95**, e00730-20
24. Scheffner, M., Huibregtse, J. M., Vierstra, R. D., and Howley, P. M. (1993) The HPV-16 E6 and E6-AP complex functions as a ubiquitin-protein ligase in the ubiquitination of p53. *Cell* **75**, 495–505
25. DeFilippis, R. A., Goodwin, E. C., Wu, L., and DiMaio, D. (2003) Endogenous human papillomavirus E6 and E7 proteins differentially regulate proliferation, senescence, and apoptosis in HeLa cervical carcinoma cells. *J. Virol.* **77**, 1551–1563
26. Glaunsinger, B. A., Lee, S. S., Thomas, M., Banks, L., and andJavier, R. (2000) Interactions of the PDZ-protein MAGI-1 with adenovirus E4-ORF1 and high-risk papillomavirus E6 oncoproteins. *Oncogene* **19**, 5270–5280

27. Thomas, M., Laura, R., Hepner, K., Guccione, E., Sawyers, C., Lasky, L., *et al.* (2002) Oncogenic human papillomavirus E6 proteins target the MAGI-2 and MAGI-3 proteins for degradation. *Oncogene* **21**, 5088–5096
28. Kiyono, T., Hiraiwa, A., Fujita, M., Hayashi, Y., Akiyama, T., and andIshibashi, M. (1997) Binding of high-risk human papillomavirus E6 oncoproteins to the human homologue of the Drosophila discs large tumor suppressor protein. *Proc. Natl. Acad. Sci. U. S. A.* **94**, 11612–11616
29. Thomas, M., Massimi, P., Navarro, C., Borg, J. P., and Banks, L. (2005) The hScrib/Dlg apico-basal control complex is differentially targeted by HPV-16 and HPV-18 E6 proteins. *Oncogene* **24**, 6222–6230
30. Hawley-Nelson, P., Vousden, K. H., Hubbert, N. L., Lowy, D. R., and Schiller, J. T. (1989) HPV16 E6 and E7 proteins cooperate to immortalize human foreskin keratinocytes. *EMBO J.* **8**, 3905–3910
31. Richard, C., Lanner, C., Naryzhny, S. N., Sherman, L., Lee, H., Lambert, P. F., *et al.* (2010) The immortalizing and transforming ability of two common human papillomavirus 16 E6 variants with different prevalences in cervical cancer. *Oncogene* **29**, 3435–3445
32. Sedman, S. A., Barbosa, M. S., Vass, W. C., Hubbert, N. L., Haas, J. A., Lowy, D. R., *et al.* (1991) The full-length E6 protein of human papillomavirus type 16 has transforming and trans-activating activities and cooperates with E7 to immortalize keratinocytes in culture. *J. Virol.* **65**, 4860–4866
33. Lim, J., Iftner, T., and Simon, C. (2021) Native isolation of 3xHA-tagged protein complexes to characterize protein-protein interactions. *Curr. Protoc.* **1**, e29
34. Liu, X., Clements, A., Zhao, K., and Marmorstein, R. (2006) Structure of the human Papillomavirus E7 oncoprotein and its mechanism for inactivation of the retinoblastoma tumor suppressor. *J. Biol. Chem.* **281**, 578–586
35. Zanier, K. (2012) Solution structure analysis of the HPV16 E6 oncoprotein reveals a self-association mechanism required for E6-mediated degradation of P53. *Structure* **20**, 604–617
36. Dyson, H. J., and Wright, P. E. (2005) Intrinsically unstructured proteins and their functions. *Nat. Rev. Mol. Cell Biol.* **6**, 197–208
37. Vreven, T., Hwang, H., Pierce, B. G., and Weng, Z. (2012) Prediction of protein-protein binding free energies. *Protein Sci.* **21**, 396–404
38. Liu, Z., and Huang, Y. (2014) Advantages of proteins being disordered. *Protein Sci.* **23**, 539–550
39. Moore, P. S., and Chang, Y. (2010) Why do viruses cause cancer? Highlights of the first century of human tumour virology. *Nat. Rev. Cancer* **10**, 878–889
40. Vandermark, E. R., Deluca, K. A., Gardner, C. R., Marker, D. F., Schreiner, C. N., Strickland, D. A., *et al.* (2012) Human papillomavirus type 16 E6 and E 7 proteins alter NF-kB in cultured cervical epithelial cells and inhibition of NF-kB promotes cell growth and immortalization. *Virology* **425**, 53–60
41. Spitkovsky, D., Hehner, S. P., Hofmann, T. G., Moller, A., and Schmitz, M. L. (2002) The human papillomavirus oncoprotein E7 attenuates NF-kappa B activation by targeting the Ikappa B kinase complex. *J. Biol. Chem.* **277**, 25576–25582
42. Nees, M., Geoghegan, J. M., Hyman, T., Frank, S., Miller, L., and Woodworth, C. D. (2001) Papillomavirus type 16 oncogenes down-regulate expression of interferon-responsive genes and upregulate proliferation-associated and NF-kappaB-responsive genes in cervical keratinocytes. *J. Virol.* **75**, 4283–4296
43. Havard, L., Rahmouni, S., Boniver, J., and Delvenne, P. (2005) High levels of p105 (NFKB1) and p100 (NFKB2) proteins in HPV16-transformed keratinocytes: role of E6 and E7 oncoproteins. *Virology* **331**, 357–366
44. Li, J., Jia, H., Xie, L., Wang, X., Wang, X., He, H., *et al.* (2009) Association of constitutive nuclear factor-kappaB activation with aggressive aspects and poor prognosis in cervical cancer. *Int. J. Gynecol. Cancer* **19**, 1421–1426
45. Messa, L., Celegato, M., Bertagnin, C., Mercorelli, B., Alvisi, G., Banks, L., *et al.* (2021) The dimeric form of HPV16 E6 is crucial to drive YAP/TAZ upregulation through the targeting of hScrib. *Cancers (Basel)* **13**, 4083
46. Hatterschide, J., Castagnino, P., Kim, H. W., Sperry, S. M., Montone, K. T., Basu, D., *et al.* (2022) YAP1 activation by human papillomavirus E7 promotes basal cell identity in squamous epithelia. *Elife* **11**, e75466
47. Tang, X., Zhang, Q., Nishitani, J., Brown, J., Shi, S., and Le, A. D. (2007) Overexpression of human papillomavirus type 16 oncoproteins enhances hypoxia-inducible factor 1 alpha protein accumulation and vascular endothelial growth factor expression in human cervical carcinoma cells. *Clin. Cancer Res.* **13**, 2568–2576
48. Lopez-Ocejo, O., Viloria-Petit, A., Bequet-Romero, M., Mukhopadhyay, D., Rak, J., and Kerbel, R. S. (2000) Oncogenes and tumor angiogenesis: the HPV-16 E6 oncoprotein activates the vascular endothelial growth factor (VEGF) gene promoter in a p53 independent manner. *Oncogene* **19**, 4611–4620
49. Toussaint-Smith, E., Donner, D. B., and Roman, A. (2004) Expression of human papillomavirus type 16 E6 and E7 oncoproteins in primary foreskin keratinocytes is sufficient to alter the expression of angiogenic factors. *Oncogene* **23**, 2988–2995
50. Li, F., and andCui, J. (2015) Human telomerase reverse transcriptase regulates vascular endothelial growth factor expression *via* human papillomavirus oncogene E7 in HPV-18-positive cervical cancer cells. *Med. Oncol.* **32**, 199
51. Suarez, I., and andTrave, G. (2018) Structural insights in multifunctional papillomavirus oncoproteins. *Viruses* **10**, 37
52. Banning, C., Votteler, J., Hoffmann, D., Koppensteiner, H., Warmer, M., Reimer, R., *et al.* (2010) A flow cytometry-based FRET assay to identify and analyse protein-protein interactions in living cells. *PLoS One* **5**, e9344
53. Schuck, P. (2000) Size-distribution analysis of macromolecules by sedimentation velocity ultracentrifugation and lamm equation modeling. *Biophys. J.* **78**, 1606–1619
54. Roos, N., Breiner, B., Preuss, L., Lilie, H., Hipp, K., Herrmann, H., *et al.* (2020) Optimized production strategy of the major capsid protein HPV 16L1 non-assembly variant in E. coli protein. *Expr. Purif.* **175**, 105690
55. Tropea, J. E., Cherry, S., and Waugh, D. S. (2009) Expression and purification of soluble His(6)-tagged TEV protease. *Met. Mol. Biol.* **498**, 297–307
56. Barthels, F., Marincola, G., Marciniak, T., Konhauser, M., Hammerschmidt, S., Bierlmeier, J., *et al.* (2020) Asymmetric Disulfanylbenzamides as irreversible and selective inhibitors of Staphylococcus aureus Sortase. *A ChemMedChem* **15**, 839–850
57. Zaidi, N., Herrmann, T., Baechle, D., Schleicher, S., Gogel, J., Driessen, C., *et al.* (2007) A new approach for distinguishing cathepsin E and D activity in antigen-processing organelles. *FEBS J.* **274**, 3138–3149
58. Jores, T., Klinger, A., Gross, L. E., Kawano, S., Flinner, N., Duchardt-Ferner, E., *et al.* (2016) Characterization of the targeting signal in mitochondrial beta-barrel proteins. *Nat. Commun.* **7**, 12036

Evidence for direct interaction between the oncogenic proteins E6 and E7 of high-risk Human Papillomavirus (HPV)

JiaWen Lim[1], Hauke Lilie[3], Hubert Kalbacher[4], Nora Roos[1], Desiree Isabella Frecot[1], Maximilian Feige[1], Marcel Conrady[1], Tobias Votteler[1], Alexandra Cousido-Siah[2], Giada Corradini Bartoli[1], Thomas Iftner[1], Gilles Trave[2], Claudia Simon[1*]

Affiliations:

1 Institute of Medical Virology and Epidemiology of Viral Diseases, University Hospital Tuebingen, Germany

2 Equipe Labellisée Ligue 2015, Department of Integrative Biology, Institut de Génétique et de Biologie Moléculaire et Cellulaire, CNRS, INSERM, UdS, Illkirch, France

3 Institute of Biochemistry and Biotechnology, Martin-Luther-University Halle-Wittemberg, Germany

4 Interfaculty Institute of Biochemistry, Eberhard-Karls-University Tuebingen, Germany

*Corresponding author:

Claudia.simon@med.uni-tuebingen.de

Thomas.Iftner@med.uni-tuebingen.de

List of supporting information

Supporting information 1 (SI1): Protein sequences of the E6 and E7

Table S1: The UniProtKB accession number and protein sequences of all mentioned E6 and E7 proteins

Proteins	UniProtKB accession number	Protein sequences
HPV16E6	P03126	MFQDPQERPRKLPQLCTELQTTIHDIILECVYCKQQLLRRE VYDFAFRDLCIVYRDGNPYAVCDKCLKFYSKISEYRHYCYS LYGTTLEQQYNKPLCDLLIRCINCQKPLCPEEKQRHLDKKQ RFHNIRGRWTGRCMSCCRSSRTRRETQL
HPV16E7	P03129	MHGDTPTLHEYMLDLQPETTDLYCYEQLNDSSEEEDEIDG PAGQAEPDRAHYNIVTFCCKCDSTLRLCVQSTHVDIRTLE DLLMGTLGIVCPICSQKP
HPV18E6	P06463	MARFEDPTRRPYKLPDLCTELNTSLQDIEITCVYCKTVLELT EVFEFAFKDLFVVYRDSIPHAACHKCIDFYSRIRELRHYSD SVYGDTLEKLTNTGLYNLLIRCLRCQKPLNPAEKLRHLNEK RRFHNIAGHYRGQCHSCCNRARQERLQRRRETQV
HPV18E7	P06788	MHGPKATLQDIVLHLEPQNEIPVDLLCHEQLSDSEEENDEI DGVNHQHLPARRAEPQRHTMLCMCCKCEARIELVVESSA DDLRAFQQLFLNTLSFVCPWCASQQ
HPV31E6	P17386	MFKNPAERPRKLHELSSALEIPYDELRLNCVYCKGQLTETE VLDFAFTDLTIVYRDDTPHGVCTKCLRFYSKVSEFRWYRY SVYGTTLEKLTNKGICDLLIRCITCQRPLCPEEKQRHLDKKK RFHNIGGRWTGRCIACWRRPRTETQV
HPV31E7	P17387	MRGETPTLQDYVLDLQPEATDLHCYEQLPDSSDEEDVIDS PAGQAEPDTSNYNIVTFCCQCKSTLRLCVQSTQVDIRILQE LLMGSFGIVCPNCSTRL
HPV6E6	P06462	MESANASTSATTIDQLCKTFNLSMHTLQINCVFCKNALTTA EIYSYAYKHLKVLFRGGYPYAACACCLEFHGKINQYRHFD YAGYATTVEEETKQDILDVLIRCYLCHKPLCEVEKVKHILTK ARFIKLNCTWKGRCLHCWTTCMEDMLP
HPV6E7	P06464	MHGRHVTLKDIVLDLQPPDPVGLHCYEQLVDSSEDEVDEV DGQDSQPLKQHFQIVTCCCGCDSNVRLVVQCTETDIREV QQLLLGTLNIVCPICAPKT
HPV38E6	Q80907	MELPKPQTVQQLSDKLTVPVEDLLLPCRFCNSFLTYIELRE FDYKNLQLIWTQEDFVFACCSSCAYASAQYECQQFYELTV FGREIEQVEQQTIGLIVIRCQYCLKCLDLIEKLDICCSHQAFH KVRGNWKGRCRHCKAIE
HPV38E7	Q80908	MIGKQATLRDIVLEELVQPIDLHCHEELPDLPEDIEASVVEE EPAYTPYKIIVLCGGCEVRLKLYVWATDAGIRNLQDCLLGD VRLLCPTCREDIRNGGR

Supporting information 2 (SI2): FACS-FRET analysis

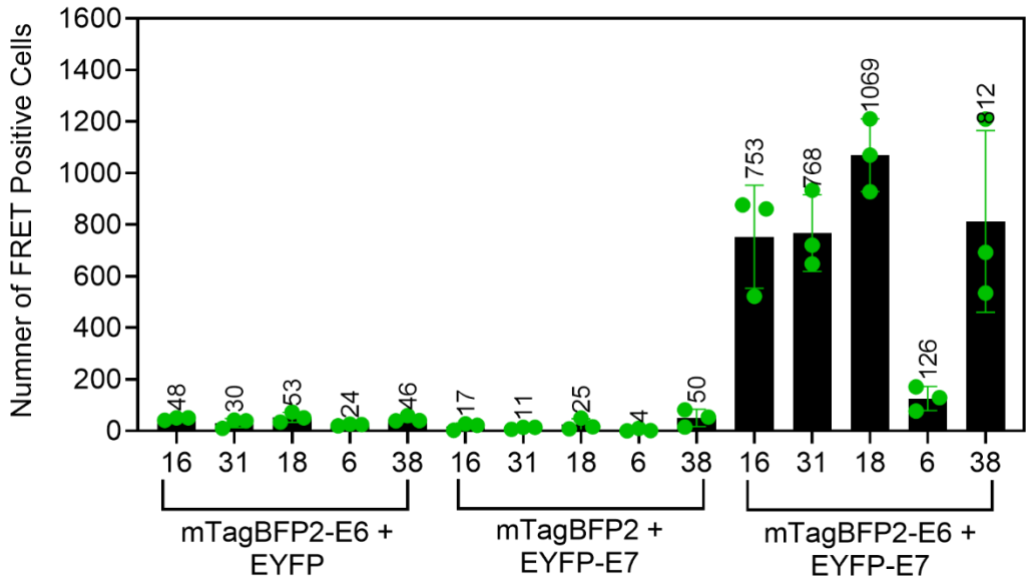

Figure S2. E6 interacts with E7 FACS-FRET assay. C33A co-expressing mTagBFP2-E6 and EYFP-E7 were subjected to FACS-FRET. The low number of FRET-positive cells in the controls of mTagBFP-E6 + EYFP and mTagBFP2 + EYFP-E7 indicate no interaction seen. The E6 and E7 proteins from high-risk alpha HPV16, HPV31, HPV18, and beta HPV38 showed positive cells above the threshold of 500 cells. The number of FRET-positive cells for HPV6 is below the threshold; thus, the interaction is unclear. Data are derived from the mean value of three independent biological replicates. The error bars are plotted to represent the standard deviation of the mean value from the three independent biological replicates. The green dots represent the scatter dot plot of the three independent biological replicates. Please see Table S2B for detailed statistical data.

Table S2A: Statistical analysis data for Figure 2

FRET pair	HPV type	*n*	Mean	Standard deviation	p-value
mTagBFP2-E6 + EYFP	16	3	1.0	0.1	NA
	31	3	0.9	0.5	NA
	18	3	1.0	0.2	NA
	6	3	2.8	1.7	NA
	38	3	1.3	0.2	NA
mTagBFP2- + EYFP-E7	16	3	0.1	0.1	NA
	31	3	0.1	0.0	NA
	18	3	0.1	0.1	NA
	6	3	0.0	0.0	NA
	38	3	0.4	0.2	NA
mTagBFP2-E6 + EYFP-E7	16	3	13.0	1.7	0.006
	31	3	16.3	2.3	0.006
	18	3	15.0	1.2	0.002
	6	3	8.6	3.4	0.049
	38	3	17.9	2.5	0.006

*NA indicates not applicable

Table S2B: Statistical analysis data for Figure S2

FRET pair	HPV type	*n*	Mean	Standard deviation
mTagBFP2-E6 + EYFP	16	3	47	5
	31	3	30	17
	18	3	52	19
	6	3	24	3
	38	3	46	11
mTagBFP2 + EYFP-E7	16	3	17	13
	31	3	11	4
	18	3	24	22
	6	3	3	5
	38	3	50	33
mTagBFP2-E6 + EYFP-E7	16	3	753	200
	31	3	767	148
	18	3	1069	141
	6	3	125	47
	38	3	812	352

Supporting information 3 (SI3): % signal and number of double positive cells for FACS-FRET

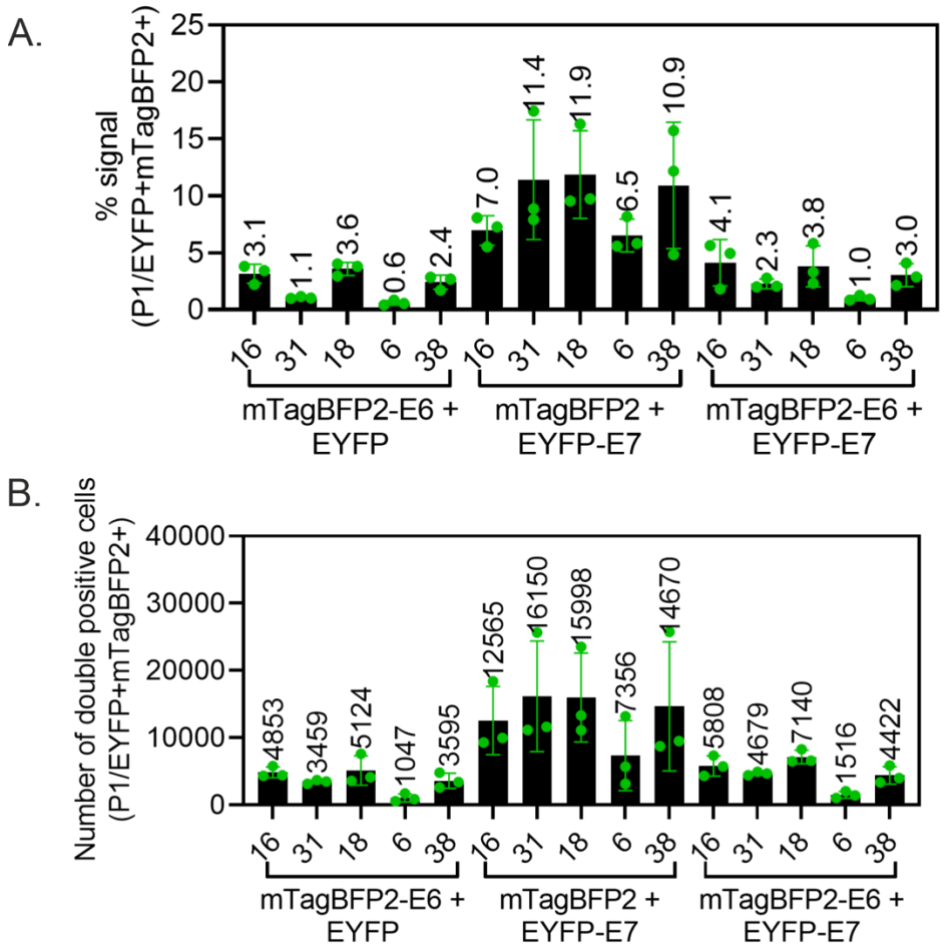

Figure S3. % signal and the number of double positive cells.
C33A co-expressing the mTagBFP2-E6 and EYFP-E7, as indicated, are subjected to FACS-FRET measurement. Viable cells are gated for EYFP and mTagBFP2 to examine cells expressing both mTagBFP-E6 and EYFP-E7 in % signal (**A.**) and the number of cells (**B**.) Data are derived from the mean value of three independent biological replicates with the mean value stated above each bar. The error bars are plotted to represent the standard deviation of the mean value from the three independent biological replicates. The green dots represent the scatter dot plot of the three independent biological replicates. Please see Table S3A and Table S3B for detailed statistical data.

Table S3A. Statistical analysis data for Figure SI3A

FRET pair	HPV type	*n*	Mean	Standard deviation
mTagBFP2-E6 + EYFP	16	3	3.1	0.8
	31	3	1.1	0.1
	18	3	3.6	0.6
	6	3	0.6	0.2
	38	3	2.4	0.6
mTagBFP2- + EYFP-E7	16	3	7.0	1.3
	31	3	11.4	5.3
	18	3	11.9	3.8
	6	3	6.5	1.4
	38	3	10.9	5.6
mTagBFP2-E6/EYFP-E7	16	3	4.1	2.0
	31	3	2.3	0.4
	18	3	3.8	1.8
	6	3	1.0	0.2
	38	3	3.0	1.0

Table S3B. Statistical analysis data for Figure SI3B

FRET pair	HPV type	*n*	Mean	Standard deviation
mTagBFP2-E6 + EYFP	16	3	4853	790
	31	3	3459	266
	18	3	5123	2184
	6	3	1047	588
	38	3	3595	1115
mTagBFP2 + EYFP-E7	16	3	12565	5076
	31	3	16150	8223
	18	3	15998	6611
	6	3	7356	5227
	38	3	14670	9597
mTagBFP2-E6 + EYFP-E7	16	3	5808	1505
	31	3	4678	261
	18	3	7140	997
	6	3	1515	504
	38	3	4422	1292

Supporting information 4 (SI4): CoIP full blot

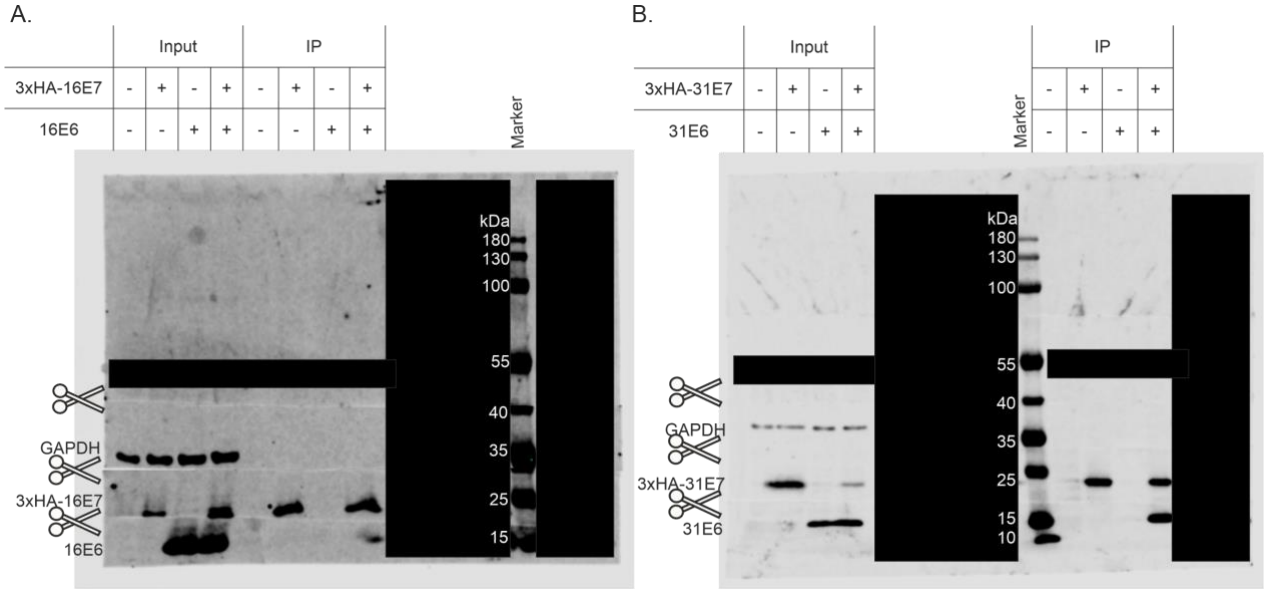

Figure S4. CoIP full blot. 70 µg cell lysates from C33A cells (input) or 25 µL of proteins precipitated with α-HA antibody (IP) were subjected to immunoblot analysis. The membrane blot was spliced after Western blotting to probe with several antibodies. First, the blots spliced above 15 kDa marker bands were probed with anti-16E6 and anti-31E6 antibodies, respectively. Then, the blots with splice site below 35 kDa marker band was probed with anti-HA antibodies for the signal of 3xHA-16E7 and 3xHA-31E7 followed by anti-GAPDH probing for the blots at splice site above 40 kDa. The antibodies probing membrane blot above the 40 kDa marker band are irrelevant for this manuscript. All spliced membranes were put together and aligned following molecular marker bands after probing with respective antibodies. Later, the aligned membrane strips were visualized at the same time at LI-COR Odyssey Fc as a single image. For presentation, the membrane blot shown in Figure 2 was cropped directly above 40 kDa marker band. The untagged E6 of alpha high-risk HPV16 **(A.)** or HPV31 **(B.)** were co-immunoprecipitated with 3xHA-16E7 or 3xHA-31E7, respectively. Irrelevant data on the same blot were covered in black.

Supporting information 5 (SI5): FP – Competition of 16E7CR1/2 with fl-16E7/MBP-16E6_4C4S

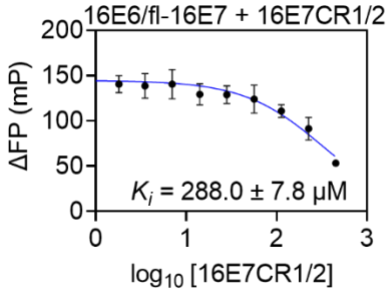

Figure S5. E6 binds the N-terminus of the E7 protein at a lower affinity. The reversibility of the fl-16E7/MBP-16E6_4C4S complex formation was observed with a competitive measurement by titrating the complex with an increasing amount of non-labeled 16E7CR1/2 (aa 1-44). A decreased FP signal indicates the reversible complex formation confirming an interaction. The binding is almost 5-fold lower compared to the GGG-16E7 FL.

Supporting information 6 (SI6): Sedimentation profile from AUC-SV measurement

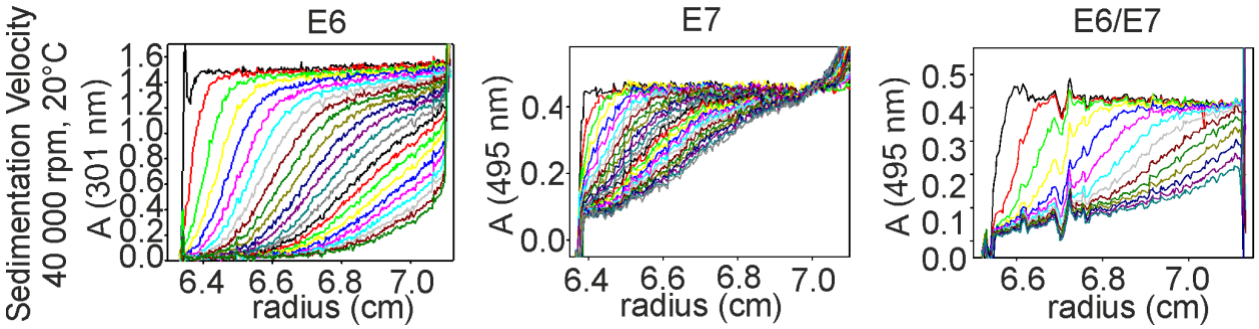

Figure S6. Sedimentation profile from sedimentation velocity measurement. MBP-16E6_4C4S-LxxLL was monitored at 301 nm wavelength. The fl-16E7 and the complex were monitored at 495 nm wavelength for the signal of the fluorescein. The shift in the sedimentation profiles indicates a binding event between MBP-16E6_4C4S-LxxLL and fl-16E7.

Supporting information 7 (SI7): Methods of proteins expression, proteins purification, proteins labeling and peptides synthesis

Protein expression

All E6 proteins were produced in *E. coli* BL21(DE3) at 16 °C after the addition of 100 µM $ZnCl_2$ and induction with 1 mM isopropyl-β-d-thiogalactopyranoside (IPTG) (MP Biomedicals, 02194029) overnight at an optical density at 600 nm (OD_{600}) of ~0.8 in Terrific Broth (TB) medium (12 g/L tryptone, 24 g/L yeast extract, 4 ml/L glycerol, 5 g/L NaCl, 0.017 M KH2PO4, and 0.072 M K2HPO4) with 30 µg/mL kanamycin as a selective antibiotic. All E7 proteins were expressed in *E. coli* BL21(DE3) using Bioreactor Labfors (INFORS AG, Bottmingen) at 20 °C in an M9 medium, following the instructions described previously in (1). MBP proteins were produced in *E. coli* BL21 and *Sortase A* (*Srt A*) in *E. coli* Rosetta 2 and expressed in the TB medium at 37°C. The expression was induced with 1 mM IPTG at an optical density at 600 nm (OD_{600}) of ~0.8 in TB using 100 µg/mL of Ampicillin as a selective antibiotic. Chloramphenicol was used additionally at 20 µg/mL for *Srt A* production in Rosetta 2. TEV protease was produced in *E. coli* BL21(DE3) and expressed in the TB medium at 37 °C. The expression was induced with 1 mM IPTG at an optical density at 600 nm (OD_{600}) of ~0.8 in TB using 30 µg/mL kanamycin as a selective antibiotic. The expression cultures were allowed to grow to OD_{600} of ~6.0 and harvested by centrifugation at 8 000 × *g* for 20 minutes at 4 °C.

Protein purification

The harvested *E. coli* biomass for production of the different E6 and E7 proteins were resuspended in 25 mL lysis buffer per 10 g wet biomass [50 mM Tris-HCl, pH 8 at 8 °C, 300 mM NaCl, 10 mM $MgCl_2$, 10 µM $ZnCl_2$, 5 % v/v glycerol, 1 mM TCEP] and approximately 4 mg of lysozyme (Carl Roth, #8259), 1 µL Benzonase® Endonuclease per 2 g wet biomass, 1 tablet cOmpleteTM EDTA-free Protease Inhibitor Cocktail per 50 mL buffer were added and incubated with gentle stirring for one hour in the cold room (4 - 8 °C). The cells were lysed by French press (Thermo Spectronic French Pressure Cell Press Model FA-078 With Pressure Cell) in 3 cycles at 600–1000 bar pressure. The lysate was centrifuged (1 hour at 30 000 × *g*, 4 °C) to remove cell debris. The supernatant was filtered through a 0.45 µm pore size, hydrophilic PVDF, 47 mm membrane (Merck, HVLP04700) before loading on the respective affinity column.

MBP-16E6_4C4S, MBP-16E6_4C4S-LxxLL(E6AP), and MBP-31E6_2C2S-LxxLL(E6AP) were applied to an MBP affinity column [self-packed amylose column, 30 ml amylose resin (New England Biolabs, #8021) equilibrated with E6-Buffer A [20 mM Tris-HCl, 200 mM NaCl, 3 mM $MgCl_2$, 10 µM $ZnCl_2$, 5 % v/v glycerol, 1 mM TCEP, pH 7.4, at 8 °C]. The unbound proteins were washed away by E6-Buffer A, followed by the wash with E6-Buffer B, a high salt buffer [E6-Buffer A containing 1 M NaCl], to remove nucleic acids and non-specific bound proteins. Proteins were eluted with E6-Buffer C [E6-Buffer A containing 10 mM maltose (Carl Roth, 8951)]. Elution fractions were pooled and centrifuged overnight at 100 000 × *g* to sediment agglomerates. The supernatant was concentrated in a 30 kDa cutoff spin column (Merck, #UFC903008) before being applied to a HiLoad 16/600 Superdex 200 pg (GE Healthcare) pre-equilibrated with SEC buffer [20 mM HEPES, 200 mM NaCl, and 1 mM TCEP, pH 7.5, at 8 °C]. Each time, 4 mL of 15 – 20 mg/mL E6 proteins were loaded. Fractions containing monomeric proteins were pooled (elution volume of ~85.5 mL for MBP-16E6_4C4S-LxxLL and 86.5 mL for MBP-16E6_4C4S), concentrated if needed (>800 µM for fluorescence polarization, >400 µM for analytical ultracentrifugation), flash frozen in liquid nitrogen, and stored at −80 °C.

His_6-TEV-GGG16E7 and His_6-TEV-GGG31E7 were subjected to Ni-NTA affinity column equilibrated with E7-Buffer A [20 mM Tris-HCl, 300 mM NaCl, 3 mM $MgCl_2$, 10 µM $ZnCl_2$, 5 % v/v glycerol, 1 mM TCEP, pH 7.4, at 8 °C]. The unbound proteins were washed away by E7-Buffer A, followed by the wash with high salt buffer E7-Buffer B [E7-Buffer A containing 1 M NaCl] to remove nucleic acids and non-specific bound proteins. Proteins were eluted with E7-Buffer C [E7-Buffer A containing 500 mM imidazole (Carl Roth, X998]. Elution fractions were pooled and centrifuged overnight at 100 000 × *g* to sediment agglomerates. The supernatant was diluted in AEX-Buffer A [20 mM Tris-HCl, 1 mM TCEP, pH 8 at 8 °C] to obtain a concentration of NaCl of less than 20 mM and applied onto an anion exchange column (HiTrap Capto Q 5mL, GE Healthcare) equilibrated with AEX-Buffer A. The unbound proteins were washed away with AEX-Buffer A. The E7 proteins were eluted with AEX-Buffer B [AEX-Buffer A containing 1 M NaCl]. Fractions containing E7 proteins were applied on HiLoad 16/600 Superdex 200 pg equilibrated with SEC buffer for size exclusion chromatography with 5 mL loaded each time. Fractions

containing His_6-TEV-GGG-E7 dimers were pooled (elution volume of ~88 mL), and concentrated to 50 µM for His_6-TEV tag cleavage.

For control experiments, the protein of MBP alone was purified from *E. coli* biomass (~20 g). The biomass was resuspended in MBP-Buffer A [20 mM Tris-HCl, 200 mM NaCl, 1 mM EDTA, pH 7.4 at 8 °C]. Approximately 8 mg of lysozyme, 1 µL Benzonase® Endonuclease per 2 g wet biomass, and 1 tablet cOmpleteTM EDTA-free Protease Inhibitor Cocktail per 50 mL buffer were added, and incubated with gentle stirring for one hour in the cold room (4 - 8 °C). Then, the cells were lysed as described above. The proteins were applied on MBPTrap HP 5 mL (GE Healthcare, 28918779) that were equilibrated with MBP-Buffer A followed by a wash with high salt buffer MBP-Buffer B (MBP-Buffer A containing 1 M NaCl) to remove nucleic acids and non-specific bound proteins. The proteins were eluted in MBP-Buffer C (MBP-Buffer A containing 10 mM maltose). The elution fractions were applied on HiLoad 16/600 Superdex 200 pg equilibrated with SEC buffer for size exclusion, with 4 mL of proteins loaded each time. Fractions containing MBP monomers were pooled (elution volume of ~88.5 mL), concentrated to >800 µM for fluorescence polarization, flash frozen in liquid nitrogen, and stored at −80 °C.

TEV protease and *Sortase A* were purified as previously described (2, 3).

Cleavage of His_6-TEV tag and *Sortase A*-based protein labeling

The purified His_6-TEV-GGG16E7 and His_6-TEV-GGG31E7 at 50 µM were incubated overnight with the in-house purified TEV protease at a molar ratio of 20:1. After overnight cleavage, the proteins were centrifuged for 1 hour at 100 000 × *g* at 4 °C to sediment aggregates. Then, the TEV protease was separated from the E7 proteins by loading 5 mL supernatant each time on HiLoad 16/600 Superdex 200 pg coupled with 1 mL HisTrap column upstream, equilibrated with SEC buffer, for an online pre-separation of the TEV protease and any non-cleaved E7 proteins containing His_6-TEV tag. The cleaved E7 proteins would run through and into HiLoad 16/600 Superdex 200 pg for size exclusion chromatography. Fractions containing GGG-E7 dimers were pooled (elution volume of ~89 mL), concentrated to > 400 µM dimeric concentration for fluorescence polarization, flash frozen in liquid nitrogen, and stored at −80 °C. The cleaved E7 proteins would now

reveal the triple-glycine motif (GGG) at its N-terminus, which is essential for *Sortase A* (*Srt A*). To label the E7 proteins, 25 µM *Sortase A* and 100 µM fluorescein-LPETGGRR were incubated with 50 µM GGG- E7 proteins after adding 10 mM $MgCl_2$ and 5 mM $CaCl_2$ co-factor. The reaction was incubated overnight with gentle stirring in the cold room (4 - 8 °C). After that, the proteins were centrifuged at 100 000 × *g* at 4 °C before applying 5 mL supernatant each time on HiLoad 16/600 Superdex 200 pg coupled with 1 mL HisTrap column upstream, equilibrated with SEC buffer, in which the His_6-*Sortase A* will be trapped in the 1 mL HisTrap column. In contrast, the fluorescein-labelled-E7 (fl-E7) proteins would run through into HiLoad 16/600 Superdex 200 pg for size exclusion chromatography. Fractions containing fl-E7 dimers were pooled (elution volume of ~89 mL), concentrated to 55 µM, flash frozen in liquid nitrogen, and stored at −80 °C.

Synthesis and purification of 16E7CR1/2 (1-44) peptides

The 16E7CR1/2 (1-44) peptide (HGDTPTLHEYMLDLQPETTDLYCYEQLNDSSEEEDEIDGPAGQ) and the corresponding fl-16E7CR1/2 (1-44) peptide were synthesized using standard Fmoc/tBu chemistry on a multiple peptide synthesizer Syro II (MultiSyntechTech, Witten, Germany) on a Rink-Amid resin (4, 5). After removing the N-terminal Fmoc group the resin was divided into two parts. One part was deprotected with reagent K for 3 hours. After precipitation in cold diethylether, the crude peptide was lyophilized.

The residual resin was coupled with 6-Carboxy-fluorescein (6-FAM, Sigma Aldrich) in a 4 molar excess using the TBTU-coupling procedure for 3 hours under light protection. Deprotection was performed according to the procedure for the free peptide. 16E7CR1/2 (1-44) peptides were purified by reversed-phase HPLC on a Reprosil C_{18} column (7 µm; 100 Å; 10x 250 mm; Dr. Maisch, Ammerbuch) using gradient elution with eluent A [0.05 % TFA in water] and eluent B [0.05 % in acetonitrile-water (80:20, v/v %)]. The gradient was from 20 % to 80 % eluent B in 30 minutes at a flow rate of 2.5 ml/min. UV detection was performed at 214 nm. All eluents are degassed under a vacuum to prevent disulfide formation.

Purities were ≥95 % as determined by analytical reversed phase-HPLC. Molecular masses of the labeled and non-labeled 16E7CR1/2 (1-44) were determined by Maldi-TOF-analysis on a Bruker Daltonics (Reflex IV, Germany) giving the correct masses$[M+H]^+$ of 4897.1 Da for the non-labeled 16E7CR1/2 peptide and 5255.3 Da for the fl-16E7CR1/2 peptide.

References

1. Roos, N., Breiner, B., Preuss, L., Lilie, H., Hipp, K., Herrmann, H. *et al.* (2020) Optimized production strategy of the major capsid protein HPV 16L1 non-assembly variant in E. coli Protein Expr Purif **175**, 105690 10.1016/j.pep.2020.105690
2. Tropea, J. E., Cherry, S., andWaugh, D. S. (2009) Expression and purification of soluble His(6)-tagged TEV protease Methods Mol Biol **498**, 297-307 10.1007/978-1-59745-196-3_19
3. Barthels, F., Marincola, G., Marciniak, T., Konhauser, M., Hammerschmidt, S., Bierlmeier, J. *et al.* (2020) Asymmetric Disulfanylbenzamides as Irreversible and Selective Inhibitors of Staphylococcus aureus Sortase A ChemMedChem **15**, 839-850 10.1002/cmdc.201900687
4. Zaidi, N., Herrmann, T., Baechle, D., Schleicher, S., Gogel, J., Driessen, C. *et al.* (2007) A new approach for distinguishing cathepsin E and D activity in antigen-processing organelles FEBS J **274**, 3138-3149 10.1111/j.1742-4658.2007.05846.x
5. Jores, T., Klinger, A., Gross, L. E., Kawano, S., Flinner, N., Duchardt-Ferner, E. *et al.* (2016) Characterization of the targeting signal in mitochondrial beta-barrel proteins Nat Commun **7**, 12036 10.1038/ncomms12036